



WESTFÄLISCHE WILHELMS-UNIVERSITÄT
MÜNSTER

PHD THESIS

$\mathcal{N} = 1$ supersymmetric
Yang-Mills theory on the lattice

Author:
Stefano PIEMONTE

Supervisor:
Prof. Dr. Gernot
MÜNSTER

8th April 2015

Theoretische Physik

$\mathcal{N} = 1$ supersymmetric Yang-Mills
theory on the lattice

Inaugural-Dissertation
zur Erlangung des Doktorgrades
der Naturwissenschaften im Fachbereich Physik
der Mathematisch-Naturwissenschaftlichen Fakultät
der Westfälischen Wilhelms-Universität Münster

vorgelegt von
Stefano Piemonte
aus Torino (Italien)
-2014-

Dekan:

Prof. Dr. Markus Donath

Erster Gutachter:

Prof. Dr. Gernot Münster

Zweiter Gutachter:

P.D. Dr. Jochen Heitger

Tag der mündlichen Prüfung(en):

.....

Tag der Promotion:

.....

This version of the thesis differs slightly from the official document submitted to the faculty. Typos are corrected while results and conclusions are unchanged.

Abstract

Supersymmetry (SUSY) relates two classes of particles of our universe, bosons and fermions. SUSY is considered nowadays a fundamental development to explain many open questions about high energy physics.

The $\mathcal{N} = 1$ super Yang-Mills (SYM) theory is a SUSY model that describes the interaction between gluons and their fermion superpartners called “gluinos”. Monte Carlo simulations on the lattice are a powerful tool to explore the non-perturbative dynamics of this theory and to understand how supersymmetry emerges at low energy. This thesis presents new results and new simulations about the properties of $\mathcal{N} = 1$ SYM, in particular about the phase diagram at finite temperature.

Zusammenfassung

Supersymmetrie (SUSY) verbindet zwei Klassen von Teilchen unseres Universums, Bosonen und Fermionen. SUSY gilt heute als fundamentale Entwicklung, um viele offene Fragen der Hochenergiephysik zu beantworten.

Die $\mathcal{N} = 1$ supersymmetrische Yang-Mills-Theorie (SYM) ist ein SUSY-Modell, das die Wechselwirkung zwischen Gluonen und ihren fermionischen Superpartnern, genannt “Gluinos”, beschreibt. Monte-Carlo-Simulationen auf dem Gitter sind ein leistungstarkes Werkzeug, um die nicht-perturbative Dynamik dieser Theorie zu erforschen und zu verstehen, wie Supersymmetrie bei niedrigen Energien in Erscheinung tritt. Diese Doktorarbeit stellt neue Ergebnisse und neue Simulationen zu den Eigenschaften der $\mathcal{N} = 1$ SYM vor, insbesondere zum Phasendiagramm bei endlicher Temperatur.

Acknowledgments

I am very grateful to my supervisor for his help during the PhD studies.

This thesis would have been impossible without the support and encouragement of Pietro Giudice, Georg Bergner and Istvan Montvay. I thank in particular Pietro Giudice for reading and commenting the first version of this thesis.

I am in debt with all the people working in the physics department for their support during these years, their help has been important to live in Germany and to finally understand (a little bit) German. I thank especially Christian Wittemeier for many useful discussions and for helping me with the translation of the abstract.

Contents

1	Introduction	13
1.1	Supersymmetry	14
1.2	The $\mathcal{N} = 1$ Supersymmetric Yang-Mills theory	15
1.3	Supersymmetry on the lattice	17
1.4	Lattice Monte Carlo methods	17
1.5	$\mathcal{N} = 1$ SYM at finite temperature	18
2	Supersymmetry	21
2.1	The cosmological constant problem	23
2.2	Supercharges	24
2.3	Properties of supersymmetric theories	26
2.3.1	Vacuum energy	26
2.3.2	Equal mass in a supermultiplet	27
2.3.3	Fermion-boson degeneracy	27
2.4	The Witten index	28
2.5	Non-renormalization theorem	30
2.6	Supersymmetry breaking	30
3	$\mathcal{N} = 1$ Super Yang-Mills model	33
3.1	Symmetries and fields content of $\mathcal{N} = 1$ SYM	33
3.2	Quantum anomalies and conserved currents	37
3.3	The bound spectrum of the theory	39
4	Supersymmetry on the lattice	43
4.1	Gluons and gauge fields on the lattice	44
4.2	The Haar measure	46
4.3	Wilson loops and gauge action	47
4.4	Gluinos on the lattice	49
4.5	The Curci-Veneziano action	50
4.6	Gluino condensate	52

5	Improved Actions	57
5.1	Lattice discretization and Symanzik improvements	58
5.2	Improving the Dirac Wilson operator	60
5.3	Tree level c_{sw} coefficient for $\mathcal{N} = 1$ SYM	62
5.4	Clover term and isospectral transformations	65
5.5	One loop c_{sw} coefficient	65
5.6	Applications to $\mathcal{N} = 1$ SUSY Yang-Mills theory	68
5.7	Tadpole improvements	68
6	Simulation algorithms for SUSY	71
6.1	Monte Carlo and importance sampling	72
6.2	Markov chains	72
6.3	Metropolis algorithm and Hybrid Monte Carlo	74
6.3.1	Hybrid Monte Carlo for lattice gauge theories	76
6.3.2	Link derivative	77
6.3.3	Numerical solution of the equations of motion	77
6.3.4	Implementation of the Hybrid Monte Carlo algorithm	78
6.3.5	Autocorrelation time	79
6.3.6	Errors in Monte-Carlo estimates	80
6.4	Majorana fermions on the lattice	80
6.5	HMC algorithm for Majorana fermions	82
6.5.1	The R algorithm	82
6.5.2	The RHMC algorithm	83
6.6	The WRHMC algorithm	85
6.6.1	Multiple time scales	85
6.6.2	Separation of scales in RHMC	86
6.7	Tools for Monte Carlo simulations	88
6.7.1	Improved integrators	88
6.7.2	Determinant breakup	89
6.7.3	Twisted mass as parameter to regularize the RHMC	89
6.7.4	Smearing	92
6.8	Testing the implementation of HMC algorithm	93
7	Scale setting in lattice SYM	97
7.1	Renormalization group equations	98
7.2	Useful observables to set the scale on the lattice	99
7.3	Mass dependent and independent schemes	100
7.4	Wilson flow	101
7.5	Measure of w_0 and t_0	103
7.6	Matching the β -function	103
7.7	Measure of the topological charge with the Wilson Flow	105

7.8	Autocorrelation time of flow observables	107
7.9	Correlations between topological charge and the scale w_0 . . .	108
7.10	Scale setting with w_0	111
8	Supermultiplets on the lattice	113
8.1	Adjoint pion and gluino mass	114
8.2	Computation of the critical point	115
8.3	η' and f_0	117
8.4	Gluino-Glue	118
8.5	Glueballs	119
8.6	The chiral limit	119
8.7	The continuum limit	120
9	Eigenvalues of the Dirac-Wilson operator	123
9.1	Symmetries of the Dirac-Wilson operator	124
9.2	Biorthogonal basis of eigenvectors	125
9.3	Degeneracy of the eigenvalues of D_W	126
9.4	Computing eigenvalues of the Dirac-Wilson operator	127
9.5	Eigenvalues and chiral anomaly	129
10	Phase diagram for $\mathcal{N} = 1$ SUSY	133
10.1	Finite temperature SUSY	135
10.2	The finite temperature phase diagram	136
10.2.1	Center symmetry and confinement	137
10.2.2	Static mesino and Polyakov loopino	138
10.2.3	Chiral phase transition	139
10.3	The deconfinement phase transition	141
10.4	The chiral phase transition	147
10.5	Phase diagram	151
11	Compactified $\mathcal{N} = 1$ super Yang-Mills theory	153
11.1	Confinement in compactified $\mathcal{N} = 1$ super Yang-Mills theory .	154
11.2	Numerical simulations	155
11.3	Phase diagram of compactified $\mathcal{N} = 1$ SYM	157
12	Conclusions	159
A	Determinants and Pfaffians	161
A.1	Grassmann variables	161
A.2	The determinant	162
A.3	The Pfaffian	164
A.4	Integration of quarks and gluinos	166

B	Data analysis	169
C	Gamma matrices	171
D	The Remez algorithm	173
E	Computation of the fermion force for the HMC algorithm	177
E.0.1	Derivative of a polynomial $P_n(\hat{Q}^\dagger \hat{Q})$	179
E.0.2	Derivative of \hat{Q}	180
E.0.3	Derivative of D_{eo}	180
E.0.4	Derivative of R_{ee} and $\log(\det(R_{ee}))$	181

Chapter 1

Introduction

Nature isn't classical, dammit, and if you want to make a simulation of nature, you'd better make it quantum mechanical, and by golly it's a wonderful problem, because it doesn't look so easy.

Richard Feynman

Elementary particles are considered the basic constituents of matter and radiation. Example of elementary particles are quarks, electrons, gluons or Higgs bosons. Quantum mechanics is the best theory available to describe the universe at scales lower or comparable to the size of an atom. From the quantum point of view fields of elementary particles are distributed over the whole space and their interactions generate the whole structure of the matter that we can see everyday. For instance the quantum behavior of electrons explains the stability of chemical matter. Particles like protons and neutrons are described by Quantum Chromodynamics (QCD) and vacuum fluctuations of quarks and gluons are the origin of the nuclear matter. Finally the Higgs mechanism is responsible for the mass of particles in the Standard Model (SM).

Supersymmetry (SUSY) is a theory in which matter and radiation are naturally paired by an extended symmetry. It has been introduced in recent years to solve many open questions left by the Standard Model. Supersymmetry has however many interesting features that could be helpful to understand better not only the high energy physics but also the low energy nuclear matter. Quantum corrections are difficult to be computed in the low energy regime, because interactions between quark and gluons are strong enough to spoil the convergence of standard perturbation methods. Supersymmetry can provide instead a fully consistent and more tractable description of

our universe to all scales, but unfortunately is far from being realized in our universe. SUSY has to be broken with some mechanism to provide a good description of our universe; or, more generally, one has to find the way to map results obtained in SUSY to non-supersymmetric theories.

A deep knowledge of strong interactions at low energy is required to understand how supersymmetry could be broken and in which way it could explain the appearance of protons from quarks and gluons. Due to strong interactions between particles, the most powerful tool to this end are computer simulations on a discrete space-time, but their implementation is “a wonderful problem, because it doesn’t look so easy”. This chapter is an overview of the contents of this thesis, to introduce the reader to the relevant topic that will be discussed in more detail in the following pages. Every section briefly summarizes motivations and insights of the main concepts regarding supersymmetry on the lattice, that will be the main subject of this thesis.

1.1 Supersymmetry

Supersymmetry is based on the idea that for every boson particle there exists a corresponding fermion partner and vice versa. Supersymmetry appears as challenge or solution of problems in many branches of physics, starting from the more abstract string theory to arrive to more practical question like dark matter or hierarchy problem. In this thesis the non perturbative dynamics of strong interacting SUSY model is considered, in the limit in which exact supersymmetry can be formulated consistently. Exact supersymmetry does not exist in nature, so it could seem rather strange to focus many efforts to study it. However there are a lot of motivations for a lattice investigation of an exact SUSY theory, non perturbative simulations allow for instance to check from first principles a possible spontaneous supersymmetry breaking and their related mechanisms.

Supersymmetric theories play a crucial role in particular in the context of the AdS/Cft correspondence, a quite complex framework that have been proposed for understanding the mysteries of QCD strong gluodynamics [1]. Quantum corrections coming from a boson are canceled by the corresponding fermion partner in SUSY theories. Finite supersymmetric theories are therefore possible without the need of an accurate fine tuning of the parameters. Many physical observables can be thus computed exactly to all order in perturbation theory, leading many remarkable results to be tested with numerical simulations. A non perturbative study of SUSY can be a test of the effective theories that have been formulated for low-energy dynamics of supersymmetry. Exact supersymmetry becomes now more appealing, since

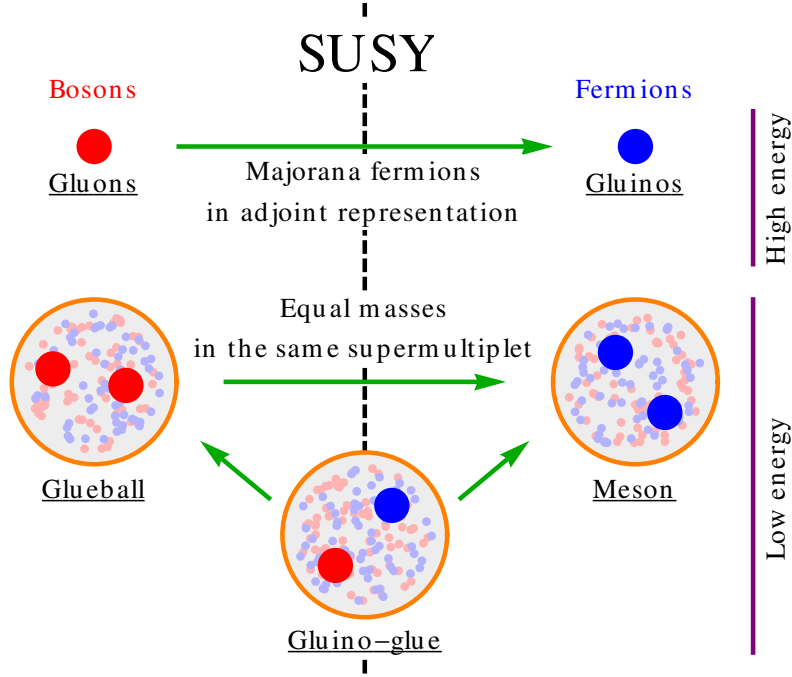


Figure 1.1: Gluons and gluinos can be found as isolated particles only at high energy and they will form colourless states at low energy due to confinement. Mesons, glueballs and gluino-gluon are the lowest energy states predicted for $\mathcal{N} = 1$ SYM and they will have the same mass if they belong to the same supermultiplet.

an orientifold equivalence can be formulated between one flavor QCD and SUSY gauge theories with one supercharge [2, 3]: it is possible in this way to provide some prediction also for QCD starting from SUSY! “One would be surprised if Nature had made no use of it”. For these reasons this thesis is focused on the study of the $\mathcal{N} = 1$ super Yang-Mills (SYM) theory on the lattice.

1.2 The $\mathcal{N} = 1$ Supersymmetric Yang-Mills theory

The $\mathcal{N} = 1$ SYM theory is the minimal supersymmetric extension of the pure gauge sector of QCD. The fundamental fields are gluons and their superpartners gluinos. The gluino is a Majorana fermion in the adjoint representation of the gauge group and it has on-shell the same number of degrees of freedom

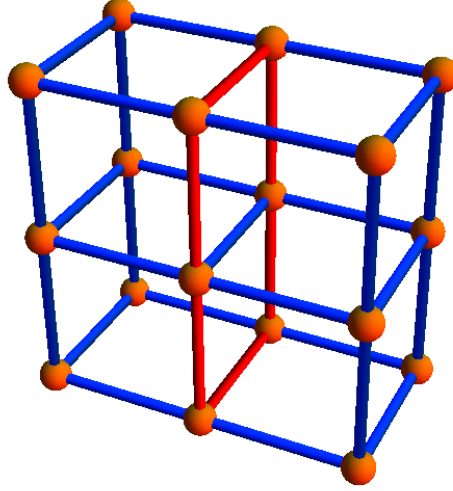


Figure 1.2: The Wilson loop is the path ordered product of all the variables on the red links.

of a gluon. The $\mathcal{N} = 1$ SYM theory is confined at low energy like QCD and elementary particles can be found only in colorless states forming a nontrivial bound spectrum of glueballs, mesons and gluino-gluon, a peculiar particle of adjoint models based on mixing of bosonic and fermionic operators. If exact supersymmetry is realized then particles are arranged in supermultiplets with equal masses and also bound states will exhibit the same pattern of mass degeneracy, see Fig. 1.1. This prediction is a good check for restoration of supersymmetry on the lattice with numerical simulations.

In QCD even-odd parity mesons have a nearly degenerate mass, for example the η' pseudoscalar meson ($J^{PC} = 0^{-+}$) has mass of 957.78 ± 0.06 MeV comparable to the mass of the scalar meson f_0 ($J^{PC} = 0^{++}$), equal to 990 ± 20 MeV. There are no explanations for this observed near degeneracy in QCD, but in the $\mathcal{N} = 1$ SYM the two corresponding adjoint mesons form a supermultiplet and the degeneracy of the mass is ensured by supersymmetry. In the large number of colors N_c of the gauge field, one flavor QCD is equivalent to $\mathcal{N} = 1$ SYM and therefore it might be possible that the small difference between the η' and f_0 mesons is a small correction of the order $1/N_c$, expected to disappear in the limit $N_c \rightarrow \infty$ [2, 3].

1.3 Supersymmetry on the lattice

A finite lattice spacing a can be introduced in order to regularize the $\mathcal{N} = 1$ theory and to simulate it in a computer. A serious problem arises immediately because the lattice breaks Lorentz invariance and so SUSY explicitly. In any case the theory can be formulated in terms of a gauge action and of a fermion action. The gauge action is based on Wilson loops, the gauge invariant product of link variables (see Fig. 1.2), while the fermion action is based on the Dirac-Wilson operator, whose inverse is related to the propagation of a gluino in the space-time. In the theory there are two free parameters, the gluino mass m and the gauge coupling g ; the strategy is to use them to fine tuning the theory to a proper continuum limit in which both the lattice spacing and the renormalized gluino mass vanish, with the hope that there supersymmetry is dynamically restored [4].

1.4 Lattice Monte Carlo methods

Computer simulations on discretized space-time are the only viable method to study the low energy behavior of QCD [5]. Computers are an important support for research in many branches of physics, not only in particle phenomenology but also for example in chaos theory, flow dynamics and quantum chemistry. Many scientific projects require nowadays long and expensive simulations impossible without the aid of large scale supercomputers. Many progresses have been achieved for Monte Carlo simulations applied to quantum field theories discretized on the lattice. Computer simulations are therefore one of the most important approach to understand better the non-perturbative regime of QCD and the limit of applicability of the gauge-gravity dualities.

Lattice Monte Carlo methods are much more involved in the case of supersymmetric Yang-Mills theories [6]. To perform numerical simulations the fermion fields are integrated out, as in QCD, because a Grassmannian variable cannot be directly stored in digital format. Unlike QCD, the result of the fermion integration is the Pfaffian of the Dirac operator due to the Majorana nature of the gluino, see App. A. The Pfaffian can be related to the determinant, but it could be a positive or negative quantity. A new serious problem arises here, because a negative quantity cannot be interpreted as a probability weight. The sign cannot be simulated directly by the Monte-Carlo algorithms and so it must be inserted and calculated separately after in the measurement process. The measure of the Pfaffian is quite nontrivial, it requires the application of specific maps defined on the complex plane to

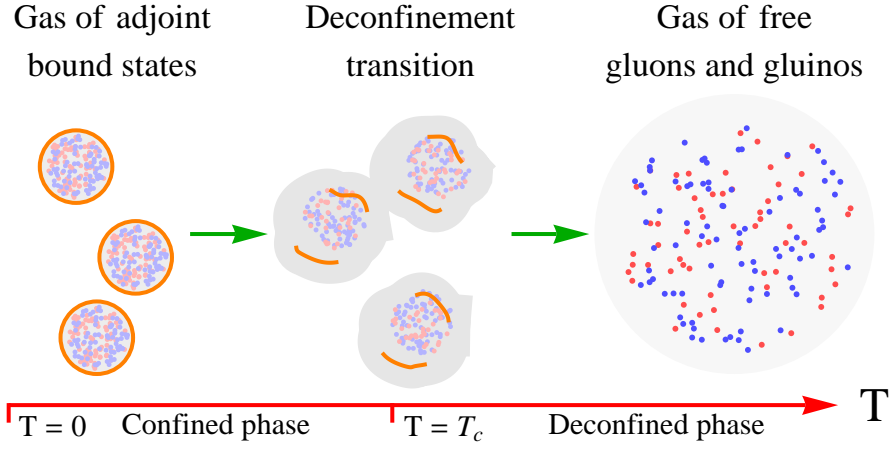


Figure 1.3: The deconfinement phase transition separates the low temperature regime from the high temperature phase where free gluons and gluinos weakly interact.

the Dirac operator, but it is a necessary step to ensure the correctness of the Monte Carlo algorithm.

A Monte Carlo algorithm to produce gauge field configurations has been implemented from scratch to simulate the $\mathcal{N} = 1$ supersymmetry, as integral part of the work for this thesis. The numerical results that will be presented in the following chapters would have been impossible without the huge effort to understand many practical informatics problems. The largest part of the work behind this thesis has been spent to code the final program. Supercomputers require for instance that the program “scales well”, meaning that it can be distributed among a large number of processors. Even several thousands of cores process in parallel the same lattice to produce a new configurations. Communications between cores are difficult, because different parts of the lattice have to be shared in different stage of the computation. An efficient routine has been implemented to solve automatically this problem.

1.5 $\mathcal{N} = 1$ SYM at finite temperature

SUSY is explicitly broken at finite temperature due to the thermal statistic difference between boson and fermion particles: fermions have antiperiodic boundary conditions in the time direction, bosons instead periodic. Therefore it could be that supersymmetric Yang-Mills theories and QCD share the same properties at finite temperature. So finite temperature is like a bridge between an “ideal world” in which SUSY exists and our real world of the

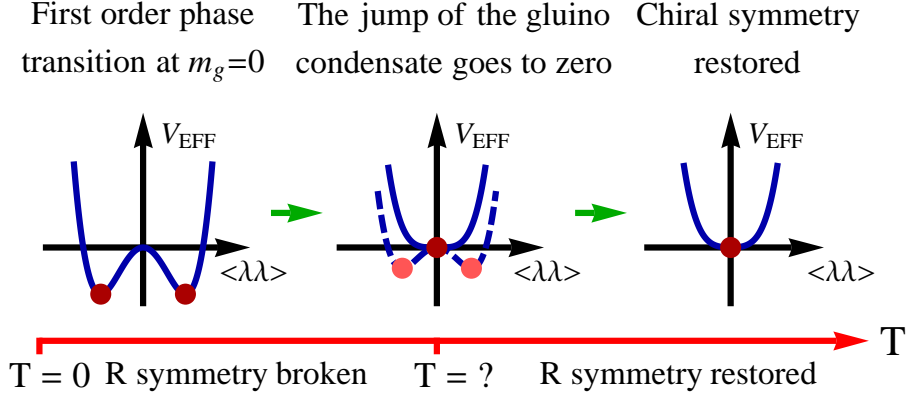


Figure 1.4: Chiral symmetry is broken at zero temperature but it is expected to be restored after a critical temperature. It is however unknown whether this critical temperature coincides or not with the deconfinement phase transition.

QCD strong interactions. “It could be”, lattice Monte Carlo simulations are needed to prove such a scenario.

The $\mathcal{N} = 1$ SYM model exhibits confinement as QCD and only colorless states will appear at zero temperature. At high temperature the theory behaves as a conformal gas of free gluons and gluinos, therefore we expect that there will be a deconfinement phase transition in which mesons and glueballs will melt down, see Fig. 1.3. The order parameter associated to the deconfinement phase transition is the Polyakov Loop, and it represents the expectation value of a single isolated fundamental quark. The deconfinement phase transition will not turn into a crossover for any value of the gluino mass because of supersymmetry. This significant difference with QCD provides the possibility of studying the deconfinement phase transition exactly also with dynamical fermions. Results about the thermodynamical phase transitions have been published in Ref. [7] and they will be presented in Ch. 10. The deconfinement temperature has been found to have a clear signal and a mild dependence on the fermion mass. A second order phase transition has been observed in the universality class of the three dimensional Z_2 Ising model for the gauge group $SU(2)$.

The $\mathcal{N} = 1$ super Yang-Mills is indeed similar to QCD because also in this model there is a classical fermion symmetry, the chiral symmetry, which is spontaneously broken. However the pattern is different, a classical $U(1)$ axial, or R symmetry in the SUSY language, is broken by anomaly down to a discrete Z_{2N_c} symmetry. This remaining symmetry is broken spontaneously down to Z_2 by a non vanishing expectation value of the gluino condensate.

At zero temperature for $SU(2)$ there are two symmetrical vacua that at high temperature are expected to form again a unique symmetrical vacua. There will be a phase transition, but it is not known at what temperature does it occur, see Fig. 1.4. Some preliminary simulations have been run to clarify this point, within the current precision the chiral symmetry restoration coincides roughly with the deconfinement phase transition. More simulations are required to fully prove such a behavior. This situation seems however really similar to QCD, where deconfinement and chiral symmetry restoration occurs around at the same temperature, but in $\mathcal{N} = 1$ SYM, thanks to SUSY, the relations between this two symmetries can be studied exactly.

Chapter 2

Quantum field theories and supersymmetries in nature

Although supersymmetry holds the promise of being a fundamental symmetry in physics, we will study these theories not because they have an immediate application to particle physics, but because they provide a fascinating laboratory in which one can probe the limits of quantum field theory.

Michio Kaku [8]

During the XX century, several important progresses have been achieved in understanding the structure and the physical foundation of the universe. While general relativity provides a good model of the large scale phenomena dominated by gravitation, quantum mechanics and quantum field theories have been successful in describing of the internal structure of the atom and of its constituents. The unification of these two important theories is one of the main challenge of physics today. Symmetries have had a central role in the development of new unified theories, for example local Lorentz invariance is crucial for general relativity and gauge symmetry is fundamental for describing the nuclear and electromagnetic interactions between elementary particles.

Supersymmetry (SUSY) is an extension of the same concept of symmetry. Additional constraints are imposed on the number and on the mutual properties between bosons and fermions, leading to a theory in which matter and radiation fields come naturally paired with degenerate masses. Supersymme-

try transforms boson particles into fermions and conversely. This new kind of symmetry is required by many quantum models of the gravitation, like SUGRA (SUPersymmetry GRAvitation) or string theory. SUSY is expected to be discovered at least at the Planck energy scale $M_P \approx 10^{19}$ GeV, where gravitational quantum effects cannot be neglected.

Supersymmetry has been introduced also as beyond Standard Model (SM) theory in order to solve difficulties and open questions in the elementary particle physics, like the “hierarchy problem” and the “vacuum stability”. Despite of the large energy scale where the degeneracy between bosons and fermions is expected to be realized, supersymmetry influences and stabilizes the low energy physics probed by current experiments. A fermion has different properties from a boson, in particular quantum corrections have different sign if they come from a boson particle instead of a fermion. SUSY has therefore a natural explanation to the surprisingly small mass of Higgs boson compared to the Planck scale M_P ; natural in the sense that it is stable with respect to quantum fluctuations. Without any accurate fine tuning of the parameters, the large quantum corrections to the Higgs mass coming from a boson are canceled by the contributions of its fermion superpartner.

Supersymmetry has been intensively studied in the last two decades not only as a model to unify gravitation and quantum mechanics, but also as a “tool” for understanding better in general quantum fields and in particular the theory of strong interactions (called QCD, Quantum ChromoDynamics). A proton can be viewed as a clouds of quarks and gluons and the coupling constant α_s measures the strength of the interactions between these elementary particles. At low energy, the coupling constant of the strong interactions is of order of the unit, $\alpha_s \sim 1$, and therefore perturbative approaches to quantum fields fail completely. Analytical results can be computed for QCD only in the high energy limit with standard perturbation theory [9, 10], but how protons and nucleons emerge in ordinary matter is still a mystery today.

In 1997 Maldacena discovered a duality between a supersymmetric quantum field theory at strong coupling and string theory in the classical gravity limit [1]. Using this duality it is possible to map the analytical calculations of string theory with perturbative couplings to a quantum field theory in the non-perturbative regime. How to apply these results valid for a supersymmetric model to QCD is still an open question. Many efforts have been recently done for understanding the relations between these two quantum fields models, the challenge is to try to find a further suitable limit of the parameters in which a supersymmetric theory reduces to standard QCD.

In the following sections the basic properties of supersymmetry will be reviewed. They will introduce better the motivations for studying these class

of theories.¹

2.1 The cosmological constant problem

In general relativity gravitational interactions between bodies are generated as the effect of the curvature R of the space-time, a four dimensional manifold with metric $g_{\mu\nu}(x)$ considered as a dynamical object. The equations of motion of the matter and of the gravitational fields can be derived from the Hilbert action

$$S = \int d^4x \sqrt{-\det(g_{\mu\nu}(x))} (R(x) - 2\Lambda).$$

The space-time independent parameter Λ is called “cosmological constant” and it can be freely added to the action without violating the basic hypothesis of the general relativity. Λ can be considered as some sort of energy of the vacuum, a kind of energy that exists even if no matter is present in the space. The effect of the cosmological constant on the evolution of our universe is to increase the rate of its expansion and therefore the value of Λ can be estimated directly from cosmological observations. Recent measurements have established that the cosmological constant is closed to zero [13].

In quantum mechanics, an harmonic oscillator has a ground state with energy E_0 different from zero and equal to

$$E_0 = \frac{1}{2} \hbar \omega.$$

A quantum field can be considered as an infinite sum (i.e. an integral) of harmonic oscillators, therefore the zero energy will be equal to

$$E_0 = \sum_{i=0}^n E_0^i = \sum_{i=0}^n (-1)^{2s_i} \frac{s_i}{2} (s_i + 1) \int d^3k \sqrt{k^2 - m_i^2}, \quad (2.1)$$

for a theory with n particles of spin s_i and mass m_i . Notice that a particle with half integer spin will contribute lowering the value of the sum because the fermion fields obey to an anticommuting algebra. E_0 is a sum of divergent terms that must be regularized, a reasonable work assumption could be that there cannot not be momenta bigger than the Planck mass M_P . Therefore the contribution E_0^i of a single boson particle will be

$$E_0^i \sim \int_0^{M_P} dk k^2 \sqrt{k^2 - m_i^2} \sim \int_0^{M_P} dk k^3 \sim M_P^4. \quad (2.2)$$

¹There are several detailed and advanced reviews available about supersymmetry. This chapter has been prepared following [11, 8, 12].

In the general relativity context, this vacuum energy has to be summed to the cosmological constant and cannot be removed by a redefinition of the zero level as in ordinary Minkowski flat space. Since the Planck mass is of order of $M_P \approx 10^{19}$ GeV, the left side of Eq. (2.2) is of order 10^{120} GeV, simply 120 orders of magnitude off from the experimental data [13]. This is the largest discrepancy between theory and experiment known in physics today, a possible renormalization of Λ should fine tune the cosmological constant accurately with large cancellations. Usually large cancellations in the parameter of the theory are a signal of a new symmetry that protects the renormalized quantities by automatically tuning them to the experimental values.

Each fermion field gives in Eq. (2.1) a negative contribution to the ground state energy, suggesting a possible kind of symmetry leading to the small value of Λ observed. If for each boson in nature there exists a corresponding fermion partner with the same quantum number (spin, number of internal degrees of freedom, etc ...), then the sum Eq. (2.1) would be exactly zero without the need of any kind of renormalization. This would automatically solve the “cosmological constant problem”. The symmetry that has this needed characteristic of equal number of fermion and boson degrees of freedom is called supersymmetry.

2.2 Supercharges

In supersymmetry an additional set of conserved charges Q_α is imposed to a quantum field theory

$$\frac{d}{dt}Q_\alpha^i = 0, \quad (2.3)$$

with the peculiar characteristic that this conserved charge transforms under Lorentz boosts and rotations non-trivially as a Majorana spinor. The supercharge Q can be viewed as an operator which transforms fermion states in boson one and vice versa

$$\begin{aligned} Q|\text{boson}\rangle &= |\text{fermion}\rangle, \\ Q|\text{fermion}\rangle &= |\text{boson}\rangle. \end{aligned}$$

and the spinor nature of Q ensures the consistency of these relations. In fact if the states are transformed by R as complete spatial rotation of 360 degrees around an axes, then the boson state does not change while the spinor acquires a minus sign

$$\begin{aligned} R|\text{boson}\rangle &= |\text{boson}\rangle, \\ R|\text{fermion}\rangle &= -|\text{fermion}\rangle, \end{aligned}$$

and then it can be deduced that also the supercharge Q gets a minus sign under a full spatial rotation as a spinor operator

$$\begin{aligned} RQ|\text{boson}\rangle &= R|\text{fermion}\rangle, \\ RQR^{-1}R|\text{boson}\rangle &= R|\text{fermion}\rangle, \\ RQR^{-1}|\text{boson}\rangle &= -|\text{fermion}\rangle, \\ RQR^{-1}|\text{boson}\rangle &= -Q|\text{boson}\rangle, \\ RQR^{-1} &= -Q. \end{aligned}$$

The spinor properties of Q have a deeper understanding and origin in quantum field theory. In fact the Coleman-Mandula theorem forbids any other possible conserved charge with an integer spin different from a scalar in an interacting quantum field theory in more than two dimensions. This theorem has been for a while considered the end of possible unification of Yang-Mills theories with space-time symmetries until SUSY was discovered as a case not covered by the hypothesis.

To derive formally the properties of the operator Q_α it is useful to consider supersymmetry as the extension of the Poincaré algebra. The symmetries of the four dimensional Minkowski space-time, i.e. the transformations that leave invariant the metric $\eta_{\mu\nu} = \text{diag}(-1, 1, 1, 1)$, are translations, boost and spatial rotations. Infinitesimal translations ϵ^μ acts on scalar fields as

$$\phi(x_\mu) \rightarrow \phi(x_\mu + \epsilon_\mu) = \phi(x) + \epsilon^\mu \partial_\mu \phi(x) = \phi(x) + i\epsilon^\mu P_\mu \phi(x) + O(\epsilon^2),$$

while infinitesimal boost and rotations $\epsilon_{\mu\nu}$ transform $\phi(x_\mu)$ as

$$\begin{aligned} \phi(x_\mu) \rightarrow \phi(x_\mu + \epsilon_{\mu\nu} x^\nu) &= \phi(x) + \epsilon^{\mu\nu} (x_\nu \partial_\mu - x_\mu \partial_\nu) \phi(x) = \\ &= \phi(x) + i\epsilon^{\mu\nu} L_{\mu\nu} \phi(x) + O(\epsilon^2). \end{aligned}$$

The Poincaré algebra than reads

$$\begin{aligned} [P_\mu, P_\nu] &= 0, \\ [L_{\mu\nu}, P_\rho] &= i(\eta_{\mu\rho} P_\nu - \eta_{\nu\rho} P_\mu), \\ [L_{\mu\nu}, L_{\rho\sigma}] &= i(\eta_{\nu\rho} L_{\mu\sigma} + \eta_{\mu\sigma} L_{\nu\rho} - \eta_{\mu\rho} L_{\nu\sigma} - \eta_{\nu\sigma} L_{\mu\rho}). \end{aligned}$$

The supercharges Q_α has now to be considered to extend the Poincaré algebra to a more generic “superalgebra”. Schematically, the superalgebra has the structure of a Z_2 -graded Lie algebra, meaning that operators can be labeled to be either “even” or “odd” obeying to the relations

$$\begin{aligned} [\text{even}, \text{even}] &\sim \text{even}, \\ [\text{even}, \text{odd}] &\sim \text{odd}, \\ \{\text{odd}, \text{odd}\} &\sim \text{even}. \end{aligned}$$

The transformation properties of a Majorana spinor under the action of the Poincaré group and the cyclic Jacoby identity force the “even”-“odd” commutator to be of the form

$$[P_\mu, Q_\alpha] = 0, \quad (2.4)$$

$$[L_{\mu\nu}, Q_\alpha] = i(\gamma_\mu\gamma_\nu - \gamma_\nu\gamma_\mu)_{\alpha\beta}Q_\beta. \quad (2.5)$$

The first equality means that the supercharges are translational invariant. The last missing point is the anticommutator algebra satisfied by two supercharges Q_α . Since the product of two spinor operators transforms as a vector and since the only vector conserved allowed by the Coleman-Mandula theorem is the energy-momentum P_μ , then it follows with the standard normalization

$$\{Q_\alpha, Q_\beta\} = (C\gamma_\mu)_{\alpha\beta}P_\mu. \quad (2.6)$$

This anticommutator conclude the superalgebra, further possible extension can be build up if a whole set Q_α^i and not only a single conserved supercharge is imposed to the quantum field theory. The most interesting cases in four dimensional flat space-time are one ($\mathcal{N} = 1$), two ($\mathcal{N} = 2$) and four ($\mathcal{N} = 4$) set of conserved supercharges. The theory considered in this thesis is a Yang-Mills model with only one conserved supercharge.

2.3 Properties of supersymmetric theories

2.3.1 Vacuum energy

One interesting property of supersymmetric theories is the exact vanishing of the vacuum energy, meaning that SUSY is able to solve the cosmological constant problem. Depending on the basis of gamma matrices chosen, from Eq. (2.6) it follows that there will be always a linear combination of anticommutators $\{Q_\alpha, Q_\beta\}$ equal to the Hamiltonian P_0 . The energy of the vacuum E_0 will be now with the gamma matrices basis defined in App. C

$$E_0 = \langle 0|P_0|0\rangle = -\frac{1}{4}(\gamma_2)_{\alpha\beta}\langle 0|(Q_\alpha Q_\beta + Q_\beta Q_\alpha)|0\rangle \quad (2.7)$$

and if supersymmetry is not broken, then the vacuum state will be annihilated by the supercharges

$$Q_\alpha|0\rangle = 0$$

so that it can be concluded that $E_0 = 0$. Supersymmetry therefore has a natural way to define and fix to zero the energy of the vacuum, without the need of renormalization and without the arbitrariness of an additive constant. In other words the vacuum energy is the order parameter for SUSY breaking.

2.3.2 Equal mass in a supermultiplet

If a boson particle with mass $M > 0$ exists, then its corresponding fermion superpartner has that same mass M . From Eq. (2.4) it follows that

$$\begin{aligned} [P_\mu P^\mu, Q_\alpha] &= 0, \\ P^2 |\text{boson}\rangle &= M_B^2 |\text{boson}\rangle \\ &= P^2 Q |\text{fermion}\rangle = Q P^2 |\text{fermion}\rangle \\ &= M_F^2 Q |\text{fermion}\rangle = M_F^2 |\text{boson}\rangle, \end{aligned}$$

and therefore $M_F = M_B$: states related by supersymmetry transformations have degenerate masses. These states form what are formally called “supermultiplets”, analogous for instance to the multiplets of isospin in nuclear particle physics.

2.3.3 Fermion-boson degeneracy

A supermultiplet contains the same number of boson and fermion particles. The supercharge operator maps the subspace spanned by a supermultiplet into itself, therefore it makes sense to consider the trace

$$N_{B-F} = \text{Tr}_{\mathcal{S}}((-1)^F \{Q_\alpha, Q_\beta\}),$$

restricted only to the states \mathcal{S} in a given supermultiplet. The operator $(-1)^F$, formally equivalent to the R rotation operator defined before

$$\begin{aligned} (-1)^F |\text{boson}\rangle &= |\text{boson}\rangle, \\ (-1)^F |\text{fermion}\rangle &= -|\text{fermion}\rangle, \end{aligned}$$

anticommutes with the supercharges

$$\{Q_\alpha, (-1)^F\} = 0, \quad (2.8)$$

since Q_α exchanges boson with fermion states

$$\begin{aligned} Q_\alpha (-1)^F |\text{boson}\rangle &= Q_\alpha |\text{boson}\rangle = |\text{fermion}\rangle = -(-1)^F |\text{fermion}\rangle \\ &= -(-1)^F Q_\alpha |\text{boson}\rangle, \\ Q_\alpha (-1)^F |\text{fermion}\rangle &= -Q_\alpha |\text{fermion}\rangle = -|\text{boson}\rangle = -(-1)^F |\text{boson}\rangle \\ &= -(-1)^F Q_\alpha |\text{fermion}\rangle. \end{aligned}$$

The trace N_{B-F} is zero

$$\begin{aligned} N_{B-F} &= \text{Tr}_{\mathcal{S}}((-1)^F Q_\alpha Q_\beta + (-1)^F Q_\beta Q_\alpha) \\ &= -\text{Tr}_{\mathcal{S}}(Q_\alpha (-1)^F Q_\beta + Q_\beta (-1)^F Q_\alpha) \\ &= -\text{Tr}_{\mathcal{S}}((-1)^F Q_\beta Q_\alpha + (-1)^F Q_\alpha Q_\beta) \\ &= -N_{B-F}, \end{aligned}$$

using Eq. (2.8) and the cyclic property of the trace in the last step. The result that

$$N_{B-F} = \text{Tr}_{\mathcal{S}}((-1)^F \{Q_\alpha, Q_\beta\}) = \text{Tr}_{\mathcal{S}}((-1)^F (C\gamma_\mu)_{\alpha\beta} P_\mu) = 0, \quad (2.9)$$

implies that also the trace

$$\text{Tr}_{\mathcal{S}}((-1)^F) = \text{number of bosons} - \text{number of fermions} = 0$$

is zero, unless $P_\mu = 0$ for all μ , and therefore

$$\text{number of bosons} = \text{number of fermions} \quad (2.10)$$

in a given supermultiplet.

A massive supermultiplet can be constructed for example with a spin- $\frac{1}{2}$ Majorana fermion, a scalar and a pseudoscalar boson. This supermultiplet has a crucial role in the low energy effective theory of $\mathcal{N} = 1$ SYM. A massless supermultiplet contains for instance a gauge boson and its corresponding fermion partner, like for example the gluon and the gluino or the photon and the photino.

The degeneracy between boson and fermion states is valid as far as $P_\mu \neq 0$ holds. However, this is not the general case, an interesting counterexample arises when the superalgebra is in the adjoint representation, where the representation of the translation operator is trivial, $P_\mu = 0$. The representation space is constructed simply from the generators itself and indeed the number of boson generators is different from the number of fermion generators [11]. An another important case is discussed in the following section.

2.4 The Witten index

When the momentum operator acts on the translation invariant vacuum state, then $P_\mu = 0$ on this state and the rule (2.10) does not hold anymore. In particular, the number of zero energy states is not constrained and in general there could be a number of zero boson states different from the number of zero fermion states. If there are no zero energy states at all, then SUSY is broken.

Witten discovered that the question whether a supersymmetric theory could be spontaneously broken or not can be addressed by considering simply the trace

$$I_W = \text{Tr}((-1)^F),$$

this time extended over all the Hilbert space and not restricted to a single supermultiplet [14]. All the non-zero energy states are paired, that means

$$I_W = \text{number of zero boson states} - \text{number of zero fermion states},$$

and therefore there are two different possibilities:

1. $I_W \neq 0$: in this case there exists at least either one fermion zero state ($I_W < 0$) or a boson zero state ($I_W > 0$), supersymmetry is not spontaneously broken
2. $I_W = 0$: in this case the number of zero boson states is equal to the number of zero fermion states. It could be that

$$\text{number of zero boson states} = \text{number of zero fermion states} \neq 0$$

and supersymmetry is not broken, or that

$$\text{number of zero boson states} = \text{number of zero fermion states} = 0$$

and supersymmetry is broken.

The trace I_W is called Witten index; if non zero, it forbids spontaneous supersymmetry breaking. The Witten index can be computed at finite volume V , at weak coupling g or in any other limit which does not alter the fundamental behavior of the theory [14]. A variation of g or of V could result in a rearrangement of the spectrum of the states, but only pairs of fermion-boson can acquire a positive energy from the ground state. It could be for instance that a zero boson state acquires a non-zero energy E_1 , but as soon as this happens, then Eq. (2.9) holds and it forces also a zero fermion state to acquire the same amount of energy E_1 . Hence the difference between zero boson states and zero fermion states does not change by a variation of the volume or of the gauge coupling. The Witten index has been computed for the $\mathcal{N} = 1$ super Yang-Mills theory, I_W is equal to the number of colors of the gauge group and this theory cannot be spontaneously broken.

The Witten index can be regularized as

$$I_W = \text{Tr}((-1)^F \exp(-\beta H)).$$

The ground states have zero energy and the other states contributions cancel

due to boson-fermion pairing, the sum reduces to

$$\begin{aligned}
I_W &= \sum_{\substack{\text{zero} \\ \text{energy} \\ \text{states}}} (-1)^F \exp(-\beta E_i) + \sum_{\substack{\text{non-zero} \\ \text{boson} \\ \text{energy} \\ \text{states}}} \exp(-\beta E_i) - \sum_{\substack{\text{non-zero} \\ \text{fermion} \\ \text{energy} \\ \text{states}}} \exp(-\beta E_i) \\
&= \sum_{\substack{\text{zero} \\ \text{energy} \\ \text{states}}} (-1)^F \exp(-\beta 0) + 0 \\
&= \text{number of zero boson states} - \text{number of zero fermion states} \\
&= \text{Tr}((-1)^F),
\end{aligned}$$

and it is completely independent from β . The Witten index is similar in this form to the usual partition function, the boundary conditions of fermions have to be changed from antiperiodic to periodic in the time direction in the path-integral formulation due to the effect of $(-1)^F$. A remarkable result follows from the β independence of the Witten index: if fermion boundary conditions are periodic in all directions, then the free energy and all the bulk thermodynamical quantities are a constant completely independent from the temperature.

2.5 Non-renormalization theorem

The non-renormalization theorem is a formal statement about the cancellation rule of fermion and boson loop quantum corrections in a set of Feynman diagrams. The non-renormalization theorem ensures that supersymmetry is not broken to all order in perturbation theory if the model is classically supersymmetric at tree level [15]. Due to this theorem, the only possible sources of SUSY breaking can appear in an exact supersymmetric theory as non-perturbative effects, arising as essential singularity of some coupling parameter like $e^{-\frac{1}{g^2}}$.

2.6 Supersymmetry breaking

Since there are not experimental evidences for SUSY in the low energy scales probed currently by particles accelerators, supersymmetry must be broken in some way to build a consistent theory of our universe. Dynamical supersymmetry breaking refers to the possibility that some composite field acquires a non-zero vacuum expectation value breaking SUSY due to non perturbative effects in agreement to the non-renormalization theorem. An example of dynamical supersymmetry breaking can be found in Ref. [16]. However such

spontaneous supersymmetry breaking is possible if and only if the index I_W is equal to zero. For models where $I_W \neq 0$, the only viable option is to break supersymmetry explicitly by adding terms in the Lagrangian not invariant under SUSY transformations.

A soft SUSY breaking modifies the theory altering only the low energy scales, but keeping intact the ultraviolet physics. The typical example of soft SUSY breaking is the addition of a mass m to all the superpartners, like gluinos, gauginos, squarks, etc; high enough to explain the absence of those particle in the current experimental results. Independently on the value of m chosen, at very high energy its contribution will disappear and SUSY will be “effectively” restored: the important properties that are interesting to solve questions like the cosmological constant problem will be not spoiled. For Super Yang-Mills theories on the lattice this mass m will assume the important role of renormalization parameter. In contrast, an hard SUSY breaking term does not become negligible in the ultraviolet regime. Possible scenarios where hard SUSY breaking could appear are usually related to particle phenomenology.

Chapter 3

$\mathcal{N} = 1$ Super Yang-Mills model

We have argued that the pure $\mathcal{N} = 1$ supersymmetric Yang-Mills theory leads to a spectrum of massive multiplets of composite hadrons [...] which become weakly interacting in the large- N_c limit. Perhaps disappointingly, SUSY is not broken [...]

G. Veneziano and S. Yankielowicz [17]

The $\mathcal{N} = 1$ Super Yang-Mills model is the supersymmetric extension of the pure gauge sector of QCD. The theory is confined at zero temperature, but nevertheless many non-perturbative properties can be computed analytically. Predictions has been proposed about the lowest two supermultiplets of the bound spectrum [17, 18, 19], while the chiral condensate and the beta function can be remarkably computed exactly [3, 2, 20]. In this chapter these important results are summarized.

3.1 Symmetries and fields content of $\mathcal{N} = 1$ SYM

In four dimensions the simplest supersymmetric Yang-Mills theory can be constructed imposing only one conserved supercharge. The gauge fields of this theory are variables of the Lie algebra

$$A_\mu(x) = A_\mu^i(x) \tau_i^F \quad i : 1 \cdots N_c^2 - 1,$$

where τ_i^F are the Lie group generator of $SU(N)$ in the fundamental representation

$$[\tau_i^F, \tau_j^F] = if_{ij}^k \tau_k^F.$$

The particles of the gauge fields are called gluons and their corresponding supersymmetric partners are the gluinos. The gluinos are Majorana fermions in the adjoint representation, therefore they have $N_c^2 - 1$ color degrees of freedom, as many as the gluons

$$\lambda(x) \equiv \lambda_\alpha^i : 1 \cdots N_c^2 - 1.$$

Majorana conditions are imposed over λ and the bar spinor $\bar{\lambda}$

$$\bar{\lambda}_\alpha^i = (\lambda^T)_\alpha^i C_{\alpha\beta},$$

where C is the charge conjugation matrix. Majorana fermions are solutions of the Dirac equation which satisfy also the self-conjugation relation

$$\lambda^c = C\bar{\lambda}^T = \lambda \quad (3.1)$$

and this equation clearly states that for gluinos there are no essential differences between particles and antiparticles.

The symmetries of the model uniquely define the action of the theory, that has to be invariant under the transformation induced by the symmetries over the fields. Lorentz symmetry is common over all the relativistic theories and it transforms the fields as

$$\begin{aligned} \lambda_\alpha^i &= \Lambda_{\alpha\beta} \lambda_\beta^i, \\ A_\mu^i &= \Lambda_{\mu\nu} A_\nu^i, \end{aligned}$$

where Λ is the proper representation in vector or spinor space of a global boost/spatial rotation. Gauge symmetry is a characteristic of all the Yang-Mills theory, the fields change locally as

$$\lambda_\alpha^i(x) = \Omega_A(x)_{ij} \lambda_\alpha^j, \quad (3.2)$$

$$A_\mu(x) = \Omega_F(x) A_\mu(x) \Omega_F^{-1}(x) - \frac{1}{g} (\partial_\mu \Omega_F(x)) \Omega_F(x), \quad (3.3)$$

where $\Omega_F(x)$ and $\Omega_A(x)$ are local matrix transformations acting in the color space, in the fundamental and in the adjoint representation respectively. Usually the matrix transformation is in the group $SU(N)$, like $SU(3)$ or $SU(2)$, in the latter case $\Omega_F(x) \in SU(2)$ and $\Omega_A(x) \in SO(3)$.

The last symmetry that can be added to the theory is supersymmetry, which transforms and mixes gauge fields and fermion fields

$$A_\mu(x) \rightarrow A_\mu - 2i\bar{\lambda}\gamma_\mu\epsilon, \quad (3.4)$$

$$\lambda_a \rightarrow \lambda_a - \sigma_{\mu\nu}F_a^{\mu\nu}\epsilon, \quad (3.5)$$

where $\sigma_{\mu\nu}$ is proportional to the commutator $[\gamma_\mu, \gamma_\nu]$ and $F_{\mu\nu}$ is the field strength:

$$F_{\mu\nu}^a = \partial_\mu A_\nu^a - \partial_\nu A_\mu^a - igf_{ij}^a A_\mu^i A_\nu^j.$$

The infinitesimal SUSY transformation is parametrized by a global Majorana spinor ϵ in the adjoint representation, with a dimension $-1/2$ in mass units.

These transformations close the algebra of supersymmetry, in fact

$$\begin{aligned} \delta_{\epsilon_1}\delta_{\epsilon_2}A_\mu^a(x) &= -2i\bar{\lambda}^a\gamma_\mu\epsilon_1 - 2i\bar{\lambda}^a\gamma_\mu\epsilon_2 - 2i\bar{\epsilon}_1\sigma_{\rho\nu}F_a^{\rho\nu}\gamma_\mu\epsilon_2 \\ (\delta_{\epsilon_1}\delta_{\epsilon_2} - \delta_{\epsilon_2}\delta_{\epsilon_1})A_\mu^a(x) &= -2i\bar{\epsilon}_1\sigma_{\rho\nu}F_a^{\rho\nu}\gamma_\mu\epsilon_2 + 2i\bar{\epsilon}_2\sigma_{\rho\nu}F_a^{\rho\nu}\gamma_\mu\epsilon_1 \end{aligned} \quad (3.6)$$

The last commutator can be written as

$$\begin{aligned} (\delta_{\epsilon_1}\delta_{\epsilon_2} - \delta_{\epsilon_2}\delta_{\epsilon_1})A_\mu^a(x) &= -i\bar{\epsilon}_1F_a^{\rho\nu}\gamma_\rho\gamma_\nu\gamma_\mu\epsilon_2 + i\bar{\epsilon}_2F_a^{\rho\nu}\gamma_\rho\gamma_\nu\gamma_\mu\epsilon_1 \\ &= -2i\bar{\epsilon}_1F_a^{\rho\nu}\gamma_\rho\gamma_\nu\gamma_\mu\epsilon_2, \end{aligned} \quad (3.7)$$

using the fact that $F^{\rho\nu}$ is an antisymmetric tensor by definition, that $\bar{\epsilon}_i = \epsilon_i^T C$ and that $C\gamma_\mu C^{-1} = -\gamma_\mu$. Now the product of three gamma matrices can be proven to be equal to

$$\gamma_\rho\gamma_\nu\gamma_\mu = \delta_{\rho\nu}\gamma_\mu + \delta_{\nu\mu}\gamma_\rho - \delta_{\rho\mu}\gamma_\nu - i\epsilon_{\sigma\rho\nu\mu}\gamma_\sigma\gamma_5.$$

The last term proportional to $\gamma_\sigma\gamma_5$ is antisymmetric and it has to be contracted with the anticommuting Majorana spinors ϵ_1 and ϵ_2 , therefore its contribution vanishes. The commutator of two SUSY transformations can be therefore written as

$$\begin{aligned} (\delta_{\epsilon_1}\delta_{\epsilon_2} - \delta_{\epsilon_2}\delta_{\epsilon_1})A_\mu^a(x) &= iF_{\mu\nu}\nu_2^T C\gamma_\mu\epsilon_1 \\ &= \epsilon_1^\alpha\epsilon_2^\beta\{Q_\alpha, Q_\beta\}A_\mu \\ &= \epsilon_1^\alpha\epsilon_2^\beta(C\gamma_\rho)_{\alpha\beta}P_\rho A_\mu \\ &= i\epsilon_1^\alpha\epsilon_2^\beta(C\gamma_\rho)_{\alpha\beta}\partial_\rho A_\mu \\ &= iF_{\mu\nu}\epsilon_2^T C\gamma_\mu\epsilon_1 \end{aligned}$$

using the space-time realization of the translation operator $P_\mu = i\partial_\mu$ and adding and neglecting terms proportional to the equation of motion. Since the commutator of two SUSY transformations is equal to the anticommutator

of the supercharges $\{Q_\alpha, Q_\beta\}$, this proves that the transformations (3.4) are a representation of SUSY algebra in the field space.

In terms of Lorentz, gauge and SUSY symmetries and considering only the gauge sector, the most generic form of the action can be written on shell as

$$S = \int d^4x \left(-\frac{1}{4} \text{Tr}(F_{\mu\nu} F^{\mu\nu}) + \frac{1}{2} \bar{\lambda}(x) (i \not{D}) \lambda(x) \right)$$

It looks similar to the action of one flavor QCD, with an extra $\frac{1}{2}$ factor in front of the fermion part of the action to avoid double counting of contractions of Majorana fermions. The most important difference is hidden in the adjoint representation of the fermions, in fact the Dirac operator \not{D} is

$$\not{D} = \gamma_\mu (\partial_\mu + ig A_\mu^i(x) \tau_i^A),$$

where this time the Lie generators τ_i^A are in the adjoint representation

$$(\tau_i^A)_{jk} = f_{ijk}.$$

It is trivial to verify that the action is a Lorentz scalar and also invariant under gauge transformations. If one considers instead the SUSY transformations (3.4), it follows term by term and keeping only leading power of the parameter ϵ

$$\begin{aligned} F_{\mu\nu}^a &\rightarrow F_{\mu\nu}^a - 2i(\partial_\mu \bar{\lambda}^a) \gamma_\nu \epsilon + 2i(\partial_\nu \bar{\lambda}^a) \gamma_\mu \epsilon \\ &\quad - 2g f_{ij}^a (A_\mu^i \bar{\lambda}^j \gamma_\nu \epsilon + \bar{\lambda}^i \gamma_\mu \epsilon A_\nu^j) \\ \bar{\lambda}_a \gamma_\mu \lambda_b &\rightarrow \bar{\lambda}_a \gamma_\mu \lambda_b - \bar{\lambda}_a \gamma_\mu \sigma_{\rho\nu} F_b^{\rho\nu} \epsilon - \bar{\epsilon} \sigma_{\rho\nu} F_a^{\rho\nu} \gamma_\mu \lambda_b, \end{aligned}$$

so that the gauge and the fermion part of the action transform as

$$\begin{aligned} S &\rightarrow S - \int d^4x \frac{i}{2} F_{\mu\nu}^a \left((D_\mu \bar{\lambda}^a) \gamma_\nu \epsilon - (D_\nu \bar{\lambda}^a) \gamma_\mu \epsilon \right) + \\ &\quad + \frac{i}{2} \int d^4x \bar{\epsilon} \sigma_{\rho\nu} \gamma_\mu F_a^{\rho\nu} D_\mu^a \lambda + \bar{\lambda} \gamma_\mu \sigma_{\rho\nu} D_\mu^a F_a^{\rho\nu} \epsilon + \\ &\quad + ig \int d^4x \bar{\lambda}_i \gamma_\mu (\bar{\lambda}_a \gamma_\mu \epsilon) f_{ij}^a \lambda_j. \end{aligned}$$

The contribution in the first two line vanishes up to total derivatives using the Bianchi identity, the equation of motion and symmetry property of the gamma matrices. The last contribution, coming from the variation of the gauge field in the covariant derivative, vanishes in four dimensions by a Fierz rearrangement due to the Majorana condition [21].

The equations of motion do not hold off-shell anymore and a Majorana spinor has four degrees of freedom while a gauge boson only three (the two

transverse polarization states plus the unphysical longitudinal mode). In order to ensure supersymmetry also off-shell, an additional boson color field in the adjoint representation must be added to the action

$$S \rightarrow S + \int D^a(x) D_a(x),$$

without kinetic or interaction terms in order to do not alter the on-shell physics. The dimension of the field D_a is two in mass units. The transformations properties of the auxiliary field D^a under supersymmetry will be proportional then to the equation of motion of the gluon and gluino fields

$$A_\mu(x) \rightarrow A_\mu - 2i\bar{\lambda}\gamma_\mu\epsilon, \quad (3.8)$$

$$\lambda_a \rightarrow \lambda_a - \sigma_{\mu\nu} F_a^{\mu\nu} \epsilon - 2\gamma_5 D_a, \quad (3.9)$$

$$D_a \rightarrow i\bar{\epsilon}\gamma_5\gamma_\mu\partial_\mu\lambda, \quad (3.10)$$

so that on-shell transformations reduce again to the form of (3.4).

3.2 Quantum anomalies and conserved currents

The $\mathcal{N} = 1$ SYM is classically scale invariant, but anomaly appears at quantum level

$$T_{\mu\mu} = -\frac{g^2 N_c}{32\pi^2} (F_{\mu\nu}^a F_a^{\mu\nu}),$$

since the trace of the energy-momentum tensor vanishes only when $g = 0$. The physical consequence of the trace anomaly is the formation at zero temperature of a bound spectrum of composite particles, like baryons, mesons and glueballs. Trace anomaly is also present in QCD just with different numerical coefficients.

Chiral symmetry is instead associated to the transformation $U_A(1)$

$$\lambda \rightarrow \exp(i\theta\gamma_5)\lambda,$$

which leaves invariant the action but not the whole partition function. The axial current $J_\mu^5 = \bar{\lambda}\gamma_\mu\gamma_5\lambda$ is therefore anomalous

$$\partial_\mu J_\mu^5 = \frac{g^2 N_c}{32\pi^2} \epsilon_{\mu\nu\rho\sigma} \text{Tr}(F^{\mu\nu} F^{\rho\sigma})$$

and the group $U_A(1)$ is broken down to a discrete subgroup Z_{2N_c} of transformations

$$\lambda \rightarrow \exp\left(\frac{2\pi n i}{2N_c}\gamma_5\right)\lambda \quad n \in \{1, \dots, 2N_c\},$$

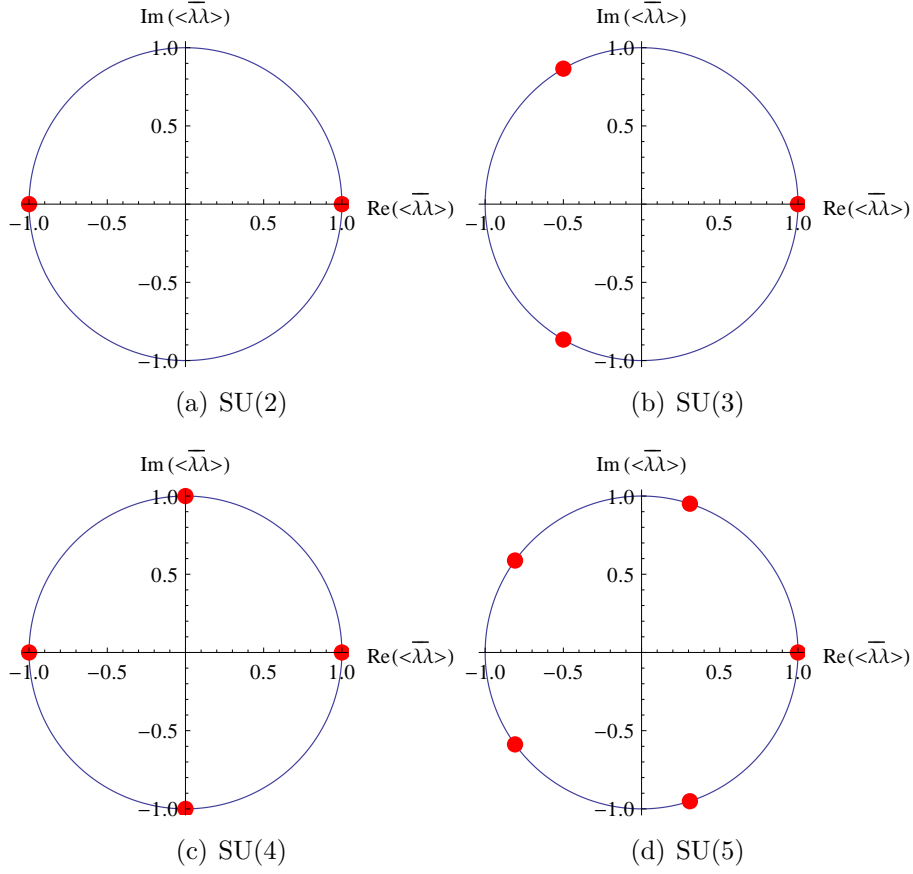


Figure 3.1: Scatter plot of the expectation value of the gluino condensate $\langle \bar{\lambda}\lambda \rangle$ for the gauge groups SU(2), SU(3), SU(4) and SU(5). Such diagrams are possible in the infinite volume limits, the gluino condensate fluctuates at finite volume around the red points with tunneling between different vacua.

which leaves invariant the whole partition function for theories with fermions in the adjoint representation. Finally the Z_{2N_c} subgroup is spontaneously broken at zero temperature down to Z_2 by a non-vanishing expectation value of the gluino condensate $\langle \bar{\lambda}\lambda \rangle$, where Z_2 represents the sign flip

$$\lambda \rightarrow -\lambda.$$

Analytical calculations have shown that the expectation value of the gluino condensate is

$$\langle \bar{\lambda}\lambda \rangle = C\Lambda^3 \exp\left(\frac{2\pi ni}{N_c}\right), \quad (3.11)$$

where C is a constant, see Fig. 3.1. The N_c different values of the gluino condensate represent N_c different vacua of the theory at zero temperature.

Thus the Witten index for the $\mathcal{N} = 1$ Super Yang Mills theory based over the gauge group $SU(N_c)$ is exactly equal to N_c and spontaneous supersymmetry breaking is impossible. This remarkable results have been obtained in [22, 23].

Many interesting conjectures arise from the existence of many different vacua in $\mathcal{N} = 1$ SYM. Domain walls are stable configurations interpolating between vacua with different expectation value of the gluino condensate. Domain walls play a special role in the large N_c limit, they should behave as branes, i.e. as planes where a QCD string can end. Branes can interact with an exchange of closed strings, interpreted in the strong interaction picture as glueballs.

Chiral symmetry and trace anomaly are also present in QCD, but in $\mathcal{N} = 1$ SYM they form a chiral supermultiplet structure together with the supercurrent

$$\partial_\mu(x^\rho \gamma_\rho) S_\mu = \frac{g^2 N_c}{16\pi^2} F_a^{\mu\nu} \sigma_{\mu\nu} \lambda^a,$$

which has a γ -trace anomaly under superconformal transformations [17].

3.3 The bound spectrum of the theory

At high temperature, the $\mathcal{N} = 1$ supersymmetry behaves as a gas of elementary gluinos and gluons. At low temperature instead the theory exhibits confinement and it is impossible to find a free isolated color charge. Gluons and gluinos will form an nontrivial bound spectrum of composite particles neutrally color charged. An effective action can be formulated to capture the interactions and the structure only of these degrees of freedom.

There are several hypothesis about the structure of the lightest particles based on low energy effective theory formulated in Ref. [17, 18, 19]. The effective Lagrangian for the chiral supermultiplet generated by the current structure discussed in the previous section is

$$\mathcal{L}_{\text{eff}} = \frac{1}{\alpha} \sqrt[3]{S^* S_D} + \frac{1}{3} \left\{ S \log \left(\frac{S}{\Lambda^3} \right) - S \right\}_F + \text{h.c.},$$

where α is a dimensionless parameter and Λ a dimensional flowing scale $\Lambda \equiv \Lambda(g)$. The chiral superfield S has on-shell two boson components

$$\begin{aligned} \phi &= c \bar{\lambda}_R \lambda_L, \\ \phi^* &= c \bar{\lambda}_L \lambda_R, \end{aligned}$$

and a fermion component

$$\chi = \frac{c}{2} F^{\mu\nu} \sigma_{\mu\nu} \lambda_L. \quad (3.12)$$

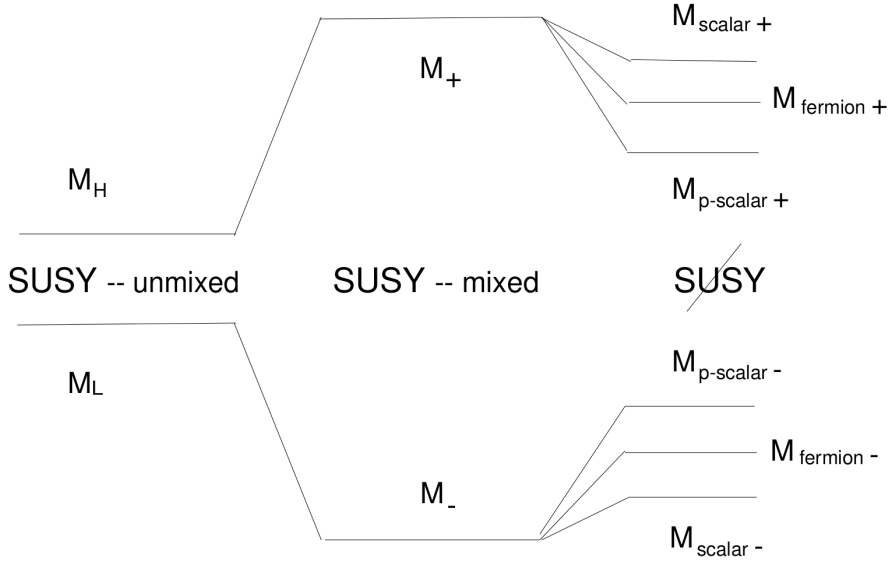


Figure 3.2: Theoretical expectation of the spectrum of $\mathcal{N} = 1$ SYM. If supersymmetry is not broken two chiral supermultiplets appear with two different masses. Mixing occurs between physical particles, therefore physical states are mixture of glueballs, mesons and gluino-glues. If supersymmetry is softly broken by a gluino mass term, the largest corrections affect the pseudoscalar states, while the scalar states are expected to exhibit only milder deviations. Picture taken from Ref. [19].

The first term of \mathcal{L}_{eff} is the Kähler potential, invariant under scale, chiral and superconformal symmetry. It gives the kinetic term for the fields, while the superpotential should take into account the correct anomaly terms of the $\mathcal{N} = 1$ SYM. The effective Lagrangian \mathcal{L}_{eff} has therefore the form of an interacting Wess-Zumino model, written on-shell as

$$\begin{aligned}
L_{\text{eff}} = & \frac{1}{\alpha\phi^*\phi}(\partial_\mu\phi^*\partial_\mu\phi + i\bar{\chi}\not{\partial}\chi) - \frac{1}{3}\left(\frac{\bar{\chi}_L\chi_R}{\phi^*} + \frac{\bar{\chi}_R\chi_L}{\phi}\right) \\
& - \frac{\alpha}{9}(\phi^*\phi)^{2/3}\log\left(\frac{\phi}{\Lambda^3}\right)\log\left(\frac{\phi^*}{\Lambda^3}\right) \\
& + \frac{2}{9}\left\{\frac{\bar{\chi}_L\chi_R}{\phi^*}\log\left(\frac{\phi^*}{\Lambda^3}\right) + \frac{\bar{\chi}_R\chi_L}{\phi}\log\left(\frac{\phi}{\Lambda^3}\right)\right\} \\
& + \frac{2}{3\alpha}(\bar{\chi}\gamma_\mu\gamma_5\chi)\left\{\frac{\phi^*\partial_\mu\phi + \phi\partial_\mu\phi^*}{(\phi^*\phi)^{5/3}}\right\}.
\end{aligned}$$

The effective potential for the scalar field ϕ has the form

$$V_{\text{eff}} = -\frac{\alpha}{9}(\phi^*\phi)^{2/3} \log\left(\frac{\phi}{\Lambda^3}\right) \log\left(\frac{\phi^*}{\Lambda^3}\right),$$

it has a minimum in agreement with Eq. (3.11) for

$$\langle\phi\rangle = \langle\phi^*\rangle = \Lambda^3,$$

with $\phi \sim \langle\bar{\lambda}\lambda\rangle$. The effective Lagrangian \mathcal{L}_{eff} describes the theory around the vacuum of the gluino condensate with $n = 0$ in Eq. (3.11).

In the effective Lagrangian the fields ϕ , ϕ^* and χ are interpreted as the two scalar and pseudoscalar meson and the gluino-gluon particle. The mass terms are equal in the above effective Lagrangian for all particles to $\frac{1}{3}\alpha\Lambda$. The pseudoscalar meson η' would be similar to a Goldstone boson for the breaking of the $U_A(1)$ axial symmetry, but it has therefore acquired a large mass proportional to the ultraviolet scale due to anomaly. The same happens to a fermion and a scalar meson due to supersymmetry, a ‘‘SUSY relic’’ could explain the similar mass between the f_0 and the η' observed in QCD as discussed in the Introduction.

The glueballs fields have been inserted in the auxiliary fields and integrated out in \mathcal{L}_{eff} . The effective Lagrangian has been extended in Ref. [18, 19] to consider also the glueball states in the low-energy effective theory. A second chiral supermultiplet has been found, formed by a pseudoscalar and scalar glueball and an another gluino-gluon. This second supermultiplet is supposed to have a lower mass than the supermultiplet of the mesons constructed above, see Fig. 3.2.

Chapter 4

Quantum fields and supersymmetry on the lattice

The gauge-field action (space-time integral of the Lagrangian) will be defined on a discrete lattice with spacing a in Euclidean space-time. The simplest way to proceed is to consider a continuum action, substitute finite-difference approximations for derivatives, and replace the space-time integral by a sum over the lattice sites.

Kenneth G. Wilson [5]

Quantum field theories defined in the continuum are plagued by divergences that appear in the calculation beyond the leading order. Further, the Feynman path integral has only an heuristic and not strictly mathematical meaning for fields defined in the continuum. In order to solve these difficulties it is possible to introduce a physical cut-off in the theory, by discretizing the continuum space time using an hypercubic lattice with points separated by a distance a . In the Fourier space, all momentum integrals are then defined in the first Brillouin zone $\left(-\frac{\pi}{a}, \frac{\pi}{a}\right]$ and therefore the ultraviolet divergences are automatically regularized. In the position space instead, all integrals are reduced simply to a sum over all lattice points,

$$\int d^4x = a^4 \sum_x,$$

and derivatives are written in terms of nearest neighborhood finite difference

$$\partial_\mu \phi(x) = \frac{\phi(x + \vec{\mu}a) - \phi(x)}{a} \equiv \frac{\nabla_\mu \phi(x)}{a}.$$

The lattice spacing a is the only dimensional parameter defined in the regularized theory and in natural units it has the dimension of an inverse of a mass ($[a] = [M^{-1}]$). Lattice regularization breaks Lorentz and translational invariance explicitly, therefore all the quantities computed on the lattice will be effected by discretization errors unless the limit $a \rightarrow 0$ is performed. Renormalization is the central concept behind the calculation of finite physical quantities that match the experimental results in the continuum limit $a \rightarrow 0$.

In this chapter the formulation of the $\mathcal{N} = 1$ supersymmetric Yang-Mills theory on the lattice is discussed.¹ After having discretized the action for the gluon and gluino fields, the main difficulties will arise in the attempt to formulate a proper continuum limit in which supersymmetry and Lorentz invariance can be consistently recovered.

4.1 Gluons and gauge fields on the lattice

A gauge field A_μ in the continuum can be viewed as a map which associates to every point of the space time a variable in the Lie algebra $\mathfrak{su}(n)$

$$A_\mu : x \rightarrow A_\mu(x) \in \mathfrak{su}(n).$$

To discretize the gauge field A_μ on the lattice is it useful to consider the path ordered exponential map

$$U[\gamma] = \mathbf{P} \left\{ \exp \left(ig \int_\gamma A_\mu dx^\mu \right) \right\},$$

defined as the product of all the infinitesimal parallel transporters between two neighbor points along the path γ

$$U[\gamma] = \lim_{\Delta x^\mu \rightarrow 0} \prod_{x \in \gamma} (1 + A_\mu(x) \Delta x^\mu). \quad (4.1)$$

It is clear from the definition that the variables $U_\gamma(x)$ belong to the Lie group $SU(N)$.

¹There are several detailed books and review about lattice QCD, some of the contents of this chapter have been prepared following [24, 25, 26].

Considering a straight path which connects a point x on the lattice to its nearest neighbor $x + \vec{\mu}$, it is possible to discretize the continuum gauge field A_μ as

$$A_\mu(x) \rightarrow U_\mu(x) = \mathbf{P} \left\{ \exp \left(ig \int_x^{x+\vec{\mu}} A_\mu dx'^\mu \right) \right\}$$

or, expanding the integral around its midpoint

$$A_\mu(x) \rightarrow U_\mu(x) = \exp(igaA_\mu(x + \vec{\mu}/2)) .$$

The indirect discretization of A_μ by the path ordered exponential map has many advantages which are clear once that the transformation properties under a generic change of gauge $\Omega(x)$ are taken in account. Remembering that in the continuum space the fields $A_\mu(x)$ transforms as

$$\begin{aligned} A'_\mu(x) &= \Omega(x)A_\mu(x)\Omega^{-1}(x) + \frac{i}{g}\Omega(x)\partial_\mu\Omega^{-1}(x) \\ &= \Omega(x) \left(A_\mu(x) + \frac{i}{g}\partial_\mu \right) \Omega^\dagger(x) \end{aligned} \quad (4.2)$$

than it follows for one element of the product (4.1)

$$\begin{aligned} 1 + igA'_\mu(y)\Delta y^\mu &= 1 + ig\Omega(y)A_\mu(y)\Omega^\dagger(y)\Delta y^\mu - \Omega(y)\partial_\mu\Omega^\dagger(y)\Delta y^\mu \\ &\simeq 1 + ig\Omega(y)A_\mu(y)\Omega^\dagger(y)\Delta y^\mu + \\ &\quad -\Omega(y)\Omega^\dagger(y) + \Omega(y)\Omega^\dagger(y + \Delta y^\mu) \\ &\simeq \Omega(y)\Omega^\dagger(y + \Delta y^\mu) + ig\Omega(y)A_\mu(y)\Omega^\dagger(y + \Delta y^\mu)\Delta y^\mu + \\ &\quad + ig\Omega(y)A_\mu(y)\partial_\mu\Omega^\dagger(y)(\Delta y^\mu)^2 \\ &\simeq \Omega(y)\Omega^\dagger(y + \Delta y^\mu) + ig\Omega(y)A_\mu(y)\Omega^\dagger(y + \Delta y^\mu)\Delta y^\mu \\ &= \Omega(y)(1 + igA_\mu(y)\Delta y^\mu)\Omega^\dagger(y + \Delta y^\mu) . \end{aligned}$$

Therefore a link variable transforms under a gauge transformation $\Omega(x)$ simply as

$$U_\mu(x) \rightarrow U_\mu(x)' = \Omega(x)U_\mu(x)\Omega^\dagger(x + \vec{\mu}) , \quad (4.3)$$

since all the intermediate transformations in the product (4.1) will be canceled. This simple transformation law helps the construction of operators and actions in a gauge invariant way for any value of the lattice spacing a .

The link variable $U_\mu(x)$ has the physical interpretation of the parallel transporter of a quark from the point x to $x + \vec{\mu}$. If the parallel transport of a gluino is considered instead, than the fields A_μ has to be written in the adjoint representation. In general

$$U_\mu^R(x) = \exp(igaA_\mu^b(x)\tau_b^R) ,$$

where τ_b^R are the Lie group generators in the representation R . In the following, $U_\mu(x)$ and $V_\mu(x)$ will denote the link variables in the fundamental and in the adjoint representation, respectively. The adjoint links $V_\mu(x)$ are related to the fundamental links $U_\mu(x)$ through the well-known formula

$$V_\mu(x)_{ab} = 2 \operatorname{tr}(U_\mu(x)^\dagger \tau_a^F U_\mu(x) \tau_b^F).$$

This relation can be demonstrated easily with the Hadamard lemma

$$\begin{aligned} V_\mu(x)^{ab} &= \frac{1}{2} \operatorname{Tr}(U_\mu^\dagger(x) \tau_a^F U_\mu(x) \tau_b^F) \\ &= \frac{1}{2} \operatorname{Tr}(\exp(-i\omega_c(x) \tau_c^F) \tau_a^F \exp(i\omega_d(x) \tau_d^F) \tau_b^F) \\ &= \frac{1}{2} \operatorname{Tr}\left(\left(\tau_a^F + i\omega_c \frac{1}{2!} [\tau_c^F, \tau_a^F] - \omega_c \omega_d \frac{1}{3!} [\tau_d^F, [\tau_c^F, \tau_a^F]] + \dots\right) \tau_b^F\right) \\ &= (\exp(i\omega_c(x) \tau_c^F))^{ab}. \end{aligned}$$

In the last row τ_a^A and τ_a^F stand for the generator in the adjoint and fundamental representation respectively. In the supersymmetric model considered in this thesis, the gauge group is $SU(2)$, therefore $U_\mu(x) \in SU(2)$ and $V_\mu(x) \in SO(3)$. The generators in the fundamental representation are normalized such that

$$\operatorname{tr}(\tau_a^F \tau_b^F) = \frac{1}{2} \delta_{ab}.$$

4.2 The Haar measure

In a quantum field theory discretized on the lattice, the functional path integral has a precise mathematical meaning in terms of standard Riemann integrals. The sum over all the possible gauge configurations is in fact replaced by the sum over all the possible elements of the gauge group $SU(N)$ for each point of the lattice

$$\int DA_\mu(x) \rightarrow \int \prod_{x,\mu} dU_\mu(x),$$

denoting by $dU_\mu(x)$ the Haar measure of the group, chosen in order to be invariant with respect to the right and left transformations

$$d(HU_\mu(x)) = d(U_\mu(x)H) = dU_\mu(x), \quad (4.4)$$

where $H \in SU(N)$. This ensures the needed gauge invariance to the measure of the path integral. For the gauge group $SU(2)$ the measure reads

$$dU_\mu(x) = \delta\left(1 - a_0^2 - \sum_i a_i^2\right) da_0 \prod_i da_i, \quad (4.5)$$

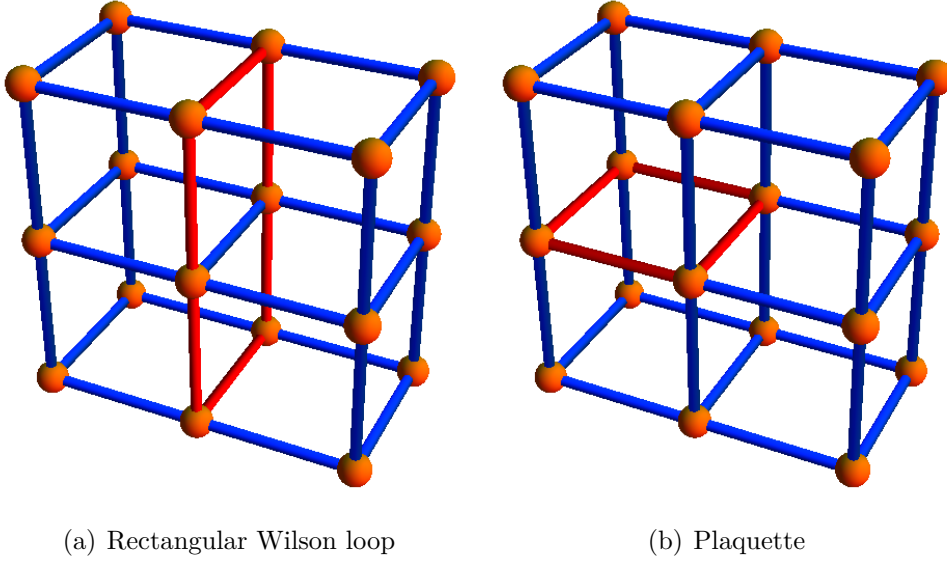


Figure 4.1: Wilson loops on the lattice. The Wilson loop is the path ordered product of all the matrices on the red links.

if an element of the group $SU(2)$ is parametrized in terms of the Pauli matrices as $U_\mu(x) = a_0 I + i a_i \sigma^i$. Even if the exact knowledge of the Haar measure is not needed when performing Monte Carlo simulations, it should be always kept in mind that the factors in front of (4.5) contribute to the action in order to ensure exact gauge invariance order by order in a perturbative expansion.

4.3 Wilson loops and gauge action

Gauge invariant operators are the natural basis to write actions and observables. The simplest gauge invariant operator on the lattice involving only links is the Wilson loop

$$\mathcal{W}[\gamma] = \text{Tr} \left(\prod_{x \in \gamma} U_\mu(x) \right), \quad (4.6)$$

that is the trace of the ordered product of the U_μ matrices along a closed lattice path, see Fig. 4.1(a). The Wilson loop reduces in the continuum to the path ordered integral

$$\mathcal{W}[\gamma] = \text{Tr} \left(\mathcal{P} \exp \left(ig \int_\gamma A_\mu dx^\mu \right) \right), \quad (4.7)$$

computed along a closed path γ . The plaquette is the smallest possible Wilson loop on the lattice enclosed on a square path of unit side, see Fig. 4.1(b).

In the continuum, the Yang-Mills action defines the propagation and the self interactions between gluons

$$S = -\frac{1}{4} \int d^4x (F_a^{\mu\nu} F_{\mu\nu}^a) \quad (4.8)$$

and it can be discretized on the lattice ensuring exact gauge invariance also for finite lattice spacing a using Wilson loops. Wilson proposed [5] to discretize the action (4.8) as

$$S_W = \frac{\beta}{N} \sum_{x, \mu < \nu} \text{ReTr} (U_\mu(x) U_\nu(x + \mu) U_{-\mu}(x + \mu + \nu) U_{-\nu}(x + \nu)) , \quad (4.9)$$

in terms only of trace of the plaquette. It is simple to verify that the Wilson action reduces to the Yang-Mills action in the naive continuum limit $a \rightarrow 0$. Defined $G_\mu(x) = agA_\mu^i(x)\tau^i$, the gauge links of Eq. (4.9) can be written as

$$\begin{aligned} U_\mu(x) &= \exp(iG_\mu(x)) , \\ U_\nu(x + \mu) &= \exp(iG_\nu(x + \mu)) = \exp(iG_\nu(x) + ia\Delta_\mu G_\nu(x)) , \\ U_{-\mu}(x + \mu + \nu) &= \exp(-iG_\mu(x + \nu)) = \exp(-iG_\mu(x) - i\Delta_\nu G_\mu(x)) , \\ U_{-\nu}(x + \nu) &= \exp(-iG_\nu(x)) , \end{aligned}$$

and using the Campbell-Baker-Hausdorff formula

$$\exp(X) \exp(Y) \simeq \exp(X + Y + \frac{1}{2}[X, Y]) ,$$

then the plaquette $U_{\mu\nu}$ is proportional to the exponential of the field strength

$$U_{\mu\nu} \simeq \exp(ia(\Delta_\mu G_\nu(x) - \Delta_\nu G_\mu(x)) - [G_\mu(x), G_\nu(x)]) \equiv \exp(iga^2 F_{\mu\nu})$$

and expanding in power series of a

$$\text{Tr}(U_{\mu\nu}) = iga^2 \sum_i \text{Tr}(\tau^i) F_i^{\mu\nu} - \frac{1}{4} g^2 a^4 \text{Tr}(\tau^i \tau^j) F_i^{\mu\nu} F_{j\mu\nu} + O(a^6) .$$

Since $\text{Tr}(T^i) = 0$ and $\text{Tr}(\tau^i \tau^j) = \delta_{i,j}$, in the naive limit the Wilson action reduces to Eq. (4.8)

$$\lim_{a \rightarrow 0} S_W = \lim_{a \rightarrow 0} \frac{\beta}{8N} g^2 a^4 \sum_{x, \mu\nu} \sum_i F_i^{\mu\nu} F_{i\mu\nu} = \frac{\beta}{8N} g^2 a^{4-d} \int d^d x \sum_i F_i^{\mu\nu} F_{i\mu\nu}$$

if the parameter β is set to $\beta = \frac{2N}{g^2}$. The weak coupling limit $g \rightarrow 0$ will be equivalent in the lattice language to the limit $\beta \rightarrow \infty$.

4.4 Gluinos on the lattice

A gluino field associates to every point of the lattice a Grassmanian anticommuting variable. A naive discretization of the Dirac equation

$$(\gamma_\mu \partial_\mu + ig\gamma_\mu A_\mu(x) + m)\lambda(x) = 0, \quad (4.10)$$

connects links to gluino field $\lambda(x \pm \vec{\mu}a)$ in the following gauge invariant form

$$\frac{1}{2a}\gamma_\mu \left(U_\mu(x)\lambda(x + \vec{\mu}a) - U_\mu(x - \vec{\mu}a)^\dagger \lambda(x - \vec{\mu}a) \right) + m\lambda(x) = 0, \quad (4.11)$$

and has a discretization error of order $O(a^2)$. The Dirac equation has a trivial constant solution $\lambda(x) = c$ for both the continuum action and its lattice counterpart in the massless case $m = 0$ in a trivial gauge background, $U_\mu(x) = 1$ and $A_\mu(x) = 0$. This constant solution has a zero momentum $p = (0, 0, 0, 0)$ in the Fourier space. However there will be on the lattice other additional fifteen solutions when $m = 0$ and $U_\mu = 1$ not present in the continuum equation, like for example

$$\lambda(x) = \exp\left(i\frac{\pi}{a}x\right)$$

since by simple complex exponential algebra ($n = x/a$)

$$\exp(i\pi(n+1)) - \exp(i\pi(n-1)) = 0.$$

These fifteen solutions are commonly called “doubblers” in the lattice language and they have non-zero momentum in the Fourier space $p_1 = (\pi/a, 0, 0, 0)$, $p_2 = (0, \pi/a, 0, 0)$, ..., $p_5 = (\pi/a, \pi/a, 0, 0)$, ..., $p_{15} = (\pi/a, \pi/a, \pi/a, \pi/a)$. They lie at the corners of the first Brillouin zone.

The inverse of the Dirac operator represents in quantum field theory the propagation of a gluino in space-time: accordingly to the Wick theorem, it will appear contracting pair of fermion fields. To each solution of the Dirac equation will correspond an infinity, or better a pole of the propagator in the momentum space. The poles are associated to states of physical particles, therefore the fifteen additional solutions represents fifteen additional particles present on the lattice. The correct flavor number is violated in the continuum limit and in particular SUSY is broken because the fifteen additional particles have no boson counterpart.

A breaking term can be added to the discretization of the Dirac equation if it is expected to vanish in the continuum limit. The Wilson term,

$$-\frac{a}{2}\nabla_\mu^* \nabla_\mu \lambda(x) = \frac{1}{2a}(U_\mu(x)\lambda(x + \vec{\mu}a) - 2\lambda(x) + U_\mu(x - \vec{\mu}a)\lambda(x - \vec{\mu}a)),$$

added to the naive discretized Dirac equation does not alter the zero momentum pole and the infrared physics but it removes doublers giving them a divergent mass proportional to $1/a$. Here ∇_μ^* and ∇_μ represent the forward and backward lattice covariant derivatives. The price of the Wilson term is hidden in the $O(a)$ discretization errors larger than the $O(a^2)$ of the naive fermions. In addition, a chiral symmetry is broken explicitly and it can be recovered only in the limit $a \rightarrow 0$, since the transformation

$$\lambda(x) \rightarrow \exp(i\theta\gamma_5)\lambda(x)$$

does not factorize anymore as in Eq. (4.10) or Eq. (4.11).

The Nielsen-Ninomiya theorem states that it is impossible to construct on the lattice a version of the Dirac equation free of doublers with a local operator which preserves exact chiral symmetry [27]. An explicit violation of four dimensional supersymmetry and chiral invariance seems unavoidable on the lattice for finite values of a . The Wilson fermion action requires thus a special care to fine tune the theory towards a proper continuum limit where chiral symmetry and SUSY are not explicitly violated. The physical equations involved in the fine-tuning will be analyzed in the special case of super Yang-Mills theories in the following section.

4.5 The Curci-Veneziano action

Curci and Veneziano proposed in 1987 an action on the lattice for supersymmetric Yang-Mills theories based on the standard plaquette action for the gauge part and on the Dirac-Wilson operator D_W

$$S_f = \frac{1}{2} \bar{\lambda} D_W \lambda = \frac{1}{2} \bar{\lambda} \left\{ \frac{\gamma^\mu (\nabla_\mu^* + \nabla_\mu) - a \nabla_\mu^* \nabla_\mu}{2} + m \right\} \lambda$$

for the gluino part of the action.

Following Ref. [4], it has to be ensured that SUSY and axial Ward identities define together a consistent supersymmetric limit, where the renormalized gluino mass vanishes. The axial Ward identity with this discretization choice reads on shell

$$\langle \Delta_\mu J_\mu^5 \dots \rangle = \langle (X_A + D_A) \dots \rangle + \delta_A \langle \dots \rangle,$$

where “ \dots ” stands for any field and $\delta_A \langle \dots \rangle$ for their variation under the axial transformation

$$\begin{aligned} \lambda(x) &\rightarrow \exp(i\phi\gamma_5)\lambda(x), \\ \bar{\lambda}(x) &\rightarrow \bar{\lambda}(x) \exp(i\phi\gamma_5). \end{aligned}$$

The axial current can be discretized as

$$J_\mu^5 = \bar{\lambda}(x) \gamma_\mu \gamma_5 V_\mu(x) \lambda(x + \mu),$$

without summation over μ in the right hand side of the equation. D_A is the explicit chiral symmetry violation term when the gluino mass m is non-zero

$$D_A = 2m \bar{\lambda}(x) \gamma_5 \lambda(x),$$

while X_A is the axial symmetry breaking induced by the Wilson term

$$X_A = -\frac{a}{2} \sum_\mu \left\{ \bar{\lambda}(x) \gamma_5 \nabla_\mu^* \nabla_\mu \lambda(x) \right\},$$

proportional to $a \gamma_5 D_\mu D_\mu$ in the naive continuum limit. The Wilson term requires therefore an additive renormalization of the gluino mass

$$M_R = m - M_A$$

and the massless limit defined by chiral symmetry will be then provided if the bare gluino mass is set to $m = M_A$. X_A will then reproduce the standard Adler-Bell-Jackiw anomaly of the continuum theory

$$\langle J_\mu^5 \rangle = \frac{N_c g^2}{32\pi} \epsilon_{\mu\nu\rho\sigma} \langle F^{\mu\nu} F^{\rho\sigma} \rangle$$

in the limit $a \rightarrow 0$.

On the other hand, a non vanishing value of the gluino mass and of the lattice spacing breaks supersymmetry and SUSY Ward identities have to be considered to show that they will approach their continuous counterpart in the limit $a \rightarrow 0$. On the lattice, the transformations (3.4) can be discretized as

$$\lambda(x) \rightarrow \lambda(x) + \sigma_{\mu\nu} F^{\mu\nu}(x) \epsilon \quad (4.12)$$

$$U_\mu(x) \rightarrow \exp(i g \bar{\epsilon} \gamma_\mu \lambda_a T^a) U_\mu(x) \quad (4.13)$$

where $F^{\mu\nu}$ is for example the clover version of the open antisymmetric plaquette. The conserved supercurrent S_μ associated to the SUSY transformations is

$$S_\mu(x) = \sigma_{\alpha\beta} \gamma_\mu F^{\mu\nu} V_\nu(x) \lambda(x + \mu) \quad (4.14)$$

and the supersymmetric Ward identity is

$$\langle \Delta_\mu S_\mu \dots \rangle = \langle (X_S + D_S) \dots \rangle + \delta_S \langle \dots \rangle,$$

where X_S is the lattice breaking term and D_S is supersymmetry violation given by the gluino mass. While D_S is simply

$$D_S = -m\sigma_{\alpha\beta}F^{\alpha\beta},$$

the explicit expression of X_S is cumbersome and not needed in the following discussion. Since Lorentz invariance and SUSY are explicitly broken on the lattice, mixing can occur even between operators of different dimensionality so that the supercurrent involves a linear combination of $\alpha S_\mu + \beta T_\mu$, where

$$T_\mu(x) = F_{\mu\nu}\gamma_\nu\lambda(x),$$

beyond tree level ($\alpha = 1 + O(g^2)$ and $\beta = O(g^2)$). The mass term in D_S is additively renormalized

$$M_R^S = m - M_S$$

and in principle is not known whether there is a relation between M_R^A and M_R^S defined by the axial and SUSY Ward identities respectively.

The target continuum theory is supersymmetric, meaning that the gluino is massless, and without any source of explicit chiral invariance breaking. The point is to ensure that all these two symmetries will be recovered at the same point on the lattice in the continuum limit $\beta \rightarrow \infty$. Curci and Veneziano have shown that

$$m - M_A = Z_{SA}(g)(m - M_S) \quad (4.15)$$

where $Z_{SA}(g) = 1 + O(g^2)$ [4]. This means that $M_R^S = 0$ implies $M_R^A = 0$, so that the chiral and the supersymmetric limit coincide [28]. This result is of great importance: even if the lattice and the Wilson formulation of fermions break the fundamental symmetries of the $\mathcal{N} = 1$ SYM, they can be recovered at the same point in the continuum limit simply by fine tuning the bare gluino mass m .

4.6 Gluino condensate

A practical definition of zero gluino mass is required in non-perturbative lattice simulations. To this end, the gluino condensate can be helpful to define the chiral critical point, that will coincide to the zero gluino mass by virtue of Eq. (4.15). An another possibility will be considered in Ch. 8. The gluino condensate $\langle \bar{\lambda}\lambda \rangle$ is a bulk quantity proportional to the derivatives of the partition function with respect to the gluino mass

$$\langle \bar{\lambda}\lambda \rangle = \frac{1}{V} \frac{\partial}{\partial m} Z(g, m). \quad (4.16)$$

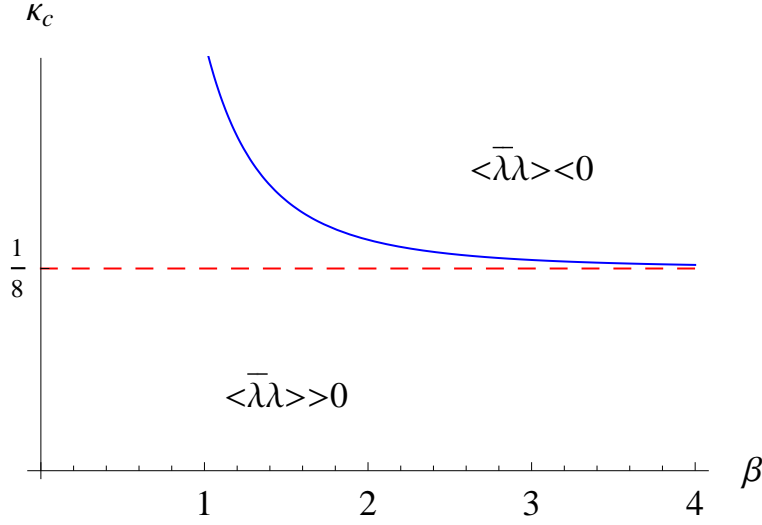


Figure 4.2: Qualitative phase diagram of the gluino condensate at zero temperature. The gluino condensate jumps when the renormalized value of the gluino mass is zero, with a first order phase transition. The dashed red line corresponds to the classical bare gluino mass equal to zero, while the blue line includes the renormalization effects of the Wilson term.

At the critical point the remaining chiral symmetry Z_{2N_c} is broken down to Z_2 and there will be N_c equivalent vacua each characterize by a distinct value of $\langle \bar{\lambda}\lambda \rangle$, see Fig. 4.2. A first order phase transition is expected at zero temperature crossing the critical point by varying the bare gluino mass, where the gluino condensate jumps from one value to an another. This transition can be identified on the lattice with numerical simulations and it can be used to find the point where the renormalized gluino mass is zero, see Fig. 4.2.

For $\mathcal{N} = 1$ SYM the partition function is

$$Z(\beta, m) = \int dA_\mu d\lambda \exp \left\{ - \int d^4x \left(\frac{1}{4} (F_{\mu\nu}^a F_{\mu\nu}^a) + \frac{1}{2} \bar{\lambda}_a (\gamma^\mu D_\mu^{ab} + m) \lambda_b \right) \right\},$$

and integrating out the Majorana fermion field λ , it can be written in terms of the determinant of the Dirac-Wilson operator

$$Z(\beta, m) = \int dU_\mu \sqrt{\det(D + m)} \exp \left\{ - \int d^4x \left(\frac{1}{4} (F_{\mu\nu}^a F_{\mu\nu}^a) \right) \right\},$$

supposing that for the lattice and the coupling under study the sign problem does not arise, see App. A. Exponentiating the determinant one has

$$Z(\beta, m) = \int dU_\mu \exp \left\{ - \int d^4x \left(\frac{1}{4} (F_{\mu\nu}^a F_{\mu\nu}^a) + \frac{1}{2} \text{Tr}(\log(D + m)) \right) \right\}$$

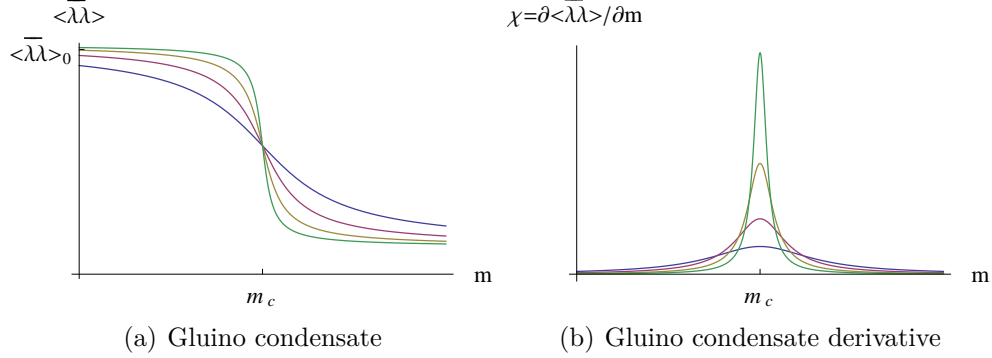


Figure 4.3: Qualitative behavior of the bare chiral condensate as function of the bare fermion mass. The value of $\langle \bar{\lambda}\lambda \rangle$ “jumps” in correspondence of the chiral phase transition at some m_c . The “jump” is more abrupt when the spatial volume of the lattice increases (blue vs green line). In this limit, differentiating the gluino condensate with respect to mass produces a more and more definite peak.

and expanding the derivative, the chiral condensate is

$$\begin{aligned} \langle \bar{\lambda}\lambda \rangle &= \frac{1}{V} \frac{1}{Z(\beta, m)} \int dU_\mu \frac{1}{2} \text{Tr}((D + m)^{-1}) \exp \left\{ +\frac{1}{2} \text{Tr}(\log(D + m)) \right\} \\ &\times \exp \left\{ - \int d^4x \left(\frac{1}{4} (F_{\mu\nu}^a F_{\mu\nu}^a) \right) \right\}, \end{aligned}$$

since $\partial_m \text{Tr}(\log(D + m)) = \text{Tr}((D + m)^{-1})$. This leads to

$$\langle \bar{\lambda}\lambda \rangle = \frac{1}{2V} \left\langle \text{Tr}((D + m)^{-1}) \right\rangle$$

This quantity on the lattice has both multiplicative and additive renormalization, the factor $\frac{1}{2}$ can be properly reabsorbed and the redefinition of the renormalization constants $Z(a\mu)$ and $b(a\mu)$.

Qualitatively the gluino condensate will jump from an upper to a lower value in correspondence of the chiral transition moving toward the zero mass limit, the jump will be more evident in the infinite volume limit. Therefore it is expected that the derivative of the gluino condensate with respect of the mass

$$\frac{\partial}{\partial m} \langle \bar{\lambda}\lambda \rangle = \frac{1}{V} \frac{\partial^2}{\partial m^2} \log(Z(\beta, m))$$

called gluino susceptibility, has a peak near the chiral phase transition (crossover at finite volume), see Fig. 4.3.

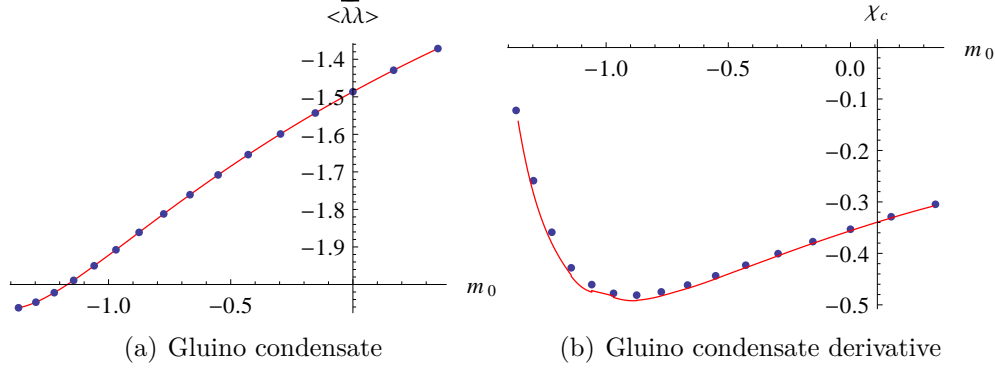


Figure 4.4: The expectation value of gluino condensate (left) has been interpolated with a cubic spline as a function of the bare fermion mass (red line), the interpolation has been derived numerically and compared with the chiral susceptibility estimated with connected and disconnected contributions (right). Simulation done on a lattice $12^3 \times 4$ at $\beta = 1.65$. The test shows a perfect agreement.

In order to compute the peak of the gluino susceptibility S_χ , the second derivative of partition function with respect to the mass has to be computed

$$S_\chi = \frac{\partial}{\partial m} \langle \bar{\lambda}\lambda \rangle = \frac{1}{V} \frac{\partial^2}{\partial m^2} \log(Z(\beta, m)).$$

Expanding the derivative, it follows

$$\begin{aligned} VS_\chi &= \frac{\partial}{\partial m} \left(\frac{1}{Z(\beta, m)} \int dU_\mu \frac{1}{2} \text{Tr}((D + m)^{-1}) \exp \left\{ + \frac{1}{2} \text{Tr}(\log(D + m)) \right\} \right. \\ &\quad \times \exp \left\{ - \int d^4x \left(\frac{1}{4} (F_{\mu\nu}^a F_{\mu\nu}^a) \right) \right\} \Bigg) \\ &= \frac{1}{4} \langle \text{Tr}((D + m)^{-1})^2 \rangle - \frac{1}{4} \langle \text{Tr}((D + m)^{-1}) \rangle^2 - \frac{1}{2} \langle \text{Tr}((D + m)^{-2}) \rangle, \end{aligned}$$

where it is important to keep carefully the order of the square power and the last term arises from

$$\begin{aligned} \partial_m((D + m)^{-1}) &= -(D + m)^{-1} (\partial_m(D + m)) (D + m)^{-1} \\ &= -(D + m)^{-2}. \end{aligned}$$

The first two term are the “classical” disconnected contributions for the standard deviation of a set of sampled data, the last term is a connected contribution which is expected to vanish in the chiral limit (i.e., zero physical

quark mass). The result is consistent with the more general result of formula 8 in [29] and with direct numerical tests presented in Fig. 4.4.

Numerical simulations have shown that the chiral condensate has a two peak structure crossing the critical value of the bare gluino mass [30], confirming the conjectures about the nature and the order of the chiral phase transition [31, 32, 33]. Further numerical results about chiral symmetry will be discussed at finite temperature in Ch. 10.

Chapter 5

Improved Actions

In the improvement, additional Taylor expansion coefficients are replaced by the ones [...] of the corresponding continuum-theory functions. Hereby, the approach to the continuum theory as $a \searrow 0$ is speed up. The terms inserted into the lattice action to perform that replacement are "irrelevant" ones of higher operator-dimension and involve also next-to-nearest neighbour couplings.

K. Symanzik [34]

Many efforts have been recently done to study the low energy behavior of super Yang-Mills theories with numerical simulations on the lattice. Most of the computer time is usually spent for extrapolating the limit $a \rightarrow 0$, where the Lorentz invariance broken by the lattice is recovered. Discretization errors are of order $O(a)$ for the Wilson formulation of the fermion action, larger than the $O(a^2)$ scaling of pure gauge theories. An improved version of Wilson fermions can be constructed following the Symanzik program [34, 35]. The strategy is to add the irrelevant operator O_{CL} to the unimproved Lagrangian

$$\begin{aligned} L_i &= L_u + c_{sw} O_{CL}, \\ O_{CL} &= -\frac{a}{4} \bar{\lambda}(x) \sigma_{\mu\nu} F^{\mu\nu} \lambda(x), \end{aligned} \tag{5.1}$$

and to tune the coefficient c_{sw} to an appropriate value where the lattice discretization errors $O(a)$ disappear from on-shell quantities (like masses of

mesons or particles scattering cross sections). The operator O_{CL} is called clover term, because of the shape depicted by the plaquettes of the lattice version of $F^{\mu\nu}$. The Sheikholeslami-Wohlert coefficient c_{sw} is a function of the gauge coupling g and it can be expanded asymptotically as

$$c_{sw} = c_{sw}^0 + c_{sw}^1 g^2 + c_{sw}^2 g^4 + \dots$$

The value of c_{sw} can be computed with standard perturbation theory. In case of QCD, the fermions are in the fundamental representation of the gauge group $SU(N)$ and c_{sw} has been computed both with perturbation theory up to one loop and non-perturbatively with the Schrödinger functional formalism [36, 37, 38]. Similar numerical calculation have been done for the two-flavor adjoint QCD theory, but so far no perturbative calculation of c_{sw} has been available. In this chapter the general idea of Symanzik improvement is discussed and the calculation of the Sheikholeslami-Wohlert coefficient up to one loop for fermions in arbitrary representation of the gauge group $SU(N)$ is presented. Applications of the clover improvement will be also considered for the special case of the $\mathcal{N} = 1$ supersymmetric Yang-Mills theory. The calculation presented in this chapter has been published in [39].

5.1 Lattice discretization and Symanzik improvements

Operators are classified in quantum field theories as relevant, irrelevant or marginal, depending on their scaling behaviour under renormalization group transformations near the critical point. Relevant operators determine the long range physics, while irrelevant operators have an influence only on short distances in the ultraviolet regimes. Once that all the degrees of freedom larger than some energy scale are integrated out, irrelevant operators will move toward zero while relevant operators will be driven away from the second order phase transition. Therefore only parameters and coupling constants related to relevant operators have to be accurately fine-tuned to reach the critical point, i.e. the continuum limit in the quantum field theory language.

A continuum operator can be discretized on the lattice in many equivalent ways, equivalent in the sense that they differ by irrelevant operators. As classical example, the derivative $\partial_\mu \phi(x)$ corresponds either to

$$\partial_\mu \phi(x) \rightarrow \nabla_L \phi(x) = \frac{\phi(x + \vec{\mu}a) - \phi(x)}{a},$$

or to

$$\partial_\mu \phi(x) \rightarrow \nabla_C \phi(x) = \frac{\phi(x + \vec{\mu}a) - \phi(x - \vec{\mu}a)}{2a},$$

but $\nabla_L \phi(x)$ has a discretization error of order $O(a)$ while $\nabla_C \phi(x)$ only of order $O(a^2)$

$$\begin{aligned} \phi(x + \vec{\mu}a) &= \phi(x) + a\partial_\mu \phi(x) + \frac{1}{2}a^2\partial_\nu\partial_\mu \phi(x) + O(a^3), \\ \phi(x - \vec{\mu}a) &= \phi(x) - a\partial_\mu \phi(x) + \frac{1}{2}a^2\partial_\nu\partial_\mu \phi(x) + O(a^3), \\ \phi(x + \vec{\mu}a) - \phi(x) &= a\partial_\mu \phi(x) + O(a^2), \\ \phi(x + \vec{\mu}a) - \phi(x - \vec{\mu}a) &= 2a\partial_\mu \phi(x) + O(a^3). \end{aligned}$$

The difference of $\nabla_L \phi(x)$ and $\nabla_C \phi(x)$ is an irrelevant operator since

$$\nabla_L \phi(x) - \nabla_C \phi(x) = \frac{\phi(x + \vec{\mu}a) - 2\phi(x) + \phi(x - \vec{\mu}a)}{2a}$$

is proportional near the continuum limit to the lattice spacing times the second derivatives and it will vanish when $a \rightarrow 0$. Other possible discretization of $\partial_\mu \phi(x)$ are possible, with smaller and smaller errors of order $O(a^k)$. When a numerical calculation of the derivative $\partial_\mu \phi(x)$ is required, the cost of the evaluation of more complex expression has to be practically compared with the advantages of having a better approximation even with larger a and so less loss of numerical accuracy.

This technique is widely employed to construct more accurate numerical integrator of ordinary and partial differential equations, for instance to integrate the classical equations of motion of a particle or a fluid. In quantum field theories the classical calculation based on Taylor expansion of operators is in general not sufficient to ensure a complete improvement of the operators. The coefficients have to be chosen by matching linear combination of operators in Ward identities with the requirement that they must be fulfilled up to the needed accuracy. The coefficients determined will not differ so much from their classical value near the continuum limit, but far from this critical point the complex and non-linear transformations generated by the renormalization group will change a lot the naive classical expectation. Non-linear equations will appear and a solution can be found in general only iteratively for example with perturbation theory or with Monte-Carlo simulations [37].

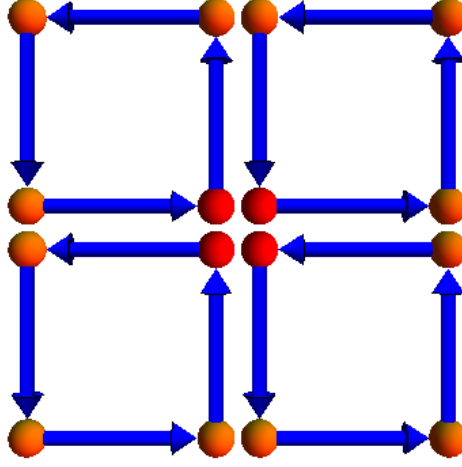


Figure 5.1: The diagram represents the lattice version of $F_{\mu\nu}$ as the sum of the plaquettes based over the red point.

5.2 Improving the Dirac Wilson operator

Let $SU(N)$ a special unitary group in an irreducible representation R with dimension d_R . Then the lattice link variables $U_\mu^R(x)$ are related to the continuum color gauge field $A_\mu^b(x)$ by the exponential map

$$U_\mu^R(x) = \exp(igaA_\mu^b(x)\tau_b^R) \quad (5.2)$$

where τ_b^R are the Lie group generators in the representation R :

$$[\tau_b^R, \tau_c^R] = if_{bc}^d \tau_d^R$$

The generators τ_b^R are $N^2 - 1$ Hermitian matrices of size $d_R \times d_R$.

On the lattice, the fermion part of the action is written in terms of the links in the arbitrary representation R

$$S_f = \sum_{x,y} \bar{\lambda}(y) D_W[U_\mu^R](y, x) \lambda(x).$$

The action of the Dirac-Wilson operator D_W over the fermion field λ is (Dirac indices suppressed)

$$\begin{aligned} D_W(x, y) \lambda(y) &= \lambda(x) - \kappa H(x, y) \lambda(y) \\ H(x, y) \lambda(y) &= \sum_\mu \left\{ (1 - \gamma_\mu) U_\mu^R(x) \lambda(x + \mu) + (1 + \gamma_\mu) U_\mu^R(x - \mu)^\dagger \lambda(x - \mu) \right\}. \end{aligned}$$

The clover term is defined in Eq. (5.1) and $F_{\mu\nu}$ is chosen as the lattice anti-symmetric sum of the plaquettes $P_{\mu\nu}$ of Fig. 5.1

$$F_{\mu\nu}(x) = \frac{1}{4i} \sum_{\mu < \nu} (P_{\mu\nu}(x) - P_{\mu\nu}(x)^\dagger).$$

The Feynman rules can be obtained expanding the exponential map of Eq. (5.2), the complete list can be found in [40].

The fermion action has lattice discretization errors of order $O(a)$. For removing them, it is possible to add to the action the lattice version of the following dimension five operators

$$\begin{aligned} O_1 &= m \text{Tr}(F^{\mu\nu} F_{\mu\nu}), \\ O_2 &= m^2 \bar{\lambda} \lambda, \\ O_3 &= m \bar{\lambda} \gamma_\mu A_\mu \lambda, \\ O_4 &= \bar{\lambda} D_\mu D_\mu \lambda, \\ O_5 &= \bar{\lambda} \sigma_{\mu\nu} F^{\mu\nu} \lambda, \end{aligned}$$

each of them multiplied by a coefficient c_i which depends on g and in principle also m , $c_i \equiv c_i(g, m)$. These coefficients can be computed perturbatively or non-perturbatively directly with lattice simulations. The first three operators lead to a renormalization of the bare gauge coupling g and of the bare fermion mass m , they are important in the context of the mass-independent renormalization scheme but they can be neglected in the following [41].

The complete calculation of the coefficients c_i that remove the discretization errors $O(a)$ is cumbersome and rather difficult, but many simplifications are possible if the removal of $O(a)$ errors is restricted to on-shell quantities [42]. Examples of on-shell quantities are the masses of particles and scattering amplitudes. Consider for instance the ratio of masses of two meson particles $m_1(a)$ and $m_2(a)$ evaluated on lattice, it will reach the continuum value up to $O(a)$ correction

$$\lim_{a \rightarrow 0} \frac{m_1(a)}{m_2(a)} = \frac{m_1^c}{m_2^c} (1 + O(a))$$

and then on-shell improvements require only the removal of such an error. On-shell improvements have the advantage to do not deal with contact terms and the Ward identities simplify further the calculation by reducing the number of operators. For example the equations of motion,

$$\langle D_\mu \lambda \phi_1 \dots \phi_n \rangle = m \langle \gamma_\mu \lambda \phi_1 \dots \phi_n \rangle + \langle \sigma_{\mu\nu} D_\nu \lambda \phi_1 \dots \phi_n \rangle,$$

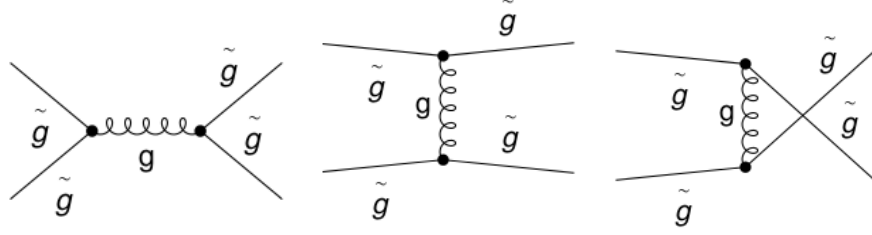


Figure 5.2: Feynman diagrams contributing to the tree-level amplitude for the gluino-gluino scattering.

with $\phi_1 \dots \phi_n$ arbitrary fields, relate the above operator O_4 to a linear combination of the operators O_3 and O_5 . Therefore this means that the use of the operator O_4 is unnecessary for on-shell improved action and so the coefficient of the operator O_5 is the only one that should be fixed [43, 44], the so-called Sheikholeslami and Wohlert coefficient c_{sw} .

5.3 Calculation of the Sheikholeslami-Wohlert coefficient at tree level for $\mathcal{N} = 1$ SYM

The calculation of the Sheikholeslami-Wohlert coefficient proceeds as in standard QCD. Many possible on-shell quantities can be considered for effectively performing the calculation of c_{sw} , the final computed value will be independent of this choice [42]. In the original calculation of Wohlert the energy levels were considered, in this calculation instead the fermion-fermion scattering is used, following Ref. [40]. This choice is natural because the fermion scattering contains in the simplest way the new interaction vertex of order g between two fermions and the gauge boson added by the clover term.

In the case of the super Yang-Mills theories, there will be the channel s , channel t and channel u (Fig. 5.2), since the gluino is a Majorana fermion. The corresponding amplitudes are

$$M_s = \frac{ig^2}{s} \bar{u}(p_1) V_\mu^A(-p_1, p_2) v(p_2) \bar{v}(p_4) V_\mu^A(-p_4, p_3) u(p_3), \quad (5.3)$$

$$M_t = \frac{ig^2}{t} \bar{u}(p_1) V_\mu^A(p_1, p_4) u(p_4) \bar{u}(p_2) V_\mu^A(p_2, p_3) u(p_3), \quad (5.4)$$

$$M_u = \frac{ig^2}{u} \bar{u}(p_1) V_\mu^A(p_1, p_3) u(p_3) \bar{u}(p_2) V_\mu^A(p_2, p_4) u(p_4), \quad (5.5)$$

where p^1 and p^2 are the momenta of the ingoing particles and p^3 and p^4 of the outgoing particle. The spinors u and v are the modes of the Fourier

transformation of the gluino field,

$$\begin{aligned}\lambda(x) &= \sum_{s=\pm} \int \frac{d^3p}{(2\pi)^3 2E_k} \left(u_s(p) b_s(p) e^{ik \cdot x} + v_s(p) d_s^\dagger(p) e^{-ik \cdot x} \right), \\ \bar{\lambda}(x) &= \sum_{s=\pm} \int \frac{d^3p}{(2\pi)^3 2E_k} \left(\bar{u}_s(p) b_s^\dagger(p) e^{-ik \cdot x} + \bar{v}_s(p) d_s(p) e^{ik \cdot x} \right),\end{aligned}$$

and they satisfy

$$(i\gamma_\mu p^\mu + m)u(p) = 0, \quad (5.6)$$

$$(-i\gamma_\mu p^\mu + m)v(p) = 0, \quad (5.7)$$

$$u(p) = C\bar{v}^T, \quad (5.8)$$

$$v(p) = C\bar{u}^T. \quad (5.9)$$

The first two identities come from the equation of motion in momentum space, while the last two can be verified directly since $\lambda(x)$ and $\bar{\lambda}(x)$ are not independent due to the $\bar{\lambda}(x) = \lambda(x)^T C$ condition.

The gluon propagator is (working with Feynman gauge $\lambda = 1$)

$$\Delta_{\mu\nu}^{AB}(q) = i\delta_{AB} \frac{g_{\mu\nu}}{q^2}$$

when $q \ll \pi/a$, that is far away from lattice distortions that however for the gauge interactions are of order $O(a^2)$.

The vertex function in the momentum space $V_\mu^A(p_1, p_2)$ can be written directly considering only the interaction gluino-gluino-gluon terms from the fermion action [45]. From the Wilson fermion action there will be two contributions

$$\begin{aligned}S_W^1 &= -a^4 \frac{ig}{2} \sum_{x,\mu} \lambda^T(x) C(1 - \gamma_\mu) A_\mu(x) \lambda(x + \mu), \\ S_W^2 &= +a^4 \frac{ig}{2} \sum_{x,\mu} \lambda^T(x + \mu) C(1 + \gamma_\mu) A_\mu(x) \lambda(x),\end{aligned}$$

while the clover term add the interaction

$$S_{CT} = -a^5 \frac{C_{sw}}{4} \sum_{x,\mu \neq \nu} \lambda^T(x) C \sigma_{\mu\nu} F_L^{\mu\nu} \lambda(x).$$

S_{CT} , S_W^2 and S_W^1 can be rewritten Taylor expanding up to $O(a^2)$ the finite differences

$$\begin{aligned}S_W^1 &= \frac{ig}{2} \psi^T(x) C \gamma_\mu A_\mu(x) \psi(x) - \frac{iga}{2} \psi^T(x) C A_\mu(x) \partial_\mu \psi(x), \\ S_W^2 &= \frac{ig}{2} \psi^T(x) C \gamma_\mu A_\mu(x) \psi(x) + \frac{iga}{2} (\partial_\mu \lambda^T(x)) C A_\mu(x) \lambda(x), \\ S_{CT} &= +a \frac{igC_{sw}}{2} \sum_{x,\mu \neq \nu} \lambda^T(x) C \sigma_{\mu\nu} (\partial_\nu A_\mu(x)) \lambda(x),\end{aligned}$$

and the vertex function then reads

$$V_\mu^A(p_1, p_2) = gT^A \left(i\gamma_\mu + a \frac{p_\mu^1 + p_\mu^2}{2} + ic_{sw} \frac{a}{2} \sigma_{\mu\nu} (p_\nu^1 - p_\nu^2) \right), \quad (5.10)$$

where p_1 is the ingoing momentum and p_2 is the outgoing momentum. Notice that an overall factor 2 is always removed in all terms, compensated by the extra 1/2 in front of the Majorana action.

The full amplitude contains factors to be improved like

$$\begin{aligned} \bar{u}(p^1) V_\mu^A(p_1, p_2) u(p^2) &= ig \bar{u}(p^1) T^A \gamma_\mu u(p^2) + ga \frac{p_\mu^1 + p_\mu^2}{2} \bar{u}(p_1) T^A u(p^2) + \\ &\quad + igc_{sw} \frac{a}{2} \bar{u}_a(p_1) (T^A)_{ab} \sigma_{\mu\nu} u_b(p^2) (p_\nu^1 - p_\nu^2). \end{aligned} \quad (5.11)$$

The first term corresponds to the continuum vertex function, while the others are the $O(a)$ lattice artifacts. Using the equations (5.6) and the properties of the matrix C

$$\begin{aligned} i(p_\nu^1 - p_\nu^2) \bar{u}_a(p^1) \sigma_{\mu\nu} u_b(p^2) &= i(p_\nu^1 - p_\nu^2) v_a^T(p_1) C \sigma_{\mu\nu} u_b(p^2) \\ &= -\frac{p_\nu^1 - p_\nu^2}{2} v_a^T(p_1) C (\gamma_\mu \gamma_\nu - \gamma_\nu \gamma_\mu) u_b(p^2) \\ &= -\frac{1}{2} v_a^T(p_1) C \gamma_\mu \not{p}^1 u_b(p^2) - \frac{1}{2} v_a^T(p_1) C \gamma_\mu \not{p}^2 u_b(p^2) + \\ &\quad + \frac{1}{2} v_a^T(p_1) C \not{p}^1 \gamma_\mu u_b(p^2) + \frac{1}{2} v_a^T(p_1) C \not{p}^2 \gamma_\mu u_b(p^2) \\ &= +\frac{1}{2} v_a^T(p_1) C \not{p}^1 \gamma_\mu u_b(p^2) - \frac{1}{2} v_a^T(p_1) C \gamma_\mu \not{p}^2 u_b(p^2) + \\ &\quad + \frac{1}{2} v_a^T(p_1) C \not{p}^1 \gamma_\mu u_b(p^2) - \frac{1}{2} v_a^T(p_1) C \gamma_\mu \not{p}^2 u_b(p^2) + \\ &\quad - p_\mu^1 v_a^T(p^1) C u_b(p^2) - p_\mu^2 v_a^T(p^1) C u_b(p^2) \\ &= +2im v_a^T(p^1) C \gamma_\mu u_b(p^2) - (p_\mu^1 + p_\mu^2) v_a^T(p^1) C u_b(p^2), \end{aligned}$$

so that the Gordon identity still holds also for Majorana fermions. The first term leads only to a mass dependent renormalization of the electric charge and in this context can be neglected. Putting this relation in Eq. (5.11)

$$\begin{aligned} \bar{u}(p^1) V_\mu^A(p_1, p_2) u(p^2) &= ig \bar{u}(p^1) T^A \gamma_\mu u(p^2) + ga \frac{p_\mu^1 + p_\mu^2}{2} \bar{u}(p^1) T^A u(p^2) + \\ &\quad - gc_{sw} \frac{a}{2} (p_\mu^1 + p_\mu^2) \bar{u}_a(p^1) (T^A)_{ab} u_b(p^2). \end{aligned}$$

Therefore $c_{sw} = 1$ for removing of the $O(a)$ errors at tree-level. The same results still holds for the other amplitudes in (5.3).

5.4 Clover term and isospectral transformations

The clover term can be calculated at tree level by requiring that $O(a)$ terms disappear from the Dirac operator

$$D_W = \frac{1}{2} \left[\gamma^\mu (\nabla_\mu^* + \nabla_\mu) - a \nabla_\mu^* \nabla_\mu \right] - c_{sw} \frac{a}{4} \sigma_{\mu\nu} F_L^{\mu\nu},$$

where

$$\begin{aligned} \nabla_\mu \psi(x) &= \frac{U_\mu(x) \psi(x + \mu) - \psi(x)}{a}, \\ \nabla_\mu^* \psi(x) &= \frac{\psi(x) - U_\mu^\dagger(x - \mu) \psi(x - \mu)}{a}. \end{aligned}$$

Clearly the Wilson term in the continuum limit is

$$\lim_{a \rightarrow 0} \nabla_\mu^* \nabla_\mu = D_\mu D_\mu.$$

The operator $D_\mu D_\mu$ is a linear combination of the clover term and of the square of the Dirac operator itself

$$\not{D} \not{D} = \gamma_\mu \gamma_\nu D_\mu D_\nu = D_\mu D_\mu - i \sigma_{\mu\nu} D_\mu D_\nu = D_\mu D_\mu + \frac{1}{2} \sigma_{\mu\nu} F_{\mu\nu};$$

collecting all terms

$$D_W = \not{D} + \frac{a}{4} \sigma_{\mu\nu} F_{\mu\nu} - c_{sw} \frac{a}{4} \sigma_{\mu\nu} F_{\mu\nu} + a \not{D} \not{D}.$$

If $c_{sw} = 1$ then the remaining $\not{D} \not{D}$ can be removed simply with an isospectral transformation of the Majorana field

$$\lambda \rightarrow \exp(\epsilon a(\not{D})) \lambda,$$

i.e. a transformation which leaves the low energy spectrum unmodified up to order $O(\epsilon^2)$ [25]. This leads to the same result of the previous section.

5.5 Calculation of the Sheikholeslami-Wohlert coefficient to one loop order in perturbation theory

As shown in the previous sections, the relevant part for the calculation of the clover coefficient comes from the fermion-fermion-gluon vertex $\Lambda(p, p')_c^\mu$

$$\Lambda(p, p')_c^\mu = g \left(i \gamma^\mu A + \frac{a}{2} (B - c_{sw}) + O(a^2) + O(p^2, p'^2) \right) \tau_c^R,$$

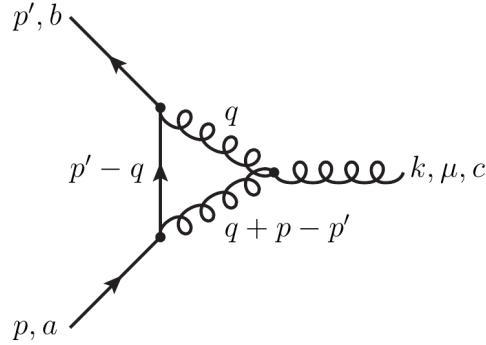


Figure 5.3: Example of one-loop diagram relevant to the calculation of the clover term. Picture taken from Ref. [40].

where p and p' are as before the momenta of the incoming fermions and c is the color of the outgoing gluon. The first term represents the continuum color vertex, while the second one is a lattice artifact proportional to a . At tree level one finds

$$B = 1 + O(g^2),$$

independent of the number of colors and of the fermion representation. Thus the clover coefficient must be set to the universal value $c_{sw}^{(0)} = 1$.

At one loop, the calculation of the vertex involves the reduction of products of matrices τ_a^R ,

$$\begin{aligned} \sum_a \tau_a^R \tau_a^R &= C_R \mathbf{1}, \\ \sum_{bc} f_{abc} \tau_b^R \tau_c^R &= i \frac{N}{2} \tau_a^R, \\ \sum_b \tau_b^R \tau_a^R \tau_b^R &= \left(C_R - \frac{N}{2} \right) \tau_a^R, \end{aligned}$$

so that the final results depend only on the number of colors of the gauge group and on the quadratic Casimir invariant C_R . The latter can be obtained using group theoretical formulas, see [46, 47].

For example, the Feynman diagram of Fig. 5.3 has a loop with one gluino line and two gluon lines. Following the gluino line backward, the first gluino-gluino-gluon vertex gives a $(\tau_d^R)^{ae}$, being a the color of the incoming gluino. The gluon interaction changes the color of the gluino from a to e , with an associated emission of a gluon of color d . Analogously, the second vertex gives a contribution $(\tau_g^R)^{eb}$, being b the color of the other incoming gluino. Gluons interact among themselves to produce the final outgoing gluon with

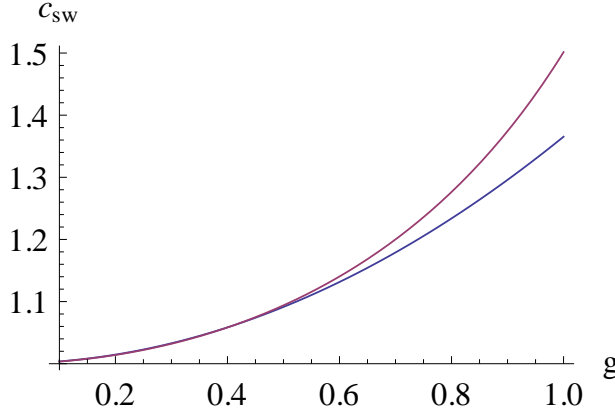


Figure 5.4: The plot compares c_{sw} between the one loop calculation and the numerical estimation for the two-flavor adjoint theory of Ref. [48].

color c , colors are contracted in this case with f_c^{gd} . The final color factor F_c is

$$F_c = (\tau_d^R)^{ae} (\tau_g^R)^{eb} f_c^{gd}, \quad (5.12)$$

summing over all intermediate states, that means summing over e , g and d . Using the second formula above, the color contribution can be rewritten as

$$F_c = i \frac{N}{2} \tau_a^R. \quad (5.13)$$

The integral in the momentum space does not depend on the specific fermion representation of the gauge group, the results that have been already computed in [40] can be simply multiplied by the new color factor.

At one loop the $O(a)$ lattice artifact coming from the vertex is

$$B = 1 + g^2(0.16764(3)C_R + 0.01503(3)N) + O(g^4),$$

which can be removed if $c_{sw}^{(1)}$ is set to

$$c_{sw}^{(1)} = 0.16764(3)C_R + 0.01503(3)N.$$

Numerical estimations of the clover term have been made in Ref. [48] in the special case of a theory with two fermions in the adjoint representation of $SU(2)$. The expansion of their results yields

$$c_{sw}^{(mc)}(g) = 1 + 0.346806g^2 + O(g^2),$$

in good agreement with our perturbative value of $c_{sw}^{(1)} = 0.36533(4)$ (Fig. 5.4).

5.6 Applications to $\mathcal{N} = 1$ SUSY Yang-Mills theory

The $\mathcal{N} = 1$ supersymmetric Yang-Mills theory describes the interactions between gluons and their supersymmetric partners, called gluinos. The gluino is a spin- $\frac{1}{2}$ Majorana fermion in the adjoint representation. A Majorana fermion obeys the condition

$$\bar{\lambda} = \lambda^T C,$$

where C is the charge conjugation operator. As a consequence there is not a distinction between particle and antiparticle, i. e. the two-point Green functions $\langle \bar{\lambda}(x)\lambda(y) \rangle$, $\langle \bar{\lambda}(x)\bar{\lambda}(y) \rangle$ and $\langle \lambda(x)\lambda(y) \rangle$ do not vanish. The main difference appears in the combinatorial factors for each Feynman diagram that has fermion loops. The one-loop diagrams for the fermion-fermion-gluon vertex have no fermion loops and therefore the previous value of $c_{sw}^{(1)}$ can be applied also to Majorana fermions. The difference between Dirac and Majorana fermions is expected to be found at order $O(g^4)$.

Recent numerical investigations of $\mathcal{N} = 1$ Super Yang-Mills theory have been presented in Refs. [49, 50], where the mass gap for particles in the same supermultiplet is found to be significantly reduced on finer and bigger lattices. The use of clover improvement could be helpful for simulating the model also on coarser lattices, since the finite lattice spacing a is an important source of supersymmetry breaking. In fact, the SUSY algebra mixes the internal field symmetry with Poincaré transformations,

$$\{Q_\alpha, Q_\beta\} = (\gamma^\mu C)_{\alpha\beta} P_\mu,$$

where P_μ is the translation operator. On the lattice only discrete translations of step a are possible, therefore the supersymmetry algebra is explicitly broken for a finite lattice spacing and it could be restored only in the continuum limit (see [4, 51]). The reduction of discretization errors given by the clover term can be helpful for restoring SUSY also on coarser lattices.

5.7 Tadpole improvements

The relation between the link $U_\mu(x)$ as a group variable and the continuum gauge field $A_\mu(x)$ as Lie algebra elements is usually defined through the exponential map of formula (5.2). The naive continuum limit $a \rightarrow 0$

$$U_\mu(x) = 1 + igaA_\mu^a(x)T_a^R + O(a^2)$$

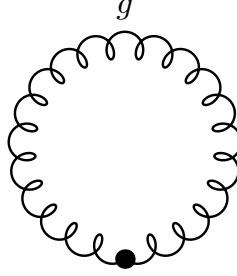


Figure 5.5: Tadpole gluon diagram responsible of the bad convergence of lattice perturbation theory.

is used as starting point in the determination of a proper discretized lattice action. The error in the expansion above is of order $O(a^2)$, but quantum fluctuations can largely modify this behavior. Consider for example the expectation value of the trace of a single link. Since it is a gauge-variant quantity, its expectation value will be zero for the Elitzur theorem [52]. However it is possible to fix the gauge on the lattice in order to be able to compare ordinary perturbation theory with lattice Monte Carlo estimations. Therefore in some gauge

$$\langle \text{tr}(U_\mu^{gf}(x)) \rangle = 1 + i g a \langle \text{tr}(A_{\mu;i}^{gf}(x) \tau^i) \rangle - g^2 a^2 \langle \text{tr}(A_{\mu;i}^{gf}(x) A_{\mu;j}^{gf}(x) \tau^i \tau^j) \rangle$$

and remembering that the trace of a single Lie generator τ^i vanishes

$$\langle \text{tr}(U_\mu^{gf}(x)) \rangle = 1 - g^2 a^2 \langle A_{\mu;i}^{gf}(x) A_{\mu;i}^{gf}(x) \rangle \quad (5.14)$$

The expectation value $\langle A_{\mu;i}^{gf}(x) A_{\mu;i}^{gf}(x) \rangle$ can be represented in momentum space at first order as a “tadpole” diagram, see Fig. 5.5. The contribution of such terms will be proportional to

$$\langle A_{\mu;i}^{gf}(x) A_{\mu;i}^{gf}(x) \rangle \propto \int_{-\frac{\pi}{2a}}^{\frac{\pi}{2a}} \frac{1}{q^2} d^4 q \propto \int_0^{\frac{\pi}{2a}} q dq = \frac{\pi^2}{4a^2},$$

since on the lattice the momentum integral are restricted on the first Brillouin zone. Putting the result in expansion of the link

$$\langle \text{tr}(U_\mu^{gf}(x)) \rangle \propto 1 - g^2 a^2 \frac{\pi^2}{4a^2} \propto 1 - O(g^2),$$

it is easy to observe that the higher contribution to the leading order are suppressed just as a power of g^2 and not as $g^2 a^2$. The quantum fluctuations generate so a slowly convergent lattice perturbation theory. This conclusion has been verified with standard perturbation theory, for example the largest

contribution to the deviation of the clover coefficient c_{sw} from its tree level value comes from the “tadpole” like loop of the gluon.

Lepage and Mackenzie in 1992 observed that it is possible to redefine the coupling in such a way to subtract the tadpole contribution in the mean-field meaning [53]. The proposal is to rescale the link variables by a factor u_0

$$U_\mu(x) \rightarrow \frac{U_\mu(x)}{u_0}$$

chosen in a clever way that the quadratic term cancels from the expansion. The factor u_0 could be for example the mean value of the link after a gauge fixing procedure, or, even simpler, the fourth root of the gauge invariant expectation value of the trace of the plaquette

$$u_0 = \sqrt[4]{\langle U_p \rangle},$$

since a plaquette has four links. This rescaling accelerates the convergence of lattice perturbation theory, it vanishes in the continuum limit if the normalization

$$\lim_{\beta \rightarrow \infty} \langle U_p \rangle = 1$$

is used. Tadpole improvement requires also the redefinition of the improvement coefficient c_{sw} by

$$c_{sw} \rightarrow \frac{c_{sw}}{u_0^3},$$

which should take effectively into account the large quantum correction of c_{sw} from the unity.

Chapter 6

Simulation algorithms for supersymmetry

Instead of choosing configurations randomly, then weighting them with $\exp(-E/kT)$, we choose configurations with a probability $\exp(-E/kT)$ and weight them evenly.

Nicholas Metropolis *et al.* [54]

Lattice regularization allows the development of powerful tools to explore the non-perturbative low energy regime of strong interacting theories. Monte Carlo methods have been introduced several decades ago to simulate classical thermodynamics [54], like for example phase transitions of Ising models. The knowledge acquired in statistical models has been useful to implement efficient algorithms also for quantum field theories.

Gauge fields are implemented straightforwardly on the lattice, while the Grassmannian nature of the gluino complicates drastically the algorithms required to perform practical simulations. In general fermions on the lattice require a huge amount of computer time and they are $O(100)$ more expensive than simulations of pure gauge fields. The main challenge today is the reduction of the cost of fermion algorithms, especially in the massless and continuum limit, to finally arrive to the fall of the so-called “Berlin Wall” [55]. Large scale supercomputers are essential to extrapolate reliable results. Fermions are a special ingredient in supersymmetry and therefore in this chapter the attention will be focused on the discussion of the main ideas behind their implementation on the lattice.

6.1 Monte Carlo and importance sampling

Lattice discretization in Euclidean space-time allows to compute expectation values of observables in gauge theories from well defined integral like

$$\langle \mathcal{O} \rangle = \frac{\int dU_\mu \mathcal{O} \exp \left(\sum_P \frac{\beta}{N} \text{ReTr}(U_P) \right)}{\int dU_\mu \exp \left(\sum_P \frac{\beta}{N} \text{ReTr}(U_P) \right)}, \quad (6.1)$$

supposing for the moment a theory without dynamical fermions. This integral can be computed directly without any perturbative expansion, but the large number of variables to be integrated, more than ten thousands, forbids practically the usage of common quadrature algorithms. However, the expression (6.1) is formally equivalent to the average of an observable \mathcal{O} in the canonical ensemble. The exponential can be interpreted as a statistical Boltzmann weight and it will suppress many configurations and regions of possible values of the link variables $U_\mu(x)$. “Importance sampling” is a technique to explore the phase space around the configurations $\{U_\mu\}_i$ that give largest contributions to the integral (6.1). The expectation value (6.1) can be then approximated as the sum of the observable evaluated over the configuration $\{U_\mu\}_i$

$$\langle \mathcal{O} \rangle \approx \frac{1}{N} \sum_i^N \mathcal{O}(\{U_\mu\}_i). \quad (6.2)$$

Markov chains are stochastic processes employed to ensure an exact equivalence between the two members of the previous equation in the limit $N \rightarrow \infty$.¹

6.2 Markov chains

A Markov chain is a discrete stochastic process formally defined by the distribution $P(C_{t-1} \rightarrow C_t)$ that provides the probability for a transition from the state C_{t-1} to a new state C_t : in a Markov chain a new state is generated with a probability which depends only on the state C_{t-1} and not on all the other previous C_k with $k < t - 1$.

The probability distribution $P(C_{t-1} \rightarrow C_t)$ can be arranged in a square stochastic matrix if the number of possible states is finite, but there are no special problems in generalizing what follows even for an uncountable set

¹There are several reviews about lattice Monte Carlo methods, this chapter has been prepared following Ref. [56].

of states. A stochastic matrix T has all entries positive and the sum of all elements in a row is equal to one

$$\begin{aligned} T_{ij} &\geq 0, \\ \sum_j T_{ij} &= 1. \end{aligned} \quad (6.3)$$

The second equation simply reads that a new state will be generated with probability one, while the first inequality reflects the probabilistic nature of T . The element T_{kl} is in fact the probability for the transition from the state $C[k]$ to $C[l]$. Therefore the probability $P[C_k \rightarrow C_m]_n$ to be in the state C_m after n steps starting from C_k is

$$P[k \rightarrow m]_n = \sum_{l_1} \cdots \sum_{l_n} T_{kl_1} T_{l_1 l_2} \cdots T_{l_{n-1} l_n} = (T \times T \times \cdots \times T)_{km} = (T^n)_{km}.$$

The states will be visited after a large number of iterations by the Markov chain with a probability independent from the initial state and dependent only on the spectral properties of T , assuming aperiodicity and ergodicity of the stochastic process. The matrix T has the largest eigenvalue equal to one $\lambda_{\max} = 1$, expressing the condition (6.3). The eigenvector v_{\max} associated defines the probability distribution $\Pi_{\infty}[i]$ of the asymptotic states C_i

$$\sum_i \Pi_{\infty}[i] T_{ij} = \Pi_{\infty}[j] \quad (6.4)$$

independent by definition from the Monte Carlo time t .

The task is now to find a matrix T in order that the asymptotic distribution is equal to the exponential of minus the target quantum action

$$\Pi_{\infty}[i] = \frac{1}{Z} \exp(-\beta S[C_i]).$$

A possible solution² can be found by looking for a stochastic process which proposes a random change T^0 of the field configuration

$$\begin{aligned} T_{ij} &= T_{ij}^0 c_{ij} \quad i \neq j \\ T_{ii} &= T_{ii}^0 + \sum_{i \neq j} T_{ij}^0 (1 - c_{ij}) \end{aligned}$$

under the symmetric restriction

$$\Pi_{\infty}[i] T_{ij} = \Pi_{\infty}[j] T_{ji}, \quad (6.5)$$

²but in principle not unique!

known under the name of “principle of detailed balance”. The matrix c_{ij} is uniquely determined using Eq. (6.5)

$$\Pi_\infty[i]T_{ij}^0 c_{ij} = \Pi_\infty[j]T_{ji}^0 c_{ji},$$

that means that the following condition must hold

$$\frac{c_{ij}}{c_{ji}} = \frac{\Pi_\infty[j]}{\Pi_\infty[i]}, \quad (6.6)$$

if it is possible to come back from the newly proposed state to the original one with the same probability

$$T_{ij}^0 = T_{ji}^0.$$

The ratio z of $\Pi_\infty[j]$ over $\Pi_\infty[i]$ is equal to

$$z \equiv \frac{\Pi_\infty[j]}{\Pi_\infty[i]} = \exp(-\beta(S[C_j] - S[C_i])),$$

imposing as solution the target quantum distribution. Supposing further that an element c_{ij} depends only on this ratio z

$$c_{ij} = F(z),$$

then from Eq. (6.6) the unknown function F has to satisfy the following relation

$$\frac{F(z)}{F(1/z)} = z.$$

There are many solutions to this functional equation, the two most important are

$$F(z) = \min(1, z), \quad (6.7)$$

that defines the “Metropolis” method and

$$F(z) = \frac{z}{1+z}, \quad (6.8)$$

that defines the “heat-bath” method.

6.3 Metropolis algorithm and Hybrid Monte Carlo

The Metropolis algorithm has been proposed many decades ago to study the equation of state of a classical gas of rigid spheres [54]. Many important

applications of the Metropolis algorithm have been found in spin system, classical and quantum fluid mechanics, statistical field theory and quantum mechanics. The core of the Metropolis method is the algorithm chosen to propose a new configuration. The spin of a single site can be randomly flipped for an Ising Z_N model, if the action of the new configuration is lower than the action of the old configuration, $\Delta S < 0$, then the spin flip is accepted. Otherwise a random number between zero and one is generated and if it is smaller than $\exp(-\Delta S)$ the new configuration is accepted, otherwise it is refused keeping the old configuration and proceeding to visit another site of the lattice.

A random change of one of the variable of a given configuration can be applied to all field models, for gauge theory the new link variables has to be generated with an uniform distribution with respect to the Haar measure. The Metropolis algorithm will effectively behaves as a sort of random walk exploring the configuration space. A random proposal can however become very inefficient especially near the continuum limit, when the correlation between distant point of the lattice appears as signal of the propagation of physical particle. In that case a random change regardless the state of the nearest neighbor is likely to be often refused. Further a change of a single site can become inefficient for models where the computation of the action has an high cost, like in theories with dynamical fermions, and a parallel change of many link variable would be feasible.

An improved algorithm is needed to provide a better new configuration to the Metropolis acceptance test. The microcanonical ensemble is generated by the uniform probabilistic weight given to all configurations with a given energy E considered as a control parameter. While the gauge coupling is an input parameter in the canonical ensemble, in the microcanonical ensemble it would become an observable as well as the mass of the particles. Practical simulations can be implemented in the microcanonical ensemble integrating numerically the equation of motion, assuming ergodicity, but numerical errors will slowly drive the simulation toward configurations with an energy far from the selected E . To solve this problem the idea is to combine both microcanonical steps in the canonical ensemble, that means to submit periodically the configuration to the metropolis step after a numerical integration of the equation of motion for a time of length t . This algorithm is called “Hybrid Monte Carlo” [57]. The numerical integrator of the equation of motion has to be chosen to be reversible and symplectic area preserving in order to satisfy the principle of detailed balance. A reversible integrator produces the same state if a numerical integration of time t and then of reversed time $-t$ is performed.

6.3.1 Hybrid Monte Carlo for lattice gauge theories

In relativistic quantum field theories the time is a dimension and not simply a parameter. Therefore an additional time dependence τ is added to the system, for example a link variable will be denoted as $U_\mu(\vec{x}, t, \tau) \equiv U_\mu(x, \tau)$. The fictitious time τ will parametrize the trajectory of the system in the phase space. The momenta are independent variables from the fields in the Hamiltonian formalism of classical mechanics, therefore the partition function can be multiplied by the quadratic Gaussian integral

$$\int \prod_{x,\mu} d\pi_\mu(x, \tau) \exp(-\text{Tr}(\pi_\mu(x, \tau)^\dagger \pi_\mu(x, \tau)))$$

and the free field $\pi_\mu(x, \tau)$ is interpreted as the canonical variable conjugate to the link $U_\mu(x, t)$. The whole partition function is

$$\begin{aligned} Z &= \int \prod_x d\lambda(x) \prod_\mu dU_\mu(x) d\pi_\mu(x, \tau) \exp \{ -H(\pi_\mu(x, \tau), U_\mu(x), \lambda(x)) \}, \\ H &= \text{Tr}(\pi_\mu(x, \tau)^\dagger \pi_\mu(x, \tau) + S_g(U_\mu(x)) + \bar{\lambda}(x) D_W[U_\mu(x)] \lambda(x), \end{aligned}$$

and H is the Hamiltonian. Since the variables $\pi_\mu(x, \tau)$ belong to the cotangent bundle and the links $U_\mu(x, \tau)$ are unitary matrices, then $\pi_\mu(x, \tau)$ is a traceless antisymmetric matrix in the Lie algebra $\mathfrak{su}(n)$

$$\pi_\mu(x, \tau) = \sum_{a=1}^{N_c^2-1} \pi_\mu(x, \tau)^a T_a.$$

The equation of motion for $U(x, \tau)$ simply reads

$$\frac{d}{d\tau} U_\mu(x, \tau) = \pi_\mu(x, \tau) U_\mu(x, \tau), \quad (6.9)$$

preserving carefully the order of the matrix multiplications. The equation of motion of the momenta $\pi_\mu(x, \tau)$ are

$$\frac{d}{d\tau} \pi_\mu(x, \tau) = -\frac{\partial}{\partial U_\mu(x, \tau)} (S_g(U_\mu) + S_f(U_\mu)) = -F, \quad (6.10)$$

but the derivative of the gauge and fermion action with respect to a gauge link has to be defined properly.

6.3.2 Derivative of a function with variables in a Lie group

To begin, it is worth to remember that a link variable $U_\mu^R(x)$ in representation R can be expanded as

$$U_\mu^R(x) = \exp(i\omega_a(x)T_R^a),$$

where $\exp(X)$ denote the exponential map. The T_R^a are the matrix generators for the representation R ; to switch the link to another representation R' only the generators have to be replaced

$$U_\mu^{R'}(x) = \exp(i\omega_a(x)T_{R'}^a),$$

while the parameters $\omega_a(x)$ are left unchanged. The same link can appear in different representation in the action. For instance, the links are in the fundamental representation for the gauge part of the action, while the same links are in the adjoint representation for the fermion part of the $\mathcal{N} = 1$ super Yang-Mills theory.

The derivative respect to the link variable of some function f of the gauge field $U_\mu^R(x)$ in the representation R is defined as

$$\mathcal{D}_{\mu'x'}f(U_\mu(x)) = \delta_{\mu,\mu'}\delta_{x,x'} \sum_a \frac{\partial}{\partial\omega_a} f(\exp(i\omega_a T_R^a)U_\mu^R(x)) \Big|_{\omega_a=0}, \quad (6.11)$$

which effectively represents the zero limit of the incremental ratio of f with respect to a variation preserving the group element structure of $U_\mu^R(x)$ [46].

The derivative of a link variable V in the adjoint representation A will be with this definition

$$\mathcal{D}_{\mu'x'c}V_\mu(x) = \delta_{\mu,\mu'}\delta_{x,x'} \frac{\partial}{\partial\omega_c} \exp(i\omega_a T_A^a)V_\mu(x) \Big|_{\omega_a=0} \quad (6.12)$$

$$= \delta_{\mu,\mu'}\delta_{x,x'} iT_A^c V_\mu(x) \quad (6.13)$$

$$\mathcal{D}_{\mu'x'c}V_\mu^\dagger(x) = -\delta_{\mu,\mu'}\delta_{x,x'} iV_\mu^\dagger(x)T_A^c \quad (6.14)$$

and similarly for the fundamental representation. A practical calculation of the derivative of the fermion action is performed in App. E.

6.3.3 Numerical solution of the equations of motion

The equation of motion (6.9) and (6.10) can be integrated numerically with a further discretization of the fictitious time τ in steps large ϵ . An update $\mathcal{U}_\pi(\epsilon)$ of the momenta is simply

$$\pi_\mu(x, \tau) \rightarrow \mathcal{U}_\pi(\epsilon)\pi_\mu(x, \tau) = \pi_\mu(x, \tau + \epsilon) = \pi_\mu(x, \tau) - \epsilon F,$$

keeping unchanged the links $U_\mu(x, \tau)$, while an update of the links $\mathcal{U}_U(\epsilon)$ is

$$U_\mu(x, \tau) \rightarrow \mathcal{U}_U(\epsilon)U_\mu(x, \tau) = U_\mu(x, \tau + \epsilon) = \exp(\epsilon\pi_\mu(x, \tau))U_\mu(x, \tau),$$

keeping the momenta fixed. The symbol “exp” denotes as usual the exponential map.

The simplest reversible scheme to numerically integrate the equations of motion can be constructed by the following chain of link and momenta updates

$$\mathcal{U}_\pi(\epsilon/2)\mathcal{U}_U(\epsilon)\mathcal{U}_\pi(\epsilon/2),$$

the specified final time $\tau_f = N\epsilon$ will be reached after N repetitions of this scheme. This integrator is called Leap-Frog and it converges toward the exact solution as $O(\epsilon^4)$. Many other numerical integrators are possible with a smaller discretization error.

6.3.4 Implementation of the Hybrid Monte Carlo algorithm

All the ingredients are now ready to finally implement the Hybrid Monte Carlo algorithm. A link configuration is generated for example randomly and the following steps are iterated starting from $k = 0$

1. Generate randomly with a Gaussian distribution the momenta $\pi_\mu(x, 0)$. Set the link to their initial configuration $U_\mu(x, 0) \equiv U_\mu(x)$. Measure the energy $E_i = H(\pi_\mu(x, 0), U_\mu(x, 0))$.
2. Integrate numerically the equations of motion for a time τ in N steps of ϵ length ($\tau = N\epsilon$), to produce a new configuration of links $U_\mu(x, \tau)$ and momenta $\pi_\mu(x, \tau)$. Compute the energy $E_f = H(\pi_\mu(x, \tau), U_\mu(x, \tau))$.
3. Accept or reject the new configuration $U_\mu(x, \tau)$ with probability

$$\min(1, \exp(E_i - E_f)).$$

Set the configuration $C_k = U_\mu(x, 0)$ or $C_k = U_\mu(x, \tau)$ accordingly and proceed to the next iteration $k = k + 1$.

The expectation value of an observable \mathcal{O} can be then computed as the mean

$$\langle \mathcal{O} \rangle \simeq \frac{1}{N} \sum_{k=k_0}^N \mathcal{O}(C_k),$$

for very large number of configurations N the starting point of the sum can be freely chosen to be $k_0 = 0$. However for finite N , it is better to skip

the first few configurations to give an adequate thermalization time to the system. An estimation of the number of configurations which have to be skipped can be done analyzing the autocorrelation time.

6.3.5 Autocorrelation time

The stochastic matrix T has one eigenvector equal to the equilibrium statistics corresponding to largest eigenvalue $\lambda_{\max} = 1$. This probability distribution is approached asymptotically for large number of steps at a rate depending on the second largest eigenvalue λ_2 . Supposing in fact to start the simulation always in the state C_1 , then the probability $\Pi_0[i]$ at $t = 0$ is

$$\Pi_0[i] = \delta_{i,1}$$

and the probability after n steps will be

$$\Pi_n[j] = (T^n)_{ji} \Pi_0[i] = (T^n)_{j1}. \quad (6.15)$$

The final result is more clear if the initial state is decomposed in eigenvectors

$$\Pi_0[i] = c_1 \Pi_\infty + c_2 v_2 + \sum_{k=3} c_k v_k, \quad (6.16)$$

so that it is possible to see that Π_∞ is reached at an exponential rate with a time constant $\tau = -\frac{1}{|\ln(\lambda_2)|}$

$$\begin{aligned} \Pi_n[j] &= (T^n)_{ji} \Pi_0[i] = c_1 \Pi_\infty + c_2 \lambda_2^n + \sum_{k=3} c_k \lambda_k^n v_k \\ &= c_1 \Pi_\infty + c_2 \exp \left\{ -n \left(-\frac{1}{|\ln(\lambda_2)|} \right) \right\} + O(n). \end{aligned} \quad (6.17)$$

The eigenvalue λ_2 determines also how much a configuration generated at the step k is correlated to the configuration at $k + n$. High correlation will result in poor exploration of the phase space and slow convergence of the sum (6.2). If λ_2 approaches the unity, than the thermalization time and the autocorrelation between two consecutive configurations will increase drastically.

The autocorrelation time can be measured from the connected correlator of observables separated by n steps

$$\langle \mathcal{O}(0) \mathcal{O}(n) \rangle_c = \frac{1}{N} \sum_k \mathcal{O}(k) \mathcal{O}(n+k) - \left(\frac{1}{N} \sum_k \mathcal{O}(k) \right)^2 \simeq \exp(-n\tau) \quad (6.18)$$

promoting effectively the Markov chain to a five dimensional theory, the four common spatial dimensions plus the Monte Carlo time. The Monte Carlo time has a physical dimension not necessarily equal to one; it contains information about how τ scales approaching the continuum limit $a \rightarrow 0$

$$\tau_R = \frac{\tau_B}{a^z}. \quad (6.19)$$

The critical coefficient z depends on the target quantum action, on the specifying update algorithm and especially on the topological properties of the model simulated. A random-walk Metropolis algorithm has a well-known classical $z = 2$, while the Hybrid Monte Carlo is characterized classically by $z = 1$. The HMC is therefore much more efficient than a standard random walk Metropolis algorithm. If there are different topological sectors, in the continuum limit they can act as a barrier because the whole configuration has to change discontinuously to modify the global topological properties. In this case z could be very large or even infinite, meaning that the five dimensional theory is non-renormalizable. To solve this problem it is possible for example to change to boundary conditions of fields from periodic to Dirichlet in the time direction, allowing the topological charge to flow through the boundaries [58, 59].

6.3.6 Errors in Monte-Carlo estimates

The equation (6.2) is only an approximation of the true expectation value $\langle \mathcal{O} \rangle$. It can be proven that the deviation of the Monte Carlo estimate from the true value scales as

$$\langle \mathcal{O} \rangle - \frac{1}{N} \sum_k \mathcal{O}(k) \sim O\left(\frac{1}{\sqrt{N}}\right), \quad (6.20)$$

meaning that errors slowly reduces at a rate independent from the dimension of the configuration space, i.e. the number of sites and links chosen to approximate the field theory. Quadrature method can converge faster, but the error will grow exponentially for large number of variables keeping fixed the number of configurations used.

A practical algorithm to estimate the error from a simulation is presented in App. B.

6.4 Majorana fermions on the lattice

Fermions are Grassmannian anticommuting variables and they cannot be represented by a real number on a computer. However, since fermions ap-

pear in the action only in the bilinear form, Majorana fermion field can be integrated out leaving the Pfaffian of the Dirac-Wilson operator

$$\int D\lambda(x) \exp \left(-\bar{\lambda}(x)(D_W + m)\lambda(x) \right) = \text{Pf}(C(D_W + m)) \quad (6.21)$$

as can be seen directly expanding the exponential and applying the rules for Grassmannian integration, see App. A. The Pfaffian of a matrix is proportional to the square root of the determinant, for the Dirac operator in the adjoint representation the Pfaffian is

$$\text{Pf}(C(D_W + m)) = \left(\prod_{\lambda_i \in \mathbb{R}} \lambda_i \right) \left(\prod_{\lambda_j \in \mathbb{C}} |\lambda_j| \right), \quad (6.22)$$

where the product over real or complex eigenvalues is considered without degeneracy. Due to the square root, naively Majorana fermions can be considered as “one half” flavor.

The Pfaffian can be positive or negative

$$\text{Pf}(M) = \text{sign}(\text{Pf}(M)) \sqrt{|\det(M)|}, \quad (6.23)$$

where the function

$$\text{sign}(\text{Pf}(CD_W)) = \begin{cases} 1 & : \text{Pf}(CD_W) \geq 0 \\ -1 & : \text{Pf}(CD_W) < 0 \end{cases} \quad (6.24)$$

is introduced for correctly handling the lost sign of the Pfaffian in the root of the square of the Dirac Wilson operator. This leads to the famous “sign problem” since a negative quantity cannot be interpreted as a Boltzmann weight. The Witten index of the $\mathcal{N} = 1$ super Yang-Mills theory is non-zero and naive arguments and practical observations suggest that the sign of the Pfaffian will be positive in the continuum limit, see Ref. [60]. At finite lattice spacing instead configurations with negative sign of the Pfaffian will appear as a lattice artefact approaching the chiral limit. The sign of the Pfaffian is inserted as a reweighting factor when computing in practical simulations at finite lattice spacing the expectation value of an observable

$$\langle \mathcal{O} \rangle = \frac{\sum_{i=1}^N \text{sgn}(C_i) \mathcal{O}(C_i)}{\sum_{i=1}^N \text{sgn}(C_i)}, \quad (6.25)$$

a severe sign problem will appear when $\sum_{i=1}^N \text{sgn}(C_i) \approx 0$ causing large fluctuations in above expression.

6.5 HMC algorithm for Majorana fermions

The computation of the square root of the determinant of the Dirac Wilson operator D_W is prohibitively expensive and it forbids a simple implementation of the Metropolis algorithm. A first manipulation can simplify the problem, considering that

$$\det(\gamma_5) = \det(C) = 1, \quad (6.26)$$

it is possible to rewrite the square root of the determinant as

$$\sqrt{|\det(M)|} = \det(\gamma_5) \sqrt{|\det(D_W)|} = \sqrt{|\det(\gamma_5 D_W)|} = \sqrt[4]{\det((\gamma_5 D_W)^2)},$$

since $\det(A)\det(B) = \det(AB)$. The matrix $(\gamma_5 D_W)^2 = D_H^2$ is Hermitian and it has positive eigenvalues, properties that can be used to write an effective action for Majorana fields that can be used in the Hybrid Monte Carlo method.

6.5.1 The R algorithm

A first attempt can use the formula

$$\det(M) = \exp \{ \text{tr}(\log(M)) \};$$

the partition function for $\mathcal{N} = 1$ SYM can be written as

$$Z = \int DU_\mu \text{sgn}(CD_W) \exp \left(-S_g + \frac{1}{4} \text{Tr} \{ \log((\gamma_5 D_W)^2) \} \right).$$

Considering the equations of motion, the derivative of the logarithm of a matrix has to be computed, leading to an expression

$$\frac{\partial}{\partial U_\mu(x)} \text{Tr} \{ \log((\gamma_5 D_W)^2) \} = 2 \text{Tr} \left\{ (\gamma_5 D_W)^{-2} \frac{\partial((\gamma_5 D_W)^2)}{\partial U_\mu(x)} \right\}$$

in which appears the inverse of the square of the Dirac-Wilson operator. The inverse of the Dirac-Wilson operator can be estimated using noise techniques, leading to the “R algorithm” [61]. A set of N random vectors $\phi_n(x)$, for example Gaussian, chosen to fulfill the conditions

$$\begin{aligned} \langle \phi_n(x) \rangle &= \sum_n \phi_n(x) = 0 \\ \langle \phi_n(x)^\dagger \phi_n(y) \rangle &= \frac{1}{N} \sum_n \phi_n(x)^\dagger \phi_n(y) = \delta_{xy}, \end{aligned}$$

can be used to approximate the inverse in the large N limit with

$$(\gamma_5 D_W)^{-1}(x, y) \approx \frac{1}{N} \sum_n \eta_n(x)^\dagger \eta_n(y)$$

if the vector $\eta_n(y)$ is the solution of the linear system

$$(\gamma_5 D_W) \eta_n = \phi_n, \quad (6.27)$$

so that

$$\begin{aligned} \frac{1}{N} \sum_n \eta_n(x)^\dagger \eta_n(y) &= (\gamma_5 D_W)^{-1}(x, z) (\gamma_5 D_W)^{-1}(w, y) \langle \phi_n(z)^\dagger \phi_n(w) \rangle \\ &= (\gamma_5 D_W)^{-1}(x, z) (\gamma_5 D_W)^{-1}(w, y) \delta_{z,w} = (\gamma_5 D_W)^{-2}(x, y), \end{aligned}$$

in the limit $N \rightarrow \infty$. The linear system of Eq. (6.27) can be solved efficiently with Krylov space methods, see Ch. 8. However the fermion force is only approximated and therefore the reversibility of the numerical trajectory can fail. The results obtained has to be extrapolated to zero integration step size ϵ to give a result free of systematic errors.

6.5.2 The RHMC algorithm

An exact algorithm can be constructed if instead a Gaussian approximation

$$\frac{1}{\det A} = \int D\phi(x) D\phi^\dagger(x) \exp \{ -\phi^\dagger(x) A(x, y) \phi(y) \}$$

is used directly for the determinant and not for only the force. The above expression converge for complex vectors $\phi(x)$ if the matrix A has positive real eigenvalues. The fermion action is written as

$$\begin{aligned} \sqrt[4]{\det(D_H^2)} &= \frac{1}{\det((D_H^2)^{-1/4})} \\ &= \int D\phi D\phi^\dagger \exp \{ -\phi^\dagger(x) ((D_H^2)^{-1/4})(x, y) \phi(y) \} \quad (6.28) \end{aligned}$$

and the fields $\phi(x)$ are called pseudofermions. They are generated at the beginning of the classical trajectory and not considered as dynamical variables.

Sampling the distribution (6.28) is straightforward, since the pseudofermion partition function is invariant under an invertible matrix transformation $\phi'(x) = M(x, y) \phi(y)$. First generate a complex random vector $\psi(x)$ with entries Gaussian distributed, then set $\phi(x)$ to

$$\phi(x) = ((D_H^2)^{1/8})(x, y) \psi(y). \quad (6.29)$$

The problem is how to compute the matrix $((D_H^2)^{1/8})(x, y)$. To this end a rational approximation of $x^{1/8}$ of the form

$$x^{1/8} = \sum_k \frac{c_k}{x + b_k} \quad (6.30)$$

is introduced, the determination of the coefficients c_k and b_k is left to the Remez algorithm discussed in App. D. Solving the Dirac equation for many different shifts

$$(D_H^2 + b_k)\eta_k = \psi, \quad (6.31)$$

allows to compute the expression (6.29) as

$$\phi(x) = \sum_k c_k \eta_k,$$

with an error that depends only on the precision of the solution of the linear system (6.31) and of the approximation (6.30) [62].

The force generated by the equation of motion can be computed if $((D_H^2)^{-1/4})(x, y)$ is expressed as new rational approximation of the form (6.30), leading to the Rational Hybrid Monte Carlo (RHMC). The alternative would be the PHMC, that uses a polynomial approximation, see App. E. The derivative of a single term of the rational approximation is

$$\frac{\partial}{\partial U_\mu(x)} \left\{ \phi^\dagger \frac{c_k}{D_H^2 + b_k} \phi \right\} = c_k \eta_k^\dagger \frac{\partial(D_H^2 + b_k)}{\partial U_\mu(x)} \eta_k, \quad (6.32)$$

if η_k is the solution of the equation (6.31) with the appropriate b_k coefficient. The derivative of the Dirac-Wilson operator is computed in App. E.

The steps of the RHMC are then iterated starting from $k = 0$

1. Generate randomly with a Gaussian distribution the momenta $\pi_\mu(x, 0)$ and a random vector $\psi(x)$. Set the link to their initial configuration $U_\mu(x, 0) \equiv U_\mu(x)$. Set the pseudofermion field to

$$\phi(x) = ((D_H[U_\mu(z, 0)]^2)^{1/8})(x, y)\psi(y), \quad (6.33)$$

where $D_H[U_\mu(z, 0)]$ is the Dirac-Wilson operator evaluated on the link field $U_\mu(z, 0)$. Measure the energy

$$E_i = H(\pi_\mu(x, 0), U_\mu(x, 0)) + \psi^\dagger(x)\psi(x).$$

2. Integrate numerically the equations of motion for a time τ in N steps of ϵ length ($\tau = N\epsilon$), keeping constant the pseudofermions, to produce a new configuration of links $U_\mu(x, \tau)$ and momenta $\pi_\mu(x, \tau)$. Compute the energy

$$E_f = H(\pi_\mu(x, \tau), U_\mu(x, \tau)) + \phi^\dagger(x)((D_H[U_\mu(z, \tau)]^2)^{-1/4})(x, y)\phi(y).$$

3. Accept or reject the new configuration $U_\mu(x, \tau)$ with probability

$$\min(1, \exp(E_i - E_f)) .$$

Set the configuration $C_k = U_\mu(x, 0)$ or $C_k = U_\mu(x, \tau)$ accordingly and proceed to the next iteration $k = k + 1$.

6.6 The WRHMC algorithm

The density of the eigenvalues near the origin increases for small quark masses. As consequence the inverse of the operator D_H^2 is dominated by the low modes and the linear system (6.31) gets close to the point $\det(D_H^2) \approx 0$ where a (unique) solution does not exist. The force of the fermion action depends on the inverse of the Dirac-Wilson operator and it will be dominated by the large fluctuations of eigenvectors corresponding to the near-zero eigenvalues.

Near-zero eigenvalues control the infrared physics which is changed only a little following a classical trajectory in the phase space. This observation provides the nice idea to separate the numerical integration of the ultraviolet from the infrared modes, in order to speedup the acceptance rate, the running time and the stability of the RHMC. This technique has been widely employed in recent lattice simulations, see for example [63]. In this section the method of Ref. [64] is applied to the RHMC, implementing a new algorithm that one could call “WRHMC” (Weighted Rational Hybrid Monte Carlo).

6.6.1 Multiple time scales

If the total Hamiltonian is the sum of several contributions

$$H_T(q, p) = H_0(q, p) + H_1(q, p) + H_2(q, p) + \dots , \quad (6.34)$$

it could be that some of the H_n ($n < q$) are computationally simple to integrate while the others not. A large decrease of the computational demand and of numerical integration errors can be achieved if in addition the forces defined by the Hamiltonians H_n

$$F_n = \frac{\partial H_n(p, q)}{\partial q} , \quad (6.35)$$

generate a separation of scales, in the sense that they can be ordered by increasing magnitude

$$\|F_n\| > \|F_{n+1}\| . \quad (6.36)$$

Sexton and Weingarten proposed a scheme to integrate better the force F_k with a step size ϵ inversely proportional to the magnitude $\|F_n\|$. Supposing for simplicity an Hamiltonian with two terms

$$H_T(q, p) = H_0(q, p) + H_1(q, p), \quad (6.37)$$

such that $\|F_0\| > \|F_1\|$, two different step sizes ϵ_0 and ϵ_1 are introduced for the numerical integration of the equations of motion of H_0 and H_1 . ϵ_0 and ϵ_1 are required to satisfy further the condition $\epsilon_1/\epsilon_0 = N$, with N integer. The updates of links and momenta are ordered such that the force F_0 is integrated precisely with N more steps

$$\mathcal{U}_\pi^1(\epsilon_1/2) \left\{ \mathcal{U}_\pi^0(\epsilon_0/2) \mathcal{U}_U(\epsilon_0) \mathcal{U}_\pi^0(\epsilon_0/2) \right\}^N \mathcal{U}_\pi^1(\epsilon_1/2),$$

where

$$\begin{aligned} \mathcal{U}_\pi^1(\epsilon) \pi_\mu(x, \tau) &= \pi_\mu(x, \tau) - \epsilon F_1, \\ \mathcal{U}_\pi^0(\epsilon) \pi_\mu(x, \tau) &= \pi_\mu(x, \tau) - \epsilon F_0. \end{aligned}$$

The ratio ϵ_1/ϵ_0 is usually tuned to

$$\frac{\epsilon_1}{\epsilon_0} = \frac{\|F_0\|}{\|F_1\|}$$

and it requires to have a rough estimate of the magnitudes $\|F_0\|$ and $\|F_1\|$.

6.6.2 Separation of scales in RHMC

The action for the $\mathcal{N} = 1$ super Yang-Mills theory on the lattice is ready for a first application of the separation of different time scales, if H_0 is set to the gluon action and H_1 to the fermion action. The computation of the gluino force requires expensive linear systems to be solved, while the gluon force has a larger magnitude and it is simple to be evaluated.

Further improvements are possible by a separation of ultraviolet and infrared modes of the Dirac-Wilson operator. To this end, a weight function $w(x)$ is introduced, like for example simply

$$w(x) = x,$$

to require to the Remes algorithm a better precision of the rational approximations of $x^{-1/4}$ for the eigenvalues far from the origin. The coefficients b_k obtained from a weighted rational approximation are different from the one when $w(x) = 1$, in particular the minimal shift b_k is usually several orders of

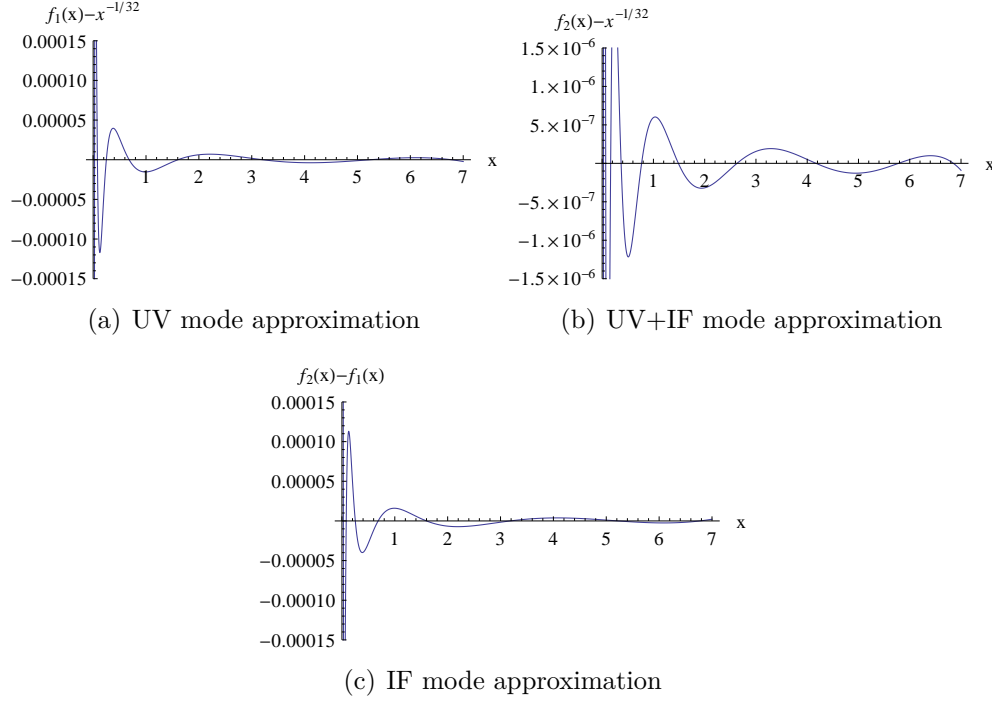


Figure 6.1: Plot of the rational approximations used to separate the force in ultraviolet and infrared part.

magnitude larger. Since the convergence to the solution of (6.31) is dictated by the smallest shift b_k , this implies a very fast computation of the force.

Three different Hamiltonians are therefore used for the HMC. H_0 is simply the gluon action, while H_1 and H_2 are coming from the split of the Dirac operator. H_1 is the fermion action generated by the approximation f_1 of $x^{-1/4}$ using $w(x) = x$, while H_2 is the action generated by the residual difference between f_2 and f_1 , the former being the approximation of $x^{-1/4}$ using $w(x) = 1$. Additional practical evaluations shows that the force coming from H_1 is already several time larger than the force generated by H_2 , therefore a three level integration scheme based over the separation of scales leads approximately to a factor three of speedup.

A practical demonstration of the idea of the algorithm is shown in Fig. 6.1, assuming the use of determinant breakup (see Sec. 6.7.2). In Fig. 6.1(a) is shown a plot of the “ultraviolet approximation” of $x^{-1/32}$, i.e. a rational functional

$$f_1(x) = \frac{0.0320359}{x + 0.446146} + \frac{0.285421}{x + 4.05823} + \frac{676.638}{x + 736.271} + \frac{0.00376429}{x + 0.0328166} \quad (6.38)$$

which approximates precisely f for $x \gtrsim 1$. In Fig. 6.1(b) is shown a plot of

the rational approximation $f_2(x)$ of $x^{-1/32}$

$$f_2(x) = \frac{0.00045153}{x + 0.00510132} + \frac{0.00287559}{x + 0.0433161} + \frac{0.0142944}{x + 0.260406} + \frac{0.0676906}{x + 1.34216} \\ + \frac{0.47533}{x + 7.87664} + \frac{1087.97}{x + 1203.89} + \frac{0.0000414535}{x + 0.000277322} \quad (6.39)$$

which is precise both in the “ultraviolet” and in the “infrared”, i.e. for $x \gtrsim 0$. The first function f_1 is used to approximate the ultraviolet modes of the Dirac Wilson operator, while $f_2(x) - f_1(x)$ is used as correction factor which effectively operates only in the infrared modes of the Dirac Wilson operator (as it can be seen from Fig. 6.1(c), the function $f_2(x) - f_1(x)$ is different from zero only when $x \lesssim 1$). The separations of scales can be accomplished integrating the action coming from $f_1(x)$ more precisely than the action coming from $f_2(x) - f_1(x)$, which depends on the infrared modes only slowly changing during a classical trajectory. Notice that the smallest number in the denominators of (6.38) is much larger than the smallest coefficient in the denominator of (6.39) ($0.03 > 0.00027$), this implies a faster convergence for $f_1(x)$ of the multishift solver and a cheap evaluation of the ultraviolet force.

6.7 Tools for Monte Carlo simulations

6.7.1 Improved integrators

Leap-frog integrators have a numerical discretization error of order $O(\epsilon^4)$, other high order schemes can further reduce the error to $O(\epsilon^6)$, $O(\epsilon^8)$ or even smaller. However these schemes increase in complexity requiring a huge computational cost. They suffer also of numerical instability, the final error can even diverge quite rapidly if the step size ϵ is not small enough.

To solve this problem Omelyan *et al.* proposed an algorithm aim to reduce the relative size of the error $O(\epsilon^4)$, but not its scaling [65]. General benefits of this approach are larger step size ϵ with the same numerical error and stability of leap-frog and only a little larger numerical effort. An example of such an integrator is

$$\mathcal{U}_\pi(\lambda\epsilon)\mathcal{U}_U(\epsilon/2)\mathcal{U}_\pi((1-2\lambda)\epsilon)\mathcal{U}_U(\epsilon/2)\mathcal{U}_\pi(\lambda\epsilon),$$

where $\lambda \approx 0.193$ is a parameter that can be tuned such that the size of the error $O(\epsilon^4)$ is minimal. An Omelyan integrator can be combined with multiple time scales schemes and in general it provides an integration of the classical trajectory three time longer than the unimproved leap-frog with the same numerical error [66].

6.7.2 Determinant breakup

The condition number c of an operator is defined as the ratio between the largest and the smallest eigenvalue (in modulus)

$$c = \frac{\lambda_{\max}}{\lambda_{\min}}.$$

A large condition number occurs when $\lambda_{\min} \rightarrow 0$ and it signals a near singular matrix. In other words, a large condition number is the origin to the difficulties in solving large linear systems with iteration methods.

The action of the gluino can be split in N equal pieces, noticing that the determinant can be factorized as

$$\sqrt[4]{\det(D_H^2)} = \left(\sqrt[4N]{\det(D_H^2)} \right)^N.$$

Each term $\sqrt[4N]{\det(D_H^2)}$ of the product is exponentiated and associated to an independent pseudofermion field. The resulting condition number c_N of the operator $(D_H^2)^{-1/4N}$ in one term of the action

$$S_f^i = \phi_i^\dagger(x)(D_H^2)^{-1/4N}(x, y)\phi_i(y)$$

is simply N -root of the original condition number c_1 of $(D_H^2)^{-1/4}$. Since $c_n = (c_1)^{1/N} < c_1$, the calculation of the force of S_f^i is cheaper and fluctuations are reduced. Near the critical point, the gluino action is factorized in many pieces to take advantage from the determinant breakup.

6.7.3 Twisted mass as parameter to regularize the RHMC

As stated before, the Dirac-Wilson operator becomes ill conditioned when κ is closer to its critical value κ_c and near zero mode start to proliferate. The Krylov space solver fails to converge and the rational approximations cannot be computed anymore with accuracy. The heatbath and metropolis step will be plagued by a systematic error almost impossible to correct and the observables will be not anymore distributed accordingly to the correct probability weight.

Many solutions have been found for reducing this problem, based on the properties of the near zero mode of the Dirac-Wilson operator. A basic idea is to regularize the square of the Hermitian Dirac-Wilson operator D_H^2 introducing a factor μ^2

$$\det(D_H^2) = \det(D_H^2 + \mu^2) \left(\frac{\det(D_H^2)}{\det(D_H^2 + \mu^2)} \right) \quad (6.40)$$

and considering determinant inside the bracket as a global correction step for the metropolis [67]. The value of μ has to be tuned to optimize the acceptance rate and the speedup given to the Krylov space solver. If μ is closed to zero then the ratio of the determinant will be almost equal to one and a good acceptance rate can be achieved. On the other hand, any larger value of μ will improve the convergence rate of the Arnoldi methods.

The RHMC algorithm can be therefore written as

1. Start from a configuration $\{U_{\text{OLD}}\}$ and propose a new configuration $\{U_{\text{NEW}}\}$ distributed accordingly to

$$\sqrt[4]{D_H^2 + \mu^2} \exp(-S_g) .$$

The RHMC trajectory and the Krylov space solver will be regularized by the positive shift introduced by μ^2 .

2. Accept or reject the new configuration with probability $P \equiv P(\{U_{\text{OLD}}\} \rightarrow \{U_{\text{NEW}}\})$

$$P = \min \left(1, \sqrt[4]{\frac{\det(D_H^2(U_{\text{NEW}})) \det(D_H^2(U_{\text{OLD}} + \mu^2))}{\det(D_H^2(U_{\text{OLD}})) \det(D_H^2(U_{\text{NEW}} + \mu^2))}} \right) . \quad (6.41)$$

The shift introduced in Eq. (6.40) on the action is effectively equivalent to introduce a “twisted mass” to the fermion action

$$D_W^T = D_W + i\mu\gamma_5 ,$$

proportional to γ_5 . Since a global reweighting is done at the end, the twisted mass can be simply considered a trick to regularize the RHMC.

The ratio of the determinants (6.41) can be evaluated stochastically. Using the properties of Gaussian integrals

$$\frac{\det(D_H^2 + \mu^2)}{\det(D_H^2)} = \int d\phi d\phi^\dagger \exp \left\{ -\phi^\dagger (D_H^2) (D_H^2 + \mu^2)^{-1} \phi \right\}$$

Adding and removing a quadratic free term $\phi^\dagger \phi$

$$\frac{\det(D_H^2 + \mu^2)}{\det(D_H^2)} = \int d\phi d\phi^\dagger \exp \left\{ -\phi^\dagger (D_H^2) (D_H^2 + \mu^2)^{-1} \phi + \phi^\dagger \phi - \phi^\dagger \phi \right\} ,$$

it is possible to write the ratio of the determinants as

$$\frac{\det(D_H^2 + \mu^2)}{\det(D_H^2)} = \left\langle \exp \left\{ -\phi^\dagger (D_H^2) (D_H^2 + \mu^2)^{-1} \phi + \phi^\dagger \phi \right\} \right\rangle_{\text{gauss}}$$

It can be proven that this formula converges if the minimal eigenvalue λ_{\min} of $(D_H^2)(D_H^2 + \mu^2)^{-1}$ is bigger than 0.5.

Therefore the following two steps are needed to evaluate the ratio of the determinants for the global metropolis step

1. Generate a random complex vector ϕ Gaussian distributed. Compute

$$\chi = (D_H^2 + \mu^2)^{-1} \phi,$$

using a conjugate gradient solver and set ρ_1 to

$$\rho_1 = \phi^\dagger \phi - \phi^\dagger D_H^2 \chi.$$

2. Repeat step 1 a sufficient number M of time and return the fourth root of the average as estimate of the ratio of the determinants

$$\sqrt[4]{\frac{\det(D_H^2 + \mu^2)}{\det(D_H^2)}} = \sqrt[4]{\frac{1}{M} \sum_i \rho_i}.$$

It can be shown that the algorithm is correct and satisfies the principle of detailed balance for every choice of the number of noise vector M . However, a small number of noise vector can give fluctuating estimation which drastically reduce the acceptance rate of Eq. (6.41), the parameter M has therefore to be tuned directly during the simulation.

To further reduce the impact of the fluctuations on the final acceptance rate it is possible to use again the idea of “determinant breakup”, factorizing the ratio to compute as

$$\left(\sqrt[4]{\frac{\det(D_H^2 + \mu^2)}{\det(D_H^2)}} \right)^{\frac{1}{N}}$$

and repeating the metropolis step a number N of time.

Global correction steps are affected by problems concerning the scaling of the acceptance rate as a function of the volume. As the volume increases, the fluctuations of the ratio of the determinants could increase proportionally and thus lead to a bad acceptance rate. The shift μ has a strong influence only over the smallest eigenvalues of D_H^2 . However, it has been suggested and numerically found that the lowest eigenvalues have a mild fluctuations when the volume increase. Therefore it can be possible to apply a twisted mass global reweighting also for large volume.

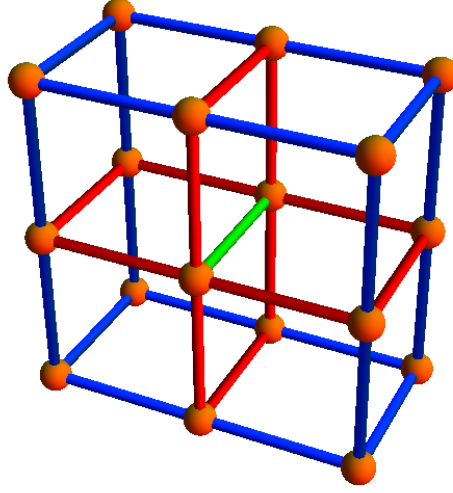


Figure 6.2: The green link is smeared using the red links.

6.7.4 Smearing

Smearing is a standard technique for reducing the fluctuations of the gauge field and improving both rotational symmetry and chiral symmetry. A single link is effectively smeared averaging it with respect to its nearest neighbors. The matrix Ω is the sum of the product of the links of the plaquettes with the link $U_\mu(x)$

$$\Omega = \sum_{\nu} \left(U_\nu(x + \mu) U_\mu(x + \nu)^\dagger U_\nu(x)^\dagger + U_\nu(x + \mu - \nu)^\dagger U_\mu(x - \nu)^\dagger U_\nu(x - \nu) \right),$$

see Fig. 6.2. The link $U_\mu(x)$ can be smeared as $U_\mu(x)\Omega$, but a projection is required since the sum of special unitary matrices is not anymore special unitary. A simple Gram-Schmidt orthogonalization does the job, but this projection is not invertible.

A “differentiable smearing” is analytical in respect to the ω_a variables of the links and it is strictly required for a well defined force in the HMC dynamics. A possible approach would be

$$U_{\text{NEW}} = \frac{X}{\sqrt{X^\dagger X}}$$

where $X = \Omega U_{\text{OLD}}$ and the square root of the matrix must be implemented as some polynomial/rational approximation. This matrix would be automatically special unitary.

Another way is to consider

$$U_{\text{NEW}} = \exp \left(\frac{1}{2}(\Omega^\dagger - \Omega) - \frac{1}{N_c} \text{Tr}(\Omega^\dagger - \Omega) \mathbf{1} \right) U_{\text{OLD}}.$$

Since the exponential map is analytical, the whole map is differentiable. In particular

$$\exp(M) = \sum_{n=0}^{\infty} \frac{M^n}{n!} \quad (6.42)$$

The whole expression can be simplified if we use the Caley-Hamilton theorem, “every matrix $n \times n$ is a zero of its characteristic polynomial”

$$P_M(M) = 0 \quad (6.43)$$

$$M^n = \sum_{i=0}^{n-1} c_i M^i \quad (6.44)$$

The formula (6.44) allows a reduction of the infinite sum in the exponential map, only powers $i \leq n$ will effectively appear in the expansion

$$\exp(M) = \sum_{i=0}^{n-1} c_i M^i$$

with coefficients c_i which are not constant and depend on the matrix M .

Smearing in this form can be used to reduce the fluctuations in the Hybrid Monte Carlo algorithm, it can be also used along a spatial slice of the lattice to remove the excited states contributions from the correlator of a physical particle.

6.8 Testing the implementation of HMC algorithm

The HMC for Majorana fermions is quite complex and coding error can unfortunately easily happen. Some trick or identities are required to check the correctness of the final implementation.

A first simple check of reversibility can test the correct implementation of the numerical integrator. A configuration is generated with a numerical integration of the classical trajectory for a time-length t , then the time is reversed and a new integration for a time-length $-t$ is performed. If the algorithm is correct, at this point both the momenta and the link fields must be equal to their original configurations.

ϵ	N_{step}	$\langle \exp(\Delta H) \rangle - 1$
0.025	5	-0.0003(150)
0.05	5	0.009(110)
0.075	5	0.11(37)
0.1	5	0.56(1.23)
0.125	5	2.6(6.4)
0.15	5	11(33)
0.2	5	270(1800)

Table 6.1: Test of the Creutz equality on a lattice $4^3 \times 8$ of RHMC for $SU(2)$ SYM. All the values are compatible with zero within the errors.

The Creutz equality,

$$\langle \exp(-\Delta H) \rangle = 1, \quad (6.45)$$

provides an another useful test of the correctness of the implementation of algorithm. ΔH is the difference of the Hamiltonian from the beginning at the end of the classical trajectory in phase space. The Creutz equality follows from the observation that if a configuration C is generated with a probability distribution function

$$P(C) = \frac{1}{Z} \exp(-S(C)),$$

then the expectation value of the ratio between two probabilities is one

$$\begin{aligned} 1 &= \left\langle \frac{P(C)}{P(C')} \right\rangle = \langle \exp \{(-S(C) + S(C'))\} \rangle \\ &= \langle \exp(-\Delta H) \rangle, \end{aligned}$$

due to the probability normalization. An example test of the equality is shown in Tab. 6.1.

For large enough volume the acceptance rate of the Metropolis algorithm should scale as

$$P_{\text{acc}} = \text{erfc} \left(\frac{\sqrt{\langle \Delta H \rangle}}{2} \right),$$

where “erfc” is the complementary error function. Notice that due to the Creutz equality in general $\langle \Delta H \rangle \geq 0$ (Jensen’s inequality). A plot to verify this scaling is shown in Fig. 6.3. The last possibility is to check directly the $O(\epsilon^4)$ scaling of the error of the leap-frog, as shown in Fig. 6.4.

The force corresponding to the fermion action has many terms acting in color, spin and real space. A correct analytical implementation can be hard especially if the clover improved Dirac-Wilson operator is employed. However

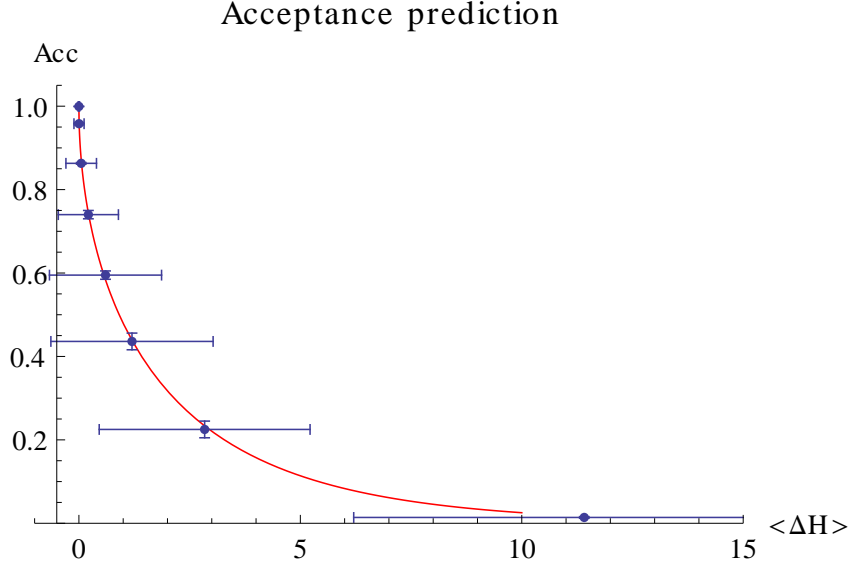


Figure 6.3: Acceptance scaling vs. $\langle \Delta H \rangle$ on a lattice $4^3 \times 8$.

a mismatch between the action and the force can be easily detected. The force can be evaluated in fact using only the knowledge of the action $S[U](x)$

$$d_a(\omega_a) = \frac{S[\exp(i\omega_a\tau^a)U](x) - S[\exp(-i\omega_a\tau^a)U](x)}{2\omega_a},$$

so that the limit can be performed numerically

$$F = \sum_a \left(\lim_{\omega_a \rightarrow 0} d_a(\omega_a) \tau^a \right).$$

To final test the correct normalization of the clover term, β and κ can be set to zero keeping κc_{sw} finite [68]. In this limit for $SU(3)$ with fundamental fermions a perturbative expansion of the plaquette expectation value is known up to $O(c_{sw}^2)$

$$\langle P \rangle = -\frac{c_{sw}}{12} \left(1 + \frac{475}{384} c_{sw} \right),$$

the comparison with a Monte Carlo simulation is shown in Fig. 6.5.

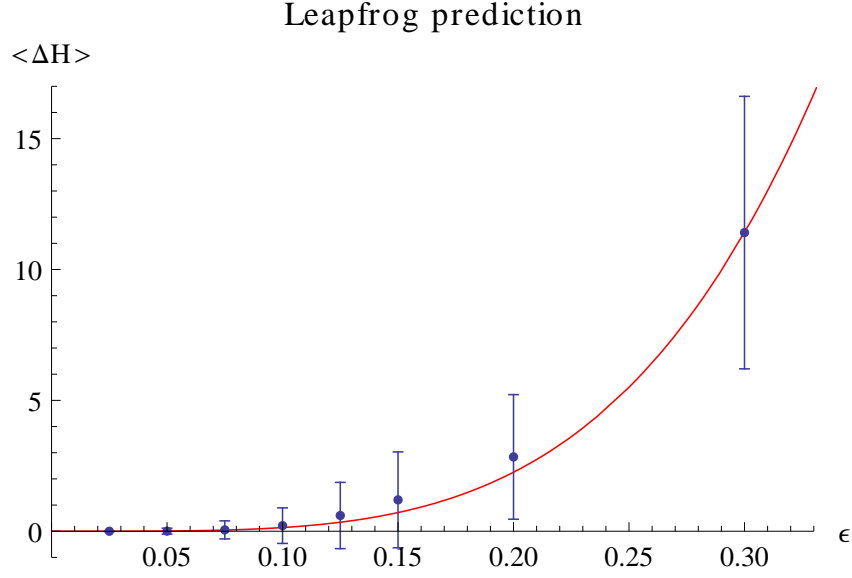


Figure 6.4: $\langle \Delta H \rangle$ as a function of the step size ϵ on a lattice $4^3 \times 8$.

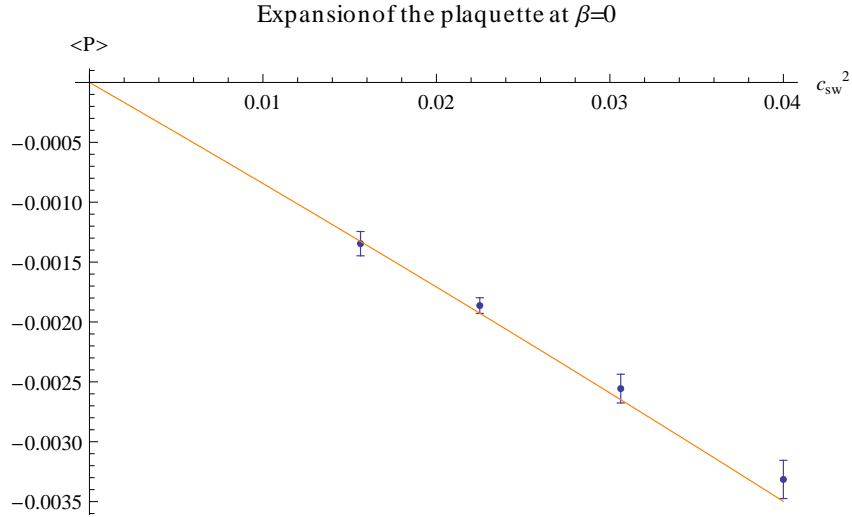


Figure 6.5: Comparison between Monte Carlo simulation and perturbative expansion of the plaquette on a lattice 8^4 .

Chapter 7

Scale setting in lattice super Yang-Mills theory

The present status provokes the questions: How well do we control our computations? Is our data ready for a continuum extrapolation?

Rainer Sommer [69]

All the observables measured on the lattice are dependent on the lattice spacing a and on the bare couplings of the action, like g or the gluino mass m . The lattice spacing is the only dimensional quantity present on the lattice regularized theory. For instance, it is possible to measure from a Monte Carlo simulation the correlation length ξ of an operator Φ for a given gauge coupling g and gluino mass m , by fitting the exponential decay of the form

$$\langle \Phi(0)\Phi(t) \rangle \simeq \exp\left(-\frac{t}{\xi}\right)$$

in terms of the free parameter ξ for large distances t . This result reads that the correlation length for that given gauge coupling g and gluino mass m is equal to ξ lattice spacings. The excitations of the field Φ will have then an associated mass M_Φ equal to

$$M_\Phi = \frac{1}{a\xi(\beta, m)} \equiv \frac{f(\beta, m)}{a},$$

dependent on β and κ .

The term “scale setting” refers to a procedure to give a value to the lattice spacing a in physical units like fermi or femtometers, or equivalently to give a physical value to the mass M_Φ for example in MeV.

7.1 Renormalization group equations

The starting point is to observe that in the continuum limit the mass M_Φ cannot be dependent on the unphysical cut-off a used to regularize the theory, therefore

$$\frac{d}{da} M_\Phi = \frac{d}{da} \frac{f(g, m)}{a} = 0.$$

Expanding this equation yields

$$\frac{d}{da} \frac{f(g, m)}{a} = 0 = -\frac{f(g, m)}{a^2} + \frac{1}{a^2} \left(a \frac{df(g, m)}{dg} \frac{dg}{da} + a \frac{df(g, m)}{dm} \frac{dm}{da} \right) \quad (7.1)$$

and nontrivial solutions exist, if and only if the gauge coupling g depends on the lattice spacing a , $g \equiv g(a)$, meaning that the gauge coupling changes varying the scale where it is measured. The gauge coupling g for the $\mathcal{N} = 1$ SYM in four dimensions, being dimensionless, can depend on the scale a only through a dimensionless functional relation of the form

$$g \equiv g(a\Lambda)$$

where Λ is a physical quantity with the dimension of a mass absent in the classical theory and generated by the quantum fluctuation via trace anomaly [70]. A theory is said to be renormalizable if the explicit dependence on the ultraviolet cut-off a can be reabsorbed by the “running” of the gauge coupling g (or also by the other couplings and parameters if any).

The expression

$$\beta(g) = -a \frac{d}{da} g(a\Lambda) = -\frac{d}{d \ln(a)} g(a\Lambda)$$

is called Callan-Symanzik β -function and it tells how the gauge coupling changes for a variation of the cut-off a .¹ The β -function can be computed in a perturbative expansion

$$\beta(g) = -b_0 g^3 - b_1 g^5 + \dots$$

and the first two coefficients are independent from the scheme chosen for the calculation. The β -function is known exactly from instanton calculation in the special case of the pure Super Yang-Mills theory based on the gauge group $SU(N_c)$

$$\beta(g) = \frac{g^3}{16\pi^3} \frac{(\mathcal{N} - 4)N_c}{1 - \frac{N_c g^2 (2 - \mathcal{N})}{8\pi^2}},$$

¹Here β has not to be confused with the inverse of the square of the gauge coupling.

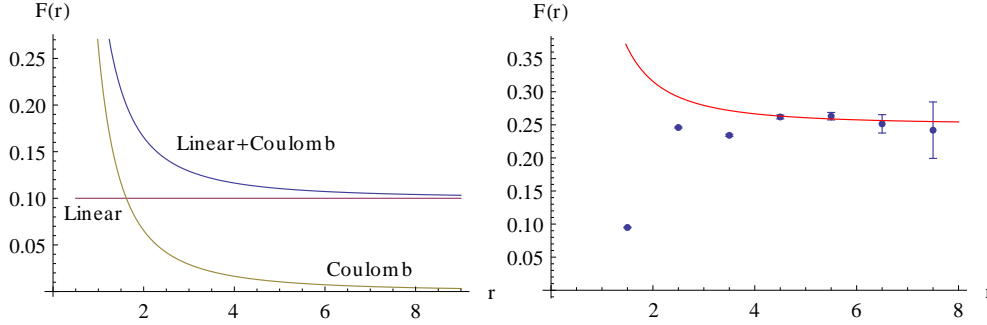


Figure 7.1: Left: Force between static quarks as a sum of a linear confining and a Coloumb term. Right: Calculation of the force on a lattice 16^4 with $\beta = 1.65$ and $\kappa = 0.1600$, $a^2\sigma = 0.250$. Smearing is applied to improve the signal, but it introduces deviations from the expected behavior for small distances.

the result is called Novikov-Shifman-Vainshtein-Zakharov (NSVZ) β -function. The first two coefficients are universal, i.e. scheme independent. When the number of supercharges is equal to four, then the β -function vanishes exactly to all-order in perturbation theory: the coupling does not run and $\mathcal{N} = 4$ SYM is a conformal theory without a mass-gap. For $\mathcal{N} = 1$ instead the functional relation

$$\frac{dg(a\Lambda)}{d\ln(a)} = \frac{g^3}{16\pi^2} \frac{3N_c}{1 - \frac{N_c g^2}{8\pi^2}}$$

can be solved and inverted to give the lattice spacing dependence as a function of the gauge coupling

$$a(g) = \frac{1}{\Lambda} \exp\left(-\frac{8\pi^2}{3N_c g^2}\right).$$

The lattice spacing $a(g)$ vanishes when the gauge coupling approaches zero and therefore $\mathcal{N} = 1$ SYM is asymptotically free. The continuum limit correspond to the limit $g \rightarrow 0$.

7.2 Useful observables to set the scale on the lattice

The knowledge of the value of lattice spacing a is crucial for converting all the measured quantities in physical units to test the agreement with the experimental data or simply to compare results between different actions.

Therefore to set scale it should be chosen an observable easy to determine with accurate precision on the lattice and affected by few systematical errors, that otherwise would disastrously propagate to all the physical predictions done by Monte Carlo simulations. During the last two decades, in particular three of them have been successfully tested for many different theories: the Sommer parameter r_0 and the Wilson flow scales t_0 and w_0 . The latter will be discussed in the following sections.

The Sommer scale r_0 and the string tension σ are pure gluonic observables in the sense that require the computation of the expectation value of Wilson loop $W(R, T)$. The potential between two static quark-antiquark pair in the fundamental representation is

$$V(R) = - \lim_{T \rightarrow \infty} \log \left(\frac{W(R, T)}{W(R, T+1)} \right)$$

In a confining theory, at large distance the potential has an expansion of the form

$$V(R) \simeq \sigma R + \frac{c_1}{R} + \frac{c_2}{R^2} + \dots$$

where σ is a parameter called “string tension” with the dimension of the square of a mass ($[\sigma] = [M^2]$). The string tension can be used to set the scale, but it assumes a linear confining potential for large distances which could not be the case when dynamical fundamental fermions are coupled to gluons. Alternatively the scale can be set implicitly by choosing a value r_0 such that

$$r_0^2 F(r_0) = 1.65,$$

where the reference value 1.65 is chosen to minimize lattice discretization errors [71, 72]. The Sommer parameter requires only expectation value of Wilson loops to be computed. While the measurement of Wilson loops is cheap, noisy signals affects the measure of the interquark force at large distances where the lattice artefact are negligible, see Fig. 7.1. Systematic errors appear when different choices of the limits and of the functional form are employed to fit the force $F(r)$, considerably increasing the complexity of the measure of the Sommer parameter r_0 .

7.3 Mass dependent and independent schemes

The equation (7.1) has also a term proportional to the derivative of the lattice spacing with respect to the gluino mass. As consequence a part of the dependence on the scale can be reabsorbed by the renormalization of the gluino mass.

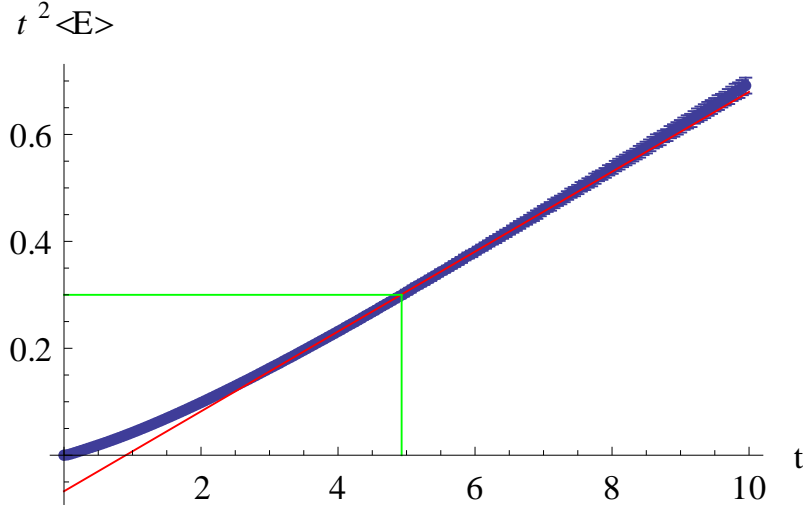


Figure 7.2: Behavior of $t^2\langle E(t) \rangle$ on a lattice 16^4 with $\beta = 1.65$ and $\kappa = 0.1600$. The green line marks the point where Eq. (7.3) holds, $\sqrt{t_0}/a = 2.22(1)$.

Observables used to set the scale are normally chosen to have a weak dependence on the fermion mass. However a mild, but not negligible, linear dependence is normally observed for r_0 as a function of the renormalized fermion mass M_R . In this situation, two different approaches can be naturally applied to set the scale. In a *mass dependent* renormalisation scheme the scale is set separately at each value of M_R , and consequently the lattice spacing depends on the gluino mass

$$a \equiv a(\beta, M_R).$$

In the second approach the lattice spacing is taken to be independent of the gluino mass M_R ,

$$a \equiv a(\beta).$$

Therefore in this case the linear behavior of r_0 is interpreted as a physical dependence of its value on the fermion mass [73]. This approach is called *mass independent* renormalisation scheme and it requires an extrapolation of the observable used to set the scale to a fixed reference value of M_R (typically but not necessarily $M_R = 0$).

7.4 Wilson flow

To improve the scale setting, beside r_0 , other efficient solutions have been found using the Wilson Flow to set precisely the scale on lattice simulations.

The Wilson flow can be considered effectively as the continuous generalization of the stout smearing. The starting point is to introduce an additional fictitious time t as fifth dimension where the gauge fields $U_\mu(x)$ generated by the Monte Carlo simulations are “continuously smoothed”. The continuous smoothing procedure is fully specified by the partial differential equation

$$\frac{\partial}{\partial t} V_\mu(x, t) = -g^2 \left\{ \frac{\partial S_{\text{gauge}}(V_\mu(x, \tau))}{\partial V_\mu(x, \tau)} \right\} V_\mu(x, t), \quad (7.2)$$

with the boundary conditions

$$V_\mu(x, t)|_{t=0} = U_\mu(x),$$

where $V_\mu(x, t)$ denotes the link at fictitious time t and $U_\mu(x)$ the link of the original lattice.

The Wilson flow removes ultraviolet divergences, meaning that local gauge invariant operators measured at positive time flow have the property to be automatically renormalized. Quantities constructed from the $V_\mu(x, \tau)$ links have a well defined continuum limit and they can be used to set reliably the scale in practical lattice simulations.

The scale t_0 has been introduced in Ref. [74] as the flow time t where the equation

$$t^2 \langle E(t) \rangle = 0.3 \quad (7.3)$$

is fulfilled, see Fig. 7.2. The scale t_0 has the same physical dimension of the string tension, i.e. the square of a length. The gauge energy $E(t)$ is defined as

$$E = \frac{1}{4} G_{\mu\nu}^a G_{\mu\nu}^a,$$

where $G_{\mu\nu}$ is the antisymmetric clover plaquette represented in Fig. 5.1.

The scale w_0 has been introduced in Ref. [75] as the square root of the flow time t where the condition

$$t \frac{d}{dt} t^2 \langle E(t) \rangle = 0.3 \quad (7.4)$$

is satisfied, therefore w_0 has the same physical dimension of the lattice spacing. It has been demonstrated that w_0 is an improved scale less sensible to lattice artifact. According to the observation of Ref. [75], the difference between the Symanzik action and the Wilson action as discretization of S_{gauge} is not relevant but the Wilson action is computationally cheap. For this reason the Wilson action is chosen to integrate the flow equation on the lattice.

Volume	β	κ	am_π	$\sqrt{t_0}/a$	w_0/a	$\tau(t_0)$
$24^3 \times 48$	1.60	0.15500	0.5788(16)	1.5672(13)	1.5102(14)	21
$24^3 \times 48$	1.60	0.15700	0.3264(23)	1.7904(11)	1.7292(37)	10
$24^3 \times 48$	1.60	0.15750	0.2015(93)	1.8986(53)	1.8410(63)	42
$32^3 \times 64$	1.75	0.14900	0.2385(4)	3.1438(67)	2.9838(59)	50
$32^3 \times 64$	1.75	0.14920	0.2035(5)	3.270(17)	3.097(25)	45
$32^3 \times 64$	1.75	0.14940	0.1604(15)	3.362(15)	3.205(20)	35
$32^3 \times 64$	1.75	0.14950	0.1294(24)	3.551(36)	3.413(40)	65
$32^3 \times 64$	1.90	0.14330	0.2874(8)	4.72(04)	4.46(05)	163
$32^3 \times 64$	1.90	0.14387	0.2123(4)	5.73(13)	5.57(19)	440
$32^3 \times 64$	1.90	0.14415	0.1742(4)	5.71(12)	5.49(11)	296
$32^3 \times 64$	1.90	0.14435	0.1413(6)	5.96(12)	5.76(14)	502

Table 7.1: This table shows the results of the measurements of the scale.

7.5 Measure of w_0 and t_0

The measure of the Wilson Flow scales has been done for three different β and many different $\kappa = \frac{1}{2m+8}$ on the ensemble of configurations generated to study the spectrum of the $\mathcal{N} = 1$ super Yang-Mills theory based on the gauge group $SU(2)$ [49, 50]. The Symanzik improved action has been used to discretize the gauge action, while the Dirac-Wilson operator with one-level stout smeared links has been used for the fermion action.

The integration of the Wilson flow has been done every six configurations, skipping the first few hundreds to ensure thermalization. The results are summarized in table 7.1. The scale w_0 and t_0 have a small dependence on the gluino mass for a given β . Employing a mass independent renormalization scheme, the scale is extrapolated to the chiral limit and set to be equal to the extrapolated value for all the fermion masses. The gluino mass is proportional to the square of the (adjoint) pion mass, defined in a partially quenched approach [76].

7.6 Matching the β -function

As discussed above, the β -function has been computed for the $\mathcal{N} = 1$ SYM model in Ref. [20], the first two perturbative coefficients are universal and scheme independent; they can be used to compare lattice results at different gauge coupling g [77]. The Wilson flow quantities t_0 and w_0 are therefore

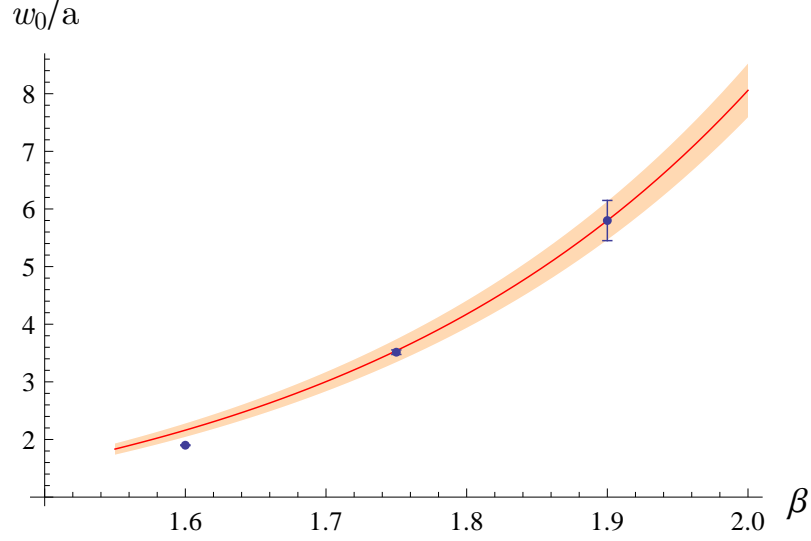


Figure 7.3: Scaling of w_0 compared to the expected asymptotic behavior (red line).

expected to scale as

$$\frac{w_0(g_1)}{w_0(g_2)} = \exp(F(g_1) - F(g_2)), \quad (7.5)$$

up to finite volume corrections and lattice discretization errors. The function $F(g)$ is the integral of the inverse of the β -function

$$F(g) = \int^g \frac{dg'}{\beta(g')} \quad (7.6)$$

and it reads explicitly for small g

$$F(g) = \frac{4\pi^2}{3g^2}$$

for the gauge group $SU(2)$ up to an unessential integration constant.

The scaling of Eq. (7.5) has been checked taking the value of w_0 at $\beta = \frac{2N_c}{g^2} = 1.9$ as reference point, see Fig. 7.3. The agreement with Eq. (7.6) is very good. The relative deviation from the exponential scaling,

$$K = \frac{w_0(1.9)}{w_0(\beta)} \exp\left\{\frac{\pi^2(\beta - 1.9)}{3}\right\}, \quad (7.7)$$

is $K \approx 1.007$ for $\beta = 1.75$ and $K \approx 1.13$ for $\beta = 1.6$, the latter induced mainly by lattice artefacts and higher order terms in the β -function.

7.7 Measure of the topological charge with the Wilson Flow

Run	Volume	β	κ	$(a^4\chi_{\text{top}}) \times 10^{-6}$
A1	$24^3 \times 48$	1.60	0.15500	160(19)
A2	$24^3 \times 48$	1.60	0.15700	102(9)
A3	$24^3 \times 48$	1.60	0.15750	85(7)
B1	$32^3 \times 64$	1.75	0.14900	17(2)
B2	$32^3 \times 64$	1.75	0.14920	12(1)
B3	$32^3 \times 64$	1.75	0.14940	11(1)
B4	$32^3 \times 64$	1.75	0.14950	10(3)
C1	$32^3 \times 64$	1.90	0.14387	1.01(14)
C2	$32^3 \times 64$	1.90	0.14415	1.59(18)
C3	$32^3 \times 64$	1.90	0.14435	1.02(8)

Table 7.2: This table shows the results of the measurements of the topological susceptibility.

The topological charge can be defined to be the integral

$$Q_{\text{top}} = \frac{1}{16\pi^2} \int d^4x (\epsilon_{\mu\nu\rho\sigma} F_a^{\mu\nu} F_a^{\rho\sigma})$$

for a given field configuration in the continuum. The topological charge is defined on the lattice with the same antisymmetric discretization of the field strength tensor of Fig. 5.1 contracted with the ϵ tensor

$$Q_{\text{lat}} = \frac{1}{16\pi^2} \sum_x \epsilon_{\mu\nu\rho\sigma} \text{Tr}(F^{\mu\nu} F^{\rho\sigma}),$$

but on the lattice the quantity Q_{lat} is affected by ultraviolet fluctuations and in general it is not an integer. A possible solution to the problem is a smoothing procedure, needed to suppress the short distance fluctuations and to recover a proper definition of the topological charge in the continuum limit [78]. To this end the Wilson flow itself has been used to smooth gauge fields, as in Ref. [79].

As shown in Fig. 7.4(a), for large enough flow time t the topological charge reaches a near integer value. Following Ref. [79], the raw lattice topological charge is converted to an integer as

$$Q_{\text{top}} = \text{round}(\alpha Q_{\text{lat}}(t)),$$

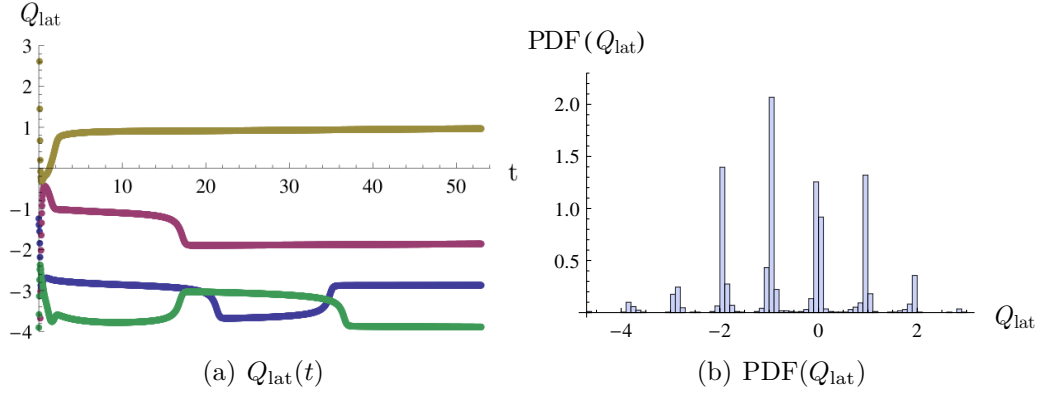


Figure 7.4: Left: Topological charge for a given configuration as a function of the flow time t , on a lattice $32^3 \times 64$, $\beta = 1.9$ and $\kappa = 0.14435$. Right: distribution of the topological charge at $t = 50$ for the same run.

choosing a large smoothing flow time t . The real constant α is chosen in order to minimize the expectation value

$$R(\alpha) = \langle (\alpha Q_{\text{lat}} - \text{round}(\alpha Q_{\text{lat}}))^2 \rangle.$$

Near the continuum limit it is expected that $\alpha \approx 1$, i.e. that the distribution of Q_{lat} is already centered nearby an integer without requiring an additional multiplication parameter, see Fig. 7.4(b) and Eq. (7.5(a)).

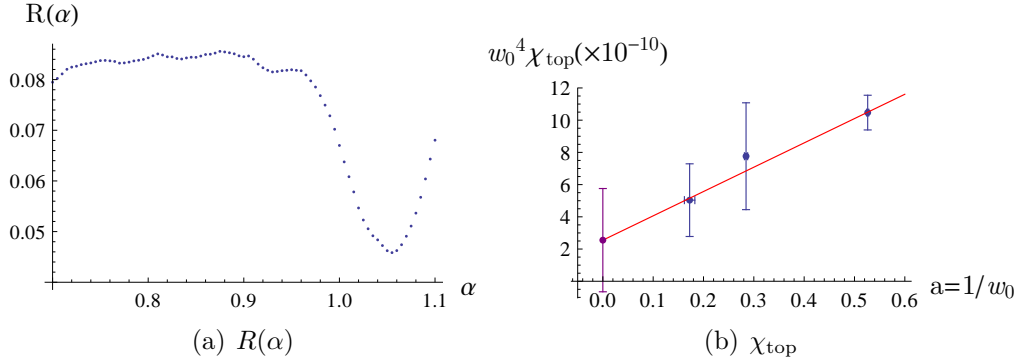


Figure 7.5: a) Plot of $R(\alpha)$ for the lattice $32^3 \times 64$ at $\beta = 1.75$ and $\kappa = 0.1494$, the minimum of $R(\alpha)$ is located at $\alpha = 1.055$. b) Extrapolation to the continuum limit of the topological susceptibility χ_{top} .

The topological susceptibility χ_{top}

$$\chi_{\text{top}} = \frac{\langle Q_{\text{top}}^2 \rangle - \langle Q_{\text{top}} \rangle^2}{V}$$

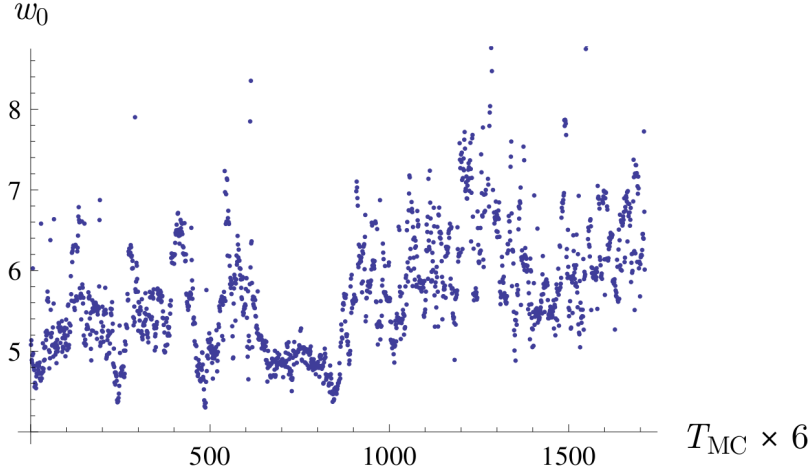


Figure 7.6: Monte Carlo history of w_0 on a lattice $32^3 \times 64$, $\beta = 1.9$ and $\kappa = 0.14435$. w_0 is measured every six configurations.

has been measured, the results are shown in Tab. 7.2. The value of χ_{top} extrapolated to the chiral limit confirms the *topological suppression* for SYM mentioned in Ref. [80].

7.8 Autocorrelation time of flow observables

The autocorrelation time of the topological charge increases drastically near the continuum limit, possibly resulting in a topological freezing depending on the boundary conditions applied to gauge fields in the time direction [58, 59]. The scales w_0 and t_0 exhibit a very long correlation time especially near the continuum limit, similar to the behavior of the autocorrelation topological charge.

Autocorrelations should scale classically as a^{-z} with $z = 1$ for the hybrid Monte Carlo (HMC) algorithm. The lattice spacing is increased roughly by a factor 3 between $\beta = 1.9$ and $\beta = 1.6$, however the autocorrelation $\tau(t_0)$ of t_0 at $\beta = 1.9$ is approximately twelve time larger than the autocorrelation of the same observable at $\beta = 1.6$. The scaling of $\tau(t_0)$ seems to indicate $z \gtrsim 2$ and therefore a possible coupling of the observables used to set the scale with the topological charge.

7.9 Correlations between topological charge and the scale w_0

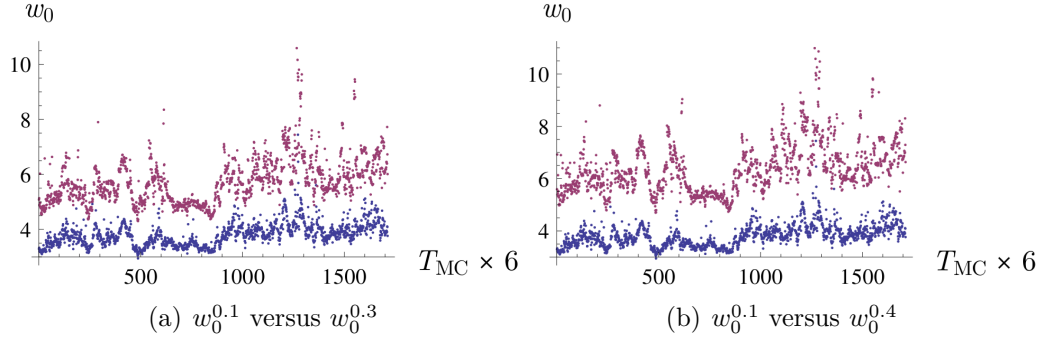


Figure 7.7: Comparison of the Monte Carlo history (a) of the $w_0^{0.1}$ with $w_0^{0.3}$ and (b) of the $w_0^{0.1}$ with $w_0^{0.4}$, on a lattice $32^3 \times 64$, $\beta = 1.9$ and $\kappa = 0.14435$. The magnitude of the peaks increases drastically when the reference value to set the w_0 scale is larger.

The Monte Carlo history of w_0 has been considered to further investigate the nature of the long autocorrelation of this observable. The w_0 scale can be defined for a single configuration without the need of an ensemble average as the time when the integrated flow for that configuration matches the specified condition of Eq. (7.4). In Fig. 7.6 is shown the Monte Carlo history of w_0 for a lattice $32^3 \times 64$, with $\beta = 1.9$ and $\kappa = 0.14435$. The value of w_0 seems to have large fluctuations with a long period and in particular very strong upward spikes emerge.

Wilson flow scales depend implicitly on the reference value chosen in Eq. (7.4). Small reference values will produce large lattice artefacts on the final results, while w_0 and t_0 will be affected by non-negligible finite volume effects for larger reference values. The scales w_0^u are defined to be the square root of the flow time where the condition

$$t \frac{d}{dt} t^2 \langle E(t) \rangle = u \quad (7.8)$$

is satisfied and u is varied to study how the correlations are affected by different choices of the reference value. Here and in the following it is set simply $w_0 \equiv w_0^{0.3}$. In Fig. 7.7 the comparison of the Monte Carlo history of $w_0^{0.1}$ in comparison with $w_0^{0.3}$ and $w_0^{0.4}$ is presented, when the value of u is small then the fluctuations and the spikes are significantly reduced, but when the value of u is increased then the spikes are even stronger.

7.9. CORRELATIONS BETWEEN TOPOLOGICAL CHARGE AND THE SCALE W_0 109

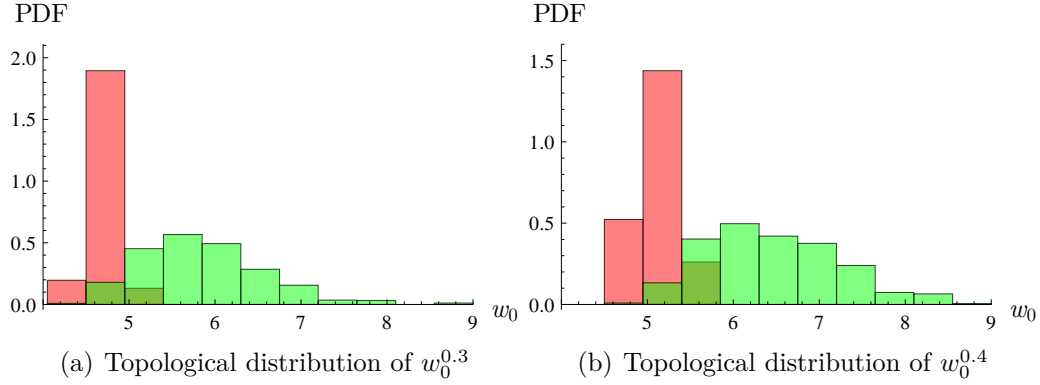


Figure 7.8: Probability distribution function of (a) $w_0^{0.3}$ and of (b) $w_0^{0.4}$ restricted to the topological sector $|Q_{\text{top}}| = 1$ (green) and $|Q_{\text{top}}| = 4$ (red), on a lattice $32^3 \times 64$, $\beta = 1.9$ and $\kappa = 0.14435$.

An increase in the value of u translates into a larger flow time needed to match the condition (7.8), which effectively means that a larger smoothing induced by the flow equation is applied to the configurations. Large flow time will remove the ultraviolet divergences and the system will be brought toward a classical configuration, as observed in the previous section. Therefore one might argue that spikes and large fluctuations are related to topological effects. Using the results of the previous section it has been possible to compute the value of w_0^u restricted only to configurations with a fixed definite topological charge.

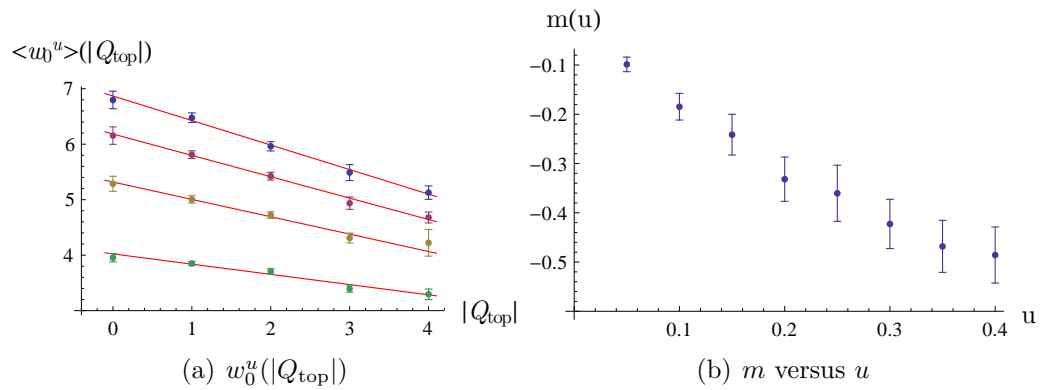


Figure 7.9: a) Linear fit of the dependence of w_0^u on the topological sector for u equal to 0.1 (green), 0.2 (yellow), 0.3 (purple) and 0.4 (blue). b) Slope coefficient m as a function of the reference value u .

The distribution of $w_0^{0.4}$ and $w_0^{0.3}$ are shown for the same run in Fig. 7.8 for two selected topological sectors, $|Q_{\text{top}}| = 1$ and $|Q_{\text{top}}| = 4$. The distribution of $w_0^{0.3}$ restricted to the topological sector $|Q_{\text{top}}| = 1$ seem to be rather broad and it has a mean value larger than the distribution of the topological sector $|Q_{\text{top}}| = 4$. The same behavior appears for the restricted distributions of $w_0^{0.4}$, but with a slightly larger gap between the two mean value of the distribution. This result is important because it shows that there is a coupling between the value of w_0 and the topological charge. The spikes observed in Fig. 7.6 are produced by the fluctuations of w_0 when the simulation is stuck at low values of the topological charge, when the distribution of w_0 is broad. The long periodicity is induced by the interchange during the Monte Carlo time between the topological sectors around zero, characterized by large expectation value of w_0 , and the topological sectors far from the origin, with a small mean value of w_0 .

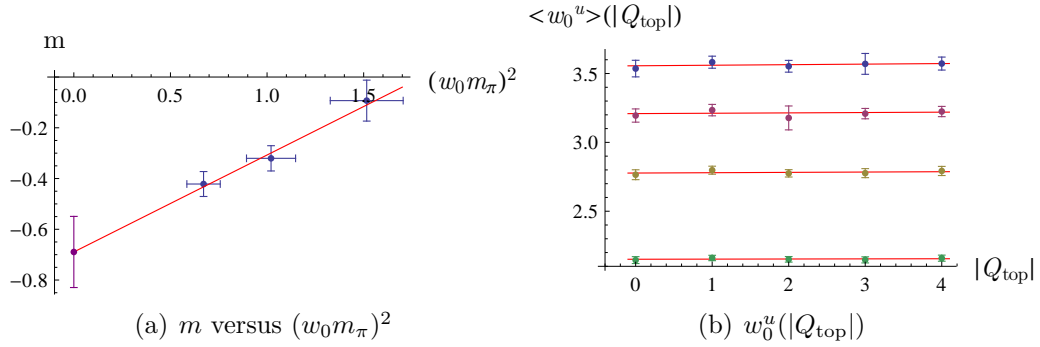


Figure 7.10: (a) Slope coefficient m as a function of $(w_0 m_\pi)^2$ at $\beta = 1.9$ for $w_0^{0.3}$. (b) The same as Fig. 7.9(a), but for $\beta = 1.75$ and $\kappa = 0.1494$. The value of m linearly extrapolated to the chiral limit is $m((w_0 m_\pi)^2 = 0) = -0.69(14)$.

In Fig. 7.9(a) is presented the expectation value of w_0^u restricted to the various topological sectors for four different u for the same run on a lattice $32^3 \times 64$, with $\beta = 1.9$ and $\kappa = 0.14435$. The behavior of $w_0^u(|Q_{\text{top}}|)$ is linear for all u but it has a stronger slope when the reference scale u is large. A linear fit has been done of the form

$$\langle w_0^u \rangle(|Q_{\text{top}}|) = m|Q_{\text{top}}| + q \quad (7.9)$$

and the resulting slope coefficients m are presented as a function of u in Fig. 7.9(b). The modulus of the slope m has an increasing behavior for large u , that means that the dependence of w_0^u on the topology is strong when u is large. This behavior confirms our previous claim about the topological origin

of the spikes in Fig. 7.7, when u is large the smoothing effects of the Wilson flow are large and the configuration is driven toward a classical point where the influence of topology is strong. As result, the autocorrelation time of $w_0^{0.4}$ is around 800 configurations, more than twice larger than the autocorrelation time of $w_0^{0.1}$ of around 300 configurations. The dependence of the slope m has been further investigated as a function of the adjoint pion mass squared, observing that it increases approaching the chiral limit, see Fig. 7.10(a).

The dependence of the scale on the topological sector could be interpreted as a finite volume effect. To conclude the analysis the same systematic calculation has been done on the lattice $32^3 \times 64$ but at $\beta = 1.75$, where the physical volume is approximately seven time larger than at $\beta = 1.9$. The dependence of the various w_0^u on $|Q_{\text{top}}|$ is presented in Fig. 7.10(b). The dependence of the flow scales on the topology is completely disappeared at this large physical volume. Finite volume effect seems to be the origin of the dependence of w_0 on the topological sector observed before on the finer lattice at $\beta = 1.9$.

7.10 Scale setting with w_0

The detailed analysis of the Wilson flow observables w_0 and t_0 leads to the conclusion that there is a substantial dependence of w_0 on the topological sector appearing as a finite volume effect, in agreement with the previous discussion on the topic for the Sommer parameter r_0 of Ref. [81, 82].

Scales based on the Wilson flow require a delicate fine-tuning to correctly handle finite volume and lattice artefact errors. However a result free from finite volume effects can be ensured if there are no couplings with the topological charge and these couplings can be determined precisely. The final results have fairly small statistical and systematic errors, thus w_0 can be used to set the scale in practical extrapolations to the chiral and to the continuum limit. Practical observations supports eventually a use of a small flow time to set the scale, at least for $\mathcal{N} = 1$ SYM model and within the current precision, the ratio of w_0^u and $w_0^{0.3}$ is flat for $u \gtrsim 0.1$ (see Tab. 7.3).

This conclusion could depend on the theory under study, in particular on the number colors N_c , on the number of fermions N_f and on their representation. However it is possible to believe that a dependence of the scale on topology is developed for sufficient large reference scales independently of the theory. Systematic studies in this direction are encouraged, in particular if the proposal of enlarging the reference flow time of Ref. [69] is accepted.

Run	$w_0^{0.05}$	$w_0^{0.10}$	$w_0^{0.15}$	$w_0^{0.20}$	$w_0^{0.25}$	$w_0^{0.30}$	$w_0^{0.35}$	$w_0^{0.40}$
A1	0.6419(10)	0.9587(15)	1.1420(17)	1.2844(19)	1.4048(22)	1.5104(21)	1.6046(26)	1.6901(26)
A2	0.7767(15)	1.1136(22)	1.3192(27)	1.4787(34)	1.6122(40)	1.7290(43)	1.8319(46)	1.9268(44)
A3	0.8341(23)	1.1853(35)	1.4048(41)	1.5760(47)	1.7182(53)	1.8419(60)	1.9511(58)	2.0495(68)
B1	1.5087(42)	2.0058(51)	2.3331(56)	2.5878(60)	2.8011(62)	2.9838(59)	3.1495(62)	3.3012(62)
B2	1.5610(84)	2.082(15)	2.417(19)	2.684(19)	2.904(23)	3.097(25)	3.256(27)	3.424(25)
B3	1.6113(74)	2.151(12)	2.504(13)	2.779(17)	3.005(18)	3.205(20)	3.385(22)	3.551(25)
B4	1.6957(15)	2.269(24)	2.651(28)	2.955(34)	3.205(37)	3.413(41)	3.623(43)	3.793(42)
C1	2.734(46)	3.687(81)	4.35(10)	4.82(14)	5.24(16)	5.60(18)	5.90(18)	6.19(18)
C2	2.717(40)	3.666(85)	4.31(11)	4.76(13)	5.13(13)	5.49(13)	5.78(15)	6.05(14)
C3	2.855(44)	3.822(81)	4.47(11)	4.97(11)	5.40(14)	5.76(14)	6.08(15)	6.38(15)

Table 7.3: This table shows the results of the measurements of the scale w_0^u , the parameters of the Runs are defined in Tab. 7.2.

Chapter 8

Supermultiplets on the lattice

Our claim here is that, contrary to widespread beliefs, SUSY and the lattice can happily coexist. [...] The simple idea behind our proposal is that, rather than try to have some version of SUSY on the lattice, one should let the lattice spoil SUSY if it so wishes. Our requirement is that SUSY, like chiral symmetry, should only be recovered in the continuum limit.

Curci and Veneziano [4]

Supersymmetry is explicitly broken for finite values of the lattice spacing a . The Curci-Veneziano action has only two parameters, the gauge coupling g and the gluino mass m , to fine tune the lattice theory to a critical point where dynamical restoration of the basic symmetries of $\mathcal{N} = 1$ SYM is expected to occur. Numerical Monte Carlo methods are required to explore the non-perturbative physics of the strong supersymmetric interactions, the critical point can be reached only with complex extrapolations. There are many possibilities to understand how far current simulations are from the target supersymmetric theory. The first idea is to measure a lattice equivalent of the Ward identities generated by SUSY transformations. Many studies in this direction has been done in the past, see Ref. [83, 49, 50]. An another interesting possibility is to check the restoration of the mass degeneracy between particles in the same supermultiplet, in order to verify the predictions that has been formulated in Ref. [84, 18, 19].

8.1 Adjoint pion and gluino mass

Simulations at fixed gauge coupling g but with different bare gluino mass m can be used to perform the first extrapolation to the chiral limit. i.e. to the point where the renormalized gluino mass vanishes. In the Wilson formulation of lattice fermions, chiral symmetry is explicitly broken by a term proportional to the lattice spacing

$$O_W = ar\bar{\lambda}D_\mu D^\mu\lambda,$$

where r is the Wilson parameter. Even if O_W is irrelevant and therefore it vanishes naively in the continuum limit $a \rightarrow 0$, the fermion mass m is not protected anymore by chiral symmetry and it can acquire large quantum correction proportional to $1/a$ coming from diagrams where loops of gauge particles connect to a fermion line. In other words, the fermion mass renormalizes additively in the Wilson formulation as a common scalar field, which means that zero bare fermion mass m does not imply zero renormalized fermion mass. Fine tuning of m is needed to bring the theory to the point where terms that break chiral symmetry explicitly vanishes to all order in perturbation theory.

In QCD with two fundamental fermions, the pattern of spontaneous chiral symmetry breaking is $SU(2)_L \times SU(2)_R \rightarrow SU(2)_V$, leading to three massless bosons by the Goldstone theorem: the three pions π^0, π^+, π^- . If the $SU(2)_L \times SU(2)_R$ symmetry is explicitly broken by a non vanishing quark mass m , then pions will acquire a mass M_π proportional to the amount of chiral symmetry breaking. Perturbative and non-perturbative arguments can be used to show that $m \propto M_\pi^2$, relation usually written in the form of the well known Gell-Mann-Oakes-Renner equation

$$m\Sigma = F_\pi^2 M_\pi^2,$$

where Σ and F_π are the chiral condensate and the pion decay constant respectively [85]. Therefore in QCD there is the natural way to set the renormalized quark mass to be proportional to square of the pion mass and to define accordingly the chiral limit.

In $\mathcal{N} = 1$ SYM, the spontaneous chiral symmetry breaking pattern is between two discrete groups $Z_{2N_c} \rightarrow Z_2$, where N_c is the number of colors of the gauge theory. Since no continuous group is broken, there will be no Goldstone bosons in $\mathcal{N} = 1$ SYM helpful to define the chiral limit and the gluino mass. Nevertheless it is possible to add to the action an extra gluino λ to mimic the two flavors structure of QCD, with the care of adding also an associated ghost boson field in order to not modify the partition

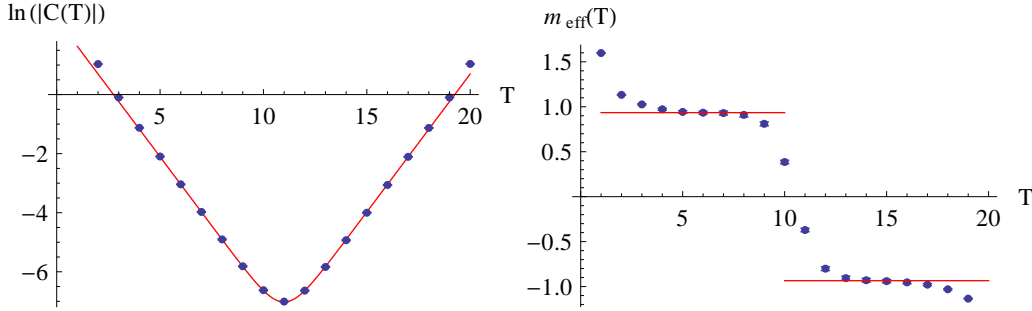


Figure 8.1: Pion mass estimation for a lattice $10^3 \times 20$ with $\beta = 1.65$ and $\kappa = 0.1875$. Logarithm of the correlator (left) and effective mass plot (right)

function. The partially quenched approach allows the construction of chiral perturbation theory and the use of the “adjoint pion mass” to define the chiral limit, such that $m \propto M_\pi^2$ also in $\mathcal{N} = 1$ SYM.

8.2 Computation of the pion mass and of the critical point

The pion mass can be extracted from the asymptotic behavior of the connected correlator

$$C(x, y) = \text{Tr}_{\text{spin,color}} \left\{ \gamma_5 D_w^{-1}(x, y) \gamma_5 D_w^{-1}(y, x) \right\}, \quad (8.1)$$

that has an exponential decay for large distance $|x - y|$ in the Euclidean space

$$C(x, y) \sim c_1 \exp(-M_\pi |x - y|) + \sum_{n>1} c_n \exp(-M_\pi^{n*} |x - y|).$$

The masses M_π^{n*} denote the contribution to the correlator coming from (pseudo-)excited states with compatible quantum numbers. Keeping in mind that the pion is not a physical particle in $\mathcal{N} = 1$ SYM, it is possible to fix the renormalized gluino mass to be proportional to the square of the adjoint pion mass M_π^2 .

An alternative and more formal definition of the gluino mass can be given in terms of the SUSY Ward identity, it has been proven numerically that both definitions gives compatible results to define the point where the gluino mass vanishes.

On the lattice, the pion correlator (8.1) can be computed once that the inverse $D_w^{-1}(x, y)$ is known. Using a point source $\psi_{\alpha'c'}(x, \alpha, c)$ located at the

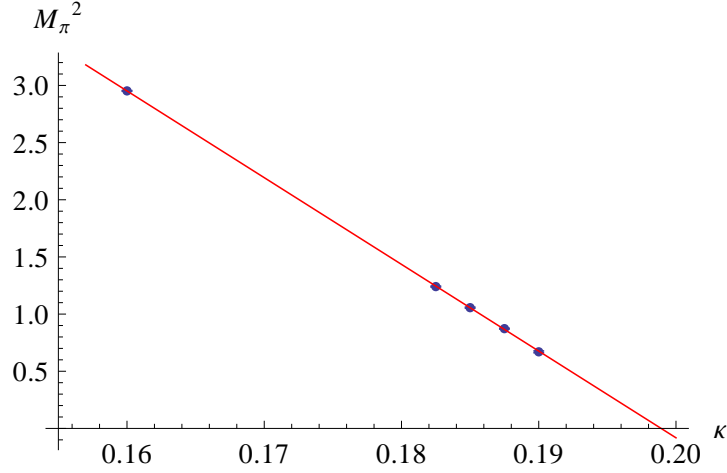


Figure 8.2: Extrapolation of the critical κ_c from a lattice $10^3 \times 20$ at $\beta = 1.65$. At $\kappa_c \simeq 0.199$ both the pion mass and the renormalized gluino mass are expected to vanish.

origin, with non zero spin and color component α' and c'

$$\psi_{\alpha'c'}(x, \alpha, c) = \delta_{x0} \delta_{\alpha\alpha'} \delta_{cc'}$$

the linear system

$$D_w \eta_{\alpha'c'} = \psi_{\alpha'c'}$$

can be solved for $\eta_{\alpha'c'}$ with standard Krylov space solver. Using γ_5 Hermiticity

$$\gamma_5 D_w^{-1} \gamma_5 = (D_w^{-1})^\dagger,$$

the correlator (8.1) can be rewritten summing over the different combination of color and spin for $\psi_{\alpha'c'}(x, \alpha, c)$ as

$$C(x, y) = \sum_{\alpha\alpha'cc'} |\eta_{\alpha'c'}(y, \alpha, c)|^2,$$

requiring the solution of $4(N_c^2 - 1)$ linear systems and not the expensive knowledge of the full inverse $D_w^{-1}(x, y)$.

A zero momentum projection is employed to practically extract the physical pion mass

$$C(t) = \sum_{\vec{x}, \vec{y}} C(\vec{x}, 0; \vec{y}, t)$$

where the sum runs over all the spatial lattice points of a time-slice of the lattice. Two contributions arise for $C(t)$ at large t due to the (anti)periodic boundary conditions

$$C(t) \sim \exp\{-M_\pi t\} + \exp\{-M_\pi(T - t)\}, \quad (8.2)$$

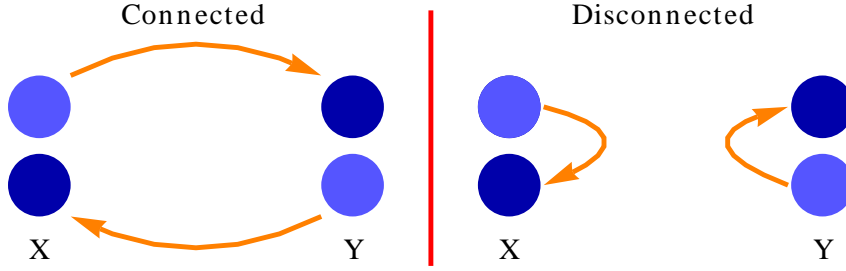


Figure 8.3: Connected and disconnected contributions. The pion has only connected contributions (left), but η' and f_0 mesons have also disconnected contributions (right).

being T the temporal extend of the lattice in the time direction. The effective mass

$$m_{\text{eff}}(t) = \log \left(\frac{C(t)}{C(t+1)} \right)$$

gives a reliable estimation of the pion mass in the window $0 \ll t \ll T/2$, otherwise it is possible to direct fit Eq. (8.2), see Fig. 8.1.

The critical bare mass where the pion mass vanishes can be extracted from a linear fit of the points (κ, M_π^2) , with $\kappa = 1/(2m+8)$, as demonstrated in Fig. 8.2. The linear behavior of the square of the pion mass extends even to relatively low regimes of κ .

8.3 η' and f_0

The η' and f_0 are two mesons with symmetries and correlation functions similar to their QCD counterpart. The mass of those meson are estimated from from the connected correlation functions of the operator

$$O_P = \bar{\lambda} \gamma_5 \lambda$$

for the η' , and of the operator

$$O_S = \bar{\lambda} \lambda$$

for the f_0 .

The correlator of the η' reads on the lattice after the fermion field con-

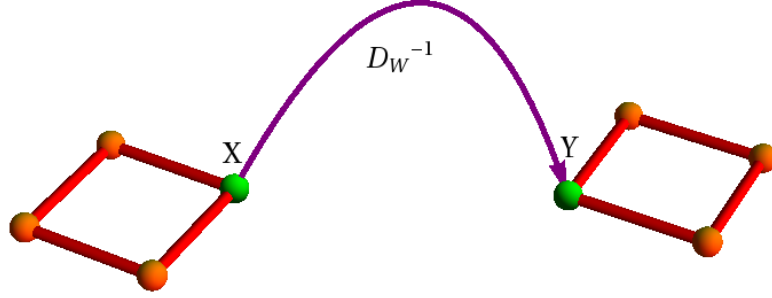


Figure 8.4: Lattice representation of the gluino-gluon correlator, the inverse of the Dirac-Wilson operator connects the field strength at two different points.

tractions

$$C_{\eta'} = \frac{1}{L^3} \sum_x \langle \text{Tr} \left(\gamma_5 (D_W^{-1})_{xy} \gamma_5 (D_W^{-1})_{yx} \right) \rangle - \frac{1}{2L^3} \sum_x \langle \text{Tr} \left(\gamma_5 (D_W^{-1})_{xx} \right) \text{Tr} \left(\gamma_5 (D_W^{-1})_{yy} \right) \rangle$$

and it has connected and disconnected contributions. A disconnected contribution can be depicted as a gluino moving forth and back to the same point in a loop, see Fig. 8.3. The disconnected contributions are dominant in the zero gluino mass limit and they have noisy signals.

8.4 Gluino-Gluon

The gluino-gluon is a spin one-half particle present only in theories with adjoint matter. Being a Majorana fermion, it has two possible states. The mass of the gluino-gluon can be extracted from the correlation function of the operator

$$O_{g\tilde{g}}(x) = (\sigma_{\mu\nu})_{\alpha\beta} F^{\mu\nu}(x) \lambda^\beta(x)$$

and gauge invariance is ensured if the field strength is written in the adjoint representation. The explicit correlator reads on the lattice

$$C(x, y) = \langle (\sigma_{ij})_{\alpha\beta} \text{Tr}(F^{ij}(x) \tau_a) D_W^{-1}[x\beta, a; y, \rho, b] \text{Tr}(F^{lm}(y) \tau_b) (\sigma_{lm})_{\rho\alpha} \rangle,$$

where a summation over all repeated indices is intended, see Fig. 8.4. The field strength can be represented on the lattice for example with the clover



Figure 8.5: Wilson loop correlation functions contain information about glueball masses.

discretization. The correlator has no disconnected contribution and therefore it has good signal. Spatial smearing can be employed both for the links in the Dirac-Wilson operator and in the field strength.

The ground state of the gluino-gluon is expected to belong to the lowest supermultiplet, while the first excited state should belong to the second supermultiplet with higher mass.

8.5 Glueballs

Glueball masses are extracted from Wilson loop connected correlators

$$C_{gg} = \langle W(x)W(y) \rangle - \langle W(x) \rangle \langle W(y) \rangle,$$

see Fig. 8.5. Wilson loop correlators are quite easy to compute, but they usually have bad signals, variational smearing is used to reduce the noise and the excited states contribution.

8.6 The chiral limit

Masses of particles are extrapolated to the chiral and to the continuum limit to see if there is a dynamically restored supersymmetry. The particles are measured for different gluino masses at a fixed lattice spacing and then the results are extrapolated to zero, see Fig. 8.6. The pink series of points are the results from $\beta = 1.6$ while the black ones from $\beta = 1.75$. The pink results are extracted therefore from a coarse lattice with a larger lattice spacing than the black points. As it can be clearly seen in the extrapolated results, the mass gap between the gluino glue and η' is significantly reduced on finer lattice, suggesting that the latest results are really pointing to the

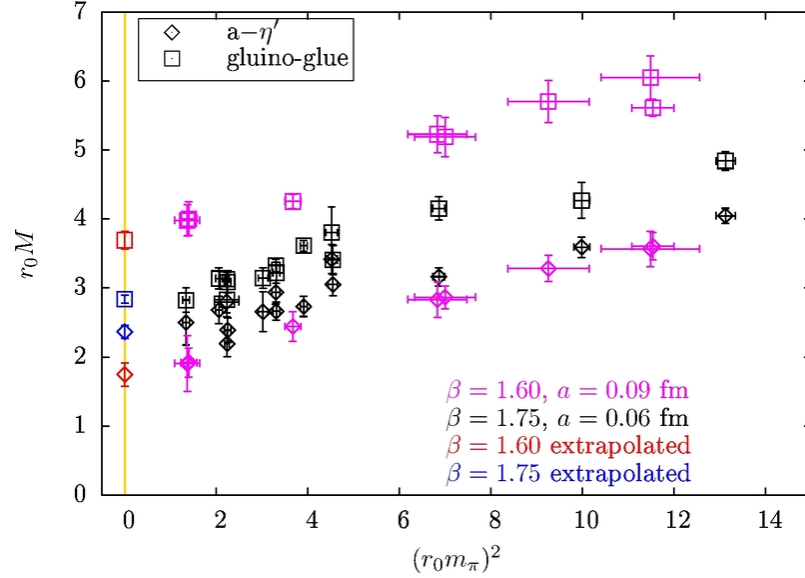


Figure 8.6: Chiral limit at $\beta = 1.75$ of the gluino-gluon and η' particles, picture taken from Ref. [49]. The yellow line marks the chiral limit, i.e. the point where the renormalized gluino mass vanishes.

supersymmetric limit in which particles in the same supermultiplet have the same mass. Further studies are needed to have at least three or four points to try an extrapolation to the continuum limit and a proper estimation of the masses of the other particles, like glueballs and excited states. A preliminary attempt in this direction is presented in the following section.

8.7 The continuum limit

The continuum limit is the extrapolation to $a \rightarrow 0$ after that the chiral limit is performed. Masses are obtained from measurements with different gauge coupling g and thus a precise determination of the lattice spacing is required. The spectrum has been measured at two different lattice spacings at $\beta = 1.6$ and $\beta = 1.75$ using a fermion action with one-level stout-smeared links [83, 49]. Preliminary results are available for a third lattice point at $\beta = 1.9$. The scale w_0 has been measured reliably in all these points in Ch. 7; the lattice spacing is proportional to $a = 1/w_0$ and it is set in mass independent renormalization scheme. The extrapolation to the continuum limit is presented in Fig. 8.7. The extrapolation is a linear function of a since the lattice discretization errors are $O(a)$ for the Wilson action without clover improvement. This behavior is clearly visible for the extrapolation of

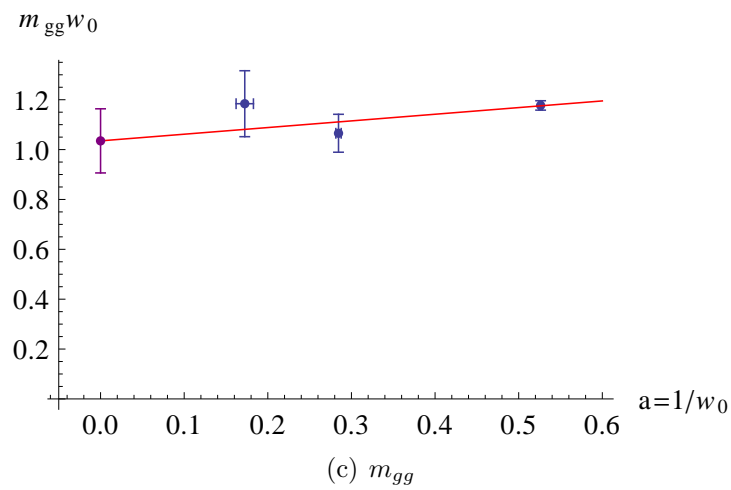
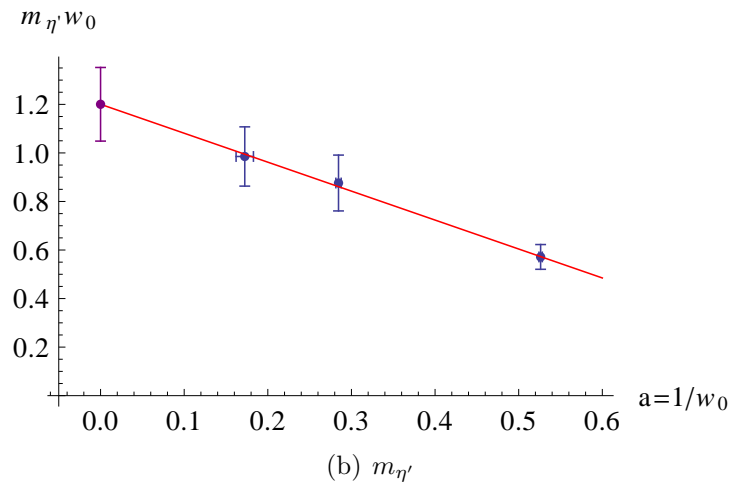
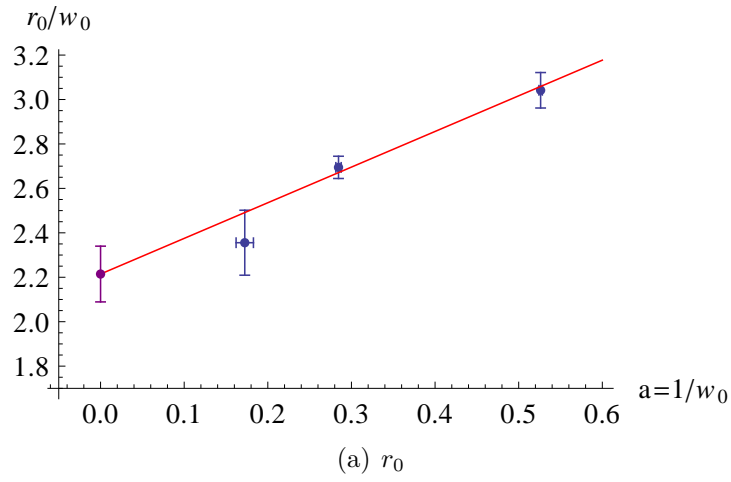


Figure 8.7: Extrapolation to the continuum limit of the Sommer parameter r_0 , the gluino-gluon mass m_{gg} and the η' mass $m_{\eta'}$.

the Sommer parameter. The mass of the η' seems to suffer larger lattice discretization errors, while the mass of the gluino-gluon is roughly constant. The Sommer parameter has even larger discretization errors. This discrepancy means that a different choice of the observable used to set the scale could lead to a significantly different behavior of the extrapolation to the continuum limit, in particular of the slope. The final value extrapolated should instead be finally equal regardless on whether r_0 or w_0 are used.

The errors on the single point are quite large, coming from large fluctuations of the chiral extrapolation, masses of bound states obtained at different gluino masses do not exhibit a precise linear behavior and have large relative errors. A larger number of configurations is needed to reduce the statistical error. New simulations with heavier gluino mass are a further cheap possibility to reduce the final error, if a linear behavior persists also for large values of the squared pion mass. Finally, a reduction of the final error could come from a careful consideration of the cross correlations between w_0 and the connected correlators of the particles.

The final extrapolation to the continuum limit of the Sommer parameter is

$$r_0/w_0 = 2.21(12) .$$

The gluino-gluon has a mass in units of w_0 of

$$w_0 m_{gg} = 1.04(13) ,$$

compatible with the mass of the η'

$$w_0 m_{\eta'} = 1.20(15) .$$

Fixing the physical value of w_0 to a conventional 800 MeV

$$w_0 \approx 0.5 r_0 \approx 0.25 \text{ fm} ,$$

the η' has a mass of 960(120) MeV, while the gluino-gluon has a mass of 832(104) MeV.

Chapter 9

Eigenvalues of the Dirac-Wilson operator

You have probably gathered by now that the solution of eigensystems is a fairly complicated business. It is. It is one of the few subjects covered in this book for which we do not recommend that you avoid canned routines. On the contrary, the purpose of this chapter is precisely to give you some appreciation of what is going on inside such canned routines, so that you can make intelligent choices about using them, and intelligent diagnoses when something goes wrong.

W.H. Press, B. P. Flannery, S. A. Teukolsky, W. T. Vetterling [86]

The Dirac-Wilson operator D_W has a central role in theories with dynamical fermions and it allows topological calculation even in pure gauge models. The smallest and especially the zero eigenvalues control the infrared behavior of QCD and of $\mathcal{N} = 1$ SYM in the continuum limit. In particular, the Banks-Casher equation relates the density of the eigenvalues of D_W near the origin with the expectation value of the chiral condensate [87]. Chiral Random Matrix Theory (ChRMT) is an effective model that has been proposed and successfully verified to describe the local and scaling properties of the eigenvalues of the Dirac-Wilson operator [88]. In this chapter the basic properties of the spectrum of D_W are discussed for $\mathcal{N} = 1$ SYM.

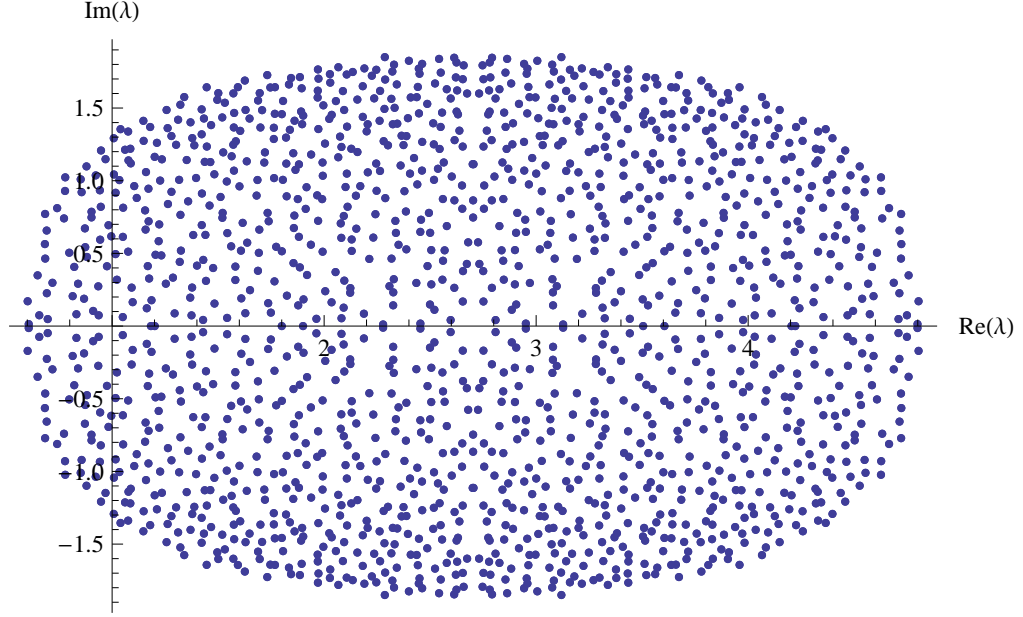


Figure 9.1: Distribution of the eigenvalues of the Dirac-Wilson operator D_W in the adjoint representation for a lattice 4^4 over a quenched $SU(2)$ gauge configuration with $\beta = 1.3$ and $\kappa = 0.1850$.

9.1 Symmetries of the Dirac-Wilson operator

The Dirac-Wilson operator satisfies the γ_5 Hermiticity relation

$$D_W^\dagger = \gamma_5 D_W \gamma_5, \quad (9.1)$$

that can be directly verified using $\gamma_5 \gamma_\mu \gamma_5 = -\gamma_\mu^\dagger$. D_W is not Hermitian, while $H = \gamma_5 D_W$ is an Hermitian operator. The γ_5 Hermiticity holds for all fermion representations and it is independent from the gauge group.

In addition, the Dirac-Wilson operator with links in the adjoint representation satisfies

$$D_W^T = C^{-1} D_W C$$

where C is the charge conjugation matrix. This property holds since the adjoint links have real elements and $C^{-1} \gamma_\mu C = -\gamma_\mu^T$. A similar statement is valid always for the adjoint representation: there is an anti-unitary operator $U = C \gamma_5 K$ which commutes with D_W

$$[C \gamma_5 K, D_W] = 0 \quad (9.2)$$

where K is the complex conjugation operator. An antiunitary operator has the property

$$\langle U\psi | U\phi \rangle = \langle \phi | \psi \rangle. \quad (9.3)$$

9.2 Biorthogonal basis of eigenvectors

The Dirac-Wilson operator is not Hermitian, meaning that right eigenvectors

$$D_W|\phi_n\rangle = \lambda_n|\phi_n\rangle \quad (9.4)$$

have to be considered separately from left eigenvectors

$$D_W^\dagger|\psi_n\rangle = \rho_n|\psi_n\rangle. \quad (9.5)$$

In general no relations exist between $|\phi_n\rangle$ and $|\psi_n\rangle$, in particular $|\phi_n\rangle \neq c|\psi_n\rangle$ with $c \in \mathbb{C}$. However taking the adjoint of Eq. (9.5),

$$\langle\psi_n|D_W = \langle\psi_n|\rho_n^*, \quad (9.6)$$

the uniqueness of the spectrum of the eigenvalues impose

$$\rho_n^* = \lambda_n. \quad (9.7)$$

Multiplying Eq. (9.4) by $\langle\psi_m|$ on the left, Eq. (9.6) by $|\phi_m\rangle$ on the right and relabeling repeated indexes

$$\langle\psi_n|D_W|\phi_m\rangle = \langle\psi_n|\phi_m\rangle\rho_n^* \quad (9.8)$$

$$\langle\psi_n|D_W|\phi_m\rangle = \lambda_m\langle\psi_n|\phi_m\rangle, \quad (9.9)$$

a subtraction of Eq. (9.8) with Eq. (9.9) yields to an equation

$$(\rho_n^* - \lambda_m)\langle\psi_n|\phi_m\rangle = 0,$$

that implies that the eigenvectors can be chosen to be biorthogonal

$$\langle\psi_n|\phi_m\rangle = \delta_{nm} \quad (9.10)$$

due to Eq. (9.7).

Left and right eigenvectors define a biorthogonal basis in terms of which the Dirac-Wilson operator can be decomposed as

$$D_W = \sum_n \lambda_n |\phi_n\rangle \langle\psi_n|,$$

under the assumption of diagonalizability [89].

9.3 Degeneracy of the eigenvalues of D_W

If $|\psi_n\rangle$ is a left eigenvector with eigenvalue λ_n^* , it follows from Eq. (9.5), Eq. (9.4) and Eq. (9.1)

$$\gamma_5 D_W \gamma_5 |\psi_n\rangle = \lambda_n^* |\psi_n\rangle.$$

Multiplying this equation by $U\gamma_5$

$$U D_W \gamma_5 |\psi_n\rangle = \lambda_n U \gamma_5 |\psi_n\rangle.$$

since the operator U has the complex conjugation operator which transforms λ_n^* in λ_n . Using the fact that U commutes with D_W from Eq. (9.2), there exists thus a second eigenvector

$$|\chi\rangle = U \gamma_5 |\psi_n\rangle$$

associated to the eigenvalue λ . Linear independence from $|\phi_n\rangle$ has to be ensured to prove a double degeneracy. It follows from

$$\begin{aligned} \langle \psi_n | U \gamma_5 | \psi_n \rangle &= \langle U U \gamma_5 \psi_n | U \psi_n \rangle \\ &= -\langle \gamma_5 \psi_n | U \psi_n \rangle \\ &= -\langle \psi_n | \gamma_5 U \psi_n \rangle \\ &= -\langle \psi_n | U \gamma_5 | \psi_n \rangle, \end{aligned}$$

where in the first line the antiunitary operator property (9.3) has been used, in the second line the fact that

$$U U = -1,$$

in the third line $\gamma_5^\dagger = \gamma_5$ and in the final line the commutation relation between U and γ_5

$$[U, \gamma_5] = 0.$$

This sequence of relations implies $\langle \psi_n | U \gamma_5 | \psi_n \rangle = \langle \psi_n | \chi \rangle = 0$. If $|\chi\rangle$ would be linearly dependent to $|\phi_n\rangle$, then this product could not be zero due to Eq. (9.10). This complete the proof that every eigenvalue of the Dirac-Wilson operator is doubly degenerate, a sort of generalization of the Kramer degeneracy [90, 88].

If $|\phi_n\rangle$ and $|\chi_n\rangle$ are two given degenerate eigenvectors corresponding to the eigenvalue λ , there are also two degenerate eigenvectors corresponding to the eigenvalue λ^*

$$\begin{aligned} U D_W |\phi_n\rangle &= U \lambda |\phi_n\rangle = D_W U |\phi_n\rangle = \lambda^* U |\phi_n\rangle, \\ U D_W |\chi_n\rangle &= U \lambda |\chi_n\rangle = D_W U |\chi_n\rangle = \lambda^* U |\chi_n\rangle, \end{aligned}$$

using again Eq. (9.2) and remembering that K acts also on λ leaving λ^* .

From these properties, the eigenvalues are organized by groups of four, for a given λ there is a corresponding λ^* , each doubly degenerate. If λ is real, then there are no other constraints apart that there will be an another pair of real eigenvalues $\tilde{\lambda} \neq \lambda$. If one of these pair across the origin, then the Pfaffian change its sign. There exist many bounds on the maximal and minimal real and imaginary part of λ , a typical distribution of the eigenvalues is presented in Fig. 9.1.

The eigenvalues of $H = \gamma_5 D_W$ are real and also doubly degenerate, but remarkably there is no known relation with the eigenvalues of D_W .

9.4 Computing eigenvalues of the Dirac-Wilson operator

The Dirac-Wilson operator is a sparse matrix of dimension $4V(N_c^2 - 1) \times 4V(N_c^2 - 1)$, assuming adjoint fermions on a lattice of finite volume $V = N_x N_y N_z N_t$. The number of non-zero elements of D_W scales linearly with the volume V of the lattice, as illustrated in Fig. 9.2. The full storage of all the elements of D_W is unpractical, even for a small lattice 8^4 and $N_c = 2$ it would require an amount of memory of the order of 40 gigabytes. The calculation of all eigenvalues at once is impossible; a good algorithm for searching eigenvalues and eigenvectors will focus only a specific region of the spectrum trying to have advantages from the sparse structure of D_W .

The “Power method” constructs a sequence of vectors which converges to the eigenvector of the eigenvalue with the largest real part. Considering for simplicity the Hermitian operator $H = \gamma_5 D_W$, each step of the iteration multiplies the previous vector by H

$$\eta_{n+1} = H\eta_n,$$

starting from a random vector η_0 . The cost of such an iteration will scale linearly with the volume due to the sparse structure of D_W . Since H is Hermitian, the initial vector η_0 can be written as a linear combination of eigenvectors ϕ_k

$$\begin{aligned}\eta_0 &= \sum_k c_k \phi_k, \\ c_k &= \phi_k^\dagger \eta_0,\end{aligned}$$

and the first iteration of the “Power Method” will output a vector η_1

$$\eta_1 = H\eta_0 = \sum_k c_k \lambda_k \phi_k. \quad (9.11)$$

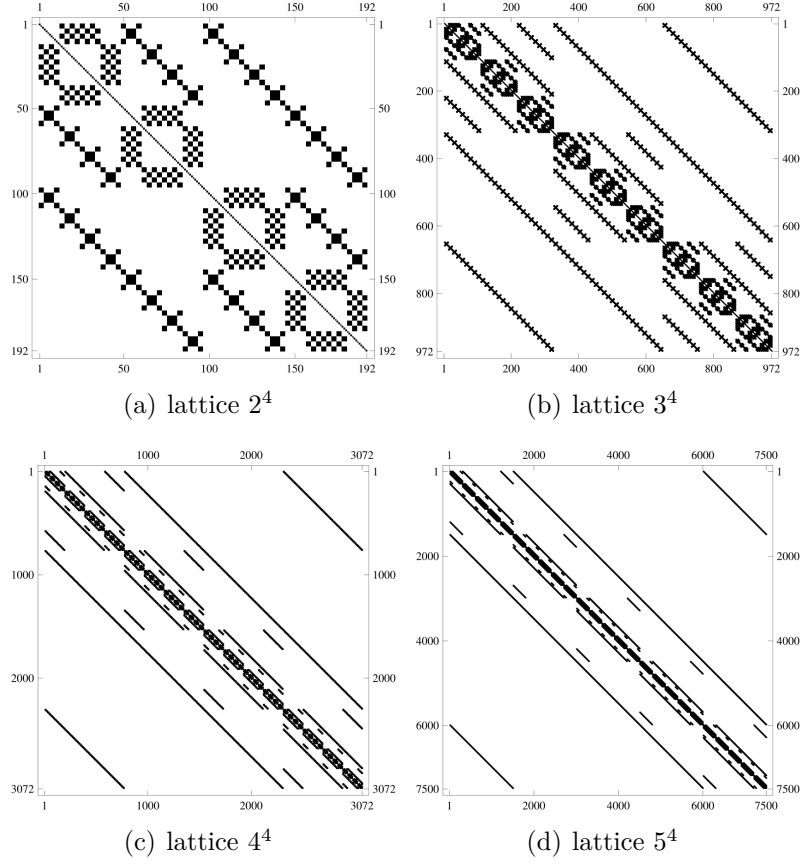


Figure 9.2: Matrix plot of the modulus of the Hermitian Dirac-Wilson operator $\gamma_5 D_W$, to each element corresponds a color proportional to its absolute value. A white pixel corresponds to an element that is zero. The sparse structure of D_W emerges when the lattice size increases, from 2^4 to 5^4 the density of non-zero entries decreases drastically.

After n iterations, the vector η_n will be

$$\eta_n = H^n \eta_0 = \sum_k c_k (\lambda_k)^n \phi_k = \lambda_0^n \phi_0 \left\{ c_0 + \left(\frac{\lambda_2}{\lambda_1} \right)^n c_2 \phi_2 + \left(\frac{\lambda_3}{\lambda_1} \right)^n c_3 \phi_3 + \dots \right\}$$

and the terms in the curly bracket will converge to c_0 in the limit $n \rightarrow \infty$ supposing an increasing ordering $\lambda_1 > \lambda_2 > \lambda_3 > \dots$. If the eigenvalues are doubly degenerate, as in the case of H in the adjoint representation, then the “Power Method” will converge to a linear combination of the subspace generated by the two largest eigenvalues. An orthogonal projection of the remaining vectors with respect to the largest ones will converge to the second, the third, and the next largest eigenvectors. This generalization is known as

Arnoldi algorithm, this method diagonalizes H restricted to the Krylov space K_n defined as

$$K_n = \text{span}\{\eta_0, H\eta_0, H^2\eta_0, \dots, H^n\eta_0\}.$$

Mapping and transformation of H are required to reach other regions of the spectrum, for example the eigenvalues closed to the origin of the complex plane can be extracted from a Krylov space generated by the inverse of H [91].

When a large number of eigenvalues and iterations is considered, the orthogonalization process can be numerically unstable and restarting the whole algorithm from the obtained approximation of the eigenvectors can be necessary. Efficient implementation of the Arnoldi algorithm with advanced technique of restarting are available in literature and coded in the ARPACK package. In the code a naive version of the Arnoldi method is implemented for extracting the spectrum close to the origin of H , while the library PARPACK is used with mappings in the complex plane to compute the sign of the Pfaffian.

9.5 Eigenvalues and chiral anomaly

The $\mathcal{N} = 1$ SYM has a classical $U(1)_A$ axial symmetry, meaning that the transformation

$$\lambda \rightarrow \lambda' = \exp(-i\omega\gamma_5)\lambda \quad (9.12)$$

leaves the action invariant when the gluino mass is exactly zero. This symmetry is known as the R-symmetry $U(1)_R$ in the SUSY language and it corresponds to the relative rotation of the left- and the right-handed Weyl components of the gluino field λ . It does not commute with the supersymmetry transformations, since there are no equivalent “pseudoscalar” rotations of the gauge field A_μ .

A fermion transformation like (9.12) acts effectively as a change of variables of the partition function $Z(\lambda)$. Provided that the action is invariant, $Z(\lambda')$ can still be unequal to $Z(\lambda)$ because of the variation of the measure $D\lambda$. The determinant of the Jacobian J can give a non trivial contribution

$$D\lambda \rightarrow \det(J)^{-1} D\lambda' = \det\{\exp(-i\omega\gamma_5)\}^{-1} D\lambda$$

as soon as J differs from the identity. Using the identity

$$\det(J) = \exp(\text{Tr} \log(J)),$$

one would naively conclude that $\det(J) = 1$

$$\det\{\exp(-i\omega\gamma_5)\} = \exp(-i\omega\text{Tr}(\gamma_5))$$

since $\text{Tr}(\gamma_5) = 0$. This conclusion is however unwarranted, since the trace extends on all the physical states of the theory and must be regularized [78]. Applying the same procedure used to define the Witten index, $\text{Tr}(\gamma_5)$ is regularized as

$$I_T = \lim_{\beta \rightarrow 0} \text{Tr}(\gamma_5 \exp(-\beta \not{D})), \quad (9.13)$$

and the trace evaluated in the continuum on the eigenvectors of \not{D} . The continuum massless Dirac operator is anti-Hermitian and has purely imaginary eigenvalues. The operator \not{D} anticommutes with γ_5

$$\{\not{D}, \gamma_5\} = 0, \quad (9.14)$$

in contrast to Eq. (9.1), and all the non-zero eigenvalues appears in complex conjugate pairs $i\lambda_n$ and $-i\lambda_n$ along the imaginary axis with eigenvector $|\phi_n\rangle$ and $\gamma_5|\phi_n\rangle$

$$\not{D}\gamma_5|\phi_n\rangle = -\gamma_5\not{D}|\phi_n\rangle = -i\lambda_n\gamma_5|\phi_n\rangle.$$

The eigenvector pairs $|\phi_n\rangle$ and $\gamma_5|\phi_n\rangle$ are orthogonal

$$\begin{aligned} i\lambda_n \langle \phi_n | \gamma_5 | \phi_n \rangle &= \langle \phi_n | \gamma_5 \not{D} | \phi_n \rangle = -\langle \phi_n | \not{D} \gamma_5 | \phi_n \rangle = (\not{D} | \phi_n \rangle)^\dagger \gamma_5 | \phi_n \rangle \\ &= -i\lambda_n \langle \phi_n | \gamma_5 | \phi_n \rangle, \end{aligned}$$

$\langle \phi_n | \gamma_5 | \phi_n \rangle = 0$ if $i\lambda_n \neq 0$. As in the case of the Witten index, I_T is completely independent from β

$$\begin{aligned} I_T &\rightarrow \text{Tr}(\gamma_5 \exp(-\beta \not{D})) \\ &= \sum_{\text{zero modes}} \langle \phi_n | \gamma_5 | \phi_n \rangle \exp(-\beta 0) + \sum_{\text{non-zero modes}} \langle \phi_n | \gamma_5 | \phi_n \rangle \exp(-\beta (i\lambda_n)^2) \\ &= \sum_{\text{zero modes}} \langle \phi_n | \gamma_5 | \phi_n \rangle, \end{aligned}$$

since due to the γ_5 orthogonality condition all the contributions from non-zero eigenvalues cancels exactly.

In the subspace spanned by the zero modes, the Dirac operator and γ_5 commutes and can be simultaneously diagonalized. The eigenvalues of γ_5 are ± 1 , $\gamma_5^2 = 1$, therefore the index I_T counts effectively the difference between zero modes of opposite chirality

$$I_T = \nu = n_+ - n_-. \quad (9.15)$$

On the other hand, a direct evaluation of the left side of Eq. (9.13) is possible with differential calculus techniques. The function used to regularize the sum $\exp(-\beta \not{D} \not{D})$ is effectively the operator solution of the heat equation

$$\frac{\partial}{\partial \beta} u(x, \beta) + \not{D} \not{D} u(x, \beta) = 0,$$

so that given the initial condition $u(x, 0)$, its evolution is

$$u(x, \beta) = (\exp(-\beta \not{D} \not{D}))u(x, 0).$$

The parameter β assumes with this interpretation an effective smoothing time similar to the fictitious time t of the Wilson flow, see Ch. 7. The operator $\exp(-\beta \not{D} \not{D})$ can be represented by the integral of the heat kernel $H(x, y; \beta)$

$$u(x, \beta) = (\exp(-\beta \not{D} \not{D}))u(x, 0) = \int d^n y H(x, y; \beta) u(y, 0);$$

in the limit $\beta \rightarrow 0$ the heat kernel reduces to the delta Dirac distribution in n dimensions

$$\lim_{\beta \rightarrow 0} H(x, y; \beta) = \delta^n(x - y).$$

From the physical point of view the operator $\exp(-\beta \not{D} \not{D})$ smooths the initial function $u(x, 0)$ and it links short range distances for β small to long range topological properties for β large. The trace of the operator $\gamma_5 \exp(-\beta \not{D} \not{D})$ can be written in terms of $H(x, y; \beta)$ as

$$\int d^n y \text{Tr}_{\text{spin, color}}(\gamma_5 H(y, y; \beta)).$$

The heat kernel can be asymptotically expanded for small β

$$H(x, y; \beta) = \frac{1}{(2\pi\beta)^{n/2}} \sum_{j=0}^{\infty} a_j(x, y) \beta^j,$$

the crucial point is the computation of the coefficients $a_j(x, y)$. It can be proven that the first $n/2 - 1$ coefficients vanish, ensuring convergence, while the difference of zero modes of opposite chirality of Eq. (9.15) is encoded all in the coefficient $a_{n/2}(x, y)$ [92].

A simpler but informal proof can be given expanding the heat kernel in the Fourier space of the free plane waves. The square of the Dirac operator is

$$\not{D} \not{D} = D_\mu D^\mu + \frac{1}{2} \sigma_{\mu\nu} F^{\mu\nu},$$

the exponential can be Taylor expanded for small field A_μ

$$\begin{aligned} \gamma_5 \exp\{-\beta \not{D} \not{D}\} &= \gamma_5 \exp\left\{-\beta \left(D_\mu D^\mu + \frac{1}{2} \sigma_{\mu\nu} F^{\mu\nu}\right)\right\} \\ &= \gamma_5 \exp\{-\beta \partial_\mu \partial^\mu\} - \frac{\beta}{2} \exp\{-\beta \partial_\mu \partial^\mu\} \gamma_5 \sigma_{\mu\nu} F^{\mu\nu} + \\ &\quad + \frac{\beta^2}{8} \exp\{-\beta \partial_\mu \partial^\mu\} \gamma_5 \sigma_{\mu\nu} \sigma_{\rho\sigma} F^{\mu\nu} F^{\rho\sigma} + \dots, \end{aligned}$$

neglecting higher order terms. The trace is evaluated on the complete set of the planar wave equation $u_s^c(k) = u_s^c \exp(ikx)$, being u_s^c a vector in spinor and color space. On this set $u_s^c(k)$ the standard γ -trace rules are valid and $\text{Tr}(\gamma_5) = 0$, $\text{Tr}(\gamma_5 \sigma_{\mu\nu}) = 0$ and $\text{Tr}(\gamma_5 \sigma_{\mu\nu} \sigma_{\rho\sigma}) = 4\epsilon_{\mu\nu\rho\sigma}$. The final trace then reads

$$I_T = \frac{\beta^2}{2} \int d^4x d^4k \exp\{-\beta k_\mu k^\mu\} \epsilon_{\mu\nu\rho\sigma} F^{\mu\nu} F^{\rho\sigma}.$$

The integration in the momentum space is then simply a factor $(4\pi\beta)^{-2}$ for small β , canceling the β^2 in front of the last equation [78]

$$I_T = \frac{1}{32\pi^2} \int d^4x \epsilon_{\mu\nu\rho\sigma} \text{Tr}_{\text{color}}(F^{\mu\nu} F^{\rho\sigma}). \quad (9.16)$$

This final integral is related to the coefficient $a_{n/2}$ of the asymptotic expansion discussed above. Note that the trace in the color space gives a factor proportional to the number of colors N_c for fermions in the adjoint representation.

The right-hand side of Eq. (9.16) is the field definition of the topological charge Q_{top} . This is the content of index theorem of Atiyah and Singer proven in 1963 [93, 94, 95], which has a significant importance for the structure of the low modes of the Dirac-Wilson operator. The index theorem states that the difference between zero modes of opposite chirality is remarkably equal to the topological charge. The Wilson term breaks Eq. (9.14) on the lattice, therefore the equivalence between topological charge and zero modes exists in this fermion formulation only in the continuum limit.

Chapter 10

Phase diagram for $\mathcal{N} = 1$ SUSY

At finite temperature supersymmetry is a broken symmetry and its effects are therefore somewhat hidden. It is plausible that finite temperature QCD and finite temperature supersymmetric gauge theory are not all that different.

Barton Zwiebach [96]

Monte Carlo simulations on the lattice have been able to explore the non-perturbative thermodynamical behavior of many different gauge models. Strong interacting particles can be found only in colorless bound states at low temperature and their liberation occurs only at high temperature due to asymptotic freedom. A deconfinement phase transition has been found for many non abelian Yang-Mills theories without fermions, see for example Ref. [97, 98]. A milder deconfinement crossover has been observed in full QCD, including also up, down, and strange quarks [99, 100, 101]. A slightly sharper transition has been found looking for the restoration of chiral symmetry. Quark condensation occurs in QCD at zero temperature and only at high temperatures chiral symmetry is realized, providing an another different (pseudo-)critical phase transition. Recent numerical investigations have shown that the restoration of chiral symmetry takes place at temperatures near the deconfinement transition [102]. The physical connection between the two critical temperatures remains, however, unclear due to the lack of an exact order parameter [103].

Only few non-perturbative results are known for supersymmetric Yang-Mills theories (SYM) about their phase diagram at finite temperature. In general, the fundamental symmetries of SYM theories have two opposite

thermodynamical behaviors. Scale and chiral invariance are expected to be restored at sufficient high temperature, but on the contrary supersymmetry itself is explicitly broken for any non zero value of the temperature due to the thermal statistic difference between boson and fermion particles. In the time direction periodic and anti-periodic boundary conditions must be imposed on fermionic and bosonic fields respectively. At zero temperature, in the infinite volume limit, this difference can be neglected and exact SUSY can be formulated consistently. At finite temperature, the temporal direction is compactified and boundary conditions will break the supersymmetry between fermions and bosons [104]. Therefore it does not exist an high temperature limit in which a possible spontaneously or explicitly broken supersymmetry can be restored by thermal fluctuations [105]. This intriguing property was subject of many theoretical studies in the past, in particular for understanding the nature and the pattern of this temperature induced SUSY breaking, see Ref. [106] for a review.

A great interest to study supersymmetric Yang-Mills theories at finite temperature comes from the application of the AdS/CFT conjecture [1] to the description of the QCD quark-gluon plasma (QGP). The equation of state of QCD approaches the conformality after the deconfinement phase transition with substantial deviation from the expected perturbative behavior, even for temperatures of the order of 800 MeV [107]. This open question could be solved in supersymmetric extensions of QCD and analytical string calculations can provide a theoretical understanding of the mysteries of QCD thermodynamics. The AdS/CFT conjecture is a duality between string theory in the classical limit and strong coupling $\mathcal{N} = 4$ SYM in four dimensions [108]. $\mathcal{N} = 4$ SYM is a conformal theory and therefore reductions are needed in order to relate the results to a theory like QCD with a mass-gap. Finite temperature is a possibility to break both supersymmetry and conformal invariance of $\mathcal{N} = 4$ SYM [108] and therefore it could be possible that many basic properties are shared between supersymmetric models at finite temperature and the QCD quark-gluon plasma.

The subject of this chapter is the phase diagram of the $\mathcal{N} = 1$ super Yang-Mills theory at finite temperature. Part of the content of this chapter has been published in Ref. [7]. The $\mathcal{N} = 1$ SYM is confined at zero temperature and a deconfinement phase transition occurs when mesons, glueballs and their bound superpartners melt down. The Polyakov loop is an exact order parameter for the deconfinement transition for any value of the fermion mass, because the gluino is in the adjoint representation. Therefore the relation between deconfinement and chiral symmetry restoration can be studied exactly in the supersymmetrical limit and numerical simulations can provide a better understanding of the thermodynamics of strong interactions. Finite

temperature does not preserve the SUSY transformations between bosons and fermions and thus thermodynamical results could be generalized also to models without supersymmetry. A comparison with the phase diagram of QCD is therefore possible. Dual gravity calculations proved that confinement implies chiral symmetry breaking for a class of supersymmetric Yang-Mills theories [108, 109].

10.1 Finite temperature SUSY

The starting point for the finite temperature formulation of any quantum field theory is the canonical partition function $Z(\beta)$

$$Z(\beta) = \text{Tr}(\exp(-\beta \hat{H}(\phi))) \quad (10.1)$$

where β is related to the inverse of the physical temperature, $\beta = \frac{1}{\kappa_B T}$. The partition function can be written in terms of a sum of energy eigenvalues E_n of the Hamiltonian \hat{H}

$$Z(\beta) = \sum_n \langle n | \exp(-\beta \hat{H}(\phi)) | n \rangle = \sum_n \exp(-\beta E_n).$$

The trace (10.1) can be evaluated also in the path integral formalism, with the same calculations of zero temperature studies it is possible to show that

$$Z(\beta) = \int D\phi \exp \left\{ - \int_0^\beta dt \int d^3x \mathcal{L}(\phi) \right\}, \quad (10.2)$$

where the time dimension is compactified with length equal to β .¹

The boundary conditions are periodic for boson fields and antiperiodic for fermion fields. The difference between the boundary conditions of fermions and bosons has the important consequence that supersymmetry is broken at any finite temperature. At zero temperature, where the length of compactified temporal dimension goes to infinity, the fields are not sensible anymore to any boundary conditions. At finite temperature instead the symmetry between bosons and fermions is broken and therefore supersymmetry is not realized anymore.

More formally, it is possible to consider the supersymmetry transformations δ_ϵ of the thermal average of a generic fermionic operator $O(\phi)$ [104]

$$\delta_\epsilon O(\phi) = \epsilon_\mu \{Q_\mu, O(\phi)\} \quad (10.3)$$

¹Here β is proportional to the inverse of the temperature, it must not be confused with the square of the inverse of the gauge coupling.

evaluated at finite temperature

$$\begin{aligned}
\langle \delta_\epsilon O \rangle_\beta &= \text{Tr}(\epsilon_\mu \{Q_\mu, O\} \exp(-\beta \hat{H})) \\
&= \text{Tr}(\epsilon_\mu Q_\mu O \exp(-\beta \hat{H})) + \text{Tr}(\epsilon_\mu O Q_\mu \exp(-\beta \hat{H})) \\
&= \text{Tr}(\epsilon_\mu O \exp(-\beta \hat{H}) Q_\mu) + \text{Tr}(\epsilon_\mu O Q_\mu \exp(-\beta \hat{H})) \\
&= \text{Tr}(\epsilon_\mu O Q_\mu \exp(-\beta \hat{H})) + \text{Tr}(\epsilon_\mu Q_\mu O \exp(-\beta \hat{H})) \quad (10.4)
\end{aligned}$$

$$\begin{aligned}
&= 2 \sum_n \langle n | \epsilon_\mu O Q_\mu | n \rangle \langle n | \exp(-\beta \hat{H}) | n \rangle \\
&= 2 \sum_n \langle n | \epsilon_\mu O Q_\mu | n \rangle \exp(-\beta E_n) \quad (10.5)
\end{aligned}$$

where in (10.4) it is used the fact that the supercharges commute with the Hamiltonian. In the zero temperature limit, β goes to infinity and only the vacuum states $|0\rangle$ with $E_0 = 0$ give a contribution to the sum. If supersymmetry is not spontaneously broken, then $Q_\mu |0\rangle = 0$ and therefore any variation of any operator with respect to supersymmetry vanishes, $\langle \delta_\epsilon O \rangle_\infty = 0$. This implies that supersymmetry is conserved. If instead $\beta \neq \infty$, then any state $|n\rangle$ gives contributions to the sum and the supersymmetric charge interchanges only fermionic and bosonic states. In general, without any other specification about the operator O , $\langle \delta_\epsilon O \rangle_\beta \neq 0$ and supersymmetry is broken.

The situation would be different if

$$Z_P(\beta) = \text{Tr}((-1)^F \exp(-\beta \hat{H}(\phi)))$$

is used instead of the standard partition function. It can be shown that $Z_P(\beta)$ corresponds to the standard partition function in the path integral formalism but where periodic boundary conditions are applied also to the fermionic fields. Now the sum (10.5) is

$$\langle \delta_\epsilon O \rangle_\beta = 2 \sum_n \langle n | \epsilon_\mu O (-1)^F Q_\mu | n \rangle \exp(-\beta E_n),$$

If supersymmetry is not broken, the states with positive energy will come in pairs and summed now with different signs due to the $(-1)^F$ operator. The contribution from all the states will be exactly zero and only the vacuum term will survive, if supersymmetry is not spontaneously broken then $\langle \delta_\epsilon O \rangle_\beta = 0$ for any temperature. From this argument it is possible to conclude that periodic boundary condition for fermions preserves supersymmetry while the antiperiodic one breaks it.

10.2 The finite temperature phase diagram

The phase diagram is considered here in function of the gluino mass and of the temperature. Different regions are characterized in the phase diagram

by the expectation value of order parameters related to confinement and to fermion condensation.

10.2.1 Center symmetry and confinement

The $\mathcal{N} = 1$ SYM is an asymptotically free theory, expected to behave at high temperatures as a conformal gas of free gluons and gluinos [31]. The order parameter for the deconfinement phase transition is the Polyakov loop

$$P_L = \frac{1}{V} \sum_{\vec{x}} \text{Tr} \left\{ \prod_{t=0}^{N_t} U_4(\vec{x}, t) \right\}.$$

The expectation value of the Polyakov loop has the physical meaning of the exponential of the negative free energy of a single static Dirac quark in the fundamental representation

$$\langle P_L \rangle = \exp \left(-\frac{F_q}{T} \right).$$

Therefore a non-vanishing value of $\langle P_L \rangle$ means that a state with a single isolated quark exists, i. e. deconfinement. Deconfinement is associated with the spontaneous breaking of the center symmetry, defined by the transformation of the gauge fields in a fixed time-slice at $t = t'$:

$$U_4(\vec{x}, t') \rightarrow U_4(\vec{x}, t')' = \exp \left(2\pi i \frac{n}{N_c} \right) U_4(\vec{x}, t') \quad n \in \{0, 1, \dots, N_c - 1\}.$$

A similar phase rotation cannot be reabsorbed by a gauge transformation due to the periodic boundary conditions applied to gluon fields in the time direction. In contrast to QCD with fermions in the fundamental representation, center symmetry is left invariant by both the gauge and the fermion part of the action in the case of $\mathcal{N} = 1$ SYM. In fact, the Wilson-Dirac operator is written in terms of links in the adjoint representation that are unaffected by complex rotations. On the other hand, the Polyakov loop transforms non-trivially under the center transformations

$$P_L \rightarrow P_L' = \exp \left(2\pi i \frac{n}{N_c} \right) P_L,$$

and it is thus an exact order parameter for the deconfinement transition for any value of the gluino mass m . The pattern for the center symmetry breaking is hence the same as in pure $\text{SU}(N_c)$ gauge theories, and it is possible that the Svetitsky-Yaffe conjecture [110] is valid for $\mathcal{N} = 1$ SYM. This conjecture implies a deconfinement transition of second order for the gauge group $\text{SU}(2)$, corresponding to the universality class of the Z_2 Ising model in three dimensions.

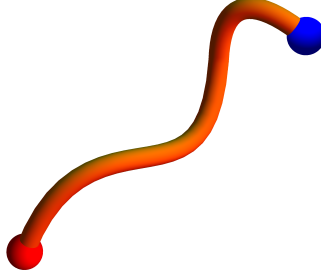


Figure 10.1: Two test particles are strongly interacting and the chromodynamical flux is confined into a small tube. In the case of $\mathcal{N} = 1$ SYM, the flux tube can be effectively described as either bosonic or fermionic string.

10.2.2 Static mesino and Polyakov loopino

Even if supersymmetry is broken at finite temperature, it could be in any case interesting to ask what SUSY transformations imply for the order parameter of the deconfinement phase transition. A single Polyakov loop is changed into a fermion under SUSY transformation as

$$P_L(x) \rightarrow D_L^\alpha(x) = \sum_{t'} \sum_i G_i^{i\alpha}(t')$$

$$G_i^{i\alpha} = (U_4(x, 0) \cdots U_4(x, t'))_j^i (\gamma_4)^\alpha_\beta \lambda_\beta^a(x, t') (T_a)_k^j (U_4(x, t') \cdots U_4(x, N_t))_l^k$$

with the insertion of a gluino λ smeared along the Wilson line. The operator D_L is the supersymmetrical partner of P_L , a “Polyakov loopino”, and it has effectively the quantum number of a Majorana fermion. Gauge invariance of $D_L^\alpha(x)$ is ensured by the adjoint representation of the gluino field, since clearly

$$\begin{aligned} U_4(x, t) &\rightarrow \Omega_F(x, t) U_4(x, t) \Omega_F^\dagger(x, t+1) \\ \lambda_\beta^a(x, t) T_a &\rightarrow \Omega_A(x, t)_b^a \lambda_\beta^b T_a \\ \Omega_A(x, t)_b^a &= 2\text{Tr}(\Omega_F(x, t) T^a \Omega_F(x, t)^\dagger T_b) \\ \lambda_\beta^a(x, t) T_a &\rightarrow \Omega_F(x, t) (\lambda_\beta^a(x, t) T_a) \Omega_F(x, t)^\dagger \end{aligned} \quad (10.6)$$

and therefore the matrix gauge transformations $\Omega_F(x, t)$ cancels at the insertion of the gluino field as well as at the other points of the Polyakov loop.

While the correlator of two Polyakov loop P_L represents the expectation value of a meson, the correlator $C^{\alpha\beta}(x-y)$ of two $D_L^\alpha(x)$

$$C^{\alpha\beta}(x-y) = \langle D_L^\alpha(x) D_L^\beta(y) \rangle$$

represents the expectation value of a mesino. When external static quarks in the fundamental representation couple to a pure supersymmetric gluodynamics, their quantum states will be a mixture of mesons and their superpartner mesinos [111]. From the effective string point of view, the chromodynamical flux is confined inside a small fluctuating tube connecting the two external sources due to the linear behavior of the strong potential. The fluctuation of the flux tube is then quantized in terms of a bosonic effective string. In the $\mathcal{N} = 1$ SYM, gluinos are the supersymmetrical partner of the gluons and they are expected to give contributions to the chromodynamical flux, therefore also a fermionic string is expected to emerge in the infrared regime of the long range strong supersymmetric interactions.

It is well known that a non vanishing expectation value of the Polyakov loop $\langle P_L \rangle$ implies the disappearance of the string tension, the linear term of the logarithm of the Polyakov loop correlator. From first principles, since SUSY is broken at finite temperature, this does not ensure automatically that also the correlator $C^{\alpha\beta}(x-y)$ would loose its linear behavior when $\langle P_L \rangle \neq 0$. It would then be an interesting investigation the study of the behavior of $C^{\alpha\beta}(x-y)$ at finite temperature.

10.2.3 Chiral phase transition

As discussed in the previous chapter, the $\mathcal{N} = 1$ SYM has a classical $U(1)_A$ axial symmetry broken by quantum fluctuations. The chiral Ward identity has a dependence on N_c absent in QCD

$$\partial_\mu J_5^\mu = \partial_\mu (\bar{\lambda} \gamma^\mu \gamma_5 \lambda) = N_c \frac{g^2}{32\pi^2} \epsilon_{\mu\nu\rho\sigma} F^{\mu\nu} F^{\rho\sigma},$$

typical of gauge models with fermions in the adjoint representation.

The anomalous contribution to the axial transformations can be absorbed in the periodicity of the parameter Θ :

$$\Theta \rightarrow \Theta - 2N_c\omega \tag{10.7}$$

if the angle ω assumes one of the values $\omega = \frac{n\pi}{N_c}$, $n = 0, \dots, 2N_c - 1$. The remaining chiral symmetries thus form the group Z_{2N_c} . Numerical investigations [30] have confirmed the conjecture [31, 32, 33] that this invariance is spontaneously broken at zero temperature by a non-vanishing expectation

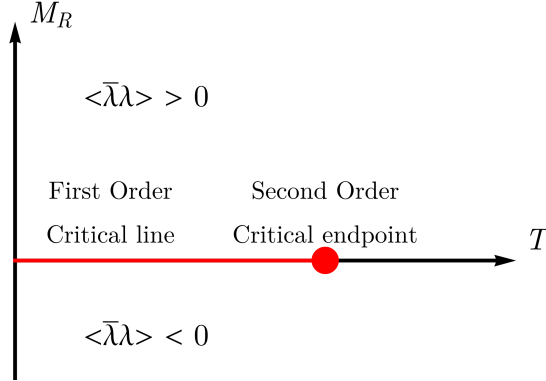


Figure 10.2: Expected phase diagram for chiral symmetry breaking of $\mathcal{N} = 1$ SYM with gauge group $SU(2)$. The chiral condensate $\langle \bar{\lambda}\lambda \rangle$ is the order parameter of the chiral phase transition. Each non-zero value of the renormalized gluino mass M_R introduces a source of chiral symmetry breaking. At low temperatures, moving from positive to negative gluino masses M_R , the chiral condensate jumps from a positive to a negative expectation value. The phase transition is therefore of first order with a coexistence of two different phases. The line of first order phase transitions is expected to terminate in a second order endpoint.

value of the gluino condensate $\langle \bar{\lambda}\lambda \rangle \neq 0$ to a remaining Z_2 symmetry corresponding to the sign flip $\lambda \rightarrow -\lambda$. The complete pattern of chiral symmetry breaking is thus

$$U(1)_A \rightarrow Z_{2N_c} \rightarrow Z_2. \quad (10.8)$$

The phase transition associated with the spontaneous breaking $Z_{2N_c} \rightarrow Z_2$ is of first order at zero temperature: the expectation value of the chiral condensate jumps from positive to negative. The system is in this respect similar to a Z_{N_c} Ising model ($Z_{N_c} = Z_{2N_c}/Z_2$), with the gluino condensate corresponding to the spontaneous magnetization and the renormalized gluino mass to the external magnetic field. This similarity suggests that for the gauge group $SU(2)$ there is a critical temperature T_c^{chiral} of a second order phase transition and a phase with restored Z_4 symmetry at high temperatures, see Fig. 10.2.

There are three possible scenarios for the relation of deconfinement and chiral symmetry restoration. T_c^{chiral} might coincide with the deconfinement transition temperature $T_c^{\text{deconf.}}$, but other scenarios are possible from first principles. If they do not coincide either a mixed deconfined phase with broken chiral symmetry or a mixed confined phase with restored chiral symmetry exists, see Fig. 10.3.

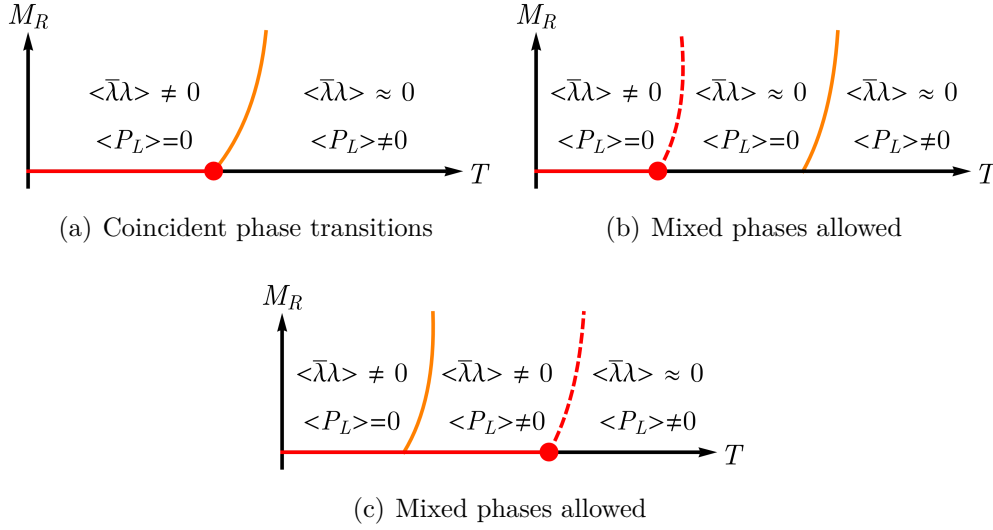


Figure 10.3: Possible scenarios for the phase diagram of $\mathcal{N} = 1$ SYM. The two chiral phases are separated by a crossover for $M_r \neq 0$ (dashed red lines) and by a phase transition in the massless limit. The orange line represents the deconfinement phase transition, present for any value of M_R . (a) In the supersymmetric limit chiral and deconfinement transition coincide. (b) A mixed confined phase occurs with chiral symmetry restored. (c) A mixed deconfined phase occurs with chiral symmetry broken.

Finally, the remaining part of the $U(1)_R$ symmetry broken by the anomaly could be effectively restored in high temperature limit.

10.3 The deconfinement phase transition

Simulations have been done for different spatial and temporal lattice extents to study the deconfinement phase transition, with lattice sizes $N_s^3 \times N_\tau = 8^3 \times 4, 12^3 \times 4, 16^3 \times 4$ and $10^3 \times 5$. Different spatial volumes estimate the influence of finite size effects and different temporal extents probe for lattice artifacts. The details of the simulations, done around critical point, are summarized in Table 10.1. The autocorrelation between consecutive configurations generated by the RHMC algorithm increases drastically near the critical point of the deconfinement transition and more statistics is needed to compensate this effect. Many tunnelings between different phases are needed to estimate correctly the scaling behavior requiring a large amount of computer time.

N_τ	N_s	β	$N_{\text{conf.}}$	τ	κ_c^{dec}
4	8	1.65	150000	400	0.1600(50)
4	12	1.65	80000	1100	0.1600(50)
4	16	1.65	40000	1600	0.1580(50)
5	15	1.65	20000	1500	0.1850(25)
5	15	1.62	20000	1500	0.1925(20)
5	15	1.60	20000	1500	0.1950(20)

Table 10.1: The table summarizes the number of measurements $N_{\text{conf.}}$, produced at the κ_c^{dec} value, for estimating the deconfinement transition using the action without stout smearing. The autocorrelation time τ is computed for the Polyakov loop at the critical point.

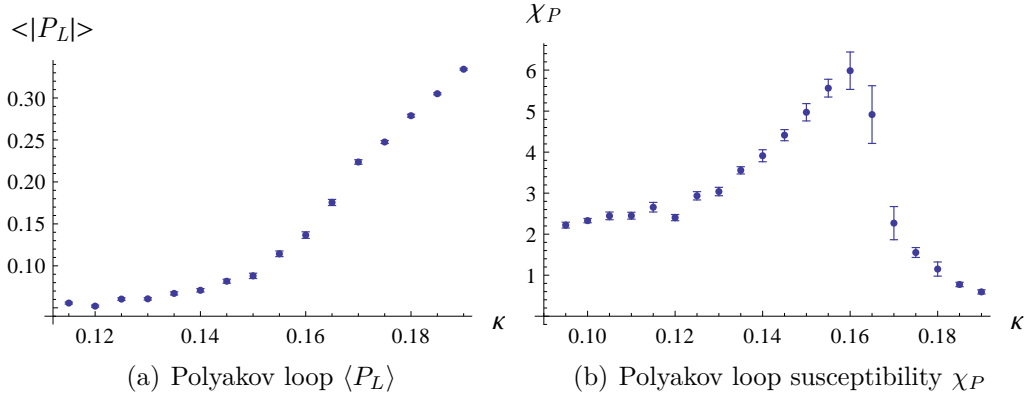


Figure 10.4: The expectation value of the Polyakov loop and of its susceptibility on a $12^3 \times 4$ lattice at $\beta = 1.65$.

The bare gluino mass

$$m = \frac{1 - 8\kappa}{2\kappa} \quad (10.9)$$

is varied for each N_τ and for each β to locate the exact point of the deconfinement phase transition. Fig. 10.4(a) demonstrates this approach for a lattice size $12^3 \times 4$ and $\beta = 1.65$, where the Polyakov loop starts to rise at $\kappa \simeq 0.15$. The point of the phase transition can be determined more precisely by the maximum of the Polyakov loop susceptibility²

$$\chi_P = V(\langle |P_L|^2 \rangle - \langle |P_L| \rangle^2). \quad (10.10)$$

²Here the susceptibility is defined in terms of the modulus of the Polyakov loop. While this choice does not alter the position of the peak, it introduces a non-zero value of χ_P below the critical point.

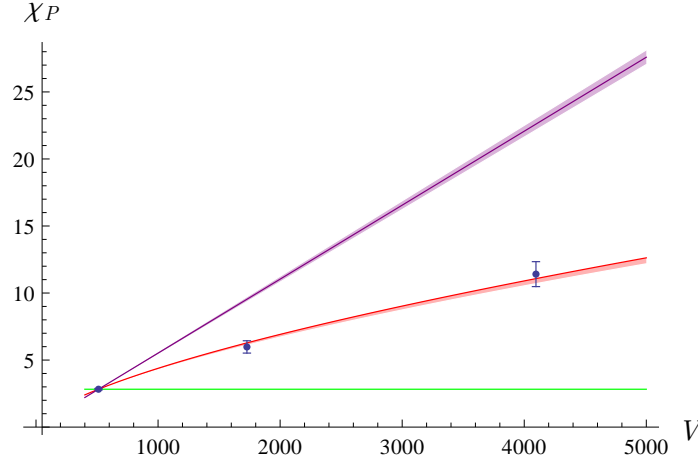


Figure 10.5: Finite size scaling for the susceptibility $\chi(|P_L|)$ at $\beta = 1.65$ and $\kappa = 0.160$. The red line is the expected scaling for a second order phase transition in the universality class of the Z_2 Ising model, the purple and the green lines represent instead a first order phase transition and a cross-over, respectively. The colored shadows indicate the errors from the extrapolation of Eq. (10.11).

The susceptibility shows a clear peak at $\kappa = 0.160(5)$, this point defines the deconfinement phase transition for a supersymmetric Yang-Mills theory broken by the renormalized gluino mass corresponding to the bare $m = -0.875$. The critical point defined in this way has only a mild finite volume dependence, which is impossible to distinguish with the current precision.

The finite size scaling of the susceptibility χ_P contains information about how the correlation length diverges in the infinite volume limit and about the order of the phase transition. The susceptibility has a scaling dependence on the volume,

$$\frac{\chi_P(V_1)}{\chi_P(V_2)} = \left(\frac{V_1}{V_2}\right)^x, \quad (10.11)$$

which is linear for a first order phase transition ($x = 1$), flat for a crossover behavior ($x = 0$), and non-linear, with $x = 0.657(4)$, for a second order phase transition in the universality class of three-dimensional Z_2 Ising model [112]. The ratios of the Polyakov loop susceptibility is computed for $V_2 = 8^3$ and $V_1 = 12^3, 16^3$ with $N_\tau = 4$ and the resulting volume dependence is shown in Fig. 10.5. The Svetitsky-Yaffe conjecture is in good agreement with the data and a possible change from the second order phase transition of pure gauge theory to first order induced by gluinos seems to be excluded.

As a further evidence for this statement the distributions of the Polyakov

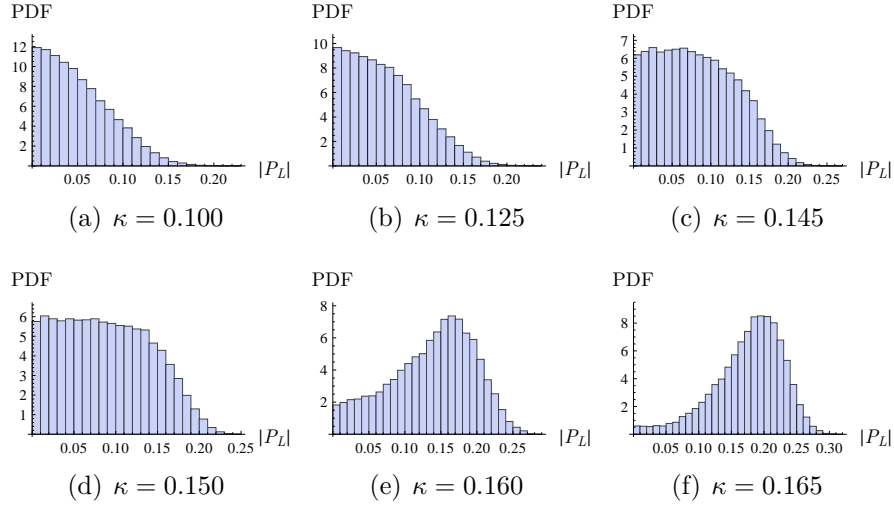


Figure 10.6: Polyakov loop distribution on a $12^3 \times 4$ lattice at $\beta = 1.65$ and various κ .

loop at different values of κ demonstrate the slow continuous emergence of a new peak in addition to the central distribution of the absolute value, see Fig. 10.6. This is in accordance with the divergence of the correlation length at a second order phase transition.

The peak of the Polyakov loop susceptibility, Eq. (10.10), defines a critical combination of bare parameters (κ, β) , see Table 10.1. The associated critical temperature,

$$T = \frac{1}{N_t a}, \quad (10.12)$$

can be compared to other relevant scales of the model and between simulations at different gauge couplings only if a common observable is used to fix the scale as explained in Ch. 7. The parameter w_0 is measured to this end at zero temperature at these values with new simulations, see Table 10.2. The supersymmetric limit can be extrapolated once that the value of the adjoint pion mass is computed in a partially quenched approach.

In the mass independent scheme the scale w_0 is first extrapolated to the chiral limit w_0^e and used for all the simulations with the same β . The temperature is $w_0^e T_c$ and the gluino mass is then proportional to $(w_0^e m_{a-\pi})^2$. The points $((w_0^e m_{a-\pi})^2, w_0^e T_c)$ are linearly interpolated, and the deconfinement temperature is extrapolated to

$$M_R^{w_0^e} \equiv (w_0^e m_{a-\pi})^2 = 0.$$

The linear fit shown in Fig. 10.7(a) clearly indicates that the deconfinement

N_τ	N_s	β	κ	$am_{a-\pi}$	w_0/a	w_0^e/a
20	10	1.65	0.1600	1.7182(09)	1.179(02)	1.428(36)
20	10	1.65	0.1825	1.1138(20)	1.310(09)	1.428(36)
20	10	1.65	0.1850	1.0277(24)	1.340(09)	1.428(36)
20	10	1.65	0.1875	0.9342(22)	1.326(13)	1.428(36)
20	10	1.62	0.1900	0.9398(26)	1.258(23)	1.359(34)
20	10	1.62	0.1925	0.8331(29)	1.297(23)	1.359(34)
20	10	1.62	0.1950	0.7067(44)	1.384(31)	1.359(34)
20	10	1.60	0.1950	0.8159(62)	1.277(20)	1.307(30)
20	10	1.60	0.1975	0.6868(40)	1.351(26)	1.307(30)
20	10	1.60	0.2000	0.4980(58)	1.553(31)	1.307(30)

Table 10.2: The table summarizes the zero temperature measurements done for setting the scale without stout smearing. w_0/a is the mass dependent value while w_0^e/a is the mass independent one, i. e. obtained by extrapolation to $(w_0 m_{a-\pi})^2 = 1$.

transition occurs at lower temperatures when the gluino mass is decreased,

$$w_0^e T_c(M_R^{w_0^e}) = 0.0190(22)M_R^{w_0^e} + 0.2432(45). \quad (10.13)$$

The final extrapolation to the supersymmetric limit $M_R^{w_0^e} = 0$ leads to

$$w_0^e T_c = 0.2432(45), \quad (10.14)$$

where the quoted error is only statistical.

Instead in a mass-dependent renormalisation scheme, the scale is not extrapolated first to the chiral limit. The lattice spacing is allowed to change with the gluino mass and the temperature $w_0 T_c$ and the gluino mass $(w_0 m_{a-\pi})^2$ will be determined with the w_0 measured at zero temperature with the same κ and β . The points $((w_0 m_{a-\pi})^2, w_0 T_c)$ with w_0 determined at the same value of the bare parameters κ and β at the phase transition are linearly interpolated,

$$w_0 T_c(M_R^{w_0}) = 0.01234(7)M_R^{w_0} + 0.2441(26), \quad (10.15)$$

where $M_R^{w_0} \doteq (w_0 m_{a-\pi})^2$. The interpolation is shown in Fig. 10.7(b). The slope is different due to the change of renormalisation scheme. However, the final extrapolation to the supersymmetric limit leads to the compatible result

$$w_0 T_c = 0.2441(26),$$

but with a smaller error due to the more precise determination of the scale for points with heavier gluino masses.

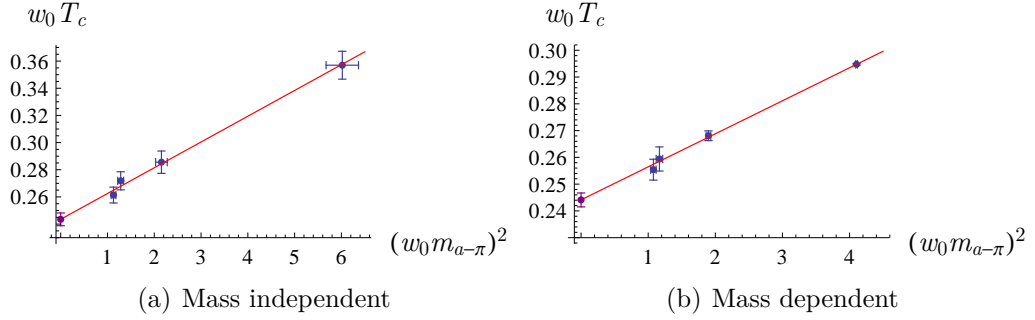


Figure 10.7: The critical temperature of the deconfinement phase transition is extrapolated to the supersymmetric limit by extrapolating the results to the point where $(w_0 m_{a-\pi})^2$ is equal to zero. The four points plotted in the two figures can be found in Table 10.2.

For a comparison of $\mathcal{N} = 1$ SYM and pure gauge theory, the scale w_0/a has been computed at infinite gluino mass on a lattice 18^4 and $\beta = 1.829$. The chosen β is the critical value for the deconfinement transition of pure SU(2) Yang-Mills theory with a Symanzik improved gauge action at $N_\tau = 6$ [113]. The measured value of

$$w_0/a = 1.7649(78) \quad (10.16)$$

leads to

$$w_0 T_c = 0.2941(13) \quad (10.17)$$

for pure SU(2) Yang-Mills theory.

The ratio of the deconfinement temperatures for pure and supersymmetric Yang-Mills theory is thus

$$\frac{T_c(\text{SYM})}{T_c(\text{pure Yang-Mills})} = 0.826(18), \quad (10.18)$$

where the comparison is of course dependent on the observable chosen to set scale. Introducing physical units by setting $T_c = 240$ MeV for the critical temperature in pure gauge theory, a physical value of the deconfinement phase transition temperature for $\mathcal{N} = 1$ SU(2) supersymmetric Yang-Mills theory can be obtained

$$T_c = 198(4) \text{ MeV}. \quad (10.19)$$

In the analysis of the deconfinement transition there are no evidences for contributions from negative Pfaffians even at the largest values of κ .

10.4 The chiral phase transition

The order parameter of the chiral phase transition is the gluino condensate. A non-zero expectation value of this parameter signals the breaking of the Z_4 remnant of the $U(1)_R$ symmetry. The bare gluino condensate is defined as the derivative of the logarithm of the partition function with respect to the bare gluino mass parameter,

$$\langle \bar{\lambda}\lambda \rangle_B \doteq -\frac{T}{V} \frac{\partial}{\partial m} \log(Z(\beta, m)). \quad (10.20)$$

Chiral symmetry is broken by the Curci-Veneziano action with the Wilson-Dirac operator for the fermions, and the bare gluino condensate $\langle \bar{\lambda}\lambda \rangle_B$ acquires an additive and multiplicative renormalisation

$$\langle \bar{\lambda}\lambda \rangle_R = Z_{\bar{\lambda}\lambda}(\beta) (\langle \bar{\lambda}\lambda \rangle_B - b_0). \quad (10.21)$$

At zero temperature a first order transition is expected when the bare gluino mass is changed, crossing a critical value corresponding to $M_R = 0$. Close to such a transition the histogram of $\langle \bar{\lambda}\lambda \rangle$ shows a two peak structure in a finite volume. The transition can be identified with the point where the symmetry of the two peaks changes, as done in [30]. Such an analysis is independent of the renormalisation described in Eq. (10.21). At finite temperatures the first order chiral phase transition extends to a phase transition line at $M_R = 0$, terminating in a second order end-point. Beyond that point the transition changes from first order to a cross over, see Fig. 10.3. For this reason, considerations on the renormalisation procedure become important for the precise localization of the phase transition.

The additive renormalisation is removed by a subtraction of the zero temperature result³

$$\langle \bar{\lambda}\lambda \rangle_S = \langle \bar{\lambda}\lambda \rangle_B^{T=0} - \langle \bar{\lambda}\lambda \rangle_B^T.$$

The calculation of the renormalisation constant $Z_{\bar{\lambda}\lambda}(\beta)$ can be avoided in a fixed scale approach, where the bare coupling β and κ are fixed and the temperature is changed by a variation of N_τ .

The bare gluino condensate is obtained from the trace of the inverse Wilson-Dirac operator,

$$\begin{aligned} -\frac{T}{V} \frac{\partial}{\partial m} \log(Z(\beta, m)) &= -\frac{1}{Z(\beta, m)} \frac{T}{V} \frac{\partial}{\partial m} \left\langle \exp \left(\frac{1}{2} \text{tr} \log(D_W(m)) \right) \right\rangle_{S_g} \\ &= -\frac{T}{V} \left\langle \frac{1}{2} \text{tr}(D_W^{-1}) \right\rangle. \end{aligned}$$

³Notice that with this convention the chiral condensate will be zero at zero temperature and non-zero at very high temperature.

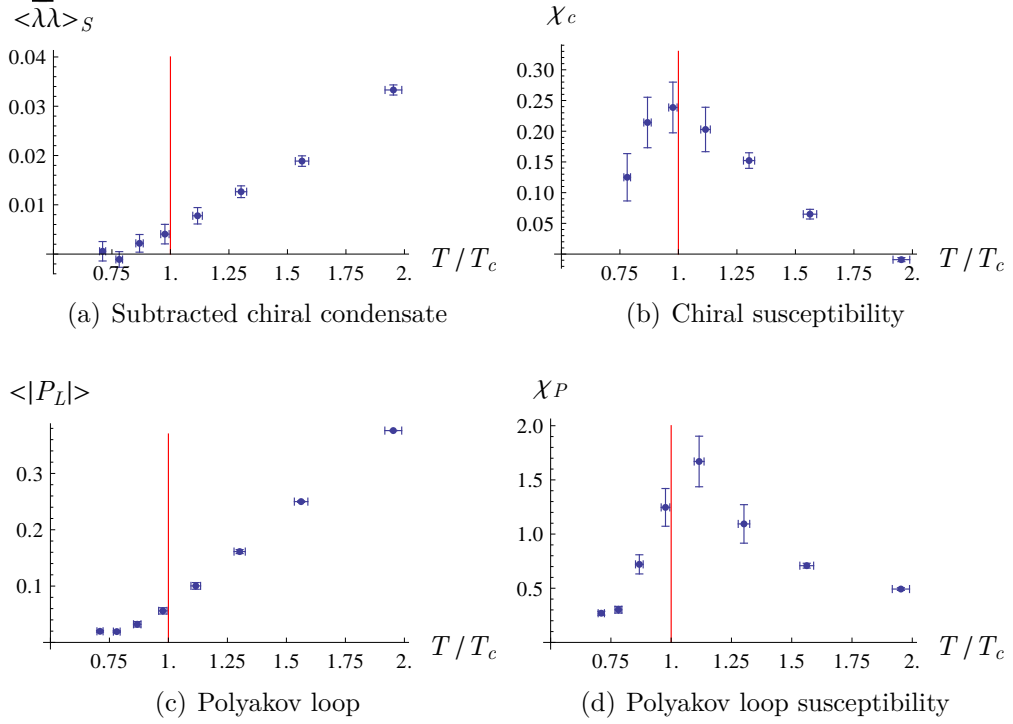


Figure 10.8: a-b) Chiral condensate and its susceptibility on a $12^3 \times N_\tau$ lattice at $\beta = 1.7$, $\kappa = 0.192$; c-d) Polyakov loop and its susceptibility at the same parameters. T_c refers to the deconfinement transition temperature obtained from an extrapolation to the supersymmetric limit using Eq. (10.15).

Here and in the following $\langle O \rangle_{S_g}$ denotes the functional integral with respect to the gauge part of the action, i. e. $Z(\beta, m) = \left\langle \exp \left(\frac{1}{2} \text{tr} \log(D_W(m)) \right) \right\rangle_{S_g}$, where a positive Pfaffian is assumed. The trace of the inverse Wilson-Dirac operator is evaluated with 20 random noise vectors using the stochastic estimator technique. The simulations are done on a lattice $12^3 \times N_\tau$, with $N_\tau \in \{4, \dots, 11\}$, $\beta = 1.7$, and $\kappa = 0.192$. A simulation at zero temperature, i. e. $N_\tau = 12$, has been performed to determine the adjoint pion mass $am_{a-\pi} = 0.388(9)$ and the value of the scale $w_0/a = 2.070(38)$.

The subtracted chiral condensate starts to rise at $N_\tau \simeq 7$, but its behavior is quite smooth due the crossover nature of the transition away from the supersymmetric limit, see Fig. 10.8(a). For a better identification of the pseudo-critical transition point, the peak of the chiral susceptibility χ_c is determined. This observable is equal to the derivative of the gluino condensate

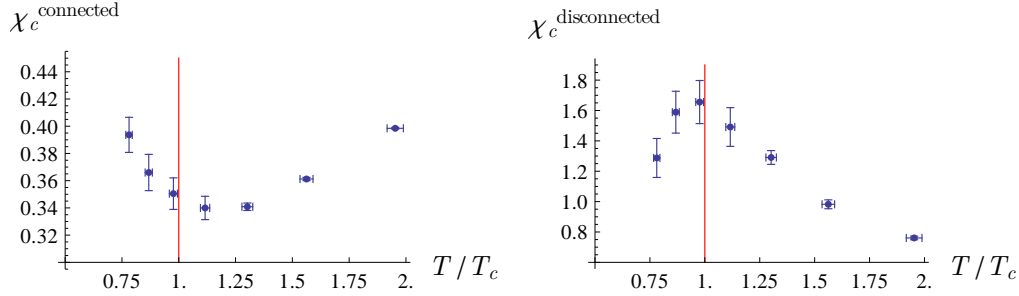


Figure 10.9: Comparison of connected (left) and disconnected (right) contributions to the chiral susceptibility on a $12^3 \times N_\tau$ lattice at $\beta = 1.7$, $\kappa = 0.192$. Notice the different scale used in the two plots.

and it has connected and disconnected contributions

$$\begin{aligned}
 \chi_c &= -\frac{T}{V} \frac{\partial^2}{\partial m^2} \log(Z(g, m)) \\
 &= -\frac{T}{V} \frac{\partial}{\partial m} \left\langle \frac{1}{2} \text{tr}(D_W^{-1}) \exp \left(\frac{1}{2} \text{tr} \log(D_W(m)) \right) \right\rangle_{S_g} \\
 &= -\frac{T}{V} \left\{ \left\langle \frac{1}{4} \text{tr}(D_W^{-1})^2 \right\rangle - \left\langle \frac{1}{4} \text{tr}(D_W^{-1}) \right\rangle^2 - \left\langle \frac{1}{2} \text{tr}(D_W^{-2}) \right\rangle \right\}. \quad (10.22)
 \end{aligned}$$

The connected contribution is expected to vanish in the supersymmetric limit. In the range of parameters that considered in this investigation the disconnected contribution is already dominant and the connected contribution can be neglected for a localization of the peak, see Fig. 10.9. In that respect the relevant dynamics of the phase transition is already close to the one at a vanishing renormalized gluino mass. Even though the connected contribution is negligible, the complete observable is considered in the following, to ensure the absence of additional systematic uncertainties in our extrapolations.

The results of the simulations are shown in Fig. 10.8(b). Even though there is quite a broad central region, a visible peak can be identified corresponding to the value at $N_\tau = 9$. For comparison, the Polyakov loop is shown in Fig. 10.8(c). It acquires a non-vanishing expectation value at $N_\tau = 8$. This small deviation is consistent with the scenario of a chiral symmetry restoration and a deconfinement phase transition at the same temperature.

In order to provide an upper limit for the chiral symmetry restoration temperature, new simulations have been done approximately at the supersymmetric limit, i. e. around the value of κ where the adjoint pion mass is expected to vanish, following the approach of [30]. This corresponds to

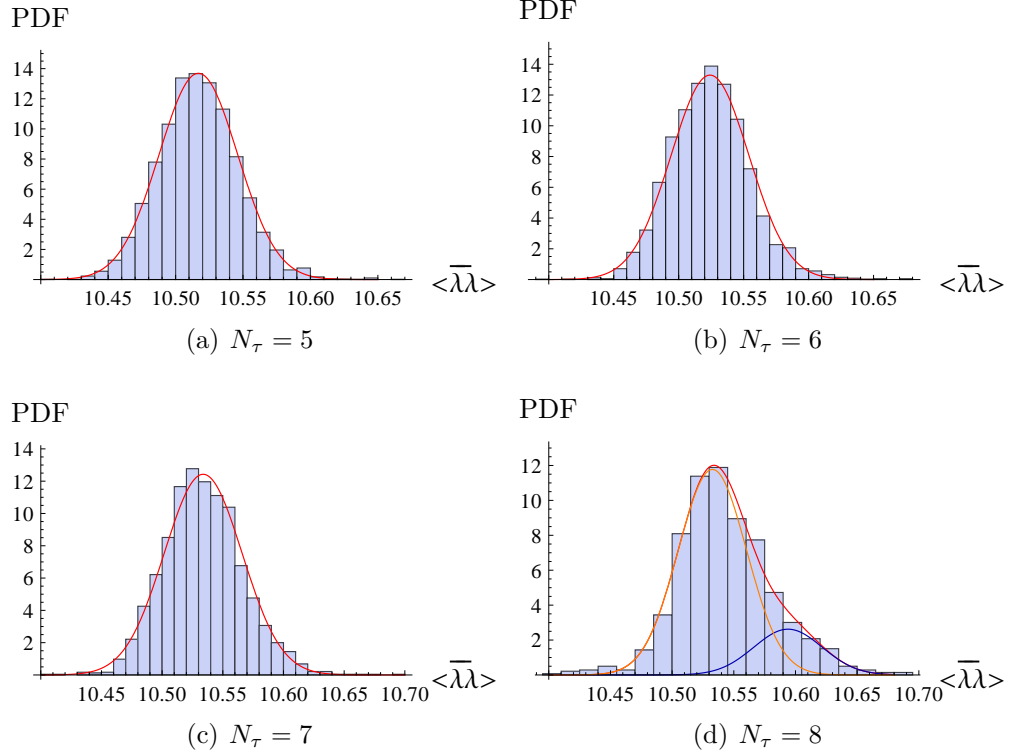


Figure 10.10: Distributions of the chiral condensate on $12^3 \times N_\tau$ lattices at $\beta = 1.7$ and $\kappa = 0.194$. For $N_\tau = 5$ the distribution is compatible with a single Gaussian, while for $N_\tau = 8$ a second peak emerges.

$\kappa = 0.194$ at $\beta = 1.7$. The lattice sizes were chosen to be $12^3 \times N_\tau$ with $N_\tau \in \{5, 6, 7, 8\}$. Note that these simulations cannot be done at large values of N_τ , due to the long time needed for a convergence of the conjugate gradient algorithm in zero temperature limit. The distributions are displayed in Fig. 10.10. At high temperatures, like $N_\tau = 5$, the distribution is close to a Gaussian without any indications for a double peak in the gluino condensate. At $N_\tau = 8$, on the other hand, a small second peak emerges from the distribution. Therefore, at these low temperatures the transition, close to the supersymmetric limit, becomes consistent with a first order chiral phase transition. Moreover, this suggests that the transition happens in the region between $N_\tau = 7$ and $N_\tau = 8$. It is another indication that the chiral phase transition and the deconfinement transition are close to each other: assuming that the value of w_0 does not change so much going from $\kappa = 0.192$ to $\kappa = 0.194$ an upper limit for the supersymmetric chiral critical temperature can be estimated to be $T_\chi(M_R = 0) \lesssim 1.5 T_c$.

The sign of the Pfaffian has been measured on 200 configurations. At $\kappa = 0.192$ no negative sign occurs, whereas at $\kappa = 0.194$ around 8% of the configurations have a negative sign on the $12^3 \times 8$ lattice. Hence the simulations at the supersymmetric limit provide only an estimate of the transition point. In further studies the contributions with a negative sign have to be taken into account more carefully; alternatively, with a larger amount of computing time, the supersymmetric limit can be extrapolated from a region without a relevant sign problem.

10.5 Phase diagram

The phase diagram of $\mathcal{N} = 1$ super Yang-Mills theory can be finally drawn based on the results discussed in the previous sections. The deconfinement phase transition has a good signal for all values of the gluino mass and the finite volume scaling seems to be in agreement with a second order phase transition in the universality class of the three dimensional Z_2 Ising model. The chiral phase transition emerges in the chiral limit and it occurs roughly at the same temperature of the deconfinement phase transition. Numerical simulations seem to support the phase diagram (a) of Fig. 10.3, but further studies closer to the continuum and to the massless limit are required to fully support this scenario. A very different phase diagram has been found for a similar gauge model but with four Majorana fermions in the adjoint representation of the gauge group in Ref. [114], chiral symmetry restoration occurs in this theory after the deconfinement phase transition. From this perspective $\mathcal{N} = 1$ SYM appears more similar to QCD.

Chapter 11

Compactified $\mathcal{N} = 1$ super Yang-Mills theory

Prove that for any compact simple gauge group G , a non-trivial quantum Yang-Mills theory exists on \mathbb{R}^4 and has a mass gap $\Delta > 0$.

A. Jaffe and E. Witten, The Millennium Prize Problems

Confinement is still an open mystery of QCD. The hope is to find an approach to study strong interactions analytically even deep in the strong coupling region. New techniques are required to realize this dream, a very famous approach is the 't-Hooft limit [115]. Yang-Mills theories simplify drastically if the gauge coupling g is sent to zero and the number of colors N_c to infinity keeping fixed the 't-Hooft coupling $g^2 N_c$. In particular, scattering and vacuum energies receive their largest contribution in perturbation theory only from planar Feynman diagrams.

Volume independence and correlation function factorization have been conjectured in the large N_c limit, in the sense that the theory in a hypercubic lattice 1^d with only one site is equivalent to the full theory in L^d [116]. Unfortunately confinement is not preserved in this limit, the center symmetry of the Polyakov loop is broken and the hypothesis that lead to the volume reduction are not fulfilled [117]. A possibility to solve this problem is to couple the gauge fields with quarks in the adjoint representation of the gauge group. Fermions of the $\mathcal{N} = 1$ super Yang-Mills theory fulfill this requirement. The model can be thus compactified in a torus $\mathbb{R}^3 \times T$ and studied for small compactification radius. Gluinos are expected to restore confinement, if periodic boundary conditions are applied to them in the time direction [118].

Under this assumption, confinement mechanisms can be studied analytically for small compactification radius. In this chapter preliminary numerical evidences are shown for these conjectures. The picture of the phase diagram of compactified $\mathcal{N} = 1$ SYM has been presented in Ref. [119].

11.1 Confinement in compactified $\mathcal{N} = 1$ super Yang-Mills theory

Fermion boundary conditions have a strong influence on confinement in the compactified $\mathcal{N} = 1$ super Yang-Mills theory. As seen in the previous chapter, the study of the theory at finite temperature requires antiperiodic boundary conditions to be applied to fermions in the compactified time direction. The temperature is proportional to the inverse of the compactification radius R . In the “thermal theory” supersymmetry is explicitly broken unless $R \rightarrow \infty$. As discussed before, confinement is also broken at high temperature for a small critical R of length approximately equal to one fermi in QCD units.

The situation is different if one spatial direction is compactified, or equivalently, if periodic boundary conditions are applied to all fields in all directions. In the Hamiltonian formalism, these boundary conditions are equivalent to the trace of the Witten index

$$\text{tr}[(-1)^F e^{-H/R}] = \sum_{\text{boson states}} e^{(-E_n/R)} - \sum_{\text{fermion states}} e^{(-E_n/R)} = \int_{\text{PBC}} \mathcal{D}\lambda \mathcal{D}A_\mu e^{-S[\lambda, A]},$$

in this case supersymmetry is not broken and it is expected to play a relevant role on deconfinement. In particular, confinement is expected to persist for all compactification radius R . Gluinos cancel quantum contributions coming from gauge bosons in the “compact theory”, the effective potential of the Polyakov loop is flat at one-loop in perturbation theory for $\mathcal{N} = 1$ SYM (where $N_f = 1/2$)

$$V_{\text{eff}} = \left(N_f - \frac{1}{2}\right) \frac{2}{\pi^2 L^4} \sum_{n=1}^{\infty} |\text{Tr}(\Omega^n)|^2, \quad (11.1)$$

being Ω the path ordered product of the temporal Wilson line [120, 118]. Supersymmetry guarantees that such a behavior holds to all order in perturbation theory. Confinement in compactified $\mathcal{N} = 1$ SYM is hence the result of non-perturbative instanton contributions to the effective potential [121]. The effective potential becomes instead attractive if additional Majorana fermions are coupled to gauge fields: center symmetry is stabilized for $N_f > 1/2$ (Dirac counting of degrees of freedom).

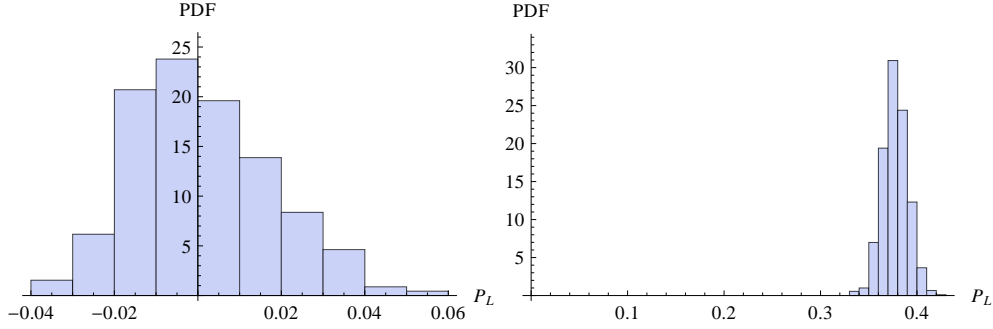


Figure 11.1: Histograms of the Polyakov loop with periodic boundary conditions with $\beta = 1.7$ and $\kappa = 0.1915$ on a lattice Left) $14^3 \times 8$ and Right) $14^3 \times 4$.

Supersymmetry is dynamically realized on the lattice in the continuum limit and the gluino mass has to be fine-tuned in the Curci-Veneziano action. The exact cancellation between fermions and bosons is broken, a lattice study of the compactified $\mathcal{N} = 1$ SYM is however a good test for understanding how and in which limit supersymmetry is restored. Numerical simulations can prove further the conjectures of Ref. [118], in particular it has to be ensured that there are no intermediate deconfined phases between the small R regimes, where the analytical calculations are available, and large R , the final target theory where one hopes to prove confinement. In fact, the analytical calculations done at small R would be meaningless at large R if there would be an intermediate deconfined region occurring between two phase transitions $R_1 < R < R_2$. It is therefore of great importance to prove, at least numerically, that there are no phase transitions in the supersymmetric limit.

11.2 Numerical simulations

Periodic and antiperiodic fermion boundary conditions have been compared with numerical simulations on a lattice with a spatial volume 14^3 , at $\beta = 1.7$ and $\kappa = 0.1915$. The Polyakov loop expectation value is zero at $N_T = 8$, but disappointingly the theory is clearly deconfined at $N_t = 4$, regardless on the fermion boundary conditions, see Fig. 11.1. The center symmetry of the Polyakov loop is broken for small compactification radius R also when periodic boundary conditions are applied to all fields, in apparent contradiction with the conjectures that have been formulated. However confinement is expected to survive continuously in the compact theory only in the chiral limit, the “Witten index partition function” could be more influenced by the

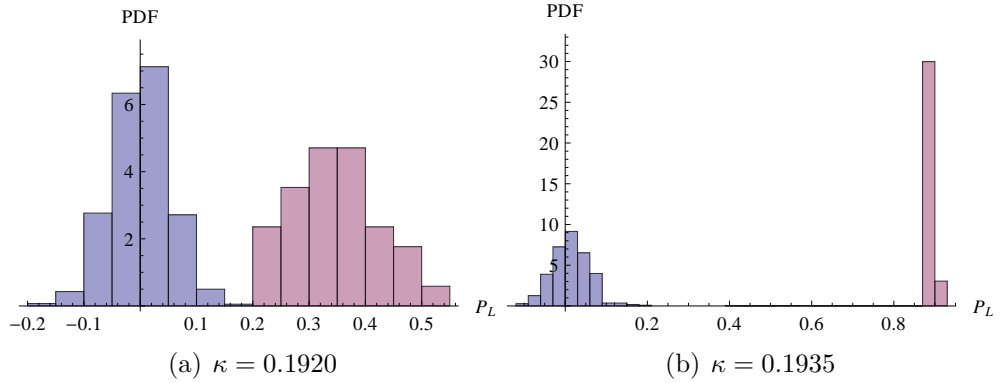


Figure 11.2: Histograms of the Polyakov loop with periodic (violet) and antiperiodic (purple) fermion boundary conditions on a lattice $10^3 \times 1$, with $\beta = 1.7$ and a) $\kappa = 0.1920$ b) $\kappa = 0.1935$.

gluino mass term.

Monte Carlo simulations are on the other hand computationally more expensive in the massless limit. Preliminary tests have been done to understand if periodic boundary conditions applied to fermions preserve confinement at least for very small compactification radius. The lattice has been reduced to $10^3 \times 1$. In this setup only one site is present in the time direction and the lattice is effectively dimensionally reduced to \mathbb{R}^3 . The histograms of the Polyakov loop are shown in Fig. 11.2. The expectation value of the Polyakov loop is zero both at $\kappa = 0.1920$ and at $\kappa = 0.1935$, closer to the critical point $\kappa_c \simeq 0.194$. When antiperiodic boundary conditions are applied to fermions, center symmetry is spontaneously broken even stronger in the massless limit. This difference is a clear evidence that periodic boundary conditions have a strong influence on confinement. A confined region exists at small compactification radius R and for sufficiently small but non vanishing gluino mass, and two deconfinement phase transitions occur when R is increased. Further simulations have been discussed in [119], observing that the deconfined region shrinks and disappears in the chiral limit. The gluino mass term breaks supersymmetry, ruining the exact cancellation between bosons and fermions which should forbid deconfinement. However, even for positive fermion mass m , the influence of gluinos is strong enough to recover confinement for small R in a wide region of the bare parameters.

The average of the plaquette expectation value in the spatial and in the time direction encodes information on how the pure gauge part of the theory reacts to a variation of the spatial volume V and of the compactification radius R . It is therefore interesting to observe that for periodic boundary

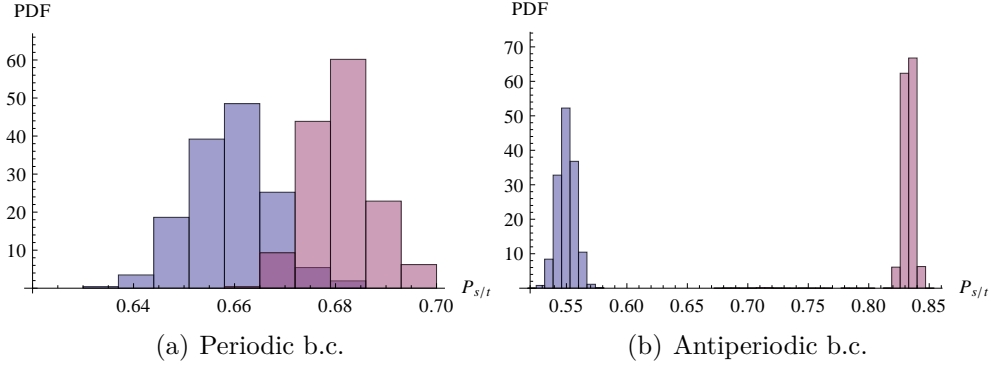


Figure 11.3: Histograms of the spatial (violet) vs. the temporal (purple) plaquette on a lattice $10^3 \times 1$, with $\beta = 1.7$ and $\kappa = 0.1935$ with periodic (Left) and antiperiodic (Right) fermion boundary conditions.

conditions the spatial plaquette is almost equal to the temporal plaquette, while a large gap is observed for fermion antiperiodic boundary conditions. The compact theory seems therefore to realize the predicted volume independence.

Monte Carlo simulations can check non-perturbatively the shape of the effective potential of the Polyakov loop. To this end, the number of Majorana fermions $N_f/2$ is considered as a continuous parameter. In Fig. 11.4 is presented the histogram of the Polyakov loop for three different $N_f/2$ at $\beta = 1.7$ and $\kappa = 0.192$. When the number of fermions is lower than the critical value, $N_f = 7/16 \simeq 0.44$, the center symmetry is broken and the Polyakov loop is non-zero although characterized by a broad distribution. The Polyakov loop is distributed instead around the origin when $N_f = 1/2$ or $N_f = 9/16 \simeq 0.56$. The raw standard deviation σ is equal to 0.036 for $N_f = 9/16$, smaller than σ at $N_f = 1/2$, equal to 0.052, in agreement with the theoretical expectation of formula 11.1.

11.3 Phase diagram of compactified $\mathcal{N} = 1$ SYM

The phase diagram of compactified $\mathcal{N} = 1$ SYM is strongly influenced by the gluino mass term. The deconfinement phase transition line continues to exist unchanged even for quite small gluino mass. However there are strong evidences that there exists a second line that appears for some gluino mass, below this second line the compact theory is again confined. This scenario

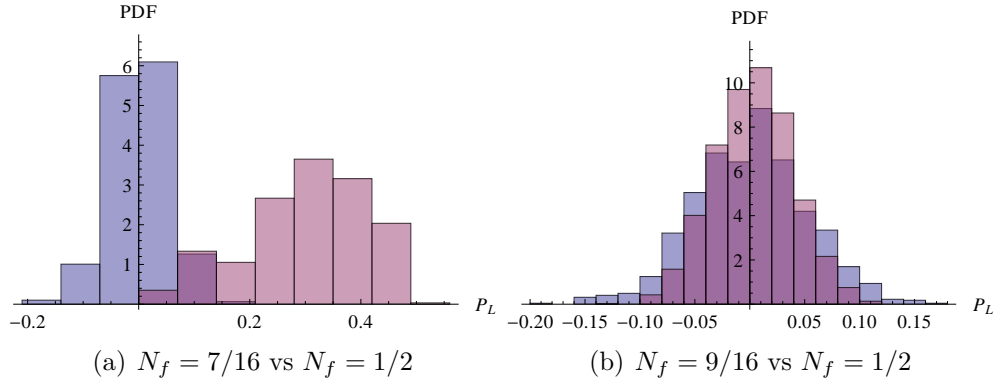


Figure 11.4: Histograms of the Polyakov loop with fermion periodic boundary conditions on a lattice $10^3 \times 1$, with $\beta = 1.7$ and $\kappa = 0.1920$. Left) Comparison between $N_f = 1/2$ (violet) and “ $N_f = 7/16$ ” (purple). Right) Comparison between $N_f = 1/2$ (violet) and “ $N_f = 9/16$ ” (purple).

is similar to the theory with two adjoint fermions $N_f = 2$ investigated in Ref. [122]. The two lines meet at some positive critical gluino mass, after which the compact theory is continuously confined [119]. More simulations are required however to prove this final picture.

Chapter 12

Conclusions

I consider that numerical methods have a comparable role with analytic thinking, experiment, and observation in physics [...] I am confident that there will be surprising breakthroughs achieved by numerical studies, perhaps even on questions as basic as: Why does the universe exist?

Kenneth Wilson [123]

The research of $\mathcal{N} = 1$ super Yang-Mills theory on the lattice has been fruitful to explore the non-perturbative regime and to test the correctness of the several conjectures that have been proposed by several authors so far.

The largest part of the work done in this thesis has been spent in the develop of the code to implement the Hybrid Monte Carlo (HMC) algorithm for $\mathcal{N} = 1$ SYM. The program is the core of all the results that has been presented in this thesis. Many algorithms have been adapted and reformulated to handle gluinos on the lattice. The separation of ultraviolet from infrared modes of the Dirac operator, used in combination with the RHMC, has been found to speedup the performance significantly with respect to the previously used algorithms.

The continuum limit is the most important ingredient behind the viability of supersymmetry on the lattice. The extrapolation to zero lattice spacing requires however a careful definition of the scale. As discussed in Ch. 7, the scale w_0 based on the Wilson flow provides a precise determination of the lattice spacing in fully agreement with the theoretical perturbative expectations. The systematical errors are under control and therefore the w_0 scale can be used to extrapolate the continuum limit of the mass spectrum. The

discovered correlation between the Wilson flow and the topological charge could lead to a deeper understanding of the topological properties of $\mathcal{N} = 1$ SYM.

The study of $\mathcal{N} = 1$ SYM at finite temperature has been able to provide the first determination of the phase diagram of the theory. The interplay between the chiral and the deconfinement phase transition has been found to be similar to QCD, where quark liberation and chiral symmetry restoration occur nearby at the same temperature. Further studies are needed to explore the equation of state, but the current numerical simulations have been able to capture already many important aspects of the thermodynamics of $\mathcal{N} = 1$ super Yang-Mills theory.

The $\mathcal{N} = 1$ SYM theory with periodic boundary conditions applied to fermions is a further important direction of research. First results have been published in Ref. [119]. The “Witten index partition function” corresponds effectively to study $\mathcal{N} = 1$ SYM with one spatial direction compactified. Periodic boundary conditions applied to fermions preserve supersymmetry. The exact cancellation between fermion and boson states leads to a theory that should be always confined and in particular invariant with respect to a change of the length of the compactified spatial dimension. This invariance provides a beautiful way to observe supersymmetry realization directly with lattice simulations: the first simulations presented in Ch. 11 are very promising and motivate future studies.

Appendix A

Determinant, Pfaffian and Grassmannian integrals

Pfaffians and determinants are the result of the Grassmannian integration of fermion fields in the path integral. In this appendix the difference between Dirac and Majorana fermions is discussed.

A.1 Grassmann variables

A set of Grassmann variables $\{\Psi_1, \dots, \Psi_n\}$ satisfies an anticommuting algebra

$$\Psi_i \Psi_j = -\Psi_j \Psi_i, \quad (\text{A.1})$$

which implies that $\Psi_i \Psi_i = 0$. The Grassmann integral is uniquely defined by

$$\int d\Psi_i a = 0, \quad (\text{A.2})$$

$$\int d\Psi_i a \Psi_i = a, \quad (\text{A.3})$$

with a real (or complex) standard commuting variable. Integrals over several variables can be computed recursively, remembering that the anticommuting rule extends over the differentials

$$d\Psi_i d\Psi_j = -d\Psi_j d\Psi_i, \quad (\text{A.4})$$

hence for example

$$\int d\Psi_1 d\Psi_2 \Psi_1 \Psi_2 = - \int d\Psi_2 d\Psi_1 \Psi_1 \Psi_2 = - \int d\Psi_2 \Psi_2 = -1. \quad (\text{A.5})$$

A.2 The determinant

The determinant of a square matrix $A \equiv a_{ij}$ of dimension $n \times n$ is defined as

$$\det(A) = \sum_{\pi \in S_n} \text{sign}(\pi) \prod_{i=1}^n a_{\pi(i)i}, \quad (\text{A.6})$$

where S_n is the permutation group of the set $\{1, 2, 3, \dots, n\}$ and $\text{sign}(\pi)$ is equal to -1 if the permutation can be reordered with an odd number of interchanges or $+1$ otherwise. If the matrix A is symmetric (or Hermitian), an orthogonal (or unitary) rotation can be applied to transform A to a diagonal matrix, where the non-zero entries are the eigenvalues. The determinant of a matrix is invariant under unitary or orthogonal basis transformations. In this case the determinant is thus just the product of all eigenvalues. It is instructive however to visualize explicitly the meaning of the above sum without any further assumptions on A .

A generic term that contributes to the sum of the determinant can be easily visualized as a path on the matrix elements. Consider for instance a 4×4 matrix. An element can be selected randomly starting from the first column (for example a_{31} , red point on the left)



and the relative row is marked as “deleted” (third row, orange line on the right). In the next step, another element is chosen randomly in the second column among the free non-“deleted” remaining a_{i2} (for example a_{12} , red point on the left)



and the its row is marked as “deleted” (first row, the new orange line on the right). This step is iterated in the third row;



the element a_{23} is selected between the free a_{i3} and the second row is marked as “deleted”. In the last step, only the fourth row is free and the remaining element a_{44} is selected,



concluding the algorithm. The multiplication of all elements encountered in the blue path represents just one contribution to the determinant, in this example $a_{31}a_{12}a_{23}a_{44}$. Its sign is given by the sign of the permutation of the indices of the chosen rows. In this case $\{3, 1, 2, 4\}$ can be rearranged to form $\{1, 2, 3, 4\}$ with two exchanges, therefore $\text{sign}(\pi) = +1$. The complete determinant is the sum of all the $n!$ possible different paths that can be obtained from this algorithm starting from the first column.

This algorithm to evaluate determinants arises naturally from a Grassmannian integration of the pseudo-Gaussian exponential

$$\int d\bar{\Psi}_1 \dots d\bar{\Psi}_n d\Psi_1 \dots d\Psi_n \exp \left\{ +(\bar{\Psi}_i a_{ij} \Psi_j) \right\}, \quad (\text{A.7})$$

where the $\bar{\Psi}$ are considered independent variables from Ψ . Only terms up to the n -th power can contribute to the Taylor expansion of the exponential, the $(n + 1)$ -th power will contain at least two equal Ψ_i which vanish due to the anticommuting rule $\Psi_i \Psi_i = 0$. The first term of the Taylor expansion of the function \exp is just one, but the Grassmann integral of a constant vanishes due to Eq. (A.2). The next term is $\bar{\Psi}_i a_{ij} \Psi_j$, summing over all repeated indices. A Grassmann integration can be performed on $\bar{\Psi}_i$ and Ψ_j , the result

$$\sum_{ij} (-1)^{(j+i)} \int \left(\prod_{p=1, p \neq i}^n d\bar{\Psi}_p \right) \left(\prod_{q=1, q \neq j}^n d\Psi_q \right) a_{ij} \quad (\text{A.8})$$

is an integral over $2(n-1)$ variables and it is zero because the integrand is again a constant. Iterating, the integral vanishes always for the terms in the Taylor expansion up to the n -th power. The n -th power $(\bar{\Psi}_i a_{ij} \Psi_j)^n$ has instead enough $\bar{\Psi}$ and Ψ to saturate the rule of Eq. (A.3). It is the product of n bilinears of the form $\bar{\Psi}_i a_{ij} \Psi_j$, they are bosonic and they can be reordered such that the j indices of the Ψ_j are in a increasing order. The first term in the product could be for example $\bar{\Psi}_2 a_{21} \Psi_1$, the next $\bar{\Psi}_2 a_{22} \Psi_2$ or $\bar{\Psi}_3 a_{31} \Psi_1$. However the term

$$\bar{\Psi}_2 a_{21} \Psi_1 \bar{\Psi}_2 a_{22} \Psi_2 \dots \quad (\text{A.9})$$

is zero regardless of what \dots is, since $\bar{\Psi}_2 \bar{\Psi}_2 = 0$. This is the equivalent to the rule “delete a row once that it has been already selected” used before. The same applies to

$$\bar{\Psi}_2 a_{21} \Psi_1 \bar{\Psi}_3 a_{31} \Psi_1 \dots, \quad (\text{A.10})$$

because $\Psi_1 \Psi_1 = 0$. Therefore Ψ_2 , Ψ_3 and all other Ψ_i have to appear one after the other starting from Ψ_1 ; this rule is equivalent to “proceed column by column” in the algorithm before. The only freedom left is the order of the different $\bar{\Psi}_j$, they can appear in many random combinations: as before the sum of all the possible “random paths” on the matrix A has to be considered. Finally the Grassmannian integration will leave numerical factors like $a_{11} a_{32} \dots a_{4n}$. The anticommuting nature of the variables Ψ and $\bar{\Psi}$ gives the equivalent of the sign of the permutation of the row-indices. The result of the integration is hence exactly the determinant of the matrix A

$$\det(A) = \int d\bar{\Psi}_1 \dots d\bar{\Psi}_n d\Psi_1 \dots d\Psi_n \exp \left\{ +(\bar{\Psi}_i a_{ij} \Psi_j) \right\}. \quad (\text{A.11})$$

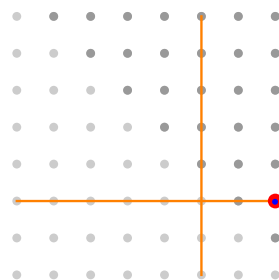
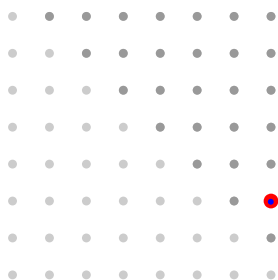
A.3 The Pfaffian

The Pfaffian of a square antisymmetric matrix $A \equiv a_{ij}$ of dimension $2n \times 2n$ is defined as

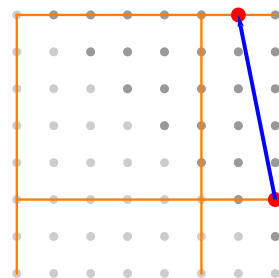
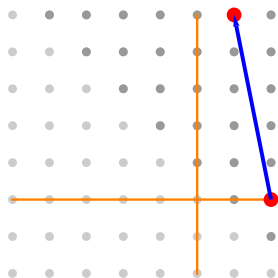
$$\det(A) = \sum_{\pi \in S_{2n}} \text{sign}(\pi) \prod_{i=1}^n a_{\pi(2i-1)\pi(2i)}, \quad (\text{A.12})$$

where S_{2n} is the permutation group of the set $\{1, 2, 3, \dots, 2n\}$ and $\text{sign}(\pi)$ is the sign of π defined as before.

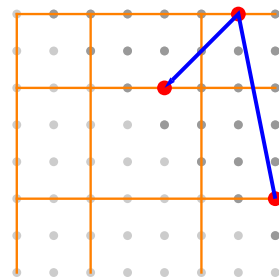
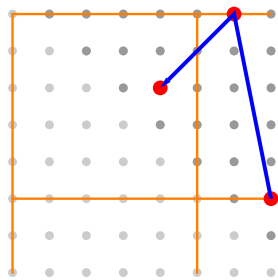
Also the Pfaffian has a geometrical meaning as sum of products of elements on paths along the entries of A . Only the upper triangular part of A has to be considered since A is antisymmetric. An element a_{in} can be selected starting from the last column



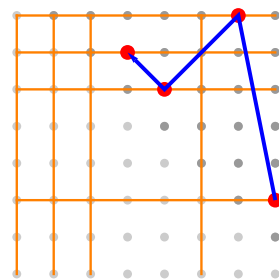
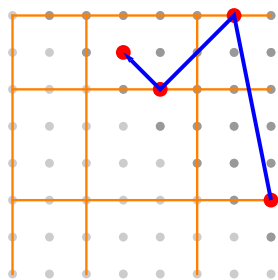
but this time the elements in the row i and in the column i are both marked as “deleted” (sixth orange row and sixth orange column for the red point a_{68} in the pictures above). Moving backward, the algorithm choose randomly a free point in the previous column and in the upper triangular part of A



for example in this case a_{17} , marking the first row and the first column as “deleted”. Moving backward, the sixth column is already marked as deleted and the algorithm jumps directly to the fifth column. In the fifth column the element a_{35} is chosen



the fifth row and the fifth column are marked as “deleted” as before. In the last step the only free element a_{24} left is selected



and the algorithm stops since all columns are now marked as “deleted”. The product of all elements in the blue path $a_{68}a_{17}a_{35}a_{42}$ represents a contribution to the sum that above defines the Pfaffian. Notice that the product has four matrix elements while the matrix has dimension eight. The sign of a given contribution is given by the sign of the permutation of the row and column indices. In this example the permutation $\{6, 8, 1, 7, 3, 5, 4, 2\}$ reduces to $\{1, 2, 3, 4, 5, 6, 7, 8\}$ with an even number of exchanges, therefore $\text{sign}(\pi) = +1$. The Pfaffian is finally just the sum of the possible paths starting from the last column.

The Pfaffian is the result of a Grassmannian integration of the form

$$\int d\lambda_1 \dots d\lambda_{2n} \exp \left\{ +\frac{1}{2}(\lambda_i a_{ij} \lambda_j) \right\}, \quad (\text{A.13})$$

where $A \equiv a_{ij}$ is an antisymmetric $2n \times 2n$ matrix (if A would have been symmetric, the integral would vanish due to the usual rule $\lambda_i \lambda_i = 0$). The factor $\frac{1}{2}$ is included to avoid double counting. Repeating the same argument as before, the only non vanishing contribution of the Taylor expansion of the exponential is the n th-power. Note again that the matrix has dimension $2n \times 2n$, the power is only n to the fact that there is just one Grassmannian variable λ , $(\lambda_i a_{ij} \lambda_j)^{n+1}$ will contain already $2(n+1)$ variables λ_i and it will be impossible that none of them is repeated at least once. The bilinears $\lambda_i a_{ij} \lambda_j$ can be rearranged in a decreasing order with respect to the second index. One notices that in the product a term $\lambda_3 a_{31} \lambda_1$ forbids another bilinear like $\lambda_3 a_{31} \lambda_1$, but also $\lambda_2 a_{23} \lambda_3$, because this time λ_3 can appear in the left or in right of an element a_{ij} . This is the equivalent to the rule “after selecting the row i , mark as deleted both the row and the column i ” used before. The argument proceeds then as in the previous section, in conclusion the new Grassmann integral is equal to the Pfaffian of A

$$\text{Pf}(A) = \int d\lambda_1 \dots d\lambda_{2n} \exp \left\{ +\frac{1}{2}(\lambda_i a_{ij} \lambda_j) \right\}. \quad (\text{A.14})$$

A.4 Difference between the integration of quarks and gluinos

The Grassmannian integral over $\bar{\Psi}$ and Ψ considered in the previous section can be naively seen as an integral over the “Grassmann complex plane”, with the identification $z = x + iy \rightarrow \Psi$ and $\bar{z} = x - iy \rightarrow \bar{\Psi}$. The integral only over λ is instead a sort of “real Grassmann integral”. Majorana and Dirac fermions are in fact in correspondence with real and complex scalar field. Complex scalar Φ or of Dirac fermion Ψ appear in the path integral

as $D\Phi^\dagger D\Phi$ or $D\bar{\Psi}D\Psi$. The path integral of a real scalar ϕ or of Majorana fermion λ has only one half of the integration variables, namely $D\phi$ or $D\lambda$, due to the “reality condition” $\phi^\dagger = \phi$ or $\bar{\lambda} = \lambda^T C$. Therefore the result of the Grassmann integration of quark fields is the determinant of the Dirac Wilson operator D_W , while gluinos leave the Pfaffian of D_W .

Any real antisymmetric matrix A of dimension $2n \times 2n$ can be reduced after an orthogonal transformation to the form

$$A = \begin{pmatrix} 0 & \lambda_1 & 0 & \cdots & 0 \\ -\lambda_1 & 0 & 0 & \cdots & 0 \\ 0 & 0 & 0 & \lambda_2 & 0 \\ 0 & -\lambda_2 & 0 & 0 & 0 \\ \vdots & \vdots & \vdots & \ddots & \vdots \\ 0 & 0 & 0 & \cdots & 0 & \lambda_k \\ & & & & -\lambda_k & 0 \\ & & & & & 0 & \ddots \\ & & & & & & 0 \end{pmatrix}, \quad (\text{A.15})$$

where 2×2 blocks contain the imaginary part of the complex conjugate pairs of the eigenvalues $\pm i\lambda_k$ of A . An orthogonal transformation of the fermion field leaves the measure of the path integral invariant, regardless on whether fermions are Majorana or Dirac. However an integration of a Dirac fermion field leads to the determinant

$$\det(A) = \prod_{i=1}^n |\lambda_n|^2, \quad (\text{A.16})$$

which is positive. An integration of the Majorana fields leads instead to the Pfaffian

$$\text{Pf}(A) = \prod_{i=1}^n \lambda_n \quad (\text{A.17})$$

and $\text{Pf}(A)$ can be positive or negative. The “delete both column and row” rule for the Pfaffian is therefore the origin of the sign problem in Monte-Carlo simulations.

Appendix B

Data analysis

Monte Carlo techniques compute the expectation value of an observable O in terms of the sum

$$\langle O \rangle = \int D\phi O(\phi) \exp(-S(\phi)) = \lim_{N \rightarrow \infty} \frac{1}{N} \sum_{C_i=1}^N O[C_i],$$

where the configurations C_i are assumed to be distributed accordingly to the weight $\exp(-S(\phi))$. In any computer simulation the number of the configurations available will be of course finite, therefore only an estimation of $\langle O \rangle$ is possible

$$\langle O \rangle \approx \langle O_N \rangle = \frac{1}{N} \sum_{C_i=1}^N O[C_i]$$

and the task is to provide an error for $\langle O_N \rangle$, that means to assign the probability that a given value of the observable O is equal to the true expectation value $\langle O \rangle$. Supposing that the simulation is able to explore the full phase space without barriers, the distribution of O_N , computed with independent simulation, will be Gaussian centered at $\langle O \rangle$, but of course it would be meaningless to perform many different simulation only to compute the standard deviation of such distribution. The clever strategy extracts all possible information from the available data set itself using the idea of resampling, that amount to generate new data set from which estimate mean and standard deviation of the original. There are two principal resampling techniques, bootstrapping and jackknife.

Given the original set $S = \{O[C_i]\}$, the resampling technique used by the bootstrapping simply produce a new set S_1 choosing randomly N elements of S without care about repetitions. For example given

$$S = \{O[C_1], O[C_2], O[C_3], O[C_4], O[C_5], O[C_6]\}$$

a possible S_1 would be

$$S_1 = \{O[C_2], O[C_4], O[C_3], O[C_4], O[C_1], O[C_1]\}.$$

This procedure is iterated M time to produce M different sets S_n . The mean value $\langle O_n \rangle$ is measured on each S_n , giving M different a resampled distribution of O . The distribution of the $\langle O_n \rangle$ is Gaussian, if there are no problems with bias or with the original statistic. It is possible to demonstrate that the best estimation bias corrected for the expectation value $\langle O \rangle$ is

$$\langle O \rangle = 2\langle O_N \rangle - \frac{1}{M} \sum_n \langle O_n \rangle,$$

where $\langle O_N \rangle$ is the raw mean of the original set; with an error σ_O

$$\sigma_O = \sqrt{\frac{N-1}{N}} \sigma_R \simeq \sqrt{\frac{1}{M} \sum_{n=1}^M \left\{ \langle O_n \rangle - \left(\frac{1}{M} \sum_{m=1}^M \langle O_m \rangle \right) \right\}^2},$$

where σ_R is the standard deviation of the resampled set of M elements generated by the $\langle O_n \rangle$.

The error would be underestimated if there is an autocorrelation between two consecutive configurations C_i . Blocking techniques are commonly used to correct this problem, the observables are first averaged block by block before applying the bootstrapping. For instance, given the set S of before, one step of blocking would result in

$$S^1 = \left\{ \frac{O[C_1] + O[C_2]}{2}, \frac{O[C_3] + O[C_4]}{2}, \frac{O[C_5] + O[C_6]}{2} \right\}.$$

This procedure is repeated until the error of the bootstrapping σ_O stabilizes. An analytical relation exists between the original error σ_O and final error σ_O^c correct to take into account the autocorrelation

$$(\sigma_O^c)^2 = \frac{(\sigma_O)^2}{2\tau_{\text{int}}}, \quad (\text{B.1})$$

being τ_{int} the integrated autocorrelation time

$$\begin{aligned} \tau_{\text{int}} &= \frac{1}{2} + \sum_{t=1}^{\infty} \frac{C(t)}{C(0)} \\ C(t) &= \frac{1}{N} \sum_{n \in S} \{O[C_{n+t}]O[C_n]\} - \left\{ \frac{1}{N} \sum_{n \in S} O[C_n] \right\}^2. \end{aligned}$$

Practically the sum cannot be extended up to infinite, a cut has to be applied [124]. The knowledge of τ_{int} allows to correct directly the error for autocorrelations, conversely the final error estimated with blocking technique allows the calculation of τ_{int} by inverting Eq. (B.1).

Appendix C

Gamma matrices

The anticommuting Clifford algebra of the gamma matrices in an Euclidean space reads

$$\{\gamma_\mu, \gamma_\nu\} = 2\delta_{\mu\nu}I \quad (\text{C.1})$$

In the representation used in the code and in the thesis, the gamma matrices are explicitly

$$\gamma_1 = \begin{pmatrix} 0 & 0 & 0 & -i \\ 0 & 0 & -i & 0 \\ 0 & i & 0 & 0 \\ i & 0 & 0 & 0 \end{pmatrix}, \quad (\text{C.2})$$

$$\gamma_2 = \begin{pmatrix} 0 & 0 & 0 & -1 \\ 0 & 0 & 1 & 0 \\ 0 & 1 & 0 & 0 \\ -1 & 0 & 0 & 0 \end{pmatrix}, \quad (\text{C.3})$$

$$\gamma_3 = \begin{pmatrix} 0 & 0 & -i & 0 \\ 0 & 0 & 0 & i \\ i & 0 & 0 & 0 \\ 0 & -i & 0 & 0 \end{pmatrix}, \quad (\text{C.4})$$

$$\gamma_4 = \begin{pmatrix} 0 & 0 & 1 & 0 \\ 0 & 0 & 0 & 1 \\ 1 & 0 & 0 & 0 \\ 0 & 1 & 0 & 0 \end{pmatrix}. \quad (\text{C.5})$$

In this basis γ_5 is Hermitian and diagonal

$$\gamma_5 = \begin{pmatrix} 1 & 0 & 0 & 0 \\ 0 & 1 & 0 & 0 \\ 0 & 0 & -1 & 0 \\ 0 & 0 & 0 & -1 \end{pmatrix} \quad (\text{C.6})$$

and the charge conjugation operator $C = \gamma_2\gamma_4$ is

$$C = \begin{pmatrix} 0 & -1 & 0 & 0 \\ 1 & 0 & 0 & 0 \\ 0 & 0 & 0 & 1 \\ 0 & 0 & -1 & 0 \end{pmatrix}. \quad (\text{C.7})$$

The matrix C satisfies the properties

$$C = -C^{-1} = -C^T. \quad (\text{C.8})$$

Finally, the $\sigma_{\mu\nu}$ matrices are defined as

$$\sigma_{\mu\nu} = \frac{i}{2}[\gamma_\mu, \gamma_\nu]. \quad (\text{C.9})$$

Appendix D

The Remez algorithm

The approximation of a function is one of the most challenging and most studied topics in analysis and in the mathematical theory of the minimization. The starting point for a polynomial or rational approximation $\tilde{f}(x)$ of a function $f(x)$ in a given interval (a, b) is to choose a norm that measures how large is the “distance” between the guess $\tilde{f}(x)$ and $f(x)$. Two different possibilities have been more often studied in literature, the first one is the “sup-norm”

$$\text{norm}(f, g) = \sup_{x \in (a, b)} |f(x) - g(x)|,$$

where f and g are two generic functions. The second one is the “integral norm” defined by

$$\text{norm}(f, g) = \int_a^b |f(x) - g(x)| dx,$$

or also in a different way as

$$\text{norm}(f, g) = \int_a^b (f(x) - g(x))^2 dx.$$

An approximation $\tilde{f}(x)$ will be possibly able to minimize only one of the previous norm but not all in the same time. In lattice QCD both of the possibilities were intensively studied and in the case of polynomial approximation both of the approaches give good results. For a rational approximation the best known way, the Remez algorithm, implies in contrast to work strictly with the “sup-norm”.

The problem to solve is the search in the space of the rational functions \mathbf{F}_r of degrees (n, m)

$$\tilde{f}(x) = \frac{P(x)}{Q(x)} = \frac{p_0 + p_1x + \cdots + p_nx^n}{q_0 + q_1x + \cdots + q_mx^m}$$

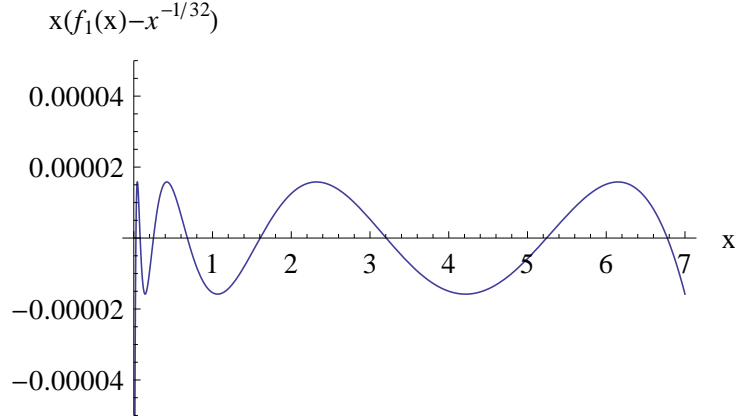


Figure D.1: Error function $\text{err}(x)$ for a rational approximation of $x^{-1/32}$ with a weight function $w(x) = x$. Notice the oscillations of $\text{err}(x)$ alternating between the same maximum and the same minimum $\approx \pm 2^{-5}$, indicating the convergence to the optimal rational approximation.

the minimum of the “sup-norm” in the interval (a, b)

$$\text{err} = \min_{\tilde{f}(x) \in \mathbf{F}_r} \left\{ \sup_{x \in (a, b)} |w(x)(f(x) - \tilde{f}(x))| \right\}, \quad (\text{D.1})$$

where the weight function $w(x)$ is introduced to give more importance to some region of (a, b) for the final approximation.

Normalizing $\tilde{f}(x)$ in such a way that $q_0 = 1$, then there are $m + n + 2$ unknown parameters, the $m + n + 1$ coefficients of the rational approximation plus the absolute error err . The error function

$$\text{err}[\tilde{f}](x) = w(x)(f(x) - \tilde{f}(x))$$

in general will have $m + n + 1$ zeros and $m + n + 2$ extremal points (i.e. maximum or minimum). The theorem of the de la Vallée-Poussin ensure that when the minimum of the absolute error (D.1) is reached then the $m + n + 2$ extremal points will have all of the value err . In other words, once that the rational approximation reaches its optimal value, the function $\text{err}[\tilde{f}](x)$ oscillates $m + n + 2$ times between $-\text{err}$ and $+\text{err}$.

The problem to solve is still highly non-linear but now it is possible to introduce a recursive algorithm for finding the optimal solution. Every polynomial or rational function approximation is uniquely defined up to a constant in terms of $m + n$ root points, where $P(x)$ or $Q(x)$ is zero. The Remez algorithm searches at every step first the best estimation of the root points given err and then the best value of err given the root points [125, 126]

1. Choose randomly $m + n$ points in (a, b) and combine them with the extrema a and b to have $m + n + 2$ root points x_i^0 . Set $k = 0$.
2. Solve the system

$$w(x_i) \frac{P_k(x_i)}{Q_k(x_i)} + (-1)^i \text{err}_k = f(x_i)w(x_i)$$

to compute the $m + n + 1$ unknown coefficients of $\frac{P_k(x_i)}{Q_k(x_i)}$ and the error err_k . Since the system is non-linear, the equation can be solved at the best numerically with a root-finding algorithm. The result will be an alternating rational approximation in correspondence of the points x_i , but it does not mean that the maxima of the error function are exactly at x_i as required to find the best approximation.

3. Move the point x_i^k to the maxima of

$$\text{err}(x) = \left| w(x) \left(f(x) - \frac{P(x)}{Q(x)} \right) \right|,$$

to have a new set of $m + n + 2$ root points x_i^{k+1} .

4. Continue to step 2, and set $k = k + 1$ until convergence, until when the error err_k is sufficiently close to the maximal value of $\text{err}(x)$, see Fig. D.1.

The convergence of the algorithm is difficult to prove, depending strictly on the initial guess for the root point. In general the algorithm is able to converge quite quickly toward the optimal solution if the function f is sufficiently smooth. Chebyshev root points could be a good initial guess, but it is possible that they are quite far from being closer to the best solution.

Appendix E

Computation of the fermion force for the HMC algorithm

The Dirac Wilson Operator D_W with clover improvement term is defined as

$$\begin{aligned} D_W \psi(x) = & \psi(x) - \kappa \sum_{\mu=0}^3 ((1 - \gamma_\mu) U_\mu(x) \psi(x + \mu) + \\ & + (1 + \gamma_\mu) U_\mu^\dagger(x - \mu) \psi(x - \mu)) + \\ & + c_{sw} \frac{\kappa}{4} \sum_{\mu=0}^4 \sum_{\nu=0; \nu \neq \mu}^4 \sigma_{\mu\nu} F^{\mu\nu} \psi(x) \end{aligned}$$

where $F_{\mu\nu}(x)$ is here defined without antisymmetrization

$$\begin{aligned} F_{\mu\nu}(x) = & \frac{1}{4} Q_{\mu\nu} \\ Q_{\mu\nu}(x) = & U_\mu(x) U_\nu(x + \mu) U_\mu^\dagger(x + \nu) U_\nu^\dagger(x) + \\ & + U_\nu^\dagger(x - \nu) U_\mu(x - \nu) U_\nu(x - \nu + \mu) U_\mu^\dagger(x) + \\ & + U_\nu(x) U_\mu^\dagger(x + \nu - \mu) U_\nu^\dagger(x - \mu) U_\mu(x - \mu) + \\ & + U_\mu^\dagger(x - \mu) U_\nu^\dagger(x - \nu - \mu) U_\mu(x - \nu - \mu) U_\nu(x - \nu) \end{aligned}$$

Due to the symmetries of $\sigma_{\mu\nu} = -\frac{1}{2}[\gamma_\mu, \gamma_\nu]$, only the traceless antiHermitian part of $Q_{\mu\nu}$ will give contribution to the clover term.

In the following the Dirac Wilson operator D_W is factorized with the

“even-odd“ preconditioning

$$\begin{aligned}
D_W &= \begin{pmatrix} R_{ee} & D_{eo} \\ D_{oe} & R_{oo} \end{pmatrix} \\
&= \begin{pmatrix} 1 & 0 \\ D_{oe}R_{ee}^{-1} & 1 \end{pmatrix} \begin{pmatrix} R_{ee} & 0 \\ 0 & R_{oo} - D_{oe}R_{ee}^{-1}D_{eo} \end{pmatrix} \begin{pmatrix} 1 & R_{ee}^{-1}D_{eo} \\ 0 & 1 \end{pmatrix} \\
&= L \times D_{WP} \times U
\end{aligned}$$

The resulting determinant of D_W is

$$\begin{aligned}
\det(D_W) &= \det(R_{ee}) \det(R_{oo}) \det(\hat{Q}), \\
\hat{Q} &= \gamma_5(1 - R_{oo}^{-1}D_{oe}R_{ee}^{-1}D_{eo}),
\end{aligned}$$

where a γ_5 is inserted to have an Hermitian operator.

The partition function reads using the “even-odd” preconditioned Dirac Wilson operator

$$Z = \int \prod_{x,\mu} DU_\mu(x) \exp(-S_g - S_f),$$

where S_f is

$$S_f = -N_f \log(\det(R_{ee})) - N_f \log(\det(R_{oo})) + \phi^\dagger \left((\hat{Q}^\dagger \hat{Q})^{-\frac{N_f}{2}} \right) \phi,$$

for a theory with N_f number of fermions ($N_f = 1/2$ in $\mathcal{N} = 1$ SYM)

As discussed in Ch. 6, in the simulation program \hat{Q} is treated stochastically by the pseudofermion ϕ , while R_{oe} and R_{eo} can be computed exactly. The hybrid Monte Carlo algorithm generates configurations in the microcanonical ensemble with a final metropolis step, following the equation of motion.

In this appendix it is calculated the expression of the fermion force

$$F = \frac{\partial}{\partial U_\mu(x)} S_f \equiv \mathcal{D}_{x\mu a}(S_f).$$

The calculation will be done by parts. First consider

$$\mathcal{D} \left(\phi^\dagger \left((\hat{Q}^\dagger \hat{Q})^{-\frac{N_f}{2}} \right) \phi \right)$$

where for the moment the indices x, μ and a of \mathcal{D} are suppressed. This derivative can be calculated directly, approximating $(\hat{Q}^\dagger \hat{Q})^{-\frac{N_f}{2}}$ with a polynomial when $N_f = 1$ or $N_f = \frac{1}{2}$ and then derive it, or in the last case one can consider that

$$\mathcal{D}((\hat{Q}^\dagger \hat{Q})^{-\frac{N_f}{2}} (\hat{Q}^\dagger \hat{Q})^{\frac{N_f}{2}}) = \mathcal{D}(\mathbf{1}) = 0$$

and so

$$\begin{aligned}\mathcal{D}((\hat{Q}^\dagger \hat{Q})^{-\frac{N_f}{2}} (\hat{Q}^\dagger \hat{Q})^{\frac{N_f}{2}}) &= \mathcal{D}((\hat{Q}^\dagger \hat{Q})^{-\frac{N_f}{2}}) (\hat{Q}^\dagger \hat{Q})^{\frac{N_f}{2}} + (\hat{Q}^\dagger \hat{Q})^{-\frac{N_f}{2}} \mathcal{D}((\hat{Q}^\dagger \hat{Q})^{\frac{N_f}{2}}) \\ &= 0, \\ \mathcal{D}((\hat{Q}^\dagger \hat{Q})^{-\frac{N_f}{2}}) &= -(\hat{Q}^\dagger \hat{Q})^{-\frac{N_f}{2}} \mathcal{D}((\hat{Q}^\dagger \hat{Q})^{\frac{N_f}{2}}) (\hat{Q}^\dagger \hat{Q})^{-\frac{N_f}{2}}\end{aligned}$$

Now for computing $\mathcal{D}((\hat{Q}^\dagger \hat{Q})^{\frac{N_f}{2}})$ and $(\hat{Q}^\dagger \hat{Q})^{-\frac{N_f}{2}}$ one can use two polynomial approximations

$$\begin{aligned}(\hat{Q}^\dagger \hat{Q})^{-\frac{N_f}{2}} &\simeq P_n^1(\hat{Q}^\dagger \hat{Q}), \\ (\hat{Q}^\dagger \hat{Q})^{\frac{N_f}{2}} &\simeq P_n^2(\hat{Q}^\dagger \hat{Q}).\end{aligned}$$

E.0.1 Derivative of a polynomial $P_n(\hat{Q}^\dagger \hat{Q})$

A polynomial $P_n(\hat{Q}^\dagger \hat{Q})$ of order n which has exactly n roots in the complex plane in complex conjugate pairs (z_i, z_i^*) can be written as

$$P_n(\hat{Q}^\dagger \hat{Q}) = c_0(\hat{Q} + z_1)^\dagger (\hat{Q} + z_2)^\dagger \dots (\hat{Q} + z_{n/2})^\dagger (\hat{Q} + z_{n/2}) \dots (\hat{Q} + z_2)(\hat{Q} + z_1).$$

It follows that the derivative $\mathcal{D}_P \equiv \mathcal{D}(P_n(\hat{Q}^\dagger \hat{Q}))$ of P_n is

$$\begin{aligned}\mathcal{D}_P &= c_0 \mathcal{D}(\hat{Q}^\dagger) (\hat{Q} + z_2)^\dagger \dots (\hat{Q} + z_{n/2})^\dagger (\hat{Q} + z_{n/2}) \dots (\hat{Q} + z_2)(\hat{Q} + z_1) + \\ &\quad + c_0 (\hat{Q} + z_1)^\dagger \mathcal{D}(\hat{Q}^\dagger) \dots (\hat{Q} + z_{n/2})^\dagger (\hat{Q} + z_{n/2}) \dots (\hat{Q} + z_2)(\hat{Q} + z_1) + \\ &\quad + \dots + \\ &\quad + c_0 (\hat{Q} + z_1)^\dagger (\hat{Q} + z_2)^\dagger \dots (\hat{Q} + z_{n/2})^\dagger (\hat{Q} + z_{n/2}) \dots (\hat{Q} + z_2) \mathcal{D}(\hat{Q}),\end{aligned}$$

It is possible to collect all terms together defining for every $k < n$

$$\psi^k = \begin{cases} \phi & \text{if } k = 0 \\ (\hat{Q} + z_k) \psi^{k-1} & \text{if } k \leq (n/2) \\ (\hat{Q} + z_{n-k+1})^\dagger \psi^{k-1} & \text{if } (n/2) < k < n \end{cases}$$

to have a more compact relation. In this way, considering that $\hat{Q}^\dagger = \hat{Q}$

$$\begin{aligned}\mathcal{D}_P &= c_0 \sum_{i=1}^n (\psi^{(n-i)})^\dagger \mathcal{D}(\hat{Q}) \psi^{(i-1)} \\ &= c_0 \sum_{i=1}^{n/2} (\psi^{(n-i)})^\dagger \mathcal{D}(\hat{Q}) \psi^{(i-1)} + c_0 \sum_{i=(n/2)+1}^n (\psi^{(n-i)})^\dagger \mathcal{D}(\hat{Q}) \psi^{(i-1)} \\ &= c_0 \sum_{i=1}^{n/2} (\psi^{(n-i)})^\dagger \mathcal{D}(\hat{Q}) \psi^{(i-1)} + c_0 \sum_{i=1}^{n/2} ((\psi^{(n-i)})^\dagger \mathcal{D}(\hat{Q}) \psi^{(i-1)})^\dagger \\ &= 2c_0 \text{Re} \left(\sum_{i=1}^{n/2} (\psi^{(n-i)})^\dagger \mathcal{D}(\hat{Q}) \psi^{(i-1)} \right),\end{aligned}$$

since the derivative operator $\mathcal{D}(\hat{Q})$ is Hermitian.

E.0.2 Derivative of \hat{Q}

The derivative of \hat{Q} can be calculated easily, even if it includes a lot of terms

$$\begin{aligned}\gamma_5 \mathcal{D}(\hat{Q}) &= -\mathcal{D}(R_{oo}^{-1})D_{oe}R_{ee}^{-1}D_{eo} - R_{oo}^{-1}\mathcal{D}(D_{oe})R_{ee}^{-1}D_{eo} - \\ &\quad - R_{oo}^{-1}D_{oe}\mathcal{D}(R_{ee}^{-1})D_{eo} - R_{oo}^{-1}D_{oe}R_{ee}^{-1}\mathcal{D}(D_{eo}).\end{aligned}$$

As before

$$\begin{aligned}\mathcal{D}(R_{oo}^{-1}R_{oo}) &= \mathcal{D}(1) = 0 \\ \mathcal{D}(R_{oo}^{-1}R_{oo}) &= \mathcal{D}(R_{oo}^{-1})R_{oo} + R_{oo}^{-1}\mathcal{D}(R_{oo}) = 0 \\ \mathcal{D}(R_{oo}^{-1}) &= -R_{oo}^{-1}\mathcal{D}(R_{oo})R_{oo}^{-1} \\ \mathcal{D}(R_{ee}^{-1}) &= -R_{ee}^{-1}\mathcal{D}(R_{ee})R_{ee}^{-1}\end{aligned}$$

and so

$$\begin{aligned}\gamma_5 \mathcal{D}(\hat{Q}) &= R_{oo}^{-1}\mathcal{D}(R_{oo})R_{oo}^{-1}D_{oe}R_{ee}^{-1}D_{eo} - R_{oo}^{-1}\mathcal{D}(D_{oe})R_{ee}^{-1}D_{eo} + \\ &\quad + R_{oo}^{-1}D_{oe}R_{ee}^{-1}\mathcal{D}(R_{ee})R_{ee}^{-1}D_{eo} - R_{oo}^{-1}D_{oe}R_{ee}^{-1}\mathcal{D}(D_{eo}).\end{aligned}$$

E.0.3 Derivative of D_{eo}

The derivative $\mathcal{D}_{EOP} \equiv \mathcal{D}_{x'\mu'c}D_{eo}(x, \alpha, a; y, \beta, b)$ of D_{eo} , and also of D_{oe} , is

$$\begin{aligned}\mathcal{D}_{EOP} &= \delta_{(x,x')}\delta_{(\mu,\mu')}(iT^c V_\mu(x))_{ab}(\gamma_5(1 - \gamma_\mu))_{\alpha\beta}\delta_{x+\mu,y} + \\ &\quad + \delta_{(x-\mu,x')}\delta_{(\mu,\mu')}(-iV_\mu(x - \mu)T^c)_{ab}(\gamma_5(1 + \gamma_\mu))_{\alpha\beta}\delta_{x-\mu,y},\end{aligned}$$

where it is omitted a constant factor of $-k$. All can be rewritten in a simpler form, contacting with two generic vectors η and ρ

$$\eta^\dagger(x)_{\alpha a}\mathcal{D}_{x'\mu'c}D_{eo}(x, \alpha, a; y, \beta, b)\rho(y)_{\beta b},$$

as

$$\begin{aligned}\eta^\dagger(x)_{\alpha a}\mathcal{D}_{EOP}\rho(y)_{\beta b} &= \eta^\dagger(x')_{\alpha a}(iT^c V_{\mu'}(x'))_{ab}(\gamma_5(1 - \gamma_{\mu'}))_{\alpha\beta}\rho(x' + \mu')_{\beta b} - \\ &\quad - \eta^\dagger(x' + \mu')_{\alpha a}(iV_{\mu'}^\dagger(x')T^c)_{ab}(\gamma_5(1 + \gamma_{\mu'}))_{\alpha\beta}\rho(x)_{\beta b};\end{aligned}$$

in compact form the left side of the last equation is

$$\text{Tr} \left\{ iT^c V_{\mu'}(x')\gamma_5(1 - \gamma_{\mu'}) \left(\rho(x' + \mu') \otimes \eta^\dagger(x') + \eta(x' + \mu') \otimes \rho^\dagger(x') \right) \right\}.$$

E.0.4 Derivative of R_{ee} and $\log(\det(R_{ee}))$

The derivative of the even and of the odd part of the Dirac Wilson operator is

$$\mathcal{D}_{x'\mu'c}(\log(\det(R_{ee}))) = \mathcal{D}_{x'\mu'c}(\text{Tr}(\log(R_{ee}))) = \text{Tr}(R_{ee}^{-1}\mathcal{D}_{x'\mu'c}(R_{ee})).$$

The even part R_{ee} is

$$R_{ee}(x, \alpha, a; y, \beta, b) = \delta_{(x,y)}\delta_{(\alpha,\beta)}\delta_{(a,b)} + \delta_{(x,y)}\frac{k}{4}c_{sw} \sum_{\nu>\mu,\mu=0}^3 (\sigma_{\mu\nu})_{\alpha\beta} F^{\mu\nu}(x)_{ab}.$$

Since there is $\delta_{(x,x')}$ everywhere, the calculation of R_{ee}^{-1} need only calculation of matrix inverse in color and Dirac space

$$R_{ee}(x, \alpha, a; y, \beta, b)^{-1} = \delta_{(x,y)}R_{ee}(\alpha, a; \beta, b)(x)^{-1}.$$

When $c_{sw} \neq 0$ the derivative is not trivial and

$$\mathcal{D}_{x'\mu'c}R_{ee}(x, \alpha, a; y, \beta, b) = \delta_{(x,y)}\frac{k}{4}c_{sw} \sum_{\nu=0,\nu\neq\mu'}^3 (\sigma_{\mu'\nu})_{\alpha\beta}\mathcal{D}_{x'\mu'c}F^{\mu\nu}(x)_{ab},$$

where the sum is only over ν . Considering that $F^{\mu\nu}(x) = \frac{1}{4}Q_{\mu\nu}$, to conclude this step one has to calculate only $\mathcal{D}_{CL} \equiv \mathcal{D}_{x'\mu c}Q^{\mu\nu}(x)$

$$\begin{aligned} \mathcal{D}_{CL} = & \delta_{(x,x')}iT_A^c V_\mu(x)V_\nu(x+\mu)V_\mu^\dagger(x+\nu)V_\nu^\dagger(x) - \\ & -\delta_{(x,x')}iV_\nu^\dagger(x-\nu)V_\mu(x-\nu)V_\nu(x-\nu+\mu)V_\mu^\dagger(x)T_A^c + \\ & +\delta_{(x-\mu,x')}iV_\nu(x)V_\mu^\dagger(x+\nu-\mu)V_\nu^\dagger(x-\mu)T_A^c V_\mu(x-\mu) - \\ & -\delta_{(x-\mu,x')}iV_\mu^\dagger(x-\mu)T_A^c V_\nu^\dagger(x-\mu-\nu)V_\mu(x-\mu-\nu)V_\nu(x-\nu) + \\ & +\delta_{(x-\mu-\nu,x')}iV_\mu^\dagger(x-\mu)V_\nu^\dagger(x-\mu-\nu)T_A^c V_\mu(x-\mu-\nu)V_\nu(x-\nu) - \\ & -\delta_{(x+\nu-\mu,x')}iV_\nu(x)V_\mu^\dagger(x+\nu-\mu)T_A^c V_\nu^\dagger(x-\mu)V_\mu(x-\mu) + \\ & +\delta_{(x-\nu,x')}iV_\nu^\dagger(x-\nu)T_A^c V_\mu(x-\nu)V_\nu(x-\nu+\mu)V_\mu^\dagger(x) - \\ & -\delta_{(x+\nu,x')}iV_\mu(x)V_\nu(x+\mu)V_\mu^\dagger(x+\nu)T_A^c V_\nu^\dagger(x) \end{aligned}$$

Notice that these derivative terms don't vanish only for six points on the lattice.

Publications and proceedings

This is the list of works that have been published during my PhD or that are in preparation to be published in the near future:

- G. Bergner, P. Giudice, I. Montvay, G. Münster, S. Piemonte: *Influence of topology on the scale setting*, in preparation
- G. Bergner, S. Piemonte: *Compactified $\mathcal{N} = 1$ supersymmetric Yang-Mills theory on the lattice: Continuity and the disappearance of the deconfinement transition*, [arXiv:1410.3668 [hep-lat]].
- G. Bergner, P. Giudice, G. Münster, S. Piemonte, D. Sandbrink: *Phase structure of the $N=1$ supersymmetric Yang-Mills theory at finite temperature*, JHEP (2014) in press, [arXiv:1405.3180 [hep-lat]].
- S. Musberg, G. Münster, S. Piemonte: *Clover fermions in the adjoint representation and simulations of supersymmetric Yang-Mills theory*, PoS(LATTICE 2013) 065 [arXiv:1311.6312 [hep-lat]].
- S. Musberg, G. Münster, S. Piemonte: *Perturbative calculation of the clover term for Wilson fermions in any representation of the gauge group $SU(N)$* , JHEP 05 (2013) 143 [arXiv:1304.5741 [hep-lat]].

Bibliography

- [1] J. M. Maldacena: “*The Large N limit of superconformal field theories and supergravity*”, Adv. Theor. Math. Phys. **2** (1998) 231, [arXiv: hep-th/9711200].
- [2] A. Armoni, M. Shifman and G. Veneziano: “*SUSY relics in one flavor QCD from a new $1/N$ expansion*”, Phys. Rev. Lett. **91** (2003) 191601, [arXiv: hep-th/0307097].
- [3] A. Armoni, M. Shifman and G. Veneziano: “*From superYang-Mills theory to QCD: Planar equivalence and its implications*”, in: *Shifman, M. (ed.) et al.: From fields to strings, vol. 1*, 353-444, [arXiv: hep-th/0403071].
- [4] G. Curci and G. Veneziano: “*Supersymmetry and the Lattice: A Reconciliation?*”, Nucl. Phys. B **292** (1987) 555.
- [5] K. G. Wilson: “*Confinement of quarks*”, Phys. Rev. D **10** (1974) 2445
- [6] I. Montvay: “*An algorithm for gluinos on the lattice*”, Nucl. Phys. B **466** (1996) 259, [arXiv: hep-lat/9510042].
- [7] G. Bergner, P. Giudice, G. Münster, S. Piemonte, D. Sandbrink: *Phase structure of the $N=1$ supersymmetric Yang-Mills theory at finite temperature* [arXiv: 1405.3180 [hep-lat]].
- [8] M. Kaku: “*Quantum Field Theory: A Modern Introduction*”, Oxford University Press (1993)
- [9] David J. Gross and Frank Wilczek: *Ultraviolet behavior of non-abelian gauge theories*, Phys. Rev. Lett. **30** (1973) 1343.
- [10] H. David Politzer: *Reliable perturbative results for strong interactions?* Phys. Rev. Lett. **30** (1973) 1346.

- [11] M. F. Sohnius “*Introducing supersymmetry*”, Physics Reports **128** (1985) 39
- [12] M. Shifman: “*Advanced topics in Quantum field theory*”, Cambridge University Press (2012)
- [13] Steven Weinberg: “*The cosmological constant problem*”, Rev. Mod. Phys. **61** (1989) 1,
- [14] E. Witten: “*Constraints on supersymmetry breaking*”, Nucl. Phys. B **202**, 253 (1982)
- [15] N. Seiberg: “*Naturalness Versus Supersymmetric Non-renormalization Theorems*”, Phys. Lett. B **318** (1993) 469, [arXiv: hep-ph/9309335].
- [16] G. C. Rossi and G. Veneziano: “*Non-perturbative breakdown of the non-renormalization theorem in supersymmetric QCD*”, Phys. Lett. B **138**, 195 (1984)
- [17] G. Veneziano and S. Yankielowicz: “*An effective lagrangian for the pure $\mathcal{N} = 1$ supersymmetric Yang-Mills theory*”, Phys. Lett. B **112**, 231 (1982)
- [18] G.R. Farrar, G. Gabadadze, M. Schwetz: “*On the Effective Action of $N=1$ Supersymmetric Yang-Mills Theory*”, Phys. Rev. D **58** (1998) 015009, [arXiv: hep-th/9711166].
- [19] G.R. Farrar, G. Gabadadze, M. Schwetz: “*The Spectrum of Softly Broken $N=1$ Supersymmetric Yang-Mills Theory*”, Phys. Rev. D **60** (1999) 035002, [arXiv: hep-th/9806204].
- [20] V. A. Novikov, M. A. Shifman, A. I. Vainshtein and V. I. Zakharov: “*Exact Gell-Mann-Low Function of Supersymmetric Yang-Mills Theories from Instanton Calculus*”, Nucl. Phys. B **229** (1983) 381.
- [21] Lars Brink, John H. Schwarz and J. Scherk: “*Supersymmetric Yang-Mills theories*”, Nucl. Phys. B **121** (1977) 77
- [22] A. Y. Morozov, M. A. Olshanetsky and M. A. Shifman: “*Gluino condensate in supersymmetric gluodynamics*”, Nucl. Phys. B **304** (1988) 291.
- [23] M. A. Shifman and A. I. Vainshtein: “*On Gluino Condensation in Supersymmetric Gauge Theories. $SU(N)$ and $O(N)$ Groups*”, Nucl. Phys. B **296** (1988) 445.

- [24] I. Montvay and G. Münster: “*Quantum Fields on a Lattice*”, Cambridge University Press (1994).
- [25] T. Degrand and C. DeTar: “*Lattice Methods for Quantum Chromodynamics*”, World Scientific Publishing Company (2006).
- [26] C. Gattringer and C. Lang: “*Quantum Chromodynamics on the Lattice: An Introductory Presentation*”, Springer (2010).
- [27] H.B. Nielsen, M. Ninomiya: “*A no-go theorem for regularizing chiral fermions*”, Phys. Lett. B **105** (1981) 219
- [28] H. Suzuki: “*Supersymmetry, chiral symmetry and the generalized BRS transformation in lattice formulations of $4D \mathcal{N} = 1$ SYM*”, Nucl. Phys. B **861** (2012) 290, [arXiv: 1202.2598 [hep-lat]].
- [29] Steven Gottlieb, W. Liu and D. Toussaint, R. L. Renken and R. L. Sugar: “*Quark-number susceptibility of high-temperature QCD*”, Phys. Rev. Lett. **59**, 2247-2250 (1987)
- [30] R. Kirchner, I. Montvay, J. Westphalen, S. Luckmann and K. Spanderer: “*Evidence for discrete chiral symmetry breaking in $N=1$ supersymmetric Yang-Mills theory*”, Phys. Lett. B **446** (1999) 209, [arXiv: hep-lat/9810062].
- [31] D. Amati, K. Konishi, Y. Meurice, G. C. Rossi and G. Veneziano: “*Nonperturbative Aspects in Supersymmetric Gauge Theories*”, Phys. Rept. **162** (1988) 169.
- [32] N. Seiberg: “*Exact results on the space of vacua of four-dimensional SUSY gauge theories*”, Phys. Rev. D **49** (1994) 6857, [arXiv: hep-th/9402044].
- [33] N. Seiberg: “*Electric - magnetic duality in supersymmetric nonAbelian gauge theories*” Nucl. Phys. B **435** (1995) 129, [arXiv: hep-th/9411149].
- [34] K. Symanzik: “*Continuum Limit and Improved Action in Lattice Theories. 1. Principles and ϕ^4 Theory*”, Nucl. Phys. B **226** (1983) 187.
- [35] K. Symanzik: “*Continuum Limit and Improved Action in Lattice Theories. 2. $O(N)$ Nonlinear σ -model in Perturbation Theory*”, Nucl. Phys. B **226** (1983) 205.

- [36] M. Lüscher and P. Weisz: “ *$O(a)$ improvement of the axial current in lattice QCD to one loop order of perturbation theory*”, Nucl. Phys. B **479** (1996) 429, [arXiv: hep-lat/9606016].
- [37] M. Lüscher, S. Sint, R. Sommer, P. Weisz and U. Wolff: “*Nonperturbative $O(a)$ improvement of lattice QCD*”, Nucl. Phys. B **491** (1997) 323, [arXiv: hep-lat/9609035].
- [38] R. Edwards, U.M. Heller and T.R. Klassen: “*The effectiveness of non-perturbative $O(a)$ improvement in lattice QCD*”, Phys. Rev. Lett. **80** (1998) 3448, [arXiv: hep-lat/9711052].
- [39] S. Musberg, G. Münster, S. Piemonte: “*Perturbative calculation of the clover term for Wilson fermions in any representation of the gauge group $SU(N)$* ”, JHEP **05** (2013) 143, [arXiv: 1304.5741 [hep-lat]].
- [40] S. Aoki and Y. Kuramashi: “*Determination of the Improvement Coefficient c_{SW} up to One-Loop Order with the Conventional Perturbation Theory*”, Phys. Rev. D **68** (2003) 094019, [arXiv: hep-lat/0306015].
- [41] Martin Lüscher, Stefan Sint, Rainer Sommer, Peter Weisz: “*Chiral symmetry and $O(a)$ improvement in lattice QCD*”, Nucl. Phys. B **478** (1996) 365.
- [42] M. Lüscher and P. Weisz “*On-shell improved lattice gauge theories*”, Comm. Math. Phys. **97**, Nr. 1-2: 59-77 1985.
- [43] B. Sheikholeslami, R. Wohlert: “*Improved continuum limit lattice action for QCD with wilson fermions*”, Nucl. Phys. B **259** (1985) 572.
- [44] R. Wohlert: “*Improved continuum limit lattice action for quarks*”, Report No. DESY 87-069 1987.
- [45] Stefano Capitani: “*Lattice Perturbation Theory*”, Phys. Rept. **382** (2003) 113, [arXiv: hep-lat/0211036].
- [46] L. D. Debbio, A. Patella, and C. Pica: “*Higher representations on the lattice: Numerical simulations. $SU(2)$ with adjoint fermions*”, Phys. Rev. D **81** (2010) 094503, [arXiv: 0805.2058 [hep-lat]].
- [47] T. van Ritbergen, A. Schellekens and J. Vermaseren: “*Group theory factors for Feynman diagrams*”, Int. J. Mod. Phys. A **14** (1999) 41, [arXiv: hep-ph/9802376].

- [48] T. Karavirta, K. Tuominen, A. Mykkanen, J. Rantaharju and K. Rummukainen: “*Non-perturbatively improved clover action for $SU(2)$ gauge + fundamental and adjoint representation fermions*”, PoS (Lattice 2010) 064, [arXiv:1011.1781 [hep-lat]].
- [49] G. Bergner, T. Berheide, I. Montvay, G. Münster, U. D. Özugurel and D. Sandbrink: “*The gluino-gluon particle and finite size effects in supersymmetric Yang-Mills theory*”, JHEP **1209** (2012) 108, [arXiv:1206.2341 [hep-lat]].
- [50] G. Bergner, I. Montvay, G. Münster, U. D. Özugurel and D. Sandbrink: “*Towards the spectrum of low-lying particles in supersymmetric Yang-Mills theory*”, JHEP **1311** (2013) 061, [arXiv:1304.2168 [hep-lat]].
- [51] G. Bergner: “*Complete supersymmetry on the lattice and a No-Go theorem*”, JHEP **1001** (2010) 024, [arXiv:0909.4791 [hep-lat]].
- [52] S. Elitzur: “*Impossibility of spontaneously breaking local symmetries*”, Phys. Rev. D **12** (1975) 3978.
- [53] G.P. Lepage, P.B. Mackenzie: “*On the Viability of Lattice Perturbation Theory*”, Phys. Rev. D **48** (1993) 2250, [arXiv:hep-lat/9209022].
- [54] N. Metropolis, A. W. Rosenbluth, M. N. Rosenbluth, A. H. Teller, E. Teller: “*Equation of State Calculations by Fast Computing Machines*”, Journal of Chemical Physics, Vol. 21, p.1087-1092 (1953)
- [55] CP-PACS and JLQCD Collaboration, A. Ukawa: “*Computational cost of full QCD simulations experienced by CP-PACS and JLQCD Collaborations*”, Nucl. Phys. Proc. Suppl. **106** 195 (2002).
- [56] M. Lüscher: “*Computational strategies in lattice QCD*”, [arXiv:1002.4232 [hep-lat]].
- [57] S. Duane; A.D. Kennedy, B. J. Pendleton, R. Duncan: “*Hybrid Monte Carlo*” Phys. Lett. B **195** (1987) 216.
- [58] M. Lüscher, S. Schaefer: “*Lattice QCD without topology barriers*” [arXiv:1105.4749 [hep-lat]].
- [59] M. Lüscher, S. Schaefer: “*Non-renormalizability of the HMC algorithm*”, JHEP **1104** (2011) 104, [arXiv:1103.1810 [hep-lat]].
- [60] I. Kanamori: “*A Method for Measuring the Witten Index Using Lattice Simulation*”, [arXiv:1006.2468 [hep-lat]].

- [61] S. Gottlieb, W. Liu, D. Toussaint, R. L. Renken, R. L. Sugar “*Hybrid-molecular-dynamics algorithms for the numerical simulation of quantum chromodynamics*” Phys. Rev. D **35** (1987) 2531
- [62] B. Jegerlehner: “*Krylov space solvers for shifted linear systems*”, [arXiv:hep-lat/9612014].
- [63] M. Lüscher: “*Deflation acceleration of lattice QCD simulations*”, JHEP **0712** (2007) 011, [arXiv:0710.5417 [hep-lat]].
- [64] W. Kamleh, M. Peardon: *Polynomial Filtered HMC – an algorithm for lattice QCD with dynamical quarks*, [arXiv:1106.5625 [hep-lat]].
- [65] I.P. Omelyan, I.M. Mryglod and R. Folk: “*Optimized verlet-like algorithms for molecular dynamics simulations*”, Phys. Rev. E **65** (2002) 056706.
- [66] T. Takaishi, P. de Forcrand: “*Testing and tuning symplectic integrators for Hybrid Monte Carlo algorithm in lattice QCD*”, Phys. Rev. E **73** (2006) 036706, [arXiv:hep-lat/0505020].
- [67] M. Lüscher, F. Palombi: *Fluctuations and reweighting of the quark determinant on large lattices*, PoS LATTICE 2008 (2008) 049, [arXiv:0810.0946 [hep-lat]].
- [68] K. Jansen, C. Liu: “*Implementation of Symanzik’s Improvement Program for Simulations of Dynamical Wilson Fermions in Lattice QCD*”, Comput. Phys. Commun. **99** (1997) 221 [arXiv:hep-lat/9603008].
- [69] R. Sommer: *Scale setting in lattice QCD*, [arXiv:1401.3270 [hep-lat]].
- [70] M. S. Alvests and C. Farina: “*Trace anomaly through the Schwinger-Dyson equation*”, Class. Quantum Grav. **10**, 1947-1957 (1992).
- [71] R. Sommer: “*A New way to set the energy scale in lattice gauge theories and its applications to the static force and alpha-s in SU(2) Yang-Mills theory*”, Nucl. Phys. B **411** (1994) 839, [arXiv:hep-lat/9310022].
- [72] S. Necco and R. Sommer: “*The $N(f) = 0$ heavy quark potential from short to intermediate distances*”, Nucl. Phys. B **622** (2002) 328, [arXiv:hep-lat/0108008].
- [73] A. K. De, A. Harindranath and J. Maiti: “*On Scale Determination in Lattice QCD with Dynamical Quarks*”, [arXiv:0803.1281 [hep-lat]].

- [74] M. Lüscher: “*Properties and uses of the Wilson flow in lattice QCD*” JHEP **1008** (2010) 071 [arXiv:1006.4518 [hep-lat]].
- [75] S. Borsanyi *et al.*: “*High-precision scale setting in lattice QCD*”, JHEP **1209** (2012) 010, [arXiv:1203.4469 [hep-lat]].
- [76] G. Münster and H. Stüwe: “*The mass of the adjoint pion in $N=1$ supersymmetric Yang-Mills theory*”, JHEP (2014), to be published, [arXiv:1402.6616 [hep-th]].
- [77] I. Jack, D.R.T. Jones, C.G. North: “*Scheme dependence and the NSVZ β -function*”, Phys. Rev. B **486** (1997) 479, [arXiv:hep-ph/9609325].
- [78] M. Creutz, “*Anomalies, gauge field topology, and the lattice*”, Annals of Physics **326** (2011), 911-925, [arXiv:1007.5502 [hep-lat]].
- [79] C. Bonati, M. D’Elia: “*Comparison of the gradient flow with cooling in $SU(3)$ pure gauge theory*”, Phys. Rev. D **89** (2014) 105005, [arXiv:1401.2441 [hep-lat]].
- [80] G. Bergner, P. Giudice, I. Montvay, G. Münster, U. D. Özugurel, S. Piemonte and D. Sandbrink, PoS(LATTICE2014) (2014) 273 [arXiv:1411.1746 [hep-lat]].
- [81] F. Bruckmann, F. Gruber, K. Jansen, M. Marinkovic, C. Urbach, M. Wagner: “*Comparing topological charge definitions using topology fixing actions*”, Eur. Phys. J. A **43** (2010) 303, [arXiv:0905.2849 [hep-lat]].
- [82] JLQCD Collaboration: “*Two-flavor QCD simulation with exact chiral symmetry*”, Phys. Rev. D **78** (2008) 014508, [arXiv:0803.3197 [hep-lat]].
- [83] K. Demmouche, F. Farchioni, A. Ferling, I. Montvay, G. Münster, E. E. Scholz, J. Wuilloud: “*Simulation of 4d $N=1$ supersymmetric Yang-Mills theory with Symanzik improved gauge action and stout smearing*”, Eur. Phys. J. C **69** (2010) 147, [arXiv:1003.2073 [hep-lat]].
- [84] G. Veneziano and S. Yankielowicz: “*An Effective Lagrangian for the Pure $N=1$ Supersymmetric Yang-Mills Theory*”, Phys. Lett. **B 113** (1982) 231.
- [85] M. Gell-Mann, R. Oakes and B. Renner: “*Behavior of current divergences under $SU(3) \times SU(3)$* ”, Phys. Rev. **175** (1968) 2195.

- [86] W. H. Press, B. P. Flannery, S. A. Teukolsky, W. T. Vetterling: “*Numerical Recipes in Fortran 77: The Art of Scientific Computing*”, chapter 11
- [87] T. Banks and A. Casher: “*Chiral symmetry breaking in confining theories*”, Nucl. Phys. B **169** (1980) 103.
- [88] J.J.M. Verbaarschot: “*QCD, Chiral Random Matrix Theory and Integrability*”, [arXiv: hep-th/0502029].
- [89] T. Tanaka: “*On Existence of a Biorthonormal Basis Composed of Eigenvectors of Non-Hermitian Operators*”, J. Phys. A: Math. Gen. **39** (2006) 7757, [arXiv: quant-ph/0603075v3].
- [90] M. Sato, K. Hasebe, K. Esaki, M. Kohmoto: “*Time-Reversal Symmetry in Non-Hermitian Systems*”, Prog. Theor. Phys. **127** (2012) 937, [arXiv: cond-mat.stat-mech/1106.1806].
- [91] G. Bergner and J. Wuilloud: “*Acceleration of the Arnoldi method and real eigenvalues of the non-Hermitian Wilson-Dirac operator*”, Comput. Phys. Commun. **183** (2012) 299, [arXiv: 1104.1363 [hep-lat]].
- [92] E. Getzler: “*A short proof of the local Atiyah-Singer index theorem*”, Topology **25** (1986) 111.
- [93] M.F. Atiyah, I.M. Singer: “*The Index of Elliptic Operators on Compact Manifolds*”, Bull. Amer. Math. Soc. **69** (1963) 422
- [94] M. F. Atiyah: *Global theory of elliptic operators*. Proc. Int. Conf. Funct. Anal. Rel. Topics **1969** (1970) 21-30.
- [95] I.M. Singer: “*Future extensions of index theory and elliptic operators*”, Prosp. in Math. Annals of Mathematics Studies in Mathematics **70** (1971) 171.
- [96] Barton Zwiebach: “*A First Course in String Theory*”, Cambridge University Press (2013) p. 560.
- [97] J. Engels, J. Fingberg and M. Weber: “*Finite Size Scaling Analysis of $SU(2)$ Lattice Gauge Theory in $(3+1)$ -dimensions*” Nucl. Phys. B **332** (1990) 737.
- [98] B. Lucini, M. Teper and U. Wenger: “*The Deconfinement transition in $SU(N)$ gauge theories*”, Phys. Lett. B **545** (2002) 197, [arXiv: hep-lat/0206029].

- [99] Y. Aoki, G. Endrodi, Z. Fodor, S. D. Katz and K. K. Szabo: “*The Order of the quantum chromodynamics transition predicted by the standard model of particle physics*”, *Nature* **443** (2006) 675, [arXiv:hep-lat/0611014].
- [100] Y. Aoki, Z. Fodor, S. D. Katz and K. K. Szabo: “*The Equation of state in lattice QCD: With physical quark masses towards the continuum limit*”, *JHEP* **0601** (2006) 089, [arXiv:hep-lat/0510084].
- [101] A. Bazavov *et al.*: “*Equation of state and QCD transition at finite temperature*”, *Phys. Rev. D* **80** (2009) 014504, [arXiv:0903.4379 [hep-lat]].
- [102] Y. Aoki, Z. Fodor, S. D. Katz and K. K. Szabo: “*The QCD transition temperature: Results with physical masses in the continuum limit*” *Phys. Lett. B* **643** (2006) 46, [arXiv:hep-lat/0609068].
- [103] S. Borsanyi *et al.* [Wuppertal-Budapest Collaboration]: “*Is there still any T_c mystery in lattice QCD? Results with physical masses in the continuum limit III*”, *JHEP* **1009** (2010) 073, [arXiv:1005.3508 [hep-lat]].
- [104] L. Girardello, M. T. Grisaru and P. Salomonson: “*Temperature and Supersymmetry*”, *Nucl. Phys. B* **178** (1981) 331.
- [105] T. E. Clark and S. T. Love: “*Supersymmetry At Finite Temperature*”, *Nucl. Phys. B* **217** (1983) 349.
- [106] A. K. Das: “*Supersymmetry and Finite Temperature*”, *Physica A* **158** (1989) 1.
- [107] M. Panero: “*Thermodynamics of the QCD plasma and the large- N limit*”, *Phys. Rev. Lett.* **103** (2009) 232001, [arXiv:0907.3719 [hep-lat]].
- [108] S. S. Gubser and A. Karch: “*From gauge-string duality to strong interactions: A Pedestrian’s Guide*”, *Ann. Rev. Nucl. Part. Sci.* **59** (2009) 145, [arXiv:0901.0935 [hep-th]].
- [109] O. Aharony, J. Sonnenschein and S. Yankielowicz: “*A Holographic model of deconfinement and chiral symmetry restoration*”, *Annals Phys.* **322** (2007) 1420, [arXiv:hep-th/0604161].
- [110] B. Svetitsky and L. G. Yaffe: “*Critical Behavior at Finite Temperature Confinement Transitions*”, *Nucl. Phys. B* **210** (1982) 423.

- [111] A. Armoni and A. Patella: “*Degeneracy Between the Regge Slope of Mesons and Baryons from Supersymmetry*”, JHEP **0907** (2009) 073, [arXiv: 0901.4508 [hep-th]].
- [112] A. M. Ferrenberg and D. P. Landau: “*Critical behavior of the three-dimensional Ising model: A high-resolution Monte Carlo study*”, Phys. Rev. B **44** (1991) 5081.
- [113] G. Cella, G. Curci, R. Tripiccione and A. Vicere: “*Scaling, asymptotic scaling and Symanzik improvement. Deconfinement temperature in $SU(2)$ pure gauge theory*”, Phys. Rev. D **49** (1994) 511, [arXiv: hep-lat/9306011].
- [114] F. Karsch and M. Lütgemeier: “*Deconfinement and chiral symmetry restoration in an $SU(3)$ gauge theory with adjoint fermions*”, Nucl. Phys. B **550** (1999) 449, [arXiv: hep-lat/9812023].
- [115] G. 't Hooft: “*A planar diagram theory for strong interactions*”, Nucl. Phys. B **72** (1974) 461.
- [116] T. Eguchi and H. Kawai: “*Reduction of Dynamical Degrees of Freedom in the Large- N Gauge Theory*”, Phys. Rev. Lett. **48** (1982) 1063.
- [117] G. Bhanot, U. M. Heller, H. Neuberger: “*The quenched Eguchi-Kawai model*”, Phys. Lett. B **113** (1982) 47.
- [118] M. Ünsal and L. G. Yaffe: “*Center-stabilized Yang-Mills theory: Confinement and large N volume independence*”, Phys. Rev. D **78** (2008) 065035, [arXiv: 0803.0344 [hep-th]].
- [119] G. Bergner, S. Piemonte: “*Compactified $\mathcal{N} = 1$ supersymmetric Yang-Mills theory on the lattice: Continuity and the disappearance of the deconfinement transition*”, [arXiv: 1410.3668 [hep-lat]].
- [120] P. Kovtun, M. Ünsal, L. G. Yaffe: “*Volume independence in large $N(c)$ QCD-like gauge theories*”, JHEP **0706** (2007) 019, [arXiv: hep-th/0702021].
- [121] N. M. Davies, T. J. Hollowood, V. V. Khoze, M. P. Mattis: “*Gluino Condensate and Magnetic Monopoles in Supersymmetric Gluodynamics*”, Nucl. Phys. B **559** (1999) 123, [arXiv: hep-th/9905015].
- [122] G. Cossu, M. D’Elia: “*Finite size phase transitions in QCD with adjoint fermions*”, JHEP **0907** (2009) 048, [arXiv: 0904.1353 [hep-lat]].

- [123] Kenneth Wilson, Letter to the lattice community (2011).
- [124] U. Wolff: “*Monte Carlo errors with less errors*”, Comput. Phys. Commun. bf 156 (2004) 143, [arXiv:hep-lat/0306017].
- [125] E. Ya. Remez: “*Sur la détermination des polynômes d’approximation de degré donnée*”, Comm. Soc. Math. Kharkov **10**, (1934) 41.
- [126] W. Fraser “*A Survey of Methods of Computing Minimax and Near-Minimax Polynomial Approximations for Functions of a Single Independent Variable*” J. ACM bf 12 (1965) 295.

Selbstständigkeitserklärung:

Hiermit erkläre ich, die vorliegende Arbeit selbstständig und ohne fremde Hilfe verfasst und nur die angegebene Literatur und Hilfsmittel verwendet zu haben.

Stefano Piemonte, 20 October 2014

Curriculum vitæ

Personal Information

Name : Stefano Piemonte

Place and Date of Birth : Turin (Italy), February the 8th 1987

Citizenship : Italian

Sex : Male

Spoken languages : Italian (Mother tongue), English (Advanced), German (Intermediate)

Mail address : spiemonte@uni-muenster.de

Actual Position

I am a Ph.D student at the university of Münster under the supervision of prof. G. Münster since October 2011. I am working on the project “The $\mathcal{N} = 1$ Supersymmetric Yang-Mills theory on the lattice” in the DESY-Münster collaboration.

Academic Degrees

Ph.D

- 5/10/2011 - today: Ph.D student at the Westfälische Wilhelms-Universität Münster, supervised by prof. G. Münster.

University

- 18/7/2011: Master's degree in physics at University of Turin, with grade 110/110 cum laude. Thesis: "Thermodynamics of lattice gauge theory" supervised by Prof. Michele Caselle and Dr. Marco Panero.
- 17/11/2009 - 18/7/2011: studies for Master's degree in Physics at University of Turin, following the accomplished of theoretical physics.
- 05/10/2009: Bachelor's degree in Physics at University of Turin, with score 110/110 cum laude. Thesis: "Random Matrix Theory and complex systems" supervised by prof. Michele Caselle.
- 15/09/2006 - 05/10/2009: studies for Bachelor's degree in Physics at University of Turin.

High school

- Jun 2006: Matura, leaving exam of secondary school, with grade 100/100.
- September 2001 - Jun 2006: Scientific Lyceum at school "N. Copernico" of Turin, following the accomplished of natural science.

Publications and proceedings

- G. Bergner, S. Piemonte: *Compactified $\mathcal{N} = 1$ supersymmetric Yang-Mills theory on the lattice: Continuity and the disappearance of the deconfinement transition*, [arXiv: 1410.3668 [hep-lat]].
- G. Bergner, P. Giudice, G. Münster, S. Piemonte, D. Sandbrink: *Phase structure of the $N=1$ supersymmetric Yang-Mills theory at finite temperature*, JHEP (2014) in press, [arXiv: 1405.3180 [hep-lat]].
- S. Musberg, G. Münster, S. Piemonte: *Clover fermions in the adjoint representation and simulations of supersymmetric Yang-Mills theory*, PoS(LATTICE 2013) 065 [arXiv: 1311.6312 [hep-lat]].
- S. Musberg, G. Münster, S. Piemonte: *Perturbative calculation of the clover term for Wilson fermions in any representation of the gauge group $SU(N)$* , JHEP 05 (2013) 143 [arXiv: 1304.5741 [hep-lat]].

Talks

- 25 June 2014: “Finite temperature supersymmetry on the lattice”, presented at 32st International Symposium on Lattice Field Theory (Lattice 2013), 23 June - 28 June 2014, New York
- 19 May 2014: “Effective string model for strong interactions”, research seminar at the University of Münster
- 24 March 2014: “Phase structure of the $\mathcal{N} = 1$ supersymmetric Yang-Mills theory at finite temperature”, Conference of the German Physics Society (“DPG tagung”) at the University of Mainz
- 4 November 2013: “The challenge of supersymmetry on the lattice and the $\mathcal{N} = 1$ SuperYang-Mills theory”, research seminar at the University of Münster
- 30 July 2013: “Clover fermions in the adjoint representation and simulations of supersymmetric Yang-Mills theory”, presented at 31st International Symposium on Lattice Field Theory (Lattice 2013), 29 July - 3 August 2013, Mainz
- 5 March 2013: “The $\mathcal{N} = 1$ Super Yang-Mills theory on the lattice”, Conference of the German Physics Society (“DPG tagung”) at the University of Dresden
- 5 December 2011: “Thermodynamics of Lattice Gauge Theory”, research seminar at the University of Münster

Teaching activities

- Summer Semester 2014: Teaching assistance in the exercise groups for Quantum Mechanics, two hours per week
- Winter Semester 2013: Teaching assistance in the exercise groups for Advanced Quantum Mechanics, two hours per week
- Summer Semester 2013: Teaching assistance in the exercise groups for Quantum Mechanics, two hours per week

Workshops and Summer schools

- September 2014: 20th "Saalburg" Summer School, Wolfersdorf, Thüringen, subject: "Foundations and New Methods in Theoretical Physics"
- June 2013: STRONGnet fellow's workshop, University of Regensburg, subject: "Monte Carlo methods and data analysis in lattice QCD "
- February 2013: First JUQUEEN Porting and Tuning Workshop 2013, Juelich Supercomputing Centre, subject: "Porting, analysis, and optimization on Juqueen"

Expertise

- Numerical algorithms: Partial and ordinary differential equation solvers, Monte Carlo methods, Metropolis and Heat-bath algorithms, Hybrid Monte Carlo
- Data analysis algorithms and tools: Jackknife, Bootstrap, R, Mathematica
- Programming languages: C/C++/QtC++, Java, Python, Fortran
- Preferred operating system: Linux

Stefano Piemonte, 20 October 2014